

Studies on noble metal electrocatalysts coated diffusion electrodes for applications in PEM based sensors and fuel cells

By

E. Jayanthi

(Enrollment No: CHEM02201404001)

Indira Gandhi Centre for Atomic Research, Kalpakkam

A thesis submitted to the

Board of Studies in Chemical Sciences

In partial fulfillment of requirements

For the Degree of

DOCTOR OF PHILOSOPHY

of

HOMI BHABHA NATIONAL INSTITUTE



July 2019

Homi Bhabha National Institute

Recommendations of the Viva Voce Committee

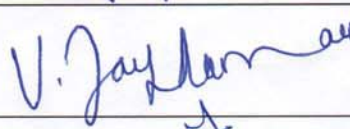
As members of the Viva Voce Committee, we certify that we have read the dissertation prepared by **E. Jayanthi** entitled "**Studies on noble metal electrocatalysts coated diffusion electrodes for applications in PEM based sensors and fuel cells**" and recommend that it may be accepted as fulfilling the thesis requirement for the award of Degree of Doctor of Philosophy.

Chairman – Dr. S. Rangarajan



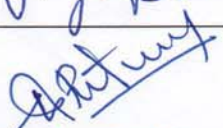
Date: 17.12.2019

Guide / Convener – Dr. V. Jayaraman



Date: 17.12.19

Examiner – Prof. C. Retna Raj



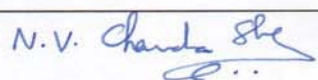
Date: 17/12/19

Member 1- Dr. Dr. B. P. Reddy



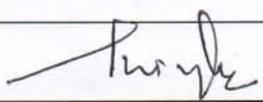
Date: 17.12.2019

Member 2- Dr. N. V. Chandra Shekar



Date: 17/12/19

Member 3- Dr. Dr. S. Ningshen




Date: 17/12/19

Final approval and acceptance of this thesis is contingent upon the candidate's submission of the final copies of the thesis to HBNI.

I/We hereby certify that I/we have read this thesis prepared under my/our direction and recommend that it may be accepted as fulfilling the thesis requirement.

Date: 17.12.2019

Place: kalpakkam



Dr. V. Jayaraman
Guide

STATEMENT BY AUTHOR

This dissertation has been submitted in partial fulfillment of requirements for an advanced degree at Homi Bhabha National Institute (HBNI) and is deposited in the Library to be made available to borrowers under rules of the HBNI.

Brief quotations from this dissertation are allowable without special permission, provided that accurate acknowledgement of source is made. Requests for permission for extended quotation from or reproduction of this manuscript in whole or in part may be granted by the Competent Authority of HBNI when in his or her judgment the proposed use of the material is in the interests of scholarship. In all other instances, however, permission must be obtained from the author.

E. Jayanthi

DECLARATION

I, hereby declare that the investigation presented in the thesis has been carried out by me. The work is original and has not been submitted earlier as a whole or in part for a degree / diploma at this or any other Institution / University.

E. Jayanthi

LIST OF PUBLICATIONS ARISING FROM THE THESIS

Journals

1. Sensing behavior of room temperature amperometric H₂ sensor with Pd electrodeposited from ionic liquid electrolyte as sensing electrode

E. Jayanthi, N. Murugesan, A. Suneesh, C. Ramesh and S. Anthonysamy, *Journal of The Electrochemical Society*, 2017, 164, H5210-H5217.
2. Comparative study of sensing behavior of brush coated, electrodeposited and pulsed electrodeposited Pt/GDE based amperometric hydrogen sensors

E. Jayanthi, N. Murugesan, S. Anthonysamy and C. Ramesh, *Sensors and Actuators B: Chemical*, 2018, 273, 488-497.
3. Proton Exchange Membrane Fuel-Cell-Based Amperometric H₂ Sensor with Pulsed Electrodeposited Electrodes Prepared Using an Ionic Liquid Electrolyte

E. Jayanthi, N. Murugesan and C. Ramesh, *Chemistry Select*, 2019, 4, 4775-4784.
4. Nafion based amperometric H₂ sensor with Pt_xPd_y alloy electrode prepared by pulsed electrodeposition

E. Jayanthi, N. Murugesan and C. Ramesh, *Journal of The Electrochemical Society* (Under review)
5. Studies on pulsed electrodeposited Pt, Pd and Pt_xPd_y alloy based gas diffusion electrodes for oxygen reduction reaction in PEMFC

E. Jayanthi, N. Murugesan and C. Ramesh, *International Journal of Hydrogen Energy* (Manuscript under preparation)

Conferences

1. Sensing behaviour of PEM fuel cell based amperometric hydrogen sensor with electrodeposited Pt electrodes,

E. Jayanthi, *N. Murugesan, C. Ramesh and S. Anthonysamy* (ICONEST -2017, IISC, Bengaluru)

2. Pulsed electrodeposition of palladium in [C4mim][Cl] ionic liquid medium for application in proton exchange membrane based H₂ sensors,

E. Jayanthi, *N. Murugesan and C. Ramesh* (INCOSURF-2018, IISC, Bengaluru)

3. Pulsed electrodeposition of PtPd alloy for the application in proton exchange membrane based H₂ sensors,

E. Jayanthi, *N. Murugesan, and C. Ramesh* (iSAEST-12, CECRI, Karaikudi)

Dedicated to my father and mother

ACKNOWLEDGEMENTS

I express my sincere thanks to my research supervisor Dr. V. Jayaraman for his guidance, support, mentoring and for completing my thesis in time. I thank my previous guide Dr. S. Anthonysamy for his support and encouragement.

I deeply acknowledge my research coordinator Dr. C. Ramesh for all the fruitful discussions, support, mentoring throughout the course of my Ph.D. Without his constant support this thesis would never have been progressed to completion. I also would like to thank his wife Dr. Nisha for her support during my Ph.D.

I would like to thank all my DC committee members Dr. S. Rangarajan, Dr. B. P. Reddy, Dr. N. V. Chandra Shekar and Dr. S. Ningshen for giving me useful suggestions to improve my knowledge as well as my research. I also thank my previous DC members Dr. U. Kamachi Mudali and Dr. Sitaram Dash for their valuable suggestions.

I sincerely thank Dr. N. Sivaraman for speeding up the revision process, support, constant encouragement and also for giving his valuable suggestions for thesis review.

I would like to thank the external examiners Dr.-Ing. Jean-Francois Drillet, DECHEMA-Forschungsinstitut, Germany and Dr. C. Retna Raj, IIT Karagpur for their valuable suggestions which had improved my thesis to a greater extend and also lead me to have better understanding about electrochemistry.

I express my sincere gratitude to Dr. K. A. Venkatesan for giving me an opportunity to work in his lab for some period that encouraged and initiated my Ph. D work.

I thank Dr. K. Ananthasivan for his constant encouragement and support.

I wish to acknowledge A. Saikumaran, Dr. Arup Dasgupta, Dr. R. Sudha, Dr. Manish Chandra and Dr. P. Venkatesh for carrying out my FESEM studies.

I would like to thank Dr. H. N. Jena, Nair Afijith Ravindhranath, Beatrice Veena and Dr.P. Magudapathy for XRD studies. I thank Dr. Amirtha pandian and Mr. Viswanathan (VIT, Vellore) for helping me with TEM characterizations and I also thank Ujjwal Kumar Maity for ICP-MS analysis.

I would like to thank my lab mates N. Murugesan, V. A. Faizal, V. Sukumaran, Devija Devarajan, Mrs. Annie and Mahima Kumar for their help, guidance and friendliness in the lab.

My special thanks to Dr. A S Suneesh, Amutha Suba, Dr. R. Rama, Robert Selvan, Dr. R. Kumaresan, Dr. Alok Rout, Dr. Prathiba, A.S. Ganapathy and K. Rama swamy for their help in the initial period of my Ph. D work. I am thankful to Dr. M. V. Krishnaiah, Dr. Suddhasattwa Ghosh, N. Sanil and E. Prabhu for fruitful discussions.

My sincere thanks to my senior Dr. Manovah david for his valuable suggestions during the course of Ph.D. I would like thank Shubra Sarkar for proof reading my thesis.

I take this opportunity to thank all my research scholar friends who had helped and motivated me during the tenure of my Ph.D.

Words are not sufficient to thank my parents, sisters, in laws and my husband for their constant support and encouragement.

I finally would like to thank IGCAR for giving me an opportunity to do my research.

E. Jayanthi

Contents

SL. No.	TITLE	PAGE No.
1	Abstract of Thesis	i
2	Synopsis	iii
3	List of Figures	x
4	List of Tables	xvii
5	List of Abbreviations	xx

Chapter 1

Introduction

1.0	Hydrogen sensors	1
1.0.1	Metal oxide sensors	2
1.0.2	Catalytic sensors	3
1.0.3	Thermal conductivity sensors	4
1.0.4	Optical sensors	5
1.0.5	Electrochemical H ₂ sensors	5
1.0.5.1	Amperometric and potentiometric hydrogen sensors	7
1.0.5.2	Proton exchange membrane based amperometric H ₂ sensor	7
1.1	Proton exchange membrane fuel cell (PEMFC)	9
1.1.1	Thermodynamics of fuel cell	10
1.1.2	Polarisation curve of fuel cell	11
1.1.2.1	Ohmic loss	12
1.1.2.2	Mass transport loss	13
1.1.2.3	Activation loss	13
1.2	Electrocatalysis in proton exchange membrane based hydrogen sensors and fuel cells	14
1.2.1	Electrocatalyst	14
1.2.2	Criteria for the selection of an electrocatalyst	15
1.2.3	Applications of electrocatalysts	16
1.2.4	Methods of preparation of electrocatalyst	16
1.2.5	Electrodeposition	18

1.2.5.1	Nucleation and growth	19
1.2.5.2	Growth modes of electrodeposition	20
1.2.5.3	Pulsed electrodeposition	21
1.2.5.4	Aqueous and non-aqueous electrolytes for electrodeposition	22
1.3	Literature survey on methods of preparation of electrocatalysts for proton exchange membrane based H ₂ sensor	24
1.4	Literature survey of electrocatalysts in proton exchange membrane fuel cell	27
1.5	Objective of the thesis	29

Chapter 2

Experimental Methods

2.1	Electrochemical studies	31
2.1.1	Potentiostat	31
2.1.2	Cyclic voltammetry	32
2.1.3	Chronoamperometry	33
2.1.4	Chronopotentiometry	34
2.1.5	Electrodeposition and pulsed electrodeposition	35
2.1.6	Electrochemical impedance spectroscopy	37
2.2	Morphological and phase characterisation	39
2.2.1	Electron microscopy	39
2.2.1.1	Scanning electron microscopy	39
2.2.1.2	Transmission electron microscopy	41
2.2.2	X-ray diffraction	42
2.2.3	Linear scratch test equipment	44
2.2.4	Inductively coupled plasma mass spectrometry	44
2.2.5	Sensor and fuel cell testing of Pt, Pd and Pt _x Pd _y alloys deposited on gas diffusion layer	45
2.2.5.1	Diffusion electrode	45
2.2.5.2	Preparation of membrane electrode assembly for sensor and fuel cell	46
2.2.5.3	Sensor testing unit	46
2.2.5.4	Fuel cell testing unit	47

2.3	Conclusions	48
-----	-------------	----

Chapter 3

Studies on deposition and characterization of electrocatalysts on carbon paper for application in PEM sensors

3.1	Introduction	49
3.2	Experimental	50
3.2.1	Preparation of gas diffusion electrodes for the application in PEMHS	50
3.2.1.1	Materials	50
3.2.1.2	Preparation/deposition of Pt electrocatalyst on gas diffusion layer	51
3.2.1.3	Preparation/deposition of Pd electrocatalyst on gas diffusion layer	53
3.2.1.4	Preparation/deposition of Pt _x Pd _y alloy electrocatalyst on gas diffusion layer	53
3.2.2	Characterization of Pt, Pd and Pt _x Pd _y alloy based gas diffusion electrodes	54
3.3	Results and discussions	55
3.3.1	Preparation of gas diffusion electrodes for the application in PEMHS	55
3.3.1.1	Preparation/deposition of Pt electrocatalyst on gas diffusion layer from aqueous electrolyte	55
3.3.1.2	Preparation/deposition of Pt electrocatalyst on gas diffusion layer from [C4mim][BF ₄] ionic liquid electrolyte	59
3.3.1.3	Preparation/deposition of Pd electrocatalyst on gas diffusion layer from aqueous electrolyte	69
3.3.1.4	Preparation/deposition of Pd electrocatalyst on gas diffusion layer from [C4mim][Cl] ionic liquid electrolyte	71
3.3.1.5	Preparation/deposition of Pt _x Pd _y alloy electrocatalyst on gas diffusion layer from aqueous electrolyte	78
3.4	Conclusions	83

Chapter 4

Development of PEM fuel cell based amperometric H₂ sensor with catalyst deposited gas diffusion electrode

4.1	Introduction	85
-----	--------------	----

4.2	Experimental	87
4.2.1	Preparation of membrane electrode assembly	87
4.2.2	Sensor assembly	88
4.2.3	Testing of sensor performance	88
4.2.4	Electrochemical characterization	90
4.3	Results and discussions	91
4.3.1	Sensing mechanism	91
4.3.2	Hydrogen sensing behaviour of PEMHS with Pt/GDL diffusion electrodes	92
4.3.2.1	Response behaviour of PEMHS with brush coated Pt/GDL, electrodeposited Pt/GDL, pulsed electrodeposited Pt/GDL as sensing electrodes prepared using aqueous electrolyte	92
4.3.2.2	Hydrogen sensing behaviour of sensors with electrodeposited Pt/GDL and pulsed electrodeposited Pt/GDL using [C4mim][BF4] as electrolyte	112
4.3.3	Hydrogen sensing behaviour of sensors with pulsed electrodeposited Pd/GDL as sensing electrode	120
4.3.3.1	Response behaviour of sensor with pulsed electrodeposited Pd/GDL using aqueous electrolyte	120
4.3.3.2	Response behaviour of sensor with electrodeposited Pd/GDL using [C4mim][Cl] ionic liquid electrolyte as sensing electrode	122
4.3.4	Hydrogen sensing behaviour of sensor with Pt _x Pd _y /GDL diffusion electrodes as sensing electrode	126
4.4	Conclusions	140

Chapter 5

Deposition, characterization and application of pulsed electrodeposited Pt_xPd_y alloy based gas diffusion electrodes in PEMFC

5.1	Introduction	143
5.2	Experimental	144
5.2.1	Pulsed electrodeposition of Pt _x Pd _y alloy electrocatalysts on gas diffusion layer	144
5.2.2	Characterization of Pt and Pt _x Pd _y alloy based gas diffusion electrodes	145
5.2.3	Preparation of membrane electrode assembly	146
5.2.4	Assembly of proton exchange membrane fuel cell	148

5.2.5	Electrochemical characterizations of membrane electrode assembly	149
5.2.6	Performance evaluation of fuel cell	149
5.3	Results and discussions	150
5.3.1	Physicochemical characterizations of Pt and Pt _x Pd _y alloy on gas diffusion layer	150
5.3.2	Electrochemical characterizations of membrane electrode assemblies	155
5.3.3	Performance evaluation of fuel cells assembled with catalyst deposited diffusion electrodes	161
5.4	Conclusions	167

Chapter 6

Summary and Scope for Future Research

6.1	Summary	169
6.1.1	Studies on deposition and characterization of electrocatalysts on carbon paper for application in PEM sensors	169
6.1.2	Development of PEM fuel cell based amperometric H ₂ sensor with catalyst deposited diffusion electrode	171
6.1.3	Deposition, characterization and application of pulsed electrodeposited Pt _x Pd _y alloy based gas diffusion electrodes in PEMFC	172
6.2	Conclusions	173
6.3	Scope for future studies	173

References

ABSTRACT OF THESIS

Platinum (Pt) electrocatalysts are in high demand due to their utilisation in proton exchange membrane based sensors (PEMHS) and proton exchange membrane fuel cell (PEMFC). High exchange current density for hydrogen oxidation and oxygen reduction reactions for Pt favours the catalyst. However, Pt being expensive will enhance production cost of sensors and fuel cells. Hence investigation for minimising the utility of Pt catalyst is a thrust area and researchers are also on look out for alternate catalysts. Palladium (Pd) is an efficient electrocatalyst and is six times less costly than Pt. Alloying Pt with Pd increase the catalytic activity but, at the same time reduce the quantity of expensive Pt. Metal based electrocatalysts namely Pt, Pd and Pt_xPd_y alloy were investigated. Mode of deposition of catalysts on gas diffusion layer (GDL) plays a crucial role in determining the electrocatalytic area and hence influences the current density of an electrochemical reaction. The present study is aimed at finding an optimal method for preparation and deposition of electrocatalyst for PEMHS and PEMFC. The Pt, Pd and Pt_xPd_y alloy electrocatalysts were prepared by electrodeposition and pulsed electrodeposition methods. Pt/C commercial catalyst was brush coated on GDL for comparison purposes. Electrodeposition of Pt and Pd electrocatalysts on GDL were also carried out using ionic liquid electrolytes to get better adhesion and microstructure. All electrodeposited and pulsed electrodeposited Pt, Pd and Pt_xPd_y alloy electrocatalysts on GDL showed spherical particles with fcc crystal structure as shown by grazing incidence X-ray diffraction and field emission scanning electron microscope studies respectively. The adhesion of electrodeposited Pd on GDL using aqueous and ionic liquid electrolytes was studied using linear scratch equipment. The formation of Pt_xPd_y alloy was confirmed by high resolution transmission electron microscope. The compositions of Pt_xPd_y alloys were analysed by energy dispersive X-ray analysis and inductively coupled plasma mass spectrometry.

Amperometric H_2 sensor gives linear response with H_2 concentration and is widely used electrochemical sensor for commercial applications. The effect of flow rate and longer response time on the response was observed in the previously reported sensors. Thus, it is not suitable for field applications. Hence, to improve the response behaviour and to minimize the catalyst loading in sensor, electrodeposited Pt, Pd and Pt_xPd_y alloy electrocatalysts on GDL were adopted for the first time. The H_2 sensing behaviour of sensor with pulsed electrodeposited electrocatalysts was found to be better compared to electrodeposition and conventional brush coating methods. Further, sensor with pulsed electrodeposited Pt and Pd

on GDL using ionic liquid electrolytes were established to give better sensitivity and response time compared to aqueous electrolytes due to the improved adhesion and higher electrochemical active area achieved by using ionic liquid electrolyte. By comparing performance of sensors with pulsed electrodeposited Pt, Pd and Pt_xPd_y alloy gas diffusion electrodes, $Pt_{54}Pd_{46}$ alloy gas diffusion electrode based sensor was having higher sensitivity, while response time was found to be shorter for $Pt_{80}Pd_{20}$ alloy in comparison to pristine Pt and Pd.

Facile fabrication of gas diffusion electrode with low loading of Pt_xPd_y alloy electrocatalyst has been achieved by pulsed electrodeposition method for application in proton exchange membrane fuel cell. Membrane electrode assembly (MEA) was made using diffusion electrodes with loading of 0.1 mg/cm^2 of $Pt_{51}Pd_{49}$ alloy as cathode and 0.05 mg/cm^2 of Pt at anode. The diffusion electrodes showed good performance in H_2 - O_2 single fuel cell. Moreover, the use of $Pt_{51}Pd_{49}$ alloy reduced the expensive Pt by 50 % since the loading of Pt in $Pt_{51}Pd_{49}$ alloy was only 0.05 mg/cm^2 . This MEA exhibits better performance than commercial Pt/C catalyst. For comparative purpose, another MEA was made using diffusion electrodes with pulsed electrodeposited Pt as cathode and anode with a loading of 0.1 mg/cm^2 and 0.05 mg/cm^2 respectively. MEA with pulsed electrodeposited $Pt_{51}Pd_{49}$ alloy on gas diffusion layer (GDL) as cathode and Pt as anode gave comparable performance with that of pulsed electrodeposited Pt on GDL as cathode.

SYNOPSIS

Chapter 1 – Introduction

Hydrogen (H_2) is an energy carrier for the global clean energy initiative ¹⁻³ and used as a clean source for the future energy supply; fuel cell and internal combustion engine. In spite of all these advantages of H_2 , it also possesses certain demerits regarding safe storage and handling owing to its flammable nature ^{4, 5}. Therefore, it is very essential to monitor its leakage. In fast breeder reactors, removal of sodium from its components is carried out by using moistened CO_2 . The reaction of sodium with moisture present in the reactive gas stream releases large quantity of H_2 ^{6, 7}. Therefore, the concentration of H_2 has to be monitored to maintain the concentration within safe levels. Thus, an extensive demand for reliable sensors for monitoring H_2 is persistent. Electrochemical sensors ⁸⁻¹⁰ are well established commercially, owing to the low power consumption and room temperature operation. Attempts have been made across the globe to lessen the amount of catalyst loading and in turn reduce agglomeration by using porous carbon supporting materials. Rashid et al. ^{11, 12} reported platinum-multi walled carbon nanotube (Pt-MWCNT) as supporting material. Here, it was reported that the usage of MWCNT has largely reduced the loading quantity of the expensive Pt by providing a high surface area for catalyst to be deposited. Lu et al. ¹³, Sakthivel et al. ¹⁴, and Murugesan et al. ⁷ have deposited electrocatalyst directly on to Nafion membrane for H_2 sensor application. They found that the change in flow rate has affected the sensor performance. However, susceptibility to the sensor response to flow rate variation is not desirable in field applications as in the case of sodium removal from fast reactor components. Hence, to provide a high surface area for electrocatalyst and also to minimize the flow rate dependency of sensor signal, gas diffusion layer (GDL) is attempted as substrate material for electrocatalyst deposition. Attempt is made to lower the amount of catalyst loading and also to minimize the effect of flow rate imposed on the sensor response by using GDL and adopting ED method for preparing the sensing electrode.

Proton exchange membrane fuel cell (PEMFC) is an emerging energy resource for the sustainable development. Commercial application of PEMFC is challenging due to the high cost of electrocatalyst used. Pt catalysts are commonly used for hydrogen oxidation reaction (HOR) and oxygen reduction reaction (ORR). The rate of ORR is five times slower compared to HOR¹⁵. Hence, the loading of Pt required is higher at cathode side than at anode. Though Pt is the outperforming catalyst for ORR in PEMFC, cost and stability are the major limitations for commercialization in a large-scale. Hence, pulsed electrodeposition method is

adopted to reduce the loading and to improve the stability. Pt, Pd and Pt_xPd_y alloy electrocatalysts are studied for application in sensors and fuel cells ^[1-3].

Efficiency and economy of catalyst deposition is a major hindrance for its utility as predominant electrocatalysts even though these noble metal electrocatalysts have potential to show superior performance. The electrodeposition method is found to be effective due to its ease of controlling the particle size with regulated catalyst loading ^[9-11]. Electrodeposition of Pt and Pd was carried out using both aqueous and ionic liquid electrolytes in order to see the morphology change and its influence on the sensor performance.

Finally, the objectives of the present study are listed as below:

1. Investigations of electrodeposition and pulse electrodeposition methods for preparation of Pt, Pd and PtPd alloy electrocatalysts on gas diffusion layer (GDL) for application in sensors and fuel cells.
2. Comparison and performance of aqueous and ionic liquid electrolytes in electrodeposition of Pt and Pd electrocatalysts.
3. The electrodeposition behaviour of Pt in 1-butyl-3-methylimidazolium tetrafluoroborate ([C4mim][BF₄]) ionic liquid is examined.
4. Performance evaluation of PEM fuel cell based amperometric H₂ sensors with diffusion electrodes having electrodeposited Pt, Pd and PtPd alloy electrocatalysts.
5. Performance evaluation of PEM fuel cell with diffusion electrodes having electrodeposited Pt, Pd and PtPd alloy electrocatalysts.

Chapter 2- Experimental methods, principles and its applications

This chapter briefs the working principles of electrodeposition and pulsed electrodeposition methods used for deposition of metals and metal alloys on GDL. This chapter also describes about the principles and applications of instruments utilized for structural and electrochemical characterizations of electrocatalysts deposited. The instruments used for physicochemical characterizations include grazing incidence X-ray diffractometer, field emission scanning electron microscope (FESEM) with energy dispersive X-ray analysis (EDAX), high-resolution transmission electron microscope (HRTEM), linear scratch equipment and multi-potentiostat.

Chapter 3- Studies on deposition and characterization of electrocatalysts on carbon paper based diffusion electrodes for application in PEM based H₂ sensors and fuel cells

This chapter deals with the studies on preparation of Pt, Pd and Pt_xPd_y alloy electrocatalysts on GDL by brush coating, electrodeposition and pulsed electrodeposition methods. Pt and Pd

catalysts were electrodeposited and pulsed electrodeposited on GDL using aqueous and ionic liquid electrolytes. Ionic liquid electrolytes used for depositing Pt and Pd are K_2PtCl_6 dissolved in 1-butyl-3-methylimidazolium tetrafluoroborate and $PdCl_2$ dissolved in 1-butyl-3-methylimidazolium chloride. This chapter also provides information on the synthesis of the above ionic liquid electrolytes and their electrochemical window determined by cyclic voltammetry. Prior to the deposition, the deposition potential of Pt and Pd in ionic liquid electrolytes were measured by cyclic voltammetry. The nucleation mechanism of Pt on GDL was studied using chronoamperometry and chronopotentiometry. To find the optimum deposition potential for getting uniform surface coverage, deposition was carried at four different potentials from reduction peak potential obtained from the cyclic voltammogram. Electrodeposition of Pt and Pd on GDL were carried out in $K_2PtCl_6 + [C4mim][BF_4]$ and $PdCl_2 + [C4mim][Cl]$ electrolytes respectively. Adhesion of electrodeposited Pd on GDL using aqueous and ionic liquid electrolytes was studied by using linear scratch technique. The deposited Pt and Pd electrocatalysts on GDL via aqueous and ionic liquid electrolytes were characterized for their crystal structure, morphology and elemental analysis by GIXRD, FESEM, and EDAX. Diffusion electrodes with brush coated Pt on GDL was attempted by using commercially procured Pt/C powder for comparative study.

Further, this chapter illustrates the effect of pulse widths on the electrodeposition of Pt by carrying out PED at four different pulse widths. The optimum pulse width was chosen for depositing Pt_xPd_y alloy on GDL using aqueous electrolyte for the application in PEM sensors and fuel cells. Crystallite sizes, lattice parameter were calculated using Scherrer's formula using the data obtained from GIXRD. Compositions and distribution of Pt and Pd in Pt_xPd_y alloy on GDL were studied by EDAX and EDAX mapping. TEM and HRTEM analysis of representative $Pt_{54}Pd_{46}$ alloy sample were carried out to find the particle size distribution and to confirm the alloy formation.

It became evident from the studies that pulsed electrodeposition produced uniform deposits of Pt, Pd and Pt_xPd_y alloy nanoparticles on GDL with minimal agglomeration in comparison to electrodeposition and brush coating methods. Thus, the PED catalysts are expected to produce higher electrocatalytic area. EDAX analysis confirmed the presence of Pt, Pd and Pt_xPd_y alloy electrocatalysts on GDL and composition of Pt_xPd_y alloys were found to be $Pt_{28}Pd_{72}$, $Pt_{54}Pd_{46}$ and $Pt_{80}Pd_{20}$. All Pt, Pd and Pt_xPd_y alloy electrocatalysts were found to have fcc crystal structure. TEM and HRTEM analysis of $Pt_{54}Pd_{46}$ alloy showed an average particle size of less than 5 nm and confirmed alloy formation for the first time by PED.

Electrodeposition and pulsed electrodeposition of Pt and Pd on GDL in [C4mim][BF₄] and [C4mim][Cl] ionic liquid electrolytes are studied. Pulsed electrodeposited Pt, Pd and Pt_xPd_y alloy on GDL electrocatalysts are developed for the first time for amperometric H₂ sensor and fuel cell applications.

Chapter 4 -Development of PEM fuel cell based amperometric H₂ sensor with catalyst deposited diffusion electrode

Brush-coated, electrodeposited and pulsed electrodeposited Pt, Pd and Pt_xPd_y alloy on GDL were tested for the amperometric H₂ sensing behaviour. These deposited Pt, Pd and Pt_xPd_y alloy electrocatalysts on GDL were used as the sensing electrode and Pt electrocatalyst on GDL was used as the counter electrode. Sensing and counter electrodes were hot-pressed onto the Nafion membrane to make membrane electrode assembly (MEA). Conductivity of Nafion membrane was determined from electrochemical impedance spectroscopy to find the suitability of the electrolyte to be used as a proton conductor. Electrochemical active surface area (ECSA) of all sensing electrodes was measured by carrying out cyclic voltammetry. Amperometric H₂ sensor performance was tested up to the lower explosive limit of H₂ in argon (1-5 %) (V/V) for Pt, Pd and Pt_xPd_y alloy catalysts based sensing electrodes.

Brush-coated, electrodeposited and pulsed electrodeposited Pt on GDL showed a variation in the signal during testing for 48 h. Hence, electrochemical impedance spectrum and cyclic voltammogram were recorded before testing and after 48 h of testing in order to see the variation in charge transfer resistance. ECSA of brush coated, electrodeposited and pulsed electrodeposited Pt was also measured. Response and recovery time of the sensor were determined from the response behaviour. Repeatability of the sensor was also recorded for all the concentrations of H₂ in argon. Calibration plot was made with their standard deviations for the concentration range 1-5 % H₂/Ar. Sensitivities of sensors were obtained from the slope of the calibration plot. Effect of relative humidity, temperature and flow rate on the sensor performance was studied for sensors with Pt deposited by PED. Sensor performance was also studied for electrodeposited and pulsed electrodeposited Pt and Pd on GDL using [C4mim][BF₄] and [C4mim][Cl] ionic liquid electrolytes. The sensing behaviour of electrodeposited Pt on GDL using [C4mim][BF₄] ionic liquid showed a better sensitivity and short response time compared to aqueous electrolyte assisted electrodeposition of Pt.

Sensing behaviour of sensor with Pd based diffusion electrodes in terms of ECSA, sensitivity, response time, recovery time and long-term stability were investigated. Diffusion electrodes for the sensors were prepared using aqueous and [C4mim][Cl] ionic liquid electrolytes. Pd diffusion electrode based sensors in three electrode mode was found to give

higher sensitivity when compared to Pt, Pt_xPd_y alloy sensor operated in two electrode mode. The sensing of Pd based sensor in two electrode mode, signal does not reached the steady state. Hence, Pd diffusion electrode sensor is more suitable to be operated as three electrode mode sensor.

Alloying of Pt with Pd is expected to improve sensitivity and response time due to the change in electronic structure of Pt compared to the pristine Pt. Hence, sensing behaviour of sensors with diffusion electrodes having three different ratios of Pt and Pd in Pt_xPd_y alloy prepared by PED method was also studied.

The hydrogen response behaviour of electrodeposited and pulsed electrodeposited Pt, Pd and Pt_xPd_y alloy revealed that use of diffusion electrode reduced dependence of sensor signal on flow rate. Sensitivity and response time for sensors operated in galvanic mode with electrocatalysts followed the order $Pt_{54}Pd_{46} > Pt$ deposited using ionic liquid $> Pt_{80}Pd_{20} > Pt$ deposited using aqueous electrolyte and $Pt_{80}Pd_{20} > Pt_{54}Pd_{46} > Pt > Pd$ respectively. Higher sensitivity and short response time was obtained for $Pt_{54}Pd_{46}$ and $Pt_{80}Pd_{20}$ alloys compared to the pristine Pt.

Chapter 5— Application of pulsed electrodeposited Pt, Pd and Pt_xPd_y alloy based gas diffusion electrodes for oxygen reduction reaction in PEMFC

PEMFC with pulsed electrodeposited Pt, Pd and Pt_xPd_y alloy diffusion electrodes using aqueous electrolyte as cathode were assembled and tested. For comparison, fuel cells with brush coated Pt based diffusion electrodes was also assembled and tested. In order to ascertain the optimal pulse width for deposition of Pt, studies were carried out at four different pulse widths. ECSA and charge transfer resistance values for the diffusion electrodes were determined by making these electrodes as cathode and Pt deposited at a fixed pulse width as anode for respective electrodes. After arriving at the optimal pulse width, diffusion electrodes with Pt, Pd and Pt_xPd_y alloy were made and performance evaluation was carried out in fuel cell configuration. Experiments were carried out with diffusion electrodes having Pt_xPd_y alloy of composition $Pt_{28}Pd_{72}$, $Pt_{54}Pd_{46}$ and $Pt_{80}Pd_{20}$. Performance of fuel cell with diffusion electrode having pulsed electrodeposited Pt, Pd and Pt_xPd_y alloys was compared. Higher current density was obtained for pulsed electrodeposited Pt and $Pt_{54}Pd_{46}$ alloy in comparison to other proportions of Pt_xPd_y alloy, pristine Pd and commercial Pt/C catalyst. The above result was also supported by ECSA and charge transfer resistance values obtained. Performance of the fuel cell catalyst in the diffusion electrode followed the order $Pt \approx Pt_{54}Pd_{46} > Pt_{20}Pd_{72} > Pt/C > Pd > Pt_{80}Pd_{20}$. Hence, $Pt_{54}Pd_{46}$ catalyst with nearly 50 % of Pt gives same performance pristine Pt.

Chapter 6 –Summary, conclusions and scope for future studies

The present investigations indicated that the electrocatalyst prepared by pulsed electrodeposition method gives higher catalytic area over brush coating and electrodeposition methods. The sensor testing studies conclude that Pt_xPd_y alloy is highly suitable for sensing H_2 with better sensitivity and response time. It is established that fuel cell performance of pulsed electrodeposited $Pt_{54}Pd_{46}$ alloy is approximately equal to that of pulsed electrodeposited Pt. Hence, the amount of Pt is reduced by employing Pt_xPd_y alloy.

Three electrode potentiostatic sensors with $Pt_{54}Pd_{46}$ as sensing electrode can be undertaken in future to improve the response behaviour. Studies can also be carried out towards developing H_2 sensors with composite proton conducting polymer electrolyte. Fuel cells with larger electrode area and also fuel cell stacks can be made with alloy electrodes and evaluated for performance. Studies can be extended with pulsed electrodeposited alloys of Pt with Pd, Ru, Cr as electrocatalyst in diffusion electrode to improve the corrosion resistance and reduce poisoning.

References

1. A. Midilli, M. Ay, I. Dincer and M. A. Rosen, *Renew. Sustainable Energy Rev.*, 2005, 9, 255-271.
2. S. A. Sherif, F. Barbir and T. Veziroglu, *Sol. Energ.*, 2005, 78, 647-660.
3. C. M. White, R. R. Steeper and A. E. Lutz, *Int. J. Hydrogen Energy*, 2006, 31, 1292-1305.
4. L. Boon-Brett, J. Bousek, G. Black, P. Moretto, P. Castello, T. Hübert and U. Banach, *Int. J. Hydrogen Energy*, 2010, 35, 373-384.
5. T. Hübert, L. Boon-Brett, G. Black and U. Banach, *Sens. Actuators B: Chem.*, 2011, 157, 329-352.
6. C. Ramesh, N. Murugesan, M. Krishnaiah, V. Ganesan and G. Periaswami, *J Solid State Electrochem.*, 2008, 12, 1109-1116.
7. N. Murugesan, C. Ramesh, N. Sanil, M. Krishnaiah, S. S. Raj and V. Ganesan, *Sens. Actuators B: Chem.*, 2013, 182, 598-604.
8. G. Korotcenkov, S. D. Han and J. R. Stetter, *Chem. Rev.*, 2009, 109, 1402-1433.
9. C. Park, S. Akbar and W. Weppner, *J Mater. Sci.*, 2003, 38, 4639-4660.
10. Z. Samec, F. Opekar and G. J. Crijns, *Electroanal.*, 1995, 7, 1054-1058.
11. M. Rashid, T.-S. Jun, Y. Jung and Y. S. Kim, *Sens. Actuators B: Chem.*, 2015, 208, 7-13.
12. M. Rashid, T.-S. Jun and Y. S. Kim, *J Korean Electrochem. Soc.*, 2014, 17, 18-25.
13. X. Lu, S. Wu, L. Wang and Z. Su, *Sens. Actuators B: Chem.*, 2005, 107, 812-817.
14. M. Sakthivel and W. Weppner, *Sens. Actuators B: Chem.*, 2006, 113, 998-1004.
15. M. Shao, *J Power Sources*, 2011, 196, 2433-2444.

List of Figures

Figure	Title	Page No.
1.1	Schematic of metal oxide sensor	3
1.2	Structure of catalytic sensor	4
1.3	Thermal conductivity sensor configuration	4
1.4	Schematic of optical sensor	5
1.5	Structure of an amperometric sensor	6
1.6	Structure of Nafion proton exchange membrane	8
1.7	Schematics of the proton exchange membrane based hydrogen sensor assembly	9
1.8	Typical polarisation curve of a fuel cell	12
1.9	Mechanism of electrochemical oxidation of gas at the catalyst surface	15
1.10	Applications of electrocatalyst in various fields	16
1.11	Growth modes of electrodeposition	21
2.1	Schematics of potentiostatic circuit	32
2.2	A typical cyclic voltammogram of reversible redox reaction (E_a – anodic potential, E_c - cathodic potential, E_s – starting potential, E_i – initial potential, E_f – final potential)	33
2.3	Plot of potential vs time for electrodeposition and pulsed electrodeposition	35
2.4	Schematics of electrolytic cell	36
2.5	Multipotentiostat with electrolytic cell (VMP-300 of M/s Biologic)	36
2.6	Equivalent circuit of simple electrochemical reaction	38
2.7	Nyquist impedance plot of simple electrochemical reaction	38
2.8	Schematics of electron-sample interaction	39
2.9	Schematic representation of scanning electron microscope	40
2.10	Schematics of transmission electron microscope (FEI-Tecnai)	41
2.11	Schematics of X-ray diffraction	43
2.12	Schematic of diffusion electrode	45
2.13	Hydraulic press (SANTEC)	46
2.14	Schematics of sensor and testing unit	47

2.15	Schematics of fuel cell test station	48
3.1	Grazing incidence X-ray diffraction pattern of deposited Pt on gas diffusion layer (a) brush coated Pt/C commercial catalyst, (b) electrodeposited and (c) pulsed electrodeposited	56
3.2	Field emission scanning electron microscope images of electrocatalyst on gas diffusion layer (a) brush coated Pt/C (50 %), (b) electrodeposited Pt and (c) pulsed electrodeposited Pt	57
3.3	Cyclic voltammogram of (a) 1-butyl-3-methylimidazolium tetrafluoroborate electrolyte (scan rate: 10 mV/s) and (b) $K_2PtCl_6 + [C4mim][BF_4]$ (scan rate: 10 mV/s) ; working electrode: GDL, counter electrode: glassy carbon, reference electrode: Pt wire	60
3.4	(a) Pt electrodeposited on gas diffusion layer at -0.58 V and (b) Pt electrodeposited on gas diffusion layer at -2.17 V	61
3.5	Chronopotentiogram of 70 mM $K_2PtCl_6 + [C4mim][BF_4]$ at 373 K	63
3.6	(a) Chronoamperogram of Pt on gas diffusion layer in $[C4mim][BF_4]$ ionic liquid electrolyte and (b) Fitting of chronoamperometric data with Scharifker Hills theoretical model of 3D progressive and instantaneous nucleation	65
3.7	Field emission scanning electron microscope images of (a) gas diffusion layer (GDL) electrodeposited Pt/GDL at the applied potential of (b) -2.4 V, (c) -2.5 V and (d) -2.6 V, and pulsed electrodeposited Pt/GDL at (e) -2.4 V (f) 1 μm resolution	68
3.8	Grazing incidence X-ray diffraction pattern of Pt on gas diffusion layer (a) electrodeposited and (b) pulsed electrodeposited	69
3.9	Field emission scanning electron microscope images of Pd on gas diffusion layer (a) electrodeposited and (b) pulsed electrodeposited	70
3.10	Grazing incidence X-ray diffraction pattern of Pd on gas diffusion layer (a) electrodeposited and (b) pulsed electrodeposited	71
3.11	Cyclic voltammogram of (a) 1-butyl-3-methylimidazolium chloride electrolyte (scan rate: 10 mV/s) and (b) $PdCl_2 + [C4mim][Cl]$ (scan rate: 10 mV/s); working electrode: GDL, counter electrode: glassy carbon, reference electrode: Pt wire	72
3.12	Field emission scanning electron microscope images of electrodeposited	74

	Pd on gas diffusion layer using [C4mim][Cl] electrolytes at the applied potentials of (a) -0.8 V, (b) -0.9 V, (c) -1 V, (d) -1.1 V, (e) -1 V at 1 μ m and (f) pulsed electrodeposited Pd at -1 V	
3.13	Energy dispersive X-ray analysis of electrodeposited Pd on gas diffusion layer using [C4mim][Cl] electrolyte	75
3.14	Grazing incidence X-ray diffraction pattern of Pd on gas diffusion layer using [C4mim][Cl] electrolyte (a) electrodeposited and (b) pulsed electrodeposited	76
3.15	Scratch plot and scanning electron micrograph of electrodeposited (a) Pd using PdCl ₂ /HCl electrolyte and (b) Pd from PdCl ₂ /[C4mim][Cl] electrolyte	78
3.16	Energy dispersive X-ray analysis of pulsed electrodeposited catalyst on gas diffusion layer using aqueous electrolyte (a) Pt ₈₀ Pd ₂₀ , (b) Pt ₅₄ Pd ₄₆ and (c) Pt ₂₈ Pd ₇₂	80
3.17	Field emission scanning electron microscope images of pulsed electrodeposited of catalyst on gas diffusion layer using aqueous electrolyte (a) Pt ₂₈ Pd ₇₂ , (b) Pt ₅₄ Pd ₄₆ and (c) Pt ₈₀ Pd ₂₀ . Energy dispersive X-ray mapping of Pt ₅₄ Pd ₄₆ alloy (d) Pt, (e) Pd and (f) merging of Pt and Pd	81
3.18	Grazing incidence X-ray diffraction pattern of pulsed electrodeposited of catalyst on gas diffusion layer using aqueous electrolyte (a) Pt ₂₈ Pd ₇₂ , (b) Pt ₈₀ Pd ₂₀ , (c) Pt ₅₄ Pd ₄₆ and (d) Pt Inset: Expanded image of Pt _x Pd _y electrodes of (111) plane	82
4.1	Hydrogen response behaviour of sensor with brush coated Pt on gas diffusion layer	94
4.2	Hydrogen response behaviour of sensor with electrodeposited Pt on gas diffusion layer using aqueous electrolyte (a) initial (b) after 48 h	95
4.3	Hydrogen response behaviour of sensor with pulsed electrodeposited Pt on gas diffusion layer using aqueous electrolyte	96
4.4	Impedance spectrum of sensors with brush coated (BC), electrodeposited (ED) and pulsed electrodeposited (PED) Pt electrocatalyst on gas diffusion layer (a) initial and (b) after 48 h	97
4.5	Cyclic voltammogram of sensor with Pt electrocatalyst on gas diffusion	100

	layer (a) brush coated, (b) electrodeposited and (c) pulsed electrodeposited	
4.6	Response and recovery times of sensor with Pt deposited on gas diffusion layer using aqueous electrolyte (a) electrodeposited Pt/GDL and (b) pulsed electrodeposited Pt/GDL	102
4.7	Pulsed electrodeposited Pt on gas diffusion layer using aqueous electrolyte based sensor (a) Repeatability of 1% H ₂ /Ar and (b) Calibration plot	104
4.8	response behaviour of sensor with pulsed electrodeposited Pt on gas diffusion layer using aqueous electrolyte for 1% H ₂ /Ar with various flow rates (50 sccm to 400 sccm)	107
4.9	Calibration plot of sensor with pulsed electrodeposited Pt on gas diffusion layer using aqueous electrolyte at different RH 60-80 %	108
4.10	Sensor with pulsed electrodeposited Pt on gas diffusion layer using aqueous electrolyte response behaviour of 1% H ₂ /Ar at five different temperatures (293-313 K)	109
4.11	Sensor with pulsed electrodeposited Pt on gas diffusion layer using aqueous electrolyte (a) Signal stability of 4% H ₂ /Ar and (b) Long-term stability	110
4.12	Sensor with electrodeposited Pt on gas diffusion layer using [C4mim][BF4] ionic liquid electrolyte (a) response behaviour and (b) repeatability for response of 4 % H ₂ /Ar	113
4.13	Sensor with pulsed electrodeposited Pt on gas diffusion layer using [C4mim][BF4] ionic liquid electrolyte (a) response behaviour and (b) repeatability for response of 4 % H ₂ /Ar	114
4.14	Cyclic voltammogram of sensors with electrodeposited and pulsed electrodeposited Pt on gas diffusion layer using [C4mim][BF4] ionic liquid electrolyte (Loading: 0.5 mg/cm ² , scan rate: 200 mV/s)	115
4.15	Response and recovery times of sensor with Pt deposited on gas diffusion layer using [C4mim][BF4] ionic liquid electrolyte	117
4.16	Calibration plot of H ₂ sensors with five different loadings of Pt deposited on gas diffusion layer using [C4mim][BF4] ionic liquid	118

	electrolyte (a) electrodeposited and (b) pulsed electrodeposited	
4.17	Long-term Stability sensors with electrodeposited and pulsed electrodeposited Pt at different loadings on gas diffusion layer using [C4mim][BF ₄] of ionic liquid electrolyte	119
4.18	Sensor with pulsed electrodeposited Pd on gas diffusion layer (a) response behaviour and (b) repeatability of 4 % H ₂ /Ar	121
4.19	Response behaviour sensor with electrodeposited Pd on GDL using [C4mim][Cl] electrolyte	123
4.20	Response and recovery times of electrodeposited Pd on GDL using [C4mim][Cl] electrolyte based sensor	124
4.21	Sensor with electrodeposited Pd on gas diffusion layer using [C4mim][Cl] ionic liquid electrolyte (a) Repeatability for 5% H ₂ /Ar and (b) Calibration plot	125
4.22	Cyclic voltammogram of sensors with pulsed electrodeposited Pt _x Pd _y alloy electrocatalyst (Loading: 0.5 mg/cm ² , scan rate: 200 mV/s)	127
4.23	Hydrogen response behaviour of sensor with pulsed electrodeposited Pt ₂₈ Pd ₇₂ alloy electrodes	128
4.24	Response behaviour of sensors with pulsed electrodeposited Pt _x Pd _y alloy electrodes (a) Pt ₅₄ Pd ₄₆ and (b) Pt ₈₀ Pd ₂₀	129
4.25	Calibration plot of sensor with pulsed electrodeposited Pt ₅₄ Pd ₄₆ and Pt ₈₀ Pd ₂₀ alloy electrodes	130
4.26	Response and recovery times of sensors with pulsed electrodeposited Pt _x Pd _y alloy on gas diffusion layer	131
4.27	(a) Effect of RH and (b) flow rate on the sensor response for Pt ₅₄ Pd ₄₆ alloy on gas diffusion layer based sensors	133
4.28	Sensor with pulsed electrodeposited Pt ₅₄ Pd ₄₆ alloy on gas diffusion layer (a) repeatability of 5 % H ₂ /Ar of Pt ₅₄ Pd ₄₆ and (b) long-term stability for 5 % H ₂ /Ar	135
5.1	Membrane electrode assemblies of PEM fuel cell with 5 cm ² and 25 cm ² electrode area	146
5.2	(a) Components of proton exchange membrane fuel cell and (b) Assembly of proton exchange membrane fuel cell	148

5.3	Fuel cell set up with test station	150
5.4	Energy dispersive X-ray analysis of pulsed electrodeposited Pt_xPd_y alloy on gas diffusion layer (a) $Pt_{28}Pd_{72}$, (b) $Pt_{51}Pd_{49}$ and (c) $Pt_{81}Pd_{19}$	151
5.5	Field emission scanning electron microscope images of pulsed electrodeposited Pt on gas diffusion layer at different pulse widths of (a) 200 ms, (b) 20 ms, (c) 2 ms and (d) 0.2 ms	152
5.6	FESEM images of pulsed electrodeposited Pt_xPd_y alloys on gas diffusion layer at 0.2 ms pulse width (a) $Pt_{28}Pd_{72}$, (b) $Pt_{51}Pd_{49}$ and (c) $Pt_{81}Pd_{19}$	153
5.7	Grazing incidence X-ray diffraction pattern of Pt, Pd and Pt_xPd_y alloy: (a) Pt (b) $Pt_{81}Pd_{19}$ (c) $Pt_{51}Pd_{49}$ (d) $Pt_{28}Pd_{72}$	153
5.8	(a) TEM image, (b) to (d) HRTEM images, (e) SAED pattern and (f) particle size distribution	155
5.9	(a) Cyclic voltammogram of pulsed electrodeposited Pt on gas diffusion layer at various pulse widths (Loading: 0.1 mg/cm^2 , scan rate: 200 mV/s) and (b) Plot of ECSA vs pulse width	156
5.10	Impedance spectrum of fuel cell with pulsed electrodeposited Pt diffusion electrode at different pulse widths as cathode and pulsed electrodeposited Pt at 0.2 ms as anode (R_1 - Ohmic resistance, R_2 - Charge transfer resistance and Q_1 - Non-ideal capacitance)	158
5.11	Electrochemical impedance spectrum of Pt/C commercial catalyst and pulsed electrodeposited Pt_xPd_y alloy electrocatalysts on gas diffusion layer (R_1 - Ohmic resistance, R_2 - Charge transfer resistance and Q_1 - Non-ideal capacitance)	159
5.12	Cyclic voltammogram of Pt/C commercial catalyst and pulsed electrodeposited Pt_xPd_y alloy electrocatalysts on gas diffusion layer (Loading: 0.1 mg/cm^2 , scan rate : 200 mV/s)	160
5.13	Proton exchange membrane fuel cell performance of pulsed electrodeposited Pt_xPd_y alloy electrocatalysts on gas diffusion layer (5 cm^2) (a) current density vs E and (b) current density vs power density	162
5.14	Plot of current density vs time at 0.5 V	163
5.15	Proton exchange membrane fuel cell performance for pulsed electrodeposited Pt, $Pt_{54}Pd_{49}$ alloy and brush coated commercial Pt/C catalyst (5 cm^2) (a) current density vs E and (b) current density vs power	164

	density	
5.16	Proton exchange membrane fuel cell performance of pulsed electrodeposited Pt ₅₁ Pd ₄₉ alloy electrocatalysts on gas diffusion layer (25 cm ²)	165

List of Tables

Table	Title	Page No.
1.1	Characteristics of different types of sensors	6
1.2	Various types of fuel cells with their electrochemical reactions	10
1.3	Comparison of different methods used for deposition of electrocatalysts	17
1.4	Viscosity, conductivity, melting point and electrochemical window of ionic liquid electrolytes	23
1.5	Comparison of electrocatalyst/Nafion based hydrogen sensor by various methods	26
1.6	Comparison of proton exchange membrane fuel cell performance of different electrocatalysts reported in literature	29
3.1	Crystallite sizes of Pt deposited on gas diffusion layer by brush coating, electrodeposition and pulsed electrodeposition methods	56
3.2	Deposition potentials of Pt in [C4mim][BF ₄], [C4mim][PF ₆] and [DEME][BF ₄] ionic liquids	66
3.3	Crystallite sizes of electrodeposited Pt on gas diffusion layer (Pt/GDL) and pulsed electrodeposited Pt/GDL from [C4mim][BF ₄] ionic liquid electrolyte	69
3.4	Crystallite sizes of electrodeposited and pulsed electrodeposited Pd on gas diffusion layer using aqueous electrolyte	71
3.5	Bragg angle and crystallite sizes of electrodeposited and pulsed electrodeposited Pd using [C4mim][Cl] electrolyte	76
3.6	Bragg angle, lattice parameter and crystallite sizes of pulsed electrodeposited Pt ₂₈ Pd ₇₂ , Pt ₅₄ Pd ₄₆ and Pt ₈₀ Pd ₂₀ on gas diffusion layer	83
4.1	Sensing and counter electrodes used for membrane electrode assembly for the application in proton exchange membrane based H ₂ sensor	88
4.2	Response behaviours of sensors with brush coated, electrodeposited and pulsed electrodeposited Pt on gas diffusion layer using aqueous electrolyte	101
4.3	Response behaviour of sensor with pulsed electrodeposited Pt on gas diffusion layer using aqueous electrolyte to H ₂ /Ar	105
4.4	Sensor signal with their standard deviations for pulsed electrodeposited Pt on gas diffusion layer	105

4.5	Comparison of amperometric H ₂ sensing behaviour of electrodeposited and pulsed electrodeposited Pt on gas diffusion layer using [C4mim][BF ₄] ionic liquid electrolyte	116
4.6	Hydrogen sensing characteristics of sensor with pulsed electrodeposited Pt _x Pd _y alloy diffusion electrodes	132
4.7	Response current with standard deviation of sensor with Pt ₅₄ Pd ₄₆ alloy diffusion electrode	136
4.8	Sensor characteristics of Pt and Pt _x Pd _y alloy electrocatalysts on gas diffusion layer based electrodes with sensors reported in literature	136
4.9	Comparison of present amperometric H ₂ sensor performances with sensors reported in literature	139
4.10	Response time reported in Huber et al. ¹² document	140
4.11	Response time reported in the present thesis	140
5.1	Electrolyte concentrations used for pulsed electrodeposition of Pt _x Pd _y alloy on gas diffusion layer	145
5.2	Loading of electrocatalyst and pulse width used for pulsed electrodeposition of Pt on gas diffusion layer as anode and cathode	147
5.3	Loading of electrocatalyst and pulse width used for pulsed electrodeposition of Pt _x Pd _y alloy on gas diffusion layer as cathode and for pulsed electrodeposition of Pt on gas diffusion layer as anode	147
5.4	PEM fuel cells assembled and tested	149
5.5	Bragg angle, lattice parameter and crystallite sizes of pulsed electrodeposited Pt ₂₈ Pd ₇₂ , Pt ₅₁ Pd ₄₉ and Pt ₈₁ Pd ₁₉ on gas diffusion layer	154
5.6	Electrochemical surface area of pulsed electrodeposited Pt on GDL at various pulse widths	157
5.7	Electrochemical impedance of pulsed electrodeposited Pt diffusion electrode at different pulse widths	158
5.8	Electrochemical impedance of Pt/C commercial catalyst and pulsed electrodeposited Pt _x Pd _y alloy electrocatalysts on gas diffusion layer	159
5.9	Electrochemical surface area of brush coated Pt/C/GDL and pulsed electrodeposited Pt _x Pd _y on GDL	160
5.10	Proton exchange membrane fuel cell performance of pulsed electrodeposited Pt _x Pd _y on gas diffusion layer at a loading of 0.1 mg/cm ²	165
5.11	Comparison of single fuel cell performance of present pulsed	166

electrodeposited Pt_xPd_y alloy electrocatalysts on GDL with reported Pt_xPd_y alloy electrocatalysts in literature

List of abbreviations

SL. No.	Full Name	Abbreviation
1	Saturated calomel electrode	SCE
2	Gas diffusion layer	GDL
3	1-butyl-3-methylimidazolium chloride	[C4mim][Cl]
4	1-butyl-3-methylimidazolium tetrafluoroborate	[C4mim][BF ₄]
5	Electrodeposition	ED
6	Pulsed electrodeposition	PED
7	Brush coating	BC
8	Membrane electrode assembly	MEA
9	Gas diffusion electrode	GDE
10	Inductively coupled plasma mass spectrometry	ICP-MS
11	Grazing incidence X-ray diffraction	GIXRD
12	High resolution transmission electron microscopy	HRTEM
13	Field emission scanning electron microscope	FESEM
14	Energy dispersive X-ray analysis	EDAX
15	Proton exchange membrane based H ₂ sensor	PEMHS
16	Cyclic voltammetry	CV
17	Proton exchange membrane fuel cell	PEMFC
18	Room temperature ionic liquids	RTIL
19	Electrochemical impedance spectroscopy	EIS
20	Secondary electrons	SEs
21	Energy dispersive X-ray analysis	EDAX
22	Grazing incidence X-ray diffraction	GIXRD
23	Joint Committee of Powder Diffraction Standards	JCPDS
24	Full width half maximum	FWHM
25	Critical load	L _c
26	Electrodeposited Pt on GDL using aqueous electrolyte	ED/Pt/GDL/AQ
27	Brush coated Pt/C catalyst on GDL	BC/Pt/C/GDL
28	Pulsed electrodeposited Pt on GDL using aqueous electrolyte	PED/Pt/GDL/AQ
29	Pulsed electrodeposited Pt on GDL using	PED/Pt/GDL/[C4mim][BF ₄]

	[C4mim][BF ₄] ionic liquid	
30	Electrodeposited Pt on GDL using [C4mim][BF ₄] ionic liquid	ED/Pt/GDL/[C4mim][BF ₄]
31	Electrodeposited Pd on GDL using aqueous electrolyte	ED/Pd/GDL/AQ
32	Pulsed electrodeposited Pd on GDL using aqueous electrolyte	PED/Pd/GDL/AQ
33	Electrodeposited Pd on GDL using [C4mim][Cl] ionic liquid	ED/Pd/GDL/[C4mim][Cl]
34	Pulsed electrodeposited Pt on GDL using [C4mim][Cl] ionic liquid	PED/Pd/GDL/[C4mim][Cl]
35	Electrochemical surface area	ECSA
36	Relative humidity	RH
37	Oxygen reduction reaction	ORR
38	Hydrogen oxidation reaction	HOR
39	Working electrode	WE
40	Counter electrode	CE
41	Reference electrode	RE
42	Selected area electron diffraction	SAED

Thesis Highlight

Name of the Student: E. Jayanthi

Name of the CI/OCC: HBNI-IGCAR

Enrolment No.: CHEM02201404001

Thesis Title: Studies on noble metal electrocatalysts coated diffusion electrodes for applications in PEM based sensors and fuel cells

Discipline: Chemical Sciences

Sub-Area of Discipline: Electrochemistry

Date of viva voce: 17/12/2018

Polymer exchange membrane (PEM) based H_2 sensors and PEM fuel cell devices are operating in galvanic mode where chemical energy is converted into electrical energy. The response behaviour of electrochemical sensors and current efficiency of fuel cell are significantly influenced by the catalytic area available for electrochemical reaction and these sites are called three phase contact sites i.e. electrolyte, gas, and electrically connected catalyst regions are in contact for the completion of the circuit in the case of electrochemical reactions. The catalyst used for the above purpose is called electrocatalyst. Platinum (Pt) and its alloys are commonly used as electrocatalysts for sensors and fuel cell owing to their physicochemical properties. The high cost of Pt catalyst is the main hurdle to be used commercially. Recently, several efforts have been made to reduce the cost of precious metal electrocatalysts without sacrificing the catalyst performances and are listed below: reduction of precious metal loading, nanostructured thin-film (NSTF) development for catalyst layer, particle size reduction for electrocatalyst, developing non-precious metal/alloy and developing novel catalyst preparation methods. Novel catalyst preparation method is used in the present study to reduce the loading of expensive electrocatalysts. Pulsed electrodeposition method is adopted for the first time to prepare the electrocatalysts for the application in H_2 sensors and fuel cell.

Facile fabrication of gas diffusion electrode with low loading of electrocatalysts has been achieved by pulsed electrodeposition method for application in PEM based H_2 sensor and PEM fuel cell. The minimum Pt electrocatalyst loading reported in literature for PEM H_2 sensor is 1 mg/cm^2 and Pt_xPd_y alloy electrocatalyst for fuel cell is 0.5 mg/cm^2 . In the present study, it is possible to reduce the loading to 0.5 mg/cm^2 and 0.1 mg/cm^2 for sensors and fuel cell respectively. This is due to finer distribution of Pt electrocatalyst is attained by pulsed electrodeposition method compared to electrodeposition and brush coating methods as shown by Fig. 1. Improved sensing characteristics of H_2 sensors and current efficiency of fuel cell are attained as indicated by Fig. 2 (a) and Fig. 2 (b) by the usage of pulsed electrodeposition method.

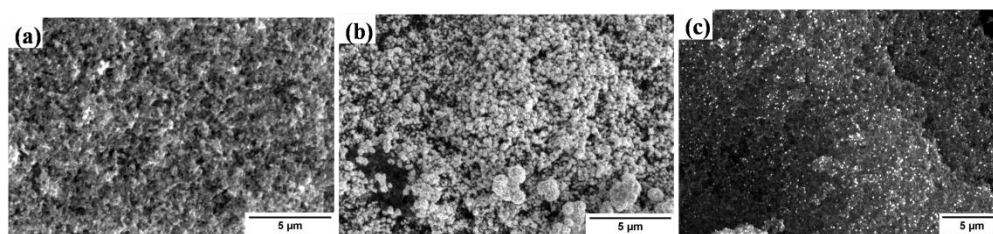


Fig. 1 FESEM images of electrocatalyst on gas diffusion layer (a) brush coated Pt/C (50 %), (b) electrodeposited Pt and (c) pulsed electrodeposited Pt

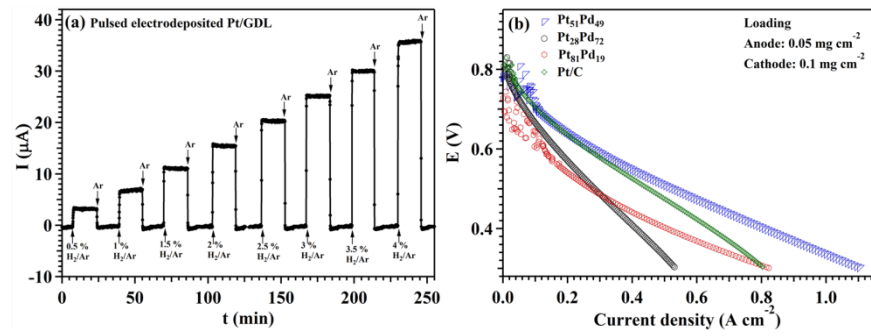


Fig. 2 Evaluation of pulsed electrodeposited electrocatalysts (a) H₂ response behavior of Pt electrocatalysts (b) PEM fuel cell performance of Pt_xPd_y alloys

Chapter 1

Introduction

1.0 Hydrogen sensors

Future of this planet largely depends on the successful utilization of molecular hydrogen (H_2) as an energy resource in the renewable energy sector. H_2 is a clean source of energy with environmentally green combustion products and has the potential to be the lead energy carrier and energy provider. In spite of all these advantages, H_2 forms an explosive mixture with air in the concentration range of 4-75% (V/V) resulting in a catastrophic damage^{1, 2}. Therefore, to prevent any unforeseen disaster, H_2 in the concentration between 0-4 % (Lower Explosion Limit of hydrogen in air) needs to be monitored using suitable sensors. Hence, H_2 sensor is high in demand to monitor its leakage wherever it is utilized or released as a by product. In sodium cooled fast reactor (SFR) technology, hydrogen sensor operable in inert ambient like argon/nitrogen in percentage range are required for processes like residual sodium removal from sodium wetted reactor components and cold trap regeneration. The components of the reactor will be removed for the purpose of service/disposal and it will have residual sodium sticking on the surface of the components. The adopted process for residual sodium removal are steam-nitrogen (SN) and water vapour CO_2 (WV- CO_2) processes depending upon the nature of the component. The reaction of sodium with steam releases H_2 as by- product. H_2 sensor is also finds application during cold trap regeneration. Cold traps are made up of stainless steel mesh (SS mesh), which are used in sodium cooled fast reactor to maintain the purity of sodium by trapping H_2 and O_2 as sodium hydrides and sodium oxides which gets collected in SS mesh. The cold trap gets saturated with hydride during the continuous operation of the reactor. Hence, once in five years cold trap needs to be regenerated and it is done by thermal decomposition of NaH, which releases a large quantity of H_2 . The released H_2 during sodium cleaning and cold trap regeneration will be sampled in inert ambient such

as argon or nitrogen. The concentration of H_2 has to be monitored to maintain the concentration within the safe level of below 4 % before being let out to the atmosphere. Therefore, both sodium cleaning and cold trap regeneration are in demand of reliable, flow rate independent and accurate H_2 sensors which can function in inert ambient. Solid electrolyte based H_2 sensors are miniaturized and is suitable to avoid leakage of electrolyte, corrosion and impurities. Operation of this sensor becomes handy compared to the liquid electrolyte based H_2 sensors. At present, several researchers are taking efforts to develop room temperature H_2 sensor operating on change in electrical resistivity ³, optical constants ⁴, potential ⁵, current ⁶, volume ⁷ and work function ⁸ to meet the ever growing demand. Mainly, five types of H_2 sensors have been discussed in this section (1) metal oxide sensors, (2) catalytic sensors, (3) thermal conductivity sensors, (4) optical sensors and (5) electrochemical sensors.

1.0.1 Metal oxide sensors

Metal oxide sensors (MOS) detect H_2 with a change in its resistance upon exposure to H_2 . This is due to the interaction of H_2 with the MO, thereby largely affecting its electronic properties. Typical metal oxide sensor is shown in Fig. 1.1. MOS with planar and tubular morphology are the various common architectures used. Among the two, the planar structure is promising with its ability to scale up in mass production. Metal oxides have been developed for sensing H_2 . SnO_2 is the most commonly used metal oxide. Recently, rare earth oxide materials are also reported for their H_2 sensing ability⁹⁻¹¹.

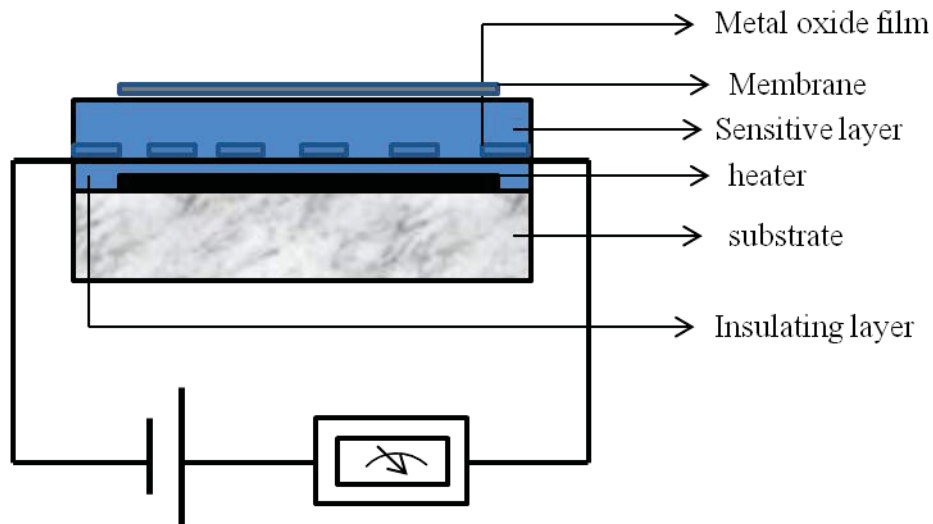


Fig. 1.1 Schematic of metal oxide sensor¹²

1.0.2 Catalytic sensors

The reaction of combustible H_2 with oxygen releases heat (exothermic) and this change is monitored and measured as a sensor signal. This type of sensor has two Pt coils where one is an active bead with the coated catalyst and the other is an inactive bead that is used as a reference which is shown in Fig. 1.2. Hydrogen gets oxidized on the catalyst surface and the heat is generated as a result of an exothermic reaction. The heat produced, changes the electrical resistance of the active bead and is measured with the help of a Wheatstone bridge. The disadvantage of using a catalytic sensor is that it requires a high temperature for its operation and also needs the presence of oxygen ^{13, 14}.

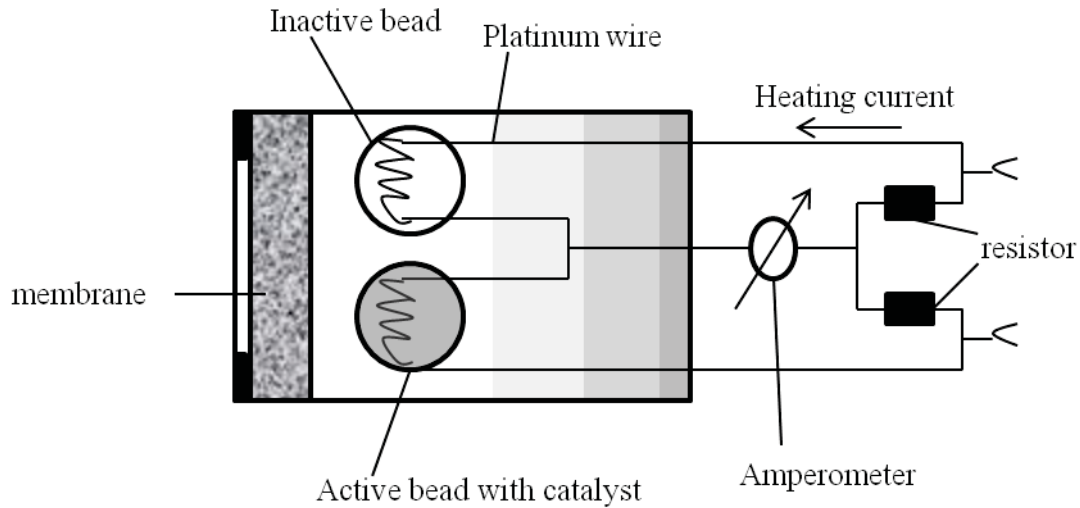


Fig. 1.2 Structure of catalytic sensor¹²

1.0.3 Thermal conductivity sensors

Thermal conductivity sensor has two identical working and reference cells as shown by Fig. 1.3. These two independent cells have heated metallic elements and over them, H_2 and reference gases are streamed. Variation in H_2 content in the “analyte gas” will modulate the temperature of the sensor. This dissimilarity is felt as a change in the resistance of the material creating a measurable imbalance in the Wheatstone bridge. At present, the thermal conductivity sensors have simpler design where no reference cell is used. The surrounding ambience temperature is taken as reference and the change in temperature as a function of H_2 concentration is measured. Thermal conductivity of H_2 sensors can be used to detect wide range of concentration but, they are less sensitive¹⁵⁻¹⁸.

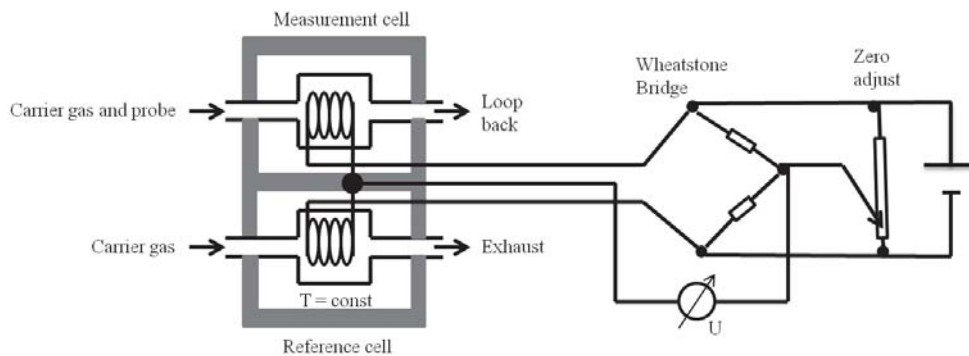


Fig. 1.3 Thermal conductivity sensor configuration¹²

1.0.4 Optical sensors

The optical property of some material changes upon exposure to the H_2 gas and this phenomenon could be utilized for the detection of H_2 . Butler et al.⁴ reported the use of palladium coated optical fibre as sensor. Schematic of optical sensor with Pd thin layer is shown in Fig. 1.4. Pd reacts with H_2 and forms palladium hydride. The optical property of palladium hydride is different from that of Pd. As a result, the effective path length of the light in the optical fibre varies and an interferometer is used to detect the variation¹⁹.

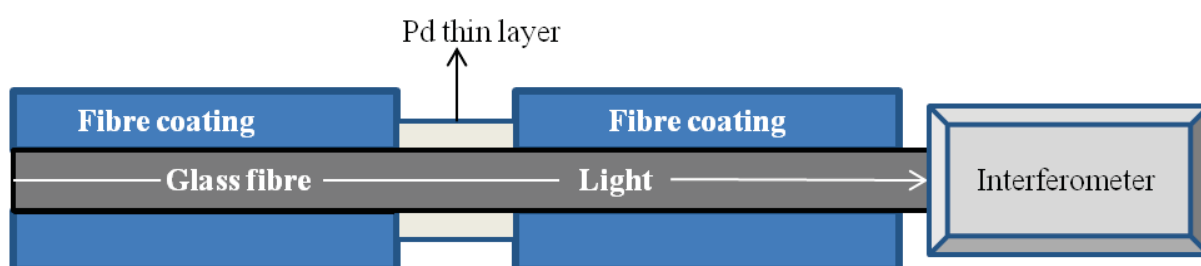


Fig. 1.4 Schematic of optical sensor¹²

1.0.5 Electrochemical H_2 sensors

Electrochemical sensors convert the chemical energy into electrical energy or vice versa. Sensor schematic is shown in Fig. 1.5. In this sensor, H_2 gets oxidized at the sensing electrode that is coated with Pt or Pd catalyst. On the other hand, O_2 is reduced at the counter electrode. Electrochemical sensors can be used in harsh environment and also provide easy way to interpret the sensor signals. Compared to all the types of sensors discussed in Table 1.1, electrochemical sensor offers fast response, simplicity, precision, and allows to be operated with minimal power consumption. Several electrochemical sensors have been developed to detect glucose, CO, H_2O_2 , yet are commonly employed for H_2 leak monitoring^{20,21}.

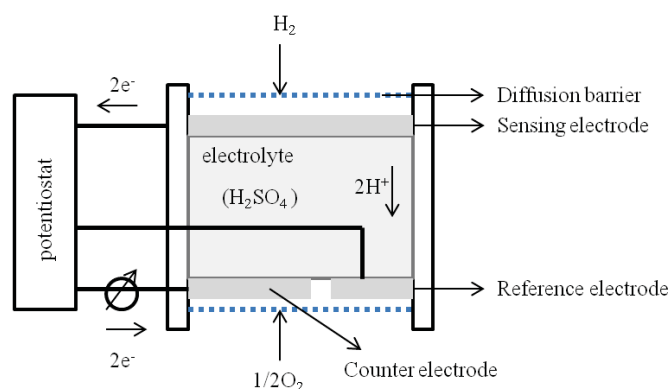


Fig. 1.5 Structure of an amperometric sensor¹²

The above classifications of sensors are based purely on the principle of operation and their characteristics are listed in Table 1.1.

Table 1.1 Characteristics of different types of sensors

Sensor	Advantages	Disadvantages	Accuracy of detection (%)	Response time (s)
Metal oxide	High sensitivity and fast response	High operation temperature and requires the presence of O ₂	±10-30	<20
Catalytic	Wide operating temperature range	High operation temperature and also needs presence of O ₂	<±5	<30
Thermal conductivity	Resistant to poisoning	Highly sensitive to the flow rate change of the gas. Poor selectivity for hydrogen in presence of moisture and CO ₂	±0.2	<10
Optical	Can operate in the absence of O ₂	Interference from ambient light	<0.1	<60
Electrochemical	Room temperature operation	Sensitive from percentage to ppm in argon.	≤± 4	<90

Table 1.1 indicates the advantages and disadvantages of different types of H₂ sensors. Electrochemical sensors are more suitable for monitoring H₂ in argon atmosphere since metal oxide and catalytic sensors need the presence of O₂ in H₂ gas stream for detection. Thermal conductivity sensors are highly sensitive to the flow rate change. Interference from ambient light is the issue with optical sensors.

1.0.5.1 Amperometric and potentiometric hydrogen sensors

Electrochemical sensors comprise both potentiometric and amperometric devices^{20, 22, 23}. Unlike potentiometric sensors, signal in amperometric sensors varies linearly with respect to H₂ concentration, works at room temperature and can operate in wide range of concentration (Table 1.1) consuming very low power with superior sensitivity, selectivity and stability^{24, 25}.

1.0.5.2 Proton exchange membrane based amperometric H₂ sensor

Proton exchange membrane based H₂ sensor (PEMHS) operates on fuel cell principle with following configuration: H₂/Pt//Nafion//Pt/O₂²⁶. PEMHS consists of sensing electrode, counter electrode and Nafion as electrolyte. Nafion, a commercial proton exchange membrane which is made up of sulfonated tetrafluoroethylene based fluoropolymer-copolymer, whose structure is shown in Fig. 1.6. Nafion is a hydrophilic membrane and forms internal pores which are associated with the clustering of sulphonic acid group. These pores facilitate the transport of proton as hydronium ion. Nafion requires substantial hydration to function as a proton exchange membrane. The sulphonic acid group of Nafion facilitates efficient transfer of proton since it has high dissociation constant ($P^{ka} \sim 6$) and has high conductivity of 0.1-0.01 S.cm⁻¹ at 373 K–383 K²⁷.

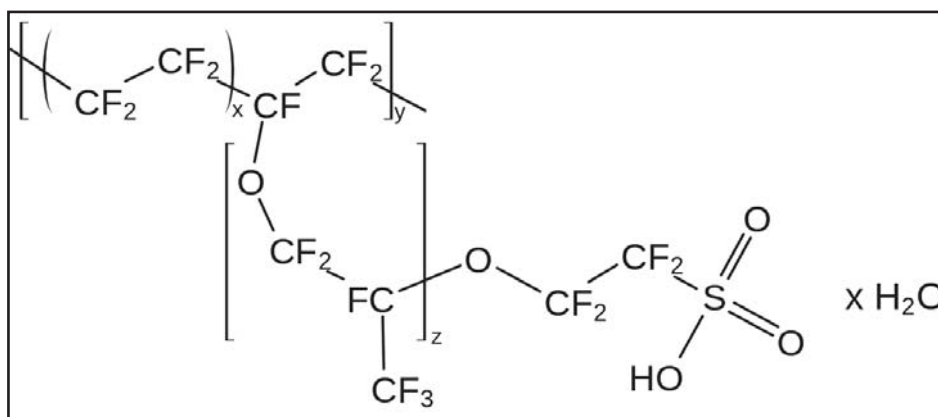
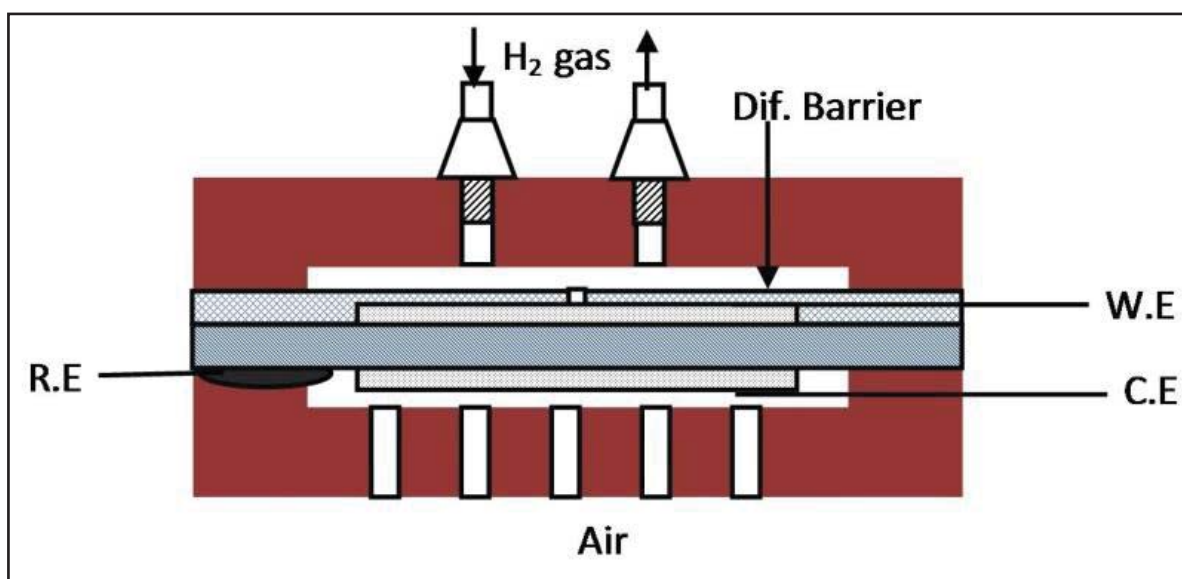


Fig. 1.6 Structure of Nafion proton exchange membrane

H₂ oxidizes at the catalyst surface of the sensing electrode and proton is transported through the Nafion to the counter electrode. Electron flows through the external circuit to the counter electrode where O₂ gets reduced at the catalyst surface by the reaction of proton, electron and oxygen. Water is the final product of the above reaction and the reaction steps are shown in eq. 1.1 and eq. 1.2. A diffusion barrier is placed at the sensing side in order to limit the flow of H₂ to the sensing electrode, so that whatever the amount of H₂ comes to the sensing electrode, it will get oxidized fully, since the flow of H₂ is a diffusion limited process. A typical assembly of sensor is shown in Fig. 1.7. Finally, the current generated during the process is monitored as a function of time and interpreted to the amount of concentration of hydrogen.





**Fig. 1.7 Schematics of the proton exchange membrane based
hydrogen sensor assembly²⁸**

1.1 Proton exchange membrane fuel cell (PEMFC)

Fuel cell is a galvanic device which consists of an anode, a cathode and an electrolyte. The principle of fuel cell operation is as follows: (1) fuel at the anode gets oxidized and transported to cathode through the ion conducting Nafion membrane and (2) electrons generated during oxidation flow towards the external circuit and reach the cathode. Fuel at the cathode is reduced by the reaction with the oxidised ion and electron. Water is generated as one of the products during the reaction. The reaction is continued as long as the fuel is supplied at their respective electrodes. Various types of fuel cells exist and all operate on the same principle. In general, fuel cells are classified based on the electrolyte used and are shown in Table 1.2.

Table 1.2 Various types of fuel cells with their electrochemical reactions

Fuel cell	Anodic reaction	Cathodic reaction	Overall cell reaction
Polymer electrolyte membrane ²⁷	$\text{H}_2 \rightarrow 2\text{H}^+ + 2\text{e}^-$	$\frac{1}{2}\text{O}_2 + 2\text{H}^+ + 2\text{e}^- \rightarrow \text{H}_2\text{O}$	$\text{H}_2 + \frac{1}{2}\text{O}_2 \rightarrow \text{H}_2\text{O}$
Alkaline ²⁹	$\text{H}_2 + 2\text{OH}^- \rightarrow 2\text{H}_2\text{O} + 2\text{e}^-$	$\frac{1}{2}\text{O}_2 + \text{H}_2\text{O} + 2\text{e}^- \rightarrow 2\text{OH}^-$	$\text{H}_2 + \frac{1}{2}\text{O}_2 \rightarrow \text{H}_2\text{O}$
Phosphoric acid ²⁹	$\text{H}_2 \rightarrow 2\text{H}^+ + 2\text{e}^-$	$\frac{1}{2}\text{O}_2 + 2\text{H}^+ + 2\text{e}^- \rightarrow \text{H}_2\text{O}$	$\text{H}_2 + \frac{1}{2}\text{O}_2 \rightarrow \text{H}_2\text{O}$
Molten carbonate ²⁹	$\text{H}_2 + \text{CO}_3^{2-} \rightarrow \text{H}_2\text{O} + \text{CO}_2 + 2\text{e}^-$	$\frac{1}{2}\text{O}_2 + \text{CO}_2 + 2\text{e}^- \rightarrow \text{CO}_3^{2-}$	$\text{H}_2 + \frac{1}{2}\text{O}_2 \rightarrow \text{H}_2\text{O}$
Solid oxide ²⁷	$\text{H}_2 + \text{O}^{2-} \rightarrow \text{H}_2\text{O} + 2\text{e}^-$	$\frac{1}{2}\text{O}_2 + 2\text{e}^- \rightarrow \text{O}^{2-}$	$\text{H}_2 + \frac{1}{2}\text{O}_2 \rightarrow \text{H}_2\text{O}$
Direct methanol ²⁹	$2\text{CH}_3\text{OH} + 2\text{H}_2\text{O} \rightarrow 2\text{CO}_2 + 12\text{H}^+ + 12\text{e}^-$	$3\text{O}_2 + 12\text{H}^+ + 12\text{e}^- \rightarrow 6\text{H}_2\text{O}$	$2\text{CH}_3\text{OH} + 3\text{O}_2 \rightarrow 2\text{CO}_2 + 2\text{H}_2\text{O}$

Among the fuel cells, proton exchange membrane fuel cell is predominantly developed for portable applications because of its compact size, low temperature and fast operation. This cell uses Nafion as ion conducting membrane, hydrogen and oxygen gases are used as a fuel and oxidant at the anode and cathode respectively. In PEMFC, hydrogen is oxidised at the anode and transported to cathode. Oxygen is reduced at the cathode by reacting with proton and electron.

1.1.1 Thermodynamics of fuel cell

Fuel cell is an energy converter by definition. The maximum energy available for conversion is given by Gibbs energy change of $\text{H}_2\text{-O}_2$ reaction. Theoretical efficiency of the fuel cell is calculated by the ratio of Gibbs energy change to the enthalpy change of the reaction under standard conditions (100 kPa, 298 K). The maximum efficiency is found to be 83 % by

substituting Gibbs energy change (237.1 kJ.mol⁻¹) and enthalpy change (286 kJ.mol⁻¹) of overall H₂-O₂ reaction in eq. (1.3).

$$\text{Energy Efficiency} = \frac{\Delta G}{\Delta H} \quad (1.3)$$

Gibbs energy of a reaction influenced by temperature and reactant concentration (or partial pressure of reactants)

$$\Delta G = \Delta G^0 + RT \ln \frac{P_{H_2O}}{P_{H_2} P_{O_2}^{1/2}} \quad (1.4)$$

where, ΔG^0 - Gibbs free energy under standard conditions, T- absolute temperature, R- gas constant; P_{H_2O} , P_{H_2} , $P_{O_2}^{1/2}$ are the partial pressures of H₂O, H₂ and O₂.

Gibbs energy of a reaction is converted to electrical energy when operated reversibly in a galvanic device. Relation between Gibbs energy and potential difference is given below

$$\Delta G = -nFE_{\text{rev}} \quad (1.5)$$

where n - number of electrons and F - Faraday's constant equal to 96485 C.mol⁻¹.

Substituting eq. (1.5) in eq. (1.4) gives the potential of the cell and is known as Nernst equation (eq. 1.6).

$$E = E^0 + RT \ln \frac{P_{H_2O}}{P_{H_2} P_{O_2}^{1/2}} \quad (1.6)$$

where E^0 – potential under standard conditions and is found to be potential of H₂ – O₂ reaction is 1.23 V.

1.1.2 Polarisation curve of fuel cell

Theoretical voltage of 1.23 V for H₂ – O₂ reaction gets polarised under experimental conditions. This voltage loss occurs mainly for three reasons such as, (1) ohmic loss of cell

components, (2) inadequate supply of fuel to the electrodes and (3) slow kinetics of electrochemical reaction. A cell without these limitations would produce a constant voltage of about 1.17 V at 373 K irrespective of the current drawn. Typical voltage vs. current response curve of fuel cell is shown in Fig. 1.8.

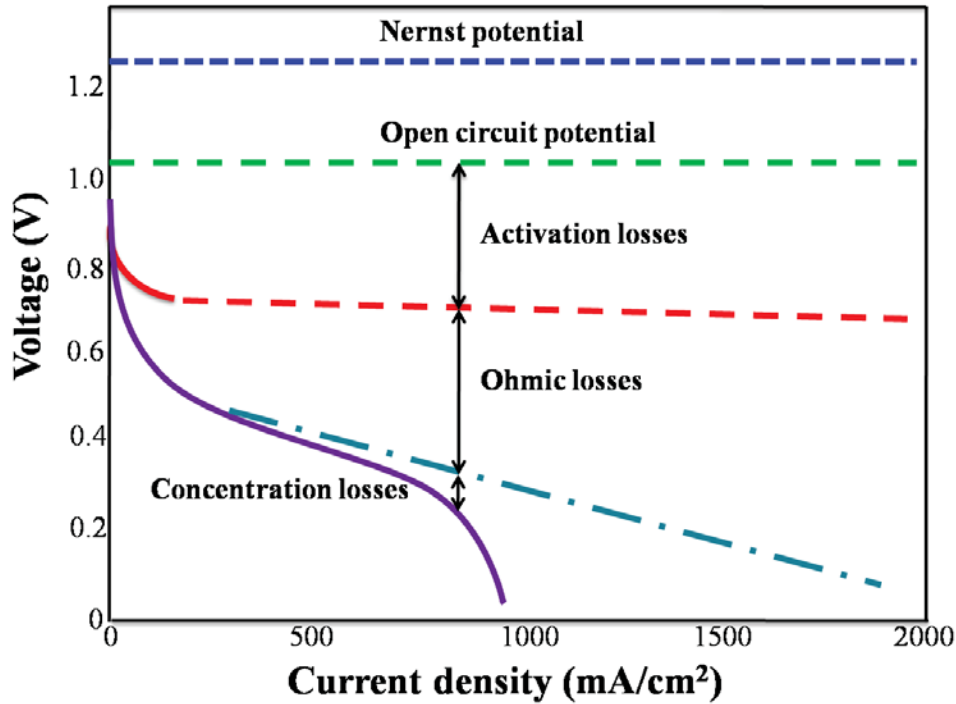


Fig. 1.8 Typical polarisation curve of a fuel cell ²⁷

1.1.2.1 Ohmic loss

Electrical resistance offered by bipolar plates, cell components and interface (between the electrolyte and electrode), ionic resistance of electrolyte and catalyst layer contributes to overall ohmic loss of fuel cell. Drop in potential follows ohm's law where it decreases linearly with increasing current (eq. 1.7).

$$-\Delta E = \Delta I R_{\Omega} \quad (1.7)$$

R_{Ω} - Internal ohmic resistance of the cell.

1.1.2.2 Mass transport loss

Fuel cannot be supplied as quickly as the kinetics of the reaction. Hence, the concentration of the fuel near the electrode surface decreases and ultimately defines the process to be diffusion limited process. This phenomenon in turn decreases the potential of the cell.

1.1.2.3 Activation loss

Activation loss occurs in the low current region of voltage-current plot. This loss is observed due to the slow kinetics of the reaction at the electrode. All electrochemical reactions involve either gain of an electron (reduction) or removal of an electron (oxidation). The rate of electrochemical reaction is purely controlled by the kinetics of the reaction when ohmic loss and mass transport losses are avoided. Hence, the kinetics determines the current flow between the electrodes and a drop in the potential is observed known as activation overpotential. Current observed due to activation overpotential is given by Butler-Volmer equation (eq. 1.8) ²⁷.

$$j = j_o (e^{-\alpha\eta F/RT} - e^{(1-\alpha)\eta F/RT}) \quad (1.8)$$

where, j_o -exchange current density, α - transfer coefficient, and η -overpotential

Exchange current density is a significant parameter in electrode reactions. Current density at thermodynamic equilibrium ($\eta = 0$) is called exchange current density. The rates of anodic and cathodic reactions are equal but, each reaction has corresponding exchange current density. Moreover the polarization from equilibrium leads to the net oxidation or reduction reaction. If the exchange current density is higher, reaction rate will be faster. Transfer coefficient determines the effect of overpotential on the rate of an electrochemical reaction and is another important parameter to ascertain the current density.

1.2 Electrocatalysis in proton exchange membrane based hydrogen sensors and fuel cells

Electrocatalysts are used to speed up the electrochemical reaction that takes place in PEMHS and PEMFC. Pt and Pd metal nanoparticles have been used extensively as electrocatalysts and are observed to be a better candidate for sensing H_2 compared to any other metals since they exhibit excellent catalytic activity, electrical conductivity, corrosion resistance and thermal stability, making them exceptional electrocatalysts³⁰. Alloying Pt with Pd decreases the use of the expensive Pt. Application of PtPd alloy electrocatalyst in amperometric H_2 sensor and fuel cell gives better performance with the reduced loading of Pt reported in literature^{31, 32}.

1.2.1 Electrocatalyst

Electrocatalyst is generally involved in electrochemical reaction which usually takes place at the electrode-electrolyte interface. It also facilitates in transportation of the electron at interface. Electrochemical reaction at the interface follows three steps: (1) transportation and adsorption of reactant at the electrode surface, (2) transfer of electrons between the reactant and the electrode and (3) desorption of the products and other intermediates from the electrode. Fig. 1.9 illustrates the mechanism of electrochemical oxidation of gas at the catalyst surface.

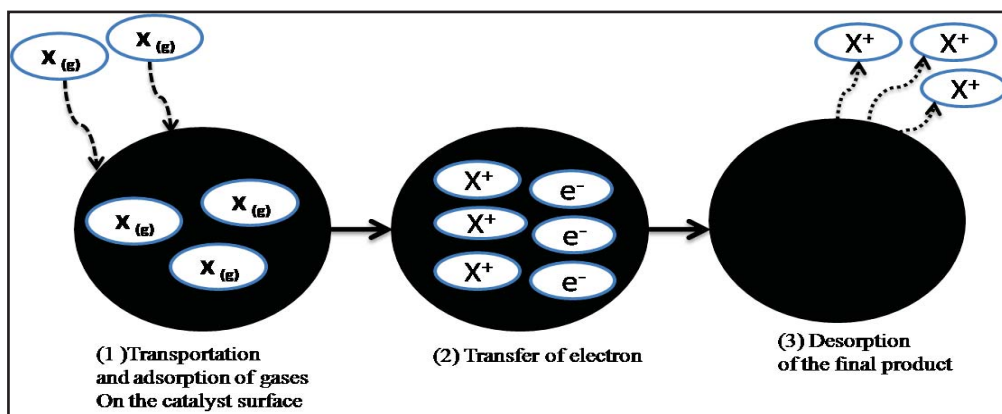


Fig. 1.9 Mechanism of electrochemical oxidation of gas at the catalyst surface

The main objective of electrocatalysis is to increase the rate of the electrochemical reaction. Electrocatalyst has a profound effect on the kinetics of the reaction. Similar to catalysis, electrocatalysis is also classified into two, as homogenous and heterogeneous electrocatalysis. In homogenous electrocatalysis, the catalyst and reactant will have the same phase; both will be dissolved in bulk. Catalyst is generally immobilised on the electrode surface or in some cases the electrode itself plays the role of a catalyst in heterogeneous catalysis.

1.2.2 Criteria for the selection of an electrocatalyst

Electrochemical reactions at the surface of electrocatalysts include oxidation at the anode and reduction at the cathode. For an effective electrocatalyst the following criteria should be met: (1) possessing high exchange current density for both cathodic and anodic reactions and (2) ability to oxidise the impurities present in reactants so that these impurities will not block the active surface area of the catalyst. Electrocatalysts should have the ability to undergo multiple adsorption-desorption cycles. Noble metals (group 8-11) are commonly used as an electrocatalyst due to their physicochemical properties and are generally used as electrocatalysts, especially Ag, Au and Pt in the periodic table. These metals are chosen owing to their high melting and boiling points and their ability to robustly resist to corrosion. Noble metal electrocatalysts are chosen based on their metal-reactant binding energy. Pt and Pd metals are found to exhibit higher activity for both oxygen reduction reaction and

hydrogen oxidation reaction in acidic electrolytes³³. There are many ways to reduce the cost of fuel cells without sacrificing performance and are³⁴⁻³⁹ listed below: Reduction of precious metal loading, Nanostructured thin-film (NSTF) development for catalyst layer, Particle size reduction for electrocatalyst, Developing non-precious metal/alloy and Developing novel catalyst preparation methods. Among the above methods we have adopted novel catalyst preparation method for the application in H₂ sensor and fuel cell in order to reduce the loading of expensive Pt, Pd and Pt_xPd_y alloy electrocatalysts.

1.2.3 Applications of electrocatalysts

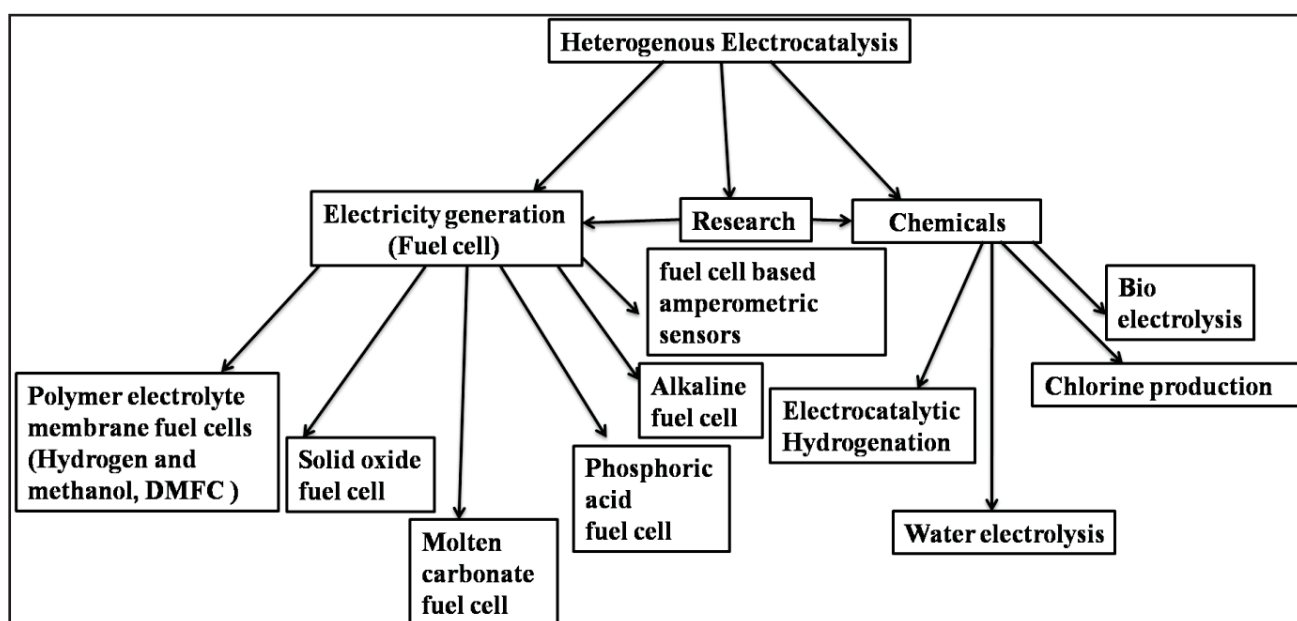


Fig. 1.10 Applications of electrocatalyst in various fields⁴⁰

Electrocatalyst finds applications in many fields such as fuel cells, electrocatalytic hydrogenation, sensors, and water electrolysis (Fig.1.10). *The current study focuses on application of electrocatalyst in fuel cell based amperometric H₂ sensors and proton exchange membrane fuel cell.*

1.2.4 Methods of preparation of electrocatalyst

Various methods have been reported for the deposition of electro-catalysts. Methods adopted so far include physical vapour depositions⁴¹, hot pressing⁴², screen printing⁴³, chemical

reduction^{44, 45}, electrophoretic painting⁴⁶ and electrodeposition⁴⁷⁻⁴⁹. Vapour deposition requires an expensive metal target, high vacuum experimental facility and catalyst wastage could not be avoided. In hot pressed method, the catalyst powders are mixed with solvents and then the catalyst slurry is coated onto the sintered glass. This sintered glass is further heated to 623 K in a hot press. The film is then transferred onto a Nafion membrane and heated to 368 K. Screen printing method involves the printing of catalyst slurry onto a Nafion membrane. In chemical reduction process, the film is coated over a Nafion membrane by chemically reducing the catalyst precursors using sodium borohydride. Commercially adopted methods for Pt/C catalyst deposition are electrophoretic, brush coating, spray coating and electrodeposition methods. There are advantages and disadvantages with respect to each methods and are listed in Table 1.3. In the case of spray coating/brush coating methods, the active sites are being covered by Nafion which eventually reduce the three phase boundary of the catalytic sites. In chemical reduction method cannot have a control over the particle growth.

Table 1.3 Comparison of different methods used for deposition of electrocatalysts

Method of deposition	Catalyst	Potential used for deposition	Particle size	Advantages	Disadvantages
Electro-phoretic	⁵⁰ Pt/C nano-powder	30–50 V	150 nm	The amount of metal deposited is linearly dependent on the current	High voltage is required to deposit Need of conducting colloidal suspensions which determines the efficiency of the process
	⁵¹ 40 wt% Pt -20 wt% Ru/CNT	0-5 V	3-6 nm		
	⁵² Pt/C	250 V/cm	-		
	⁴⁶ Pt-Ru bimetallic nanocatalysts	200 V/cm	-		
	⁵³ Pt/C	100 V/cm	245-263 nm		
	⁵⁴ Pt/C	1000 V	-		
	⁵⁵ Pt/C	33 V	-		
Chemical reduction	⁵⁶ Nafion [®] /Pt/nano-structured	-	15–40 and 5–30 nm	Ease of preparation	Cannot have control over the particle size

	polyaniline/Au/Al ₂ O ₃				
	⁵⁷ Pt-Rh/C	-	-		
	⁵⁸ TiO ₂ -CNTs/Pt	-	25 nm		
	⁵⁹ Pt nanoparticles	-	50 nm		
Spray coating/screen printing	^{47, 60, 61} Pt/C	-	-	Ease of preparation for larger area of the electrodes	most of the platinum atoms are not having three phase boundary where ionic, electronic, catalytic and <u>gas</u> are in contact with each other
Electro-deposition	⁶² Pt	-0.1 V vs Ag/AgCl	30-40 nm	Economical, preparation becomes handy	Faradic efficiency is less
	⁶³ Pt	-0.25 V vs SCE	60-80 nm		
	⁶⁴ Pd cluster	0.3 V vs. Ag/AgCl	150 nm		
	⁶⁵ PtPd alloy foams	-0.2 V vs. SMSE	-		

Electrophoretic and electrodeposition methods are found to be efficient for deposition of catalyst due to the control of particle size or thickness of the film by potential or time but an average electrophoretic method requires high voltage and also their efficiency of deposition depends on the nature of colloidal suspensions. Though electrodeposition method is less efficient compared to electrophoretic, it is economical as well as preparation handy.

1.2.5 Electrodeposition

Electrodeposition is a simple and cost-effective technique compared to several other highly sophisticated methods such as chemical or physical vapour depositions. Electrodeposition

facilitates better control over the thickness and size of nanoparticle deposits by fine tuning the reduction potential ⁶⁶. In doing so, the electrodeposition prevents the agglomeration of an electrocatalyst and therefore, this method has been found suitable and largely favourable for the preparation of electrocatalysts.

Electrodeposition is also called as “electrocrystallization”. In this process, overpotential results in the faster reduction of metal ion. A typical process of electrocrystallization is to attain supersaturation state by the electrolyte solution during this phase transition. Normally, electrodeposition of adatoms occurs on the surface of the electrode. These deposited atoms eventually dissolve if the interaction of adatom on the electrode surface is weak. However, defects or dislocations on the substrate strengthen the interaction of adatoms and stabilizes them. The defect sites are denoted as the “kink sites” which is the active site for nucleation, followed by the growth of a metal crystal.

1.2.5.1 Nucleation and growth

Thin film formation during electrodeposition is controlled by two distinct steps such as nucleation and growth. Initially, ions will be in the form of hydrated complex in the electrolyte. When the potential is applied at the electrode, hydrated complex start migrating towards the cathode owing to the potential gradient. The hydrated complex passes through a diffusion layer and an electrical double layer before reaching the electrode. This hydrated complex at the interface loses water molecules and turns out to be bare metal ions. Further, these metal ions get reduced as neutral metal atoms by obtaining an electron from the electrode. These reduced metal atoms migrate over the electrode surface and gets adsorbed onto the kink sites. The process persists until the formation of a monolayer over the entire electrode surface. Thereafter, the atoms will interact with incoming neighbouring atoms, leading to the formation of clusters. These clusters at a larger size will get desorbed with time

since they are thermodynamically unstable. Therefore, clusters grow until reaching a critical size up to which the cluster is in a thermodynamically stable state.

Nucleation is a phenomenon of generating a new phase over the existing old phase of atoms on the substrate. This process occurs when energy at the surface of the old phase is higher than that of the newly forming phase. Surface nuclei contributes to the growth, possessing a larger energy than that are at the bulk, since the nuclei at the surface are less bound to the neighboring atoms. The growth of the nuclei is decided by the increase in the size of the particle more than its critical size and the rate of nucleation. Various types of growth modes are observed during electrodeposition.

1.2.5.2 Growth modes of electrodeposition

Electrodeposition of metal on a substrate occurs in several successive steps. First step is the electroreduction of an adatom on the electrode substrate. Second step, requires a large overpotential to facilitate the formation and growth of the deposited metal. These steps are explained substantially using the following modes and are shown in Fig.1.11.

a) Volmer-Weber mode

The weak interactions of the metal on the substrate lead to this type of growth. Here, adatom-adatom interaction is stronger than the adatom-surface interaction which results in the 3D growth of the deposit.

b) Frank-van der Merwe mode

The strong interaction between the metal and a substrate leads to the epitaxial growth of the deposited metal. This kind of growth follows a layer by layer deposition of the metal along with the orientation of the atoms on the substrate producing 2D growth.

c) Stranski-Krastanov mode

This mode initially consists of an epitaxial deposition followed by isolated islands growth of the deposited metal. After that, 3D island growth takes place over the epitaxial growth.

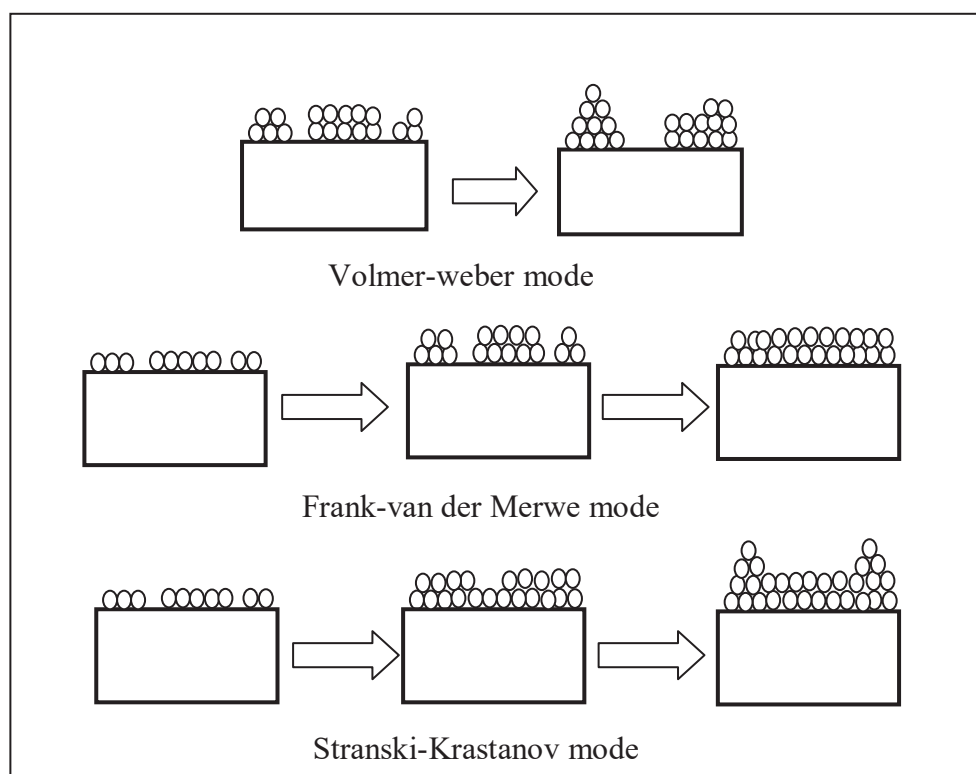


Fig. 1.11 Growth modes of electrodeposition ⁶⁷

If the nucleation rate is higher than the growth rate then it leads to the formation of a fine grained structure. Pulsed electrodeposition is a type of electrodeposition with increased nucleation rate and produces fine-grained morphology.

1.2.5.3 Pulsed electrodeposition

Potentiostatic or galvanostatic electrodeposition results in the continuous growth of the particle after the initial nucleation process. The constant growth of the diffusion layer thickness during electrodeposition decreases the current flow i.e., the passage of current decreases as the thickness of the diffusion layer increases. This reduces the deposition of catalyst at newer sites leading to non-uniformity in deposition with the formation of dendrite deposition. Among all electrodeposition techniques, pulsed electrodeposition is a well known method for obtaining a uniform and nanocrystalline deposition of electro-catalyst. In pulsed

electrodeposition, the potential is switched on (t_{on}) and off (t_{off}) between the applied reduction potential and zero potential at the electrode where electrodeposition occurs. Careful choice of these parameters allows the control of porosity, grain size and hardness of the deposit.

Pulsed electrodeposition reduces diffusion layer thickness by reorganization of the electroactive species at the interface during t_{off} . This offers deposition of metal atoms on various other sites which would bring about uniformity^{68, 69}. Further, pulsed electrodeposition provides high rate of nucleation over constant potential electrodeposition by supporting the formation of new crystals instead of growing on the existing crystals. Metals can be electrodeposited or pulsed electrodeposited by using two types of electrolytes a) aqueous electrolyte and b) non-aqueous electrolyte.

1.2.5.4 Aqueous and non-aqueous electrolytes for electrodeposition

Electrodeposition (ED) could be carried out using aqueous⁷⁰⁻⁷³ and non-aqueous electrolytes⁷⁴. ED from aqueous medium has been extensively used for the preparation of Pt and Pd electrocatalyst. Usage of aqueous electrolytes impose problems such as gas evolution, passivation of cathode or anode and has a limited potential window⁷⁵. Further, it affects the adherence of the catalyst onto the substrate as a consequence of gas evolution. These limitations of the aqueous electrolyte prevents it being used in various applications although it has an effective advantage with respect to conductivity, mass transfer and economy²⁸.

In the recent past, alternatives to aqueous electrolyte have been developed. For instance, molten salt can successfully be used as the electrolyte for depositing several metals that are not feasible to be deposited using an aqueous electrolyte. In spite of this advantage, the temperature of operation with this electrolyte is higher and the temperature is generally maintained between 300 and 1000 K. The high temperature requirement makes the use of molten salt electrolyte being limited. To overcome the limitation, molecular solvents are

suggested that have low conductivity and inhomogeneous current distribution with volatile nature. Hence, the usage of molecular solvents is limited.

Room temperature ionic liquid is made up of cation and anion which provides good conductivity for ED. In this scenario, room temperature ionic liquids (RTIL) are expected to replace water as suitable electrolytes for electrodeposition. The use of RTILs in electrodeposition is noteworthy as they are a unique class of electrolytes comprising only of ions and are devoid of any other molecular species ⁷⁶. These RTILs are eco-friendly and can be used to replace hazardous volatile organic solvents ⁷⁷. The size difference of the cations and anions in the RTILs is large and it keeps them entirely disorganized. The size factor hinders RTILs to form a stable crystal lattice as in the case of inorganic crystals. Thereby, the liquid state is maintained over a broad range of temperature, and fascinatingly RTILs almost do not have any vapor pressure ⁷⁸. Direct electrodeposition of a metal in an ionic liquid electrolyte is possible without subsequent heating due to higher thermal stability of RTILs. Further, these characteristics of RTILs reported in literature are listed in Table 1.4 and its properties can be modified and engineered by varying the combination of anions and cations according to the reaction's requirement.

Table 1.4 Viscosity, conductivity, melting point and electrochemical window of ionic liquid electrolytes

Ionic liquids	Viscosity (mPa s)	Conductivity (mS/cm)	Melting point (K)	Electrochemical window (V)
[C4mim][BF ₄]	43	1.98	284	4.9
[C4mim][PF ₆]	275	1.59	335	>4
[DEME][BF ₄]	1200	4.80	282	6
[C4mim][Cl]	64	4.6	338	2.5
[C4mim][Br]	1486	1.7	354	2.7

In general, RTILs have large, stable and tunable electrochemical window, whereas their aqueous counterpart has a narrower electrochemical window⁷⁹. These distinguished qualities of RTILs qualify them as better candidates with effective capacity to be employed in various electrochemical devices such as batteries, capacitors, fuel cells, photovoltaics, sensors and actuators⁷⁸. Moreover, RTILs are in the limelight in the areas such as electrochemistry, organic synthesis and separations. Also RTILs have the capacity to act as a template for preparing metal nanoparticles^{80, 81}. At present, RTILs have become increasingly important electrolyte media for ED because of their high electrochemical window, low vapour pressure and high ionic conductivity. RTILs can adapt to several types of precursors since they provide both hydrophobic and hydrophilic environment and also has high directional polarizability. Among RTILs, imidazolium based ionic liquids have exceptional structural organization by having a rigid planar structure with acidic hydrogen. The high degree of structural organization of imidazolium ionic liquids is responsible for the synthesis of nanostructures during ED^{82, 83}. With these inherent qualities, RTILs play a constructive role in defining the morphology and crystallite size of the deposits. These special qualities of imidazolium based RTILs qualify them to be desirable candidates for ED.

1.3 Literature survey on methods of preparation of electrocatalysts for proton exchange membrane based H₂ sensor

Vapour depositions of Pt, Pd and Pt_xPd_y alloy electrocatalysts requires high vacuum and are also capital intensive. Catalyst wastage cannot be avoided by vapour deposition methods. Hot press, screen printing or spray-coating or brush coating (BC) methods involve the preparation of a paste of Pt/C with solubilised Nafion polymer. This method has limitation due to the possibility of non-utilization of 90 % of active sites of platinum by Nafion⁴⁷. Active sites need to have three-phase contact involving gaseous reactant (H₂/O₂), electrocatalyst, and electrolyte. Excessive coverage of Pt sites by Nafion during spray coating / BC limits the Pt

particles from attaining a better contact with both the reactant gas and Nafion simultaneously. Significant agglomeration of catalyst occurs when above methods are adopted by leading to the decrease in the effective catalytic surface area. Chemical reduction method for electrocatalyst deposition includes impregnation-reduction ⁴⁴ and Takenaka-Torikai method ⁴⁵. These methods involve deposition of metal catalyst on Nafion membrane using appropriate reducing agent. However, the size and morphology of a particle cannot be controlled by these methods.

Electrodeposition of electrocatalyst from aqueous electrolytes ⁸⁴⁻⁸⁷ has been reported for PEM fuel cell application ^{34, 45-47}. Particle agglomeration is expected to be significantly reduced in the case of RTIL electrolytes compared to aqueous electrolytes, since it also acts as a surfactant during deposition. Electrodeposition of electrocatalyst from aqueous medium has a disadvantage of poor adherence of the deposit onto the substrate due to excessive H₂ evolution. However, effective adherence of electrocatalyst is expected, while using RTIL as the electrolyte medium for deposition. Since, in this method H₂ evolution does not occur. Many methods have been used for preparing the electrocatalyst such as vapour depositions, chemical reduction and hot-pressed methods for PEMHS and are shown in Table 1.3 and were discussed in sub-section 1.2.4. Table 1.5 compares the amperometric H₂ sensor characteristics of Pt and Pt_xPd_y alloy electrocatalysts prepared by different methods. Loading of electrocatalyst is found to be higher and response time of H₂ sensors was found to be larger. Both loading and response time of the sensor depends on the active area of the catalyst. Hence in order to reduce the consumption of expensive electrocatalyst and to enhance the response, ED method has been chosen for the preparation. Lu et al. ⁴⁴ and Sakthivel et.al ⁸⁸ observed non-linearity in sensor response with increasing concentration of H₂/Ar. Lu et al. ⁴⁴ reported that the sensor lost linearity above 1.15 % due to excess water and heat generated by the reaction with increasing concentration of H₂. The use of GDL facilitates

removal of H₂O molecule owing to the hydrophobicity provided by Teflonised microporous layer of gas diffusion layer (GDL) and also establishes better dispersion of electrocatalyst compared to conventional methods of coating ^{44, 88}. Therefore, electrocatalysts are electrodeposited on gas diffusion layer (GDL) to get good sensor response in the LEL range (0-4 %). To improve the availability of the active sites of catalyst, ED has been attempted on Nafion impregnated GDL. The only variable in ED is potential that is applied with respect to time. Current efficiency of ED decreases as soon as it reaches the limiting current density resulting in the denser deposits. Pulsed electrodeposition has been used to prepare size controlled electrocatalyst particles. Pulsed electrodeposition (PED) has two pulses with on and off time pulses. The ratio of current density in ED and PED have been described by Chen et al. ⁸⁹. They have found that the limiting potential of PED is always higher than the constant potential deposition. Larger the overpotential, greater will be the current density and this effect subsequently increases the nucleation rate resulting in finer grain particles in short pulse width. PED has several advantages such as uniform deposition, finer deposits, stronger adhesion, and selectivity. Electrocatalysts are prepared by both ED and PED for its application in PEMHS.

Table 1.5 Comparison of electrocatalyst/Nafion based hydrogen sensor by various methods

Electrocatalyst (sensing electrode)	Catalyst loading (mg/cm ²)	Preparation method	Concentration range (ppm)	Response time (s)	Sensitivity (μA/ppm)	Ref.
Pt/Nafion	4.99	IR method by NaBH ₄	0-4508	120-180	0.0744	⁹⁰
Pt/C/Nafion	3	HP-Method	1260-5250	100-500	0.716	⁴²
Pt/Nafion	3	IR method by HCOOH	560-11,500	20-50	0.017	⁴⁴

Pt/Nafion	3.05	IR method by NaBH ₄	1-100000	10–50	0.01	⁸⁸
Pt/Nafion	N.A.	Screen printing	50-20000	35-60	0.0022	⁴³
Pt _x Pd _y /Nafion	N.A.	TT-method	100-1000	24 to 37	1.62	⁴⁵
PtRu/Nafion	N.A.	TT-method	100-1000	40 s	0.83- 9.42	⁹¹
Pt-MWNT/Nafion	1	Decal Transfer	100-1000	33	3.60	⁹²
Ag/Pt-MWNT	1.1	CR by NaBH ₄	5–1000	180	1.1	⁹³

Note: IR- Impregnation-Reduction, TT- Takenata–Torikai, CR- Chemical reduction, HP- Hot pressed

1.4 Literature survey of electrocatalysts in proton exchange membrane fuel cell

Pt is the commonly used electrocatalyst for PEMFC. The cost of PEMFC becomes a challenge due to the rare availability of the Pt catalyst which hinders the commercialization of fuel cell. From Table 1.6, it is clear that Pt electrocatalyst is found to give high current with low loading of the catalyst. Currently, lot of efforts have been put to develop a non-Pt catalyst or to reduce the amount of Pt used in PEMFC by alloying it with other metals. Pd is found to have similar electroactivity as that of Pt be the next highest electroactive metals and also the price is one half of Pt ⁹⁴. Like Pt, Pd is currently being used in automotive industries as catalytic converters. However, catalytic activity of pure Pd for hydrogen oxidation and oxygen reduction reaction is at least five times lesser than that of Pt. Hence alloying of Pd with Pt reduces the amount of expensive Pt yet, simultaneously increases the catalytic activity compared to pure Pd or Pt. Pt_xPd_y alloy has advantages of reducing the quantity of expensive Pt metal.

Various methods have been developed so far for preparing Pt_xPd_y alloy electrocatalyst for fuel cell such as brush coating, formic acid reduction, ethylene glycol reduction, wet-impregnation method, electrodeposition and pulsed electrodeposition are shown in Table 1.6. Among these methods, pulsed electrodeposition has better control over the particle size of Pt_xPd_y alloy and the advantageous of pulsed electrodeposition is discussed in the previous section 1.2.5.3. Here also PED of Pt_xPd_y is adopted for the application in PEMFC. Table 1.6 compares PEMFC characteristics of electrocatalyst reported in literature. Pt_xPd_y catalyst is found to give similar performances as Pt/C commercial catalyst. The use of Pd greatly reduces the Pt quantity and also increases the electrocatalytic activity. From Table 1.6, it is clear that very few studies have been conducted for pulsed electrodeposition of Pt_xPd_y alloy electrocatalyst.

Table 1.6 Comparison of proton exchange membrane fuel cell performance of different electrocatalysts reported in literature

Catalyst	Method adopted for preparation	Loading of catalyst (mg/cm ²)	Current Density (mA/cm ²)	Application
Pd ₉₅ Pt ₅ /C - Anode Pt/C-cathode	Formic acid reduction	0.4	1000	PEMFC ⁹⁵
RGO/PtPd	Pulsed electrodeposition	0.3	7.6	Alkaline fuel cell ⁹⁶
Pt on Pd/C	NaBH ₄ -reduction	0.3	424	PEMFC ⁹⁷
PdPt ₃ /C	NaBH ₄ -reduction	-	22.7	Methanol oxidation ⁹⁸
Pt/C	Pulsed electrodeposition	0.68	380	PEMFC ⁹⁹
Pt/C	Pulsed potential deposition	0.219	324	PEMFC ¹⁰⁰
TiO ₂ /Pt ₇₀ Pd ₃₀	Chemical reduction	0.4	3.0	PEMFC ¹⁰¹
PtPd/C-Anode Pt/C- cathode	Brush coating	0.3	1000	PEMFC ¹⁰²
PtPd	Hydrazine hydrate reduction	0.17	3	PEMFC ¹⁰³

1.5 Objective of the thesis

Present thesis investigates electrodeposition methods to prepare the electrocatalysts with high electrochemical active area for its application in PEMHS and PEMFC.

The H₂ sensor made, will find application in monitoring H₂ released during sodium cleaning of stainless steel components and regeneration of cold trap of fast breeder reactor. In both cases, H₂/Ar or H₂/N₂ will be sampled online from the cleaning chamber/regeneration chamber in real time and measured before being let out into the atmosphere. The sampled gas of H₂/Ar will not mix with ambient air prior to the sensing by the sensor. H₂/Ar mixture from the cleaning chamber will be released out at high altitude and will get diluted in ambient air.

The low density of H_2 further facilitates upward mobility of hydrogen and hydrogen will not be present in the air near the sensor. Hence, the counter electrode side will be exposed only to air. Thus, the present sensor with air-exposed counter electrode can be used to monitor H_2 /Ar or H_2 / N_2 in real time sampling mode. In the present investigations, high electrochemical active area catalyst has been prepared to improve the sensitivity and to lessen the response time of the amperometric H_2 sensor. Further, electrodeposition and pulsed electrodeposition of Pt, Pd and Pt_xPd_y alloy electrocatalysts on GDL were carried out for the application in PEMHS. Pt and Pd electrocatalysts were electrodeposited and pulsed electrodeposited on GDL using ionic liquid electrolytes for the application in PEMHS. The H_2 sensing behaviour of sensors with electrodeposited and pulsed electrodeposited Pt, Pd and Pt_xPd_y alloys based diffusion electrodes were compared. The H_2 sensor with Pt and Pd diffusion electrodes using ionic liquid electrolyte were studied. For comparison purposes, Pt/C commercial electrocatalysts were brush coated on GDL.

The major difficulties in PEMFC lie in the usage of expensive electrocatalysts due to which commercialisation of fuel cells becomes a challenge. Pt electrocatalysts based PEMFC is found to give maximum power density. In order to reduce the Pt electrocatalyst loading in PEMFC, electrodeposition of Pt_xPd_y alloy electrocatalysts has been studied in the present work. Electrodeposition of Pt_xPd_y alloy has two advantages, (a) Alloying of Pt with Pd lessen the usage of Pt and (b) Electrodeposition methods are efficient in controlling the particles size hence higher electrochemical active area can be achieved with low loading of electrocatalyst. In the present study, three different ratios of Pt_xPd_y alloys were pulsed electrodeposited on GDL and studied their fuel cell performances as cathode catalysts and supporting electrochemical characterizations were carried out.

Chapter 2

Experimental Methods

This chapter provides brief details on the experimental techniques used for deposition and characterization of Pt, Pd and Pt_xPd_y alloy electrocatalysts on gas diffusion layer (GDL). Furthermore, studies related to the application of Pt, Pd and Pt_xPd_y alloy electrocatalysts on GDL in proton exchange membrane (PEM) based H_2 sensor and $H_2 - O_2$ PEM fuel cell are also discussed. Electrochemical characterizations by electrochemical impedance spectroscopy (EIS) of deposited electrocatalysts on GDL are explained. Electrodeposition of electrocatalysts on GDL was conducted in electrolytic cell by using multi-potentiostat whose details are illustrated. Working principles of cyclic voltammetry, chronoamperometry and chronopotentiometry pertaining to the deposition of electrocatalyst on gas diffusion layer (GDL) are illustrated. Following the description of electrodeposition facility, basic principles of Scanning Electron Microscopy (SEM) and Transmission Electron Microscopy (TEM) utilized for morphological studies of deposited electrocatalysts on GDL are explained. After that, principles of grazing incidence X-ray diffraction (GIXRD) used for characterizing the crystal structure of the deposit were elaborated. Thereafter, energy dispersive X-ray analysis (EDAX) and inductively coupled plasma mass spectrometry (ICP-MS) for compositional analyses are described.

2.1 Electrochemical studies

2.1.1 Potentiostat

Potentiostat consisting of three electrodes such as working, counter and reference electrodes connected to the cell (Fig. 2.1). It is used to control the potential of the working electrode at a constant level with respect to the reference electrode by allowing the current to pass through the counter electrode. Current of the working electrode is recorded by measuring between

counter and working electrode and potential is measured between working and reference electrodes.

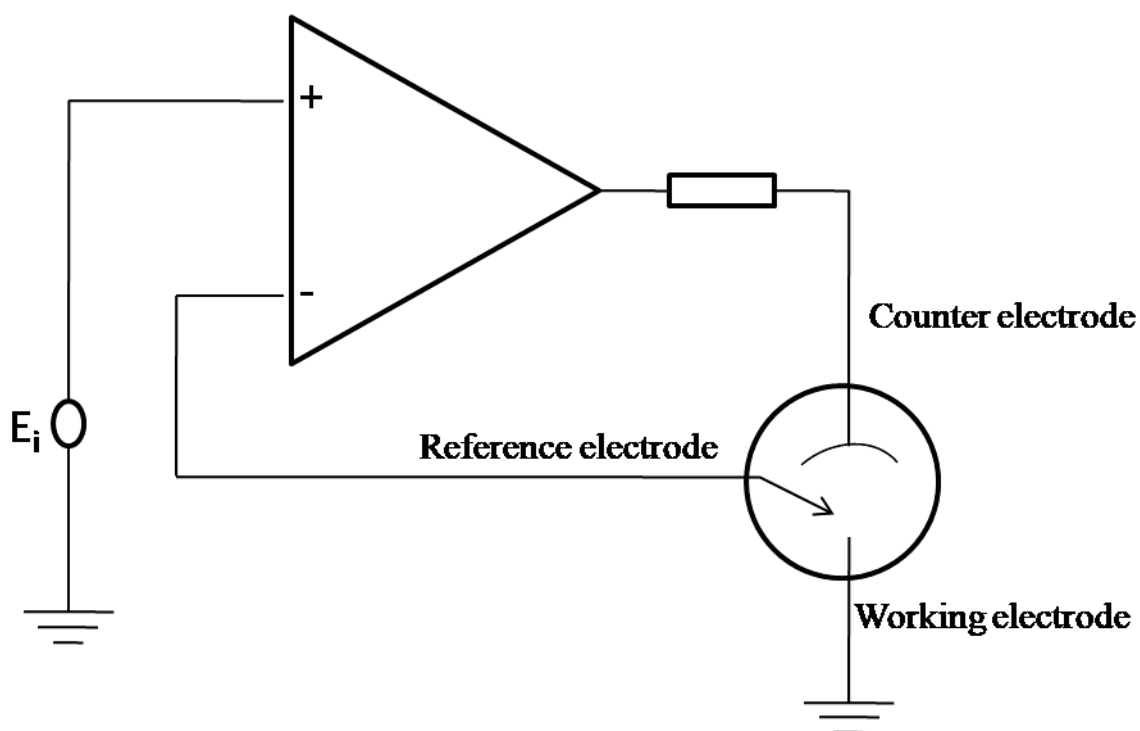


Fig. 2.1 Schematics of potentiostatic circuit

All the electrochemical studies were carried out using multi-potentiostat (VMP-300 of M/s Biologic, France) in the present work (Fig. 2.5).

2.1.2 Cyclic voltammetry

Cyclic voltammetry is an analytical technique for the determination of oxidation and reduction potentials of the electroactive species. A triangular waveform consisting of both positive and negative potential sweep applied to the working electrode with respect to time. Since potential is cycled between two potential limits back and forth, it is called cyclic voltammetry. Anodic polarisation of the electrode will result in oxidation peak and cathodic polarisation result in reduction peak. Current is generated due to the redox processes at the respective electrodes. Current is recorded with respect to the potential ramp. Plot of current vs potential is called cyclic voltammogram and the characteristics reduction and oxidation

peak of electroactive species will be obtained at negative and positive side of the voltammogram respectively. The peak at anodic side gives oxidation potential and at cathodic side gives reduction potential ^{104, 105}. A typical cyclic voltammogram is shown in Fig. 2.2.

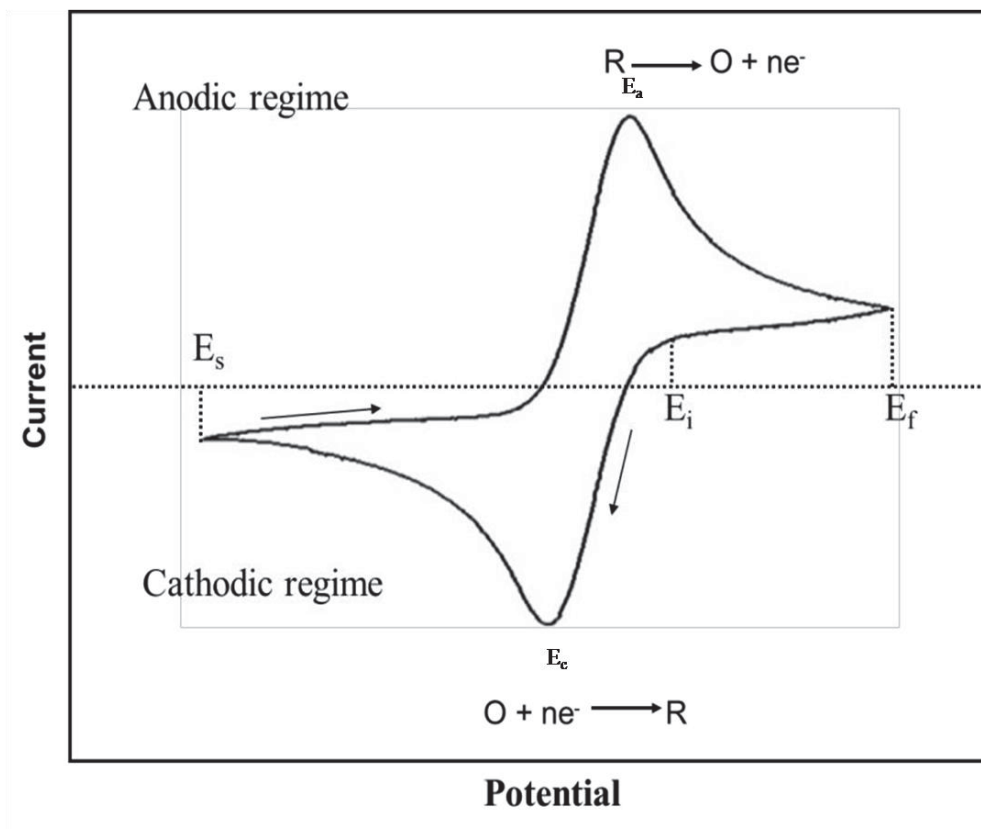


Fig. 2.2 A typical cyclic voltammogram of reversible redox reaction (E_a – anodic potential, E_c – cathodic potential, E_s – starting potential, E_i – initial potential, E_f – final potential)

In the present investigations, electrochemical window of room temperature ionic liquid electrolyte and deposition potentials of Pt and Pd were studied by cyclic voltammetry.

2.1.3 Chronoamperometry

Chronoamperometry is a potentiostatic transient technique used for the evaluation of diffusion coefficient and nucleation kinetics of an electrochemical process. To measure diffusion coefficient, potential is stepped to a value where diffusion dominates. Hence, large

overpotential is applied so that the current depends upon the diffusion of electroactive species from the bulk to the interface. The current is plotted against time and is known as chronoamperogram¹⁰⁶⁻¹⁰⁸. Cottrell equation (eq. 2.1) relating the current and diffusion coefficient is given below:

$$i = \frac{nFA \sqrt{D} C}{\sqrt{\pi t}} \quad (2.1)$$

where i -current, n - no. of electrons, F - Faraday's constant, A - area of the electrode (cm^2), C - concentration of analyte (mol.L^{-1}), D - diffusion coefficient ($\text{cm}^2.\text{s}^{-1}$) and t - time (s).

In the present studies, the nucleation kinetics of Pt was studied by chronoamperometric method.

2.1.4 Chronopotentiometry

The term chronopotentiometry says that the measurement of potential with time by keeping the current constant. The working electrode potential is measured and plotted with respect to time and is known as chronopotentiogram. When a constant current is applied between the working and counter electrode, the concentration of electroactive species decreases near the electrode-electrolyte interface. Hence, working electrode potential changes and the process persists till the concentration of electroactive species comes to zero at the interface. The time taken by the process to reach the potential change to occur is called transition time, τ ¹⁰⁹ and its relationship with current is given by Sand's equation (2.2)^{106, 107}. This equation is used for determining the diffusion coefficient of electroactive species.

$$i\tau^{1/2} = \frac{nFA \sqrt{D\pi} C}{2} \quad (2.2)$$

where i -current, τ - transition time, n - no. of electrons, F - Faraday's constant, A - area of the electrode (cm^2), C - concentration of analyte (mol.L^{-1}), D - diffusion coefficient ($\text{cm}^2.\text{s}^{-1}$) and t -time (s).

In the present work, the nucleation behaviour of Pt was studied by chronopotentiometric method.

2.1.5 Electrodeposition and pulsed electrodeposition

Electrodeposition is a simple and inexpensive technique used for the preparation of thick and thin film coatings on a substrate. The size of the particles can be easily controlled by optimizing conditions of deposition. Electrodeposition involves the reduction of metal of interest onto the base material, which acts as a working electrode with the aid of an electrolyte and a counter electrode. Electrodeposition can be carried out either by applying constant potential or (potentiostatic) or constant current (galvanostatic) modes and these can be in a constant or a pulse mode (Fig. 2.3). Electrodeposition is carried out in an electrolytic cell consisting of working, counter and reference electrodes (Fig. 2.4).

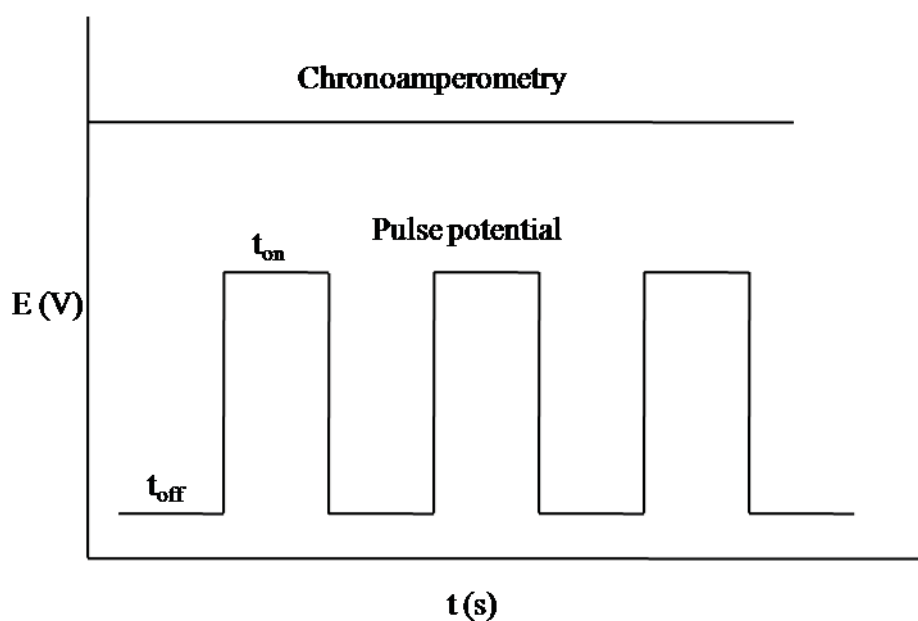


Fig. 2.3 Plot of potential vs time for electrodeposition and pulsed electrodeposition

Reduction potential is applied with respect to the reference electrode. Characteristic reduction and oxidation potential can be obtained from cyclic voltammetric studies. The metal deposited is proportional to the charge applied (Faraday's first law of electrolysis). Schematics of typical electrolytic cell are shown in Fig. 2.4. The set up for electrodeposition with potentiostat is shown Fig. 2.5. The electrodeposition facility consists of (1) electrolyte, (2) working (WE), counter (CE) and reference electrodes (RE) and (3) potentiostat.

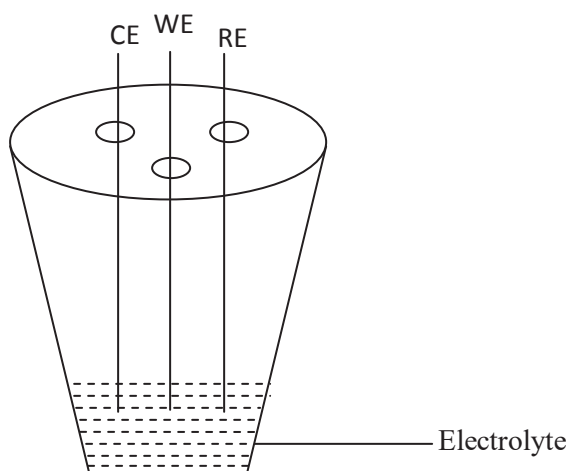


Fig. 2.4 Schematics of electrolytic cell

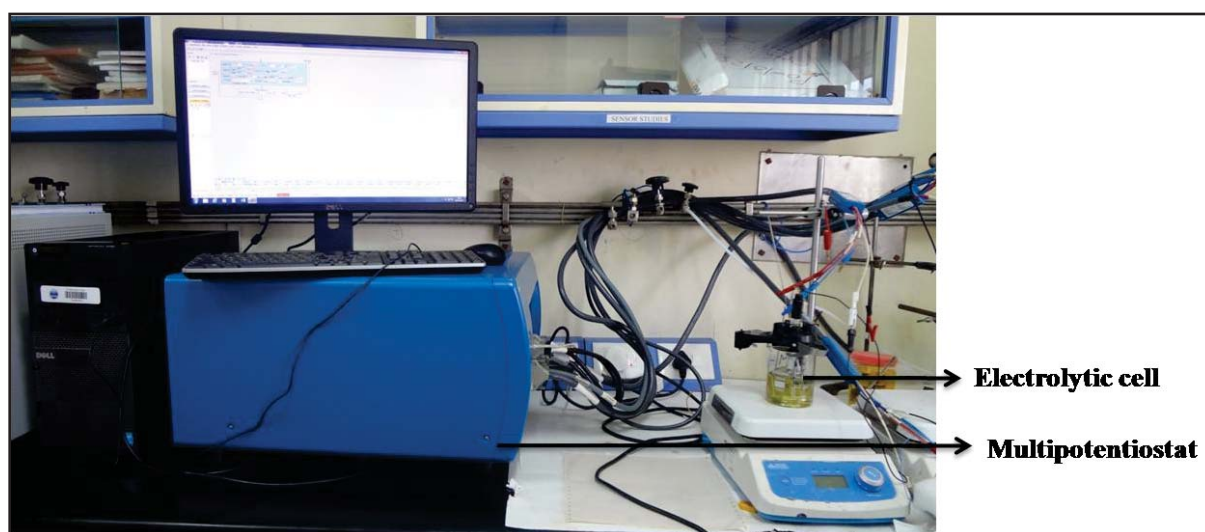


Fig. 2.5 Multipotentiostat with electrolytic cell (VMP-300 of M/s Biologic)

In the present work, Pt Pd and Pt_xPd_y alloys were electrodeposited and pulsed electrodeposited on GDL working electrode using both aqueous and ionic liquid electrolytes.

2.1.6 Electrochemical impedance spectroscopy

Ohm's law says that current (I) through a conductor between two points is directly proportional to potential (V) difference between the two points. This law is obeyed by an ideal conductor.

$$\mathbf{R} = \frac{\mathbf{V}}{\mathbf{I}} \quad (2.3)$$

In order to measure the resistance (R) of ideal electrochemical systems, direct current is applied but, in the case of non-ideal system, alternating current is used to study the impedance. Proportionality constant in Ohm's law shows complex ($e^{i\theta}$) behaviour due to sinusoidal perturbation and is called impedance¹¹⁰.

$$\mathbf{Z} = \frac{\Delta V}{\Delta I} e^{i\theta} = \mathbf{Z}_r \quad (2.4)$$

where Z_r and Z_j are real and complex impedance.

The perturbation is made either potentiostatic or galvanostatic modes in a wide frequency range and response to each frequency is recorded. Electrochemical impedance spectroscopy is an experimental tool to determine impedance of non-ideal electrochemical systems. Simple single faradaic reaction is denoted by a simple equivalent circuit shown in Fig. 2.6 consisting of electrolyte resistance (R_1), charge transfer resistance (R_2), and double layer capacitance (C_2). The impedance of this circuit is given in eq. 2.5.

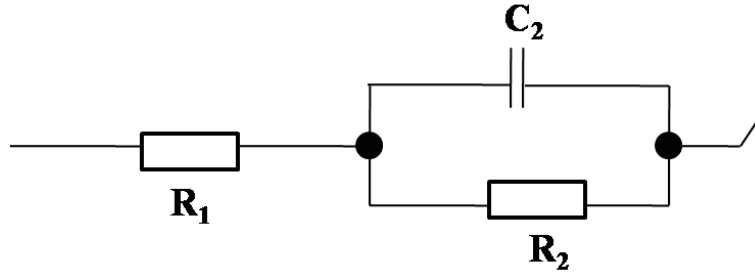


Fig. 2.6 Equivalent circuit of simple electrochemical reaction

$$Z = R_1 + \frac{R_2}{1 + i2\pi f C_2 R_2} \quad (2.5)$$

where R_1 - electrolyte resistance (Ω), R_2 - charge transfer resistance (Ω), C_2 - double layer capacitance (F) and frequency – f (Hz).

A typical impedance spectrum of this system shows a perfect semicircle at high frequency and a line appears at low frequency with one time constant as shown by Fig. 2.7. Number of time constants gets varied with respect to the electrode surface or reactivity of electrochemical reaction. The distribution of time constants are commonly represented as constant phase element in order to fit the impedance data obtained from the experiment ¹¹⁰.

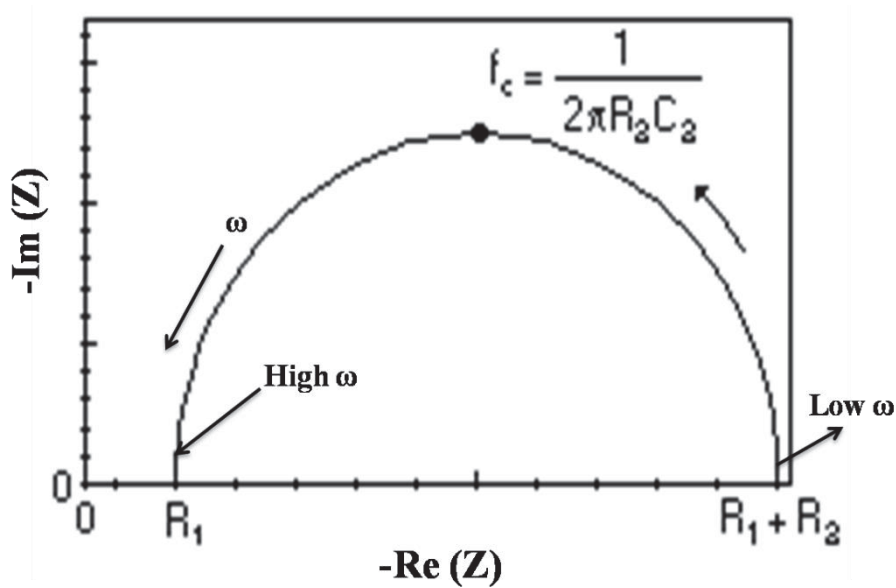


Fig. 2.7 Nyquist impedance plot of simple electrochemical reaction

2.2 Morphological and phase characterisation

2.2.1 Electron microscopy

Electron microscopy is used to find an image of the samples surface as well as its diffraction pattern by interacting with the electron beam. The electron has a shorter wavelength because of which it can be focused by electromagnetic lenses. These accelerated electrons can just pass through the material without any interaction; undergo interaction with sample results in the release of elastically and inelastically scattered electrons, and those are characteristics of a sample. The resultant signals are captured by the detector for imaging, qualitative and quantitative analysis of the sample. Schematics of electron-sample interaction are shown in Fig. 2.8.

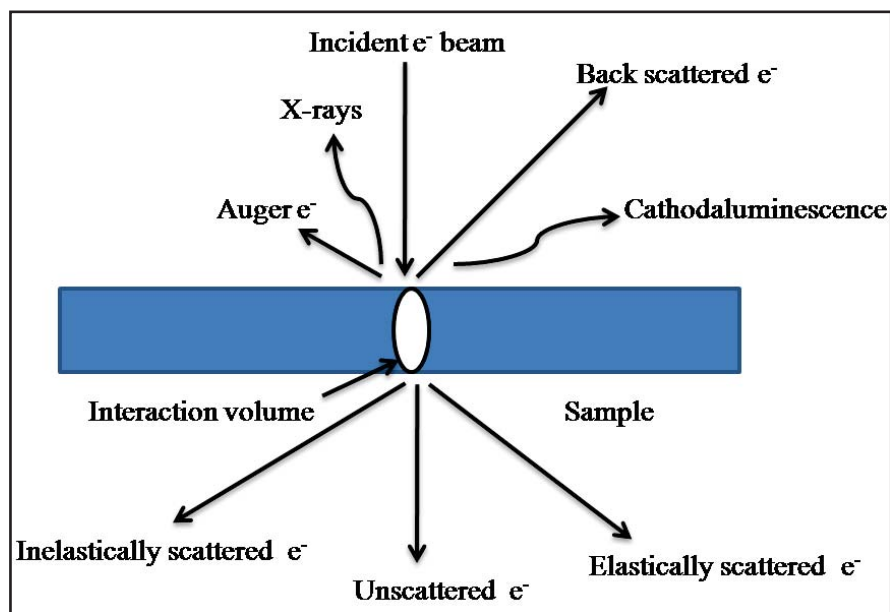


Fig. 2.8 Schematics of electron-sample interaction ¹¹¹

2.2.1.1 Scanning electron microscopy

The surface morphology of the material is studied by SEM. It can go up to a resolution of a few nm and can be operated at magnifications range from 10 x to 300,000 x. In SEM, the primary electrons are accelerated towards the target using a fine probe that scans over

sample's surface. The interaction of the electron with sample results in the release of secondary electrons, diffracted back scattered electrons, X-ray photons, back scattered electrons, visible light and heat. The emitted electron beam gives information of the sample, for instance, secondary electrons are used for imaging the sample, atomic number contrast image can be obtained from back scattered electron, X-rays furnish details about elements present in the sample and crystal structure is revealed from diffracted back scattered electrons. This technique is non-destructive other than the radiation damage caused by the electron. If the energy transfer of the electron beam to the sample exceeds the work function of the material, the electron will be ejected out from the sample's surface, and these are known secondary electrons (SEs). SEs have energy less than 50 eV and are produced from the depth of a few nm of the sample's surface. The energy of back scattered electrons are much higher than 50 eV^{112, 113}.

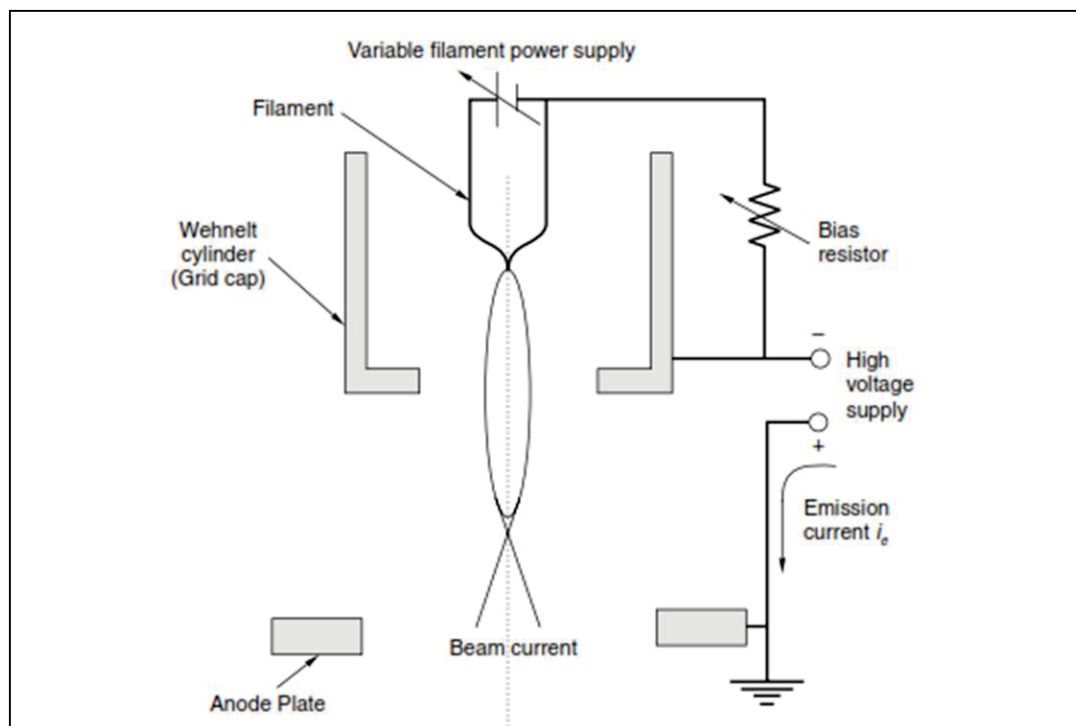


Fig. 2.9 Schematic representation of scanning electron microscope¹¹³

In EDAX equipment the output is displayed in the form of a histogram of counts versus X-ray energy. The characteristic X-rays emitted from the sample serve as fingerprints and

provide elemental information of the samples permitting semi-quantitative analysis, quantitative analysis, line profiling and spatial distribution imaging.

Field Emission Scanning Electron Microscopes (FEG Quanta, M/s Philips, Netherlands and M/s Zeiss, Germany) having EDAX facilities were employed for the morphological analysis in the present study. Semi-quantitative elemental analyses were carried out by using the EDAX facilities attached to the FESEMs.

2.2.1.2 Transmission electron microscopy

TEM is a tool for visualisation and analysis of specimens. TEM reveals information which is inaccessible by light microscopy since it uses high energy electrons. It is widely used to investigate chemical compositions and crystal structures. It produces images by capturing the electrons, which are transmitted from the specimen^{113, 114}.

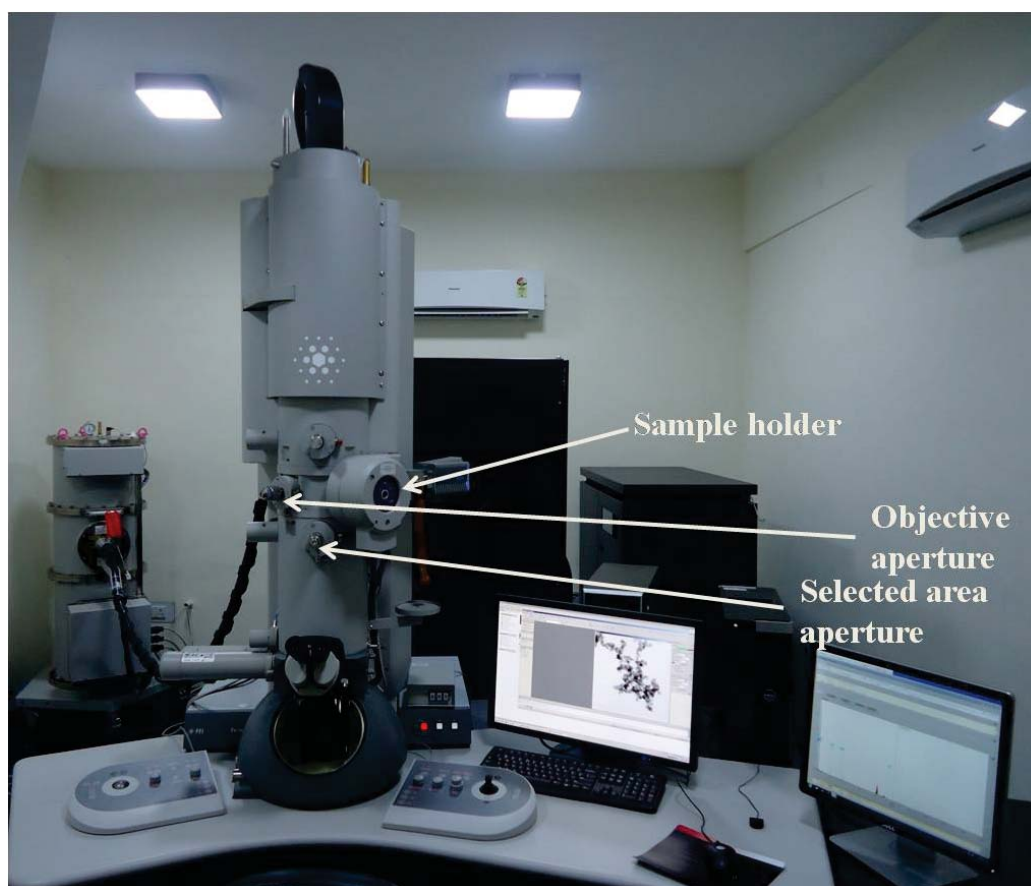


Fig. 2.10 Schematics of transmission electron microscope (FEI-Technai)

Modes of operation of TEM:

Diffraction mode: In this mode, electron diffraction pattern is formed at the back focal plane of objective lens owing to the diffraction that occurs between the incident electrons and atomic planes of the specimen. This diffraction pattern will be displayed on the fluorescent screen. The magnetic lenses are positioned below the specimen for analysing the transmitted electrons. Selected area electron diffraction (SAED) is carried out in the specific region to obtain the information on the crystal structure. SAED is produced by superposition of diffraction patterns produced from crystallites that has distinct orientations.

Imaging mode: A magnified image is produced in the objective lens (image plane).

TEM (M/s FEI-Tecnai, G² 20 Twin) was employed for the morphological and structural characterization of all the samples investigated for the present work (Fig. 2.10).

2.2.2 X-ray diffraction

Diffraction effect occurs, when electromagnetic radiation with a wavelength λ impinges and imposes on a crystallographic material having regular periodic structures with a few geometrical variations in the incident length scale (λ). Since the wavelength of X-rays is largely comparable to inter-atomic spacing, d of a crystal, it can largely interact with the solid material and can scatter to produce diffraction patterns¹¹⁵. This phenomenon occurs only when the interaction of the wavelength with the crystal planes satisfy the Bragg's diffraction criterion (eq. 2.6)

$$2d\sin\theta = n\lambda \quad (2.6)$$

where, d in this equation, is the inter-planar distance (i.e. distance is the spacing between next two adjacent planes in a vast set of planes, Fig. 2.11), θ is known as the angle of incidence, n is an integer that represents the order of diffraction, and λ is the wavelength of the incident

X-ray (in general, Cu $K_\alpha = 1.54056 \text{ \AA}$). Notably, each peak in the diffraction pattern can be positively correlated to a several set of planes in the crystal lattice. This is because, different set of planes have a different interplanar distance and according to Bragg's law condition θ must vary as the “d” varies. A schematic diagram of X-ray Diffraction (XRD) is displayed in Fig. 2.11. The diffraction pattern is recorded in the X-ray diffractometer from the Bragg-Brentano geometry. In general, the pattern of diffraction is plotted with the intensity against the diffraction angle, 2θ .

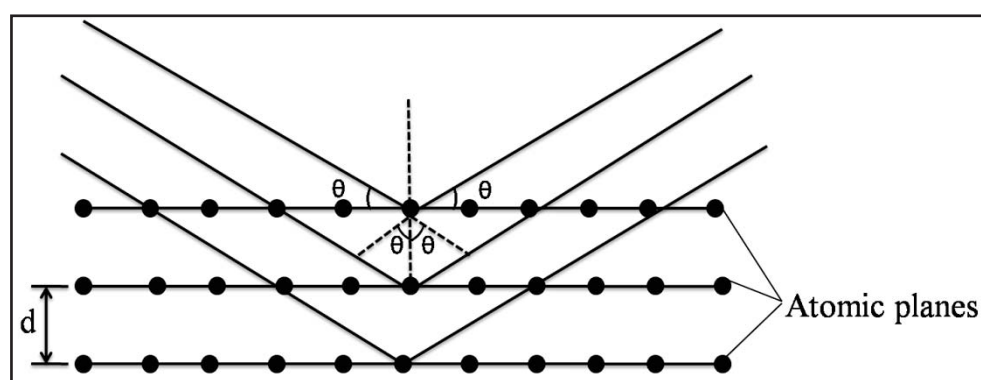


Fig. 2.11 Schematics of X-ray diffraction

Grazing incidence X-ray diffraction (GIXRD) is another technique closely associated with common XRD and it is used to record the diffraction pattern in thin films, where minimum contribution is required from substrate to acquire the pattern. In the case of GIXRD, the penetration depths of the incident X-rays are strictly restricted to about 10-100 nm by fixing the angle of incidence of X-ray to a value below 5° . Since the scattering volume in this format is very small, high brilliance X-ray sources such as rotating anode and synchrotron beams are commonly used. On the other hand, such a surface and sub-surface crystallography requires fast and efficient detectors to yield significant counts displaying the pattern. The crystal structure of the thin film samples are solely obtained by the comparison of the pattern obtained and is maintained by Joint Committee of Powder Diffraction Standards (JCPDS)

established by International Commission on Diffraction Data (ICDD). The crystallite sizes (t) of the samples are calculated using Scherer formula ¹¹⁶.

$$t = \frac{K\lambda}{\cos\theta} \quad (2.7)$$

where K is a dimensionless quantity having a value of 0.9, λ is the wavelength of X-ray radiation and θ is the diffraction angle in radians. Broadening, B is generally calculated by using the full width half maximum (FWHM) of the diffraction peak that corresponds to every plane in the diffraction pattern. In the present study, the samples were analyzed in GIXRD mode by using the X-ray diffractometer (M/s GNR-Explorer, Italy).

2.2.3 Linear scratch test equipment

The adhesion of coating on substrate was determined using linear scratch test equipment. Acoustic signal will be emitted where cracking takes place on the scratch path. The strength of the coating is depicted by critical load (L_c) and it describes about the load at which coating peels off from the substrate. The adhesion is measured by sensing first acoustic signal ^{117, 118}. A scratch was done by using rock-well type diamond indenter with radius of 200 μm hemispherical tip. The test load was increased gradually from 1 N to 6 N at 2 N/min rate for a distance of 2 mm. Depending on the nature of substrate and material used for coating, the testing parameters were calibrated as per ASTM C1624-05 standard ¹¹⁹. During the test, frictional force, acoustic emission, tangential force, penetration depth and applied normal load parameters are automatically recorded. The adhesion of thin film on substrate was measured by linear scratch test equipment (Revtest, Switzerland) in the present study.

2.2.4 Inductively coupled plasma mass spectrometry

Inductively coupled plasma mass spectrometry (ICP-MS) is mass spectrometry which can detect metals in the concentration range of part per quadrillion. Ionizing the sample using

inductively coupled plasma and then analysed by mass spectrometer. This process made possible for such a low concentration level detection. In comparison to atomic absorption spectroscopy, ICP-MS is more precise and has higher sensitivity^{120, 121}.

In the present work, the samples were analysed using ICP-MS (M/s SPECTRO MS – MSS001, Germany).

2.2.5 Sensor and fuel cell testing of Pt, Pd and Pt_xPd_y alloys deposited on gas diffusion layer

2.2.5.1 Diffusion electrode

Diffusion electrode in the present study is a gas diffusion electrode which is prepared by deposition of electrocatalysts on teflonised microporous layer on carbon paper (200 micron thickness). Teflonised microporous layer consists of nanocarbon (25 micron thickness) deposited onto carbon paper. Teflonised carbon paper used in the study is a commercial one (Anabond Sainergy Fuel cell Pvt. Ltd, Chennai). The gas diffusion electrode facilitates effective distribution of reactant gases (H₂ and O₂/air) and also transport of water (preventing clogging).

The use of gas diffusion layer is to allow the gas to reach the catalyst layer more effectively. In addition, GDL also provides the necessary electrical conductivity and helps in the removal of water from the fuel cell. Gas transport from the macroporous (carbon paper) layer to catalyst layer is the mass transfer process in PEM fuel cell and PEM based H₂ sensor. A typical diffusion electrode is shown in Fig. 2.12.

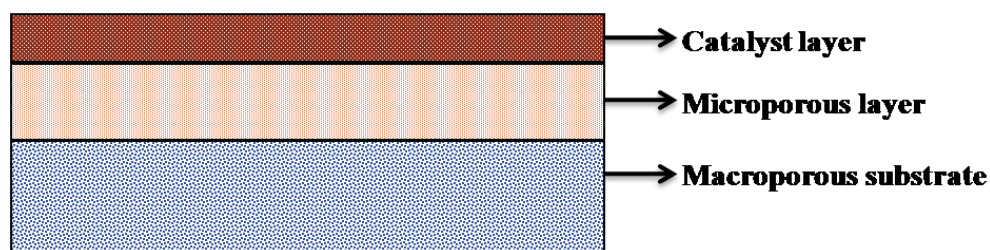


Fig. 2.12 Schematic of diffusion electrode

2.2.5.2 Preparation of membrane electrode assembly for sensor and fuel cell

Membrane electrode assemblies (MEA) for sensor and fuel cell were made by hot-pressing the anode and cathode onto either side of the Nafion membrane. Hot-pressing was done by using hydraulic press shown in Fig. 2.13 (M/s SANTEC, Delhi).



Fig. 2.13 Hydraulic press (SANTEC)

2.2.5.3 Sensor testing unit

Sensor consists of sensing electrode (anode), counter electrode (cathode) and electrolyte. Sensing electrode has inlet and outlet for the controlled flow of H_2 and that of counter electrode disc has small holes which are exposed to atmosphere for the supply of oxygen from air as shown by Fig. 2.14. The required concentrations of H_2 were mixed with argon using mass flow controller. Platinum wire used as the current collector, which was pressed onto working and counter electrodes. In three electrode mode operation platinum wire was used as the reference electrode. The schematics of the sensor and testing unit are shown in Fig. 2.14.

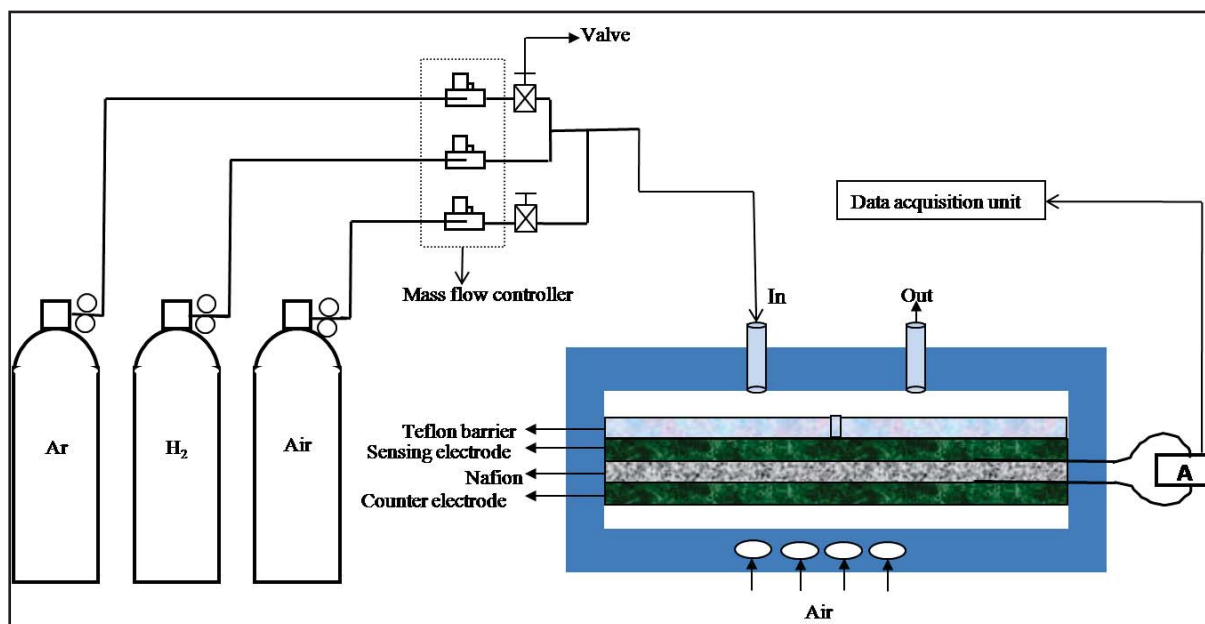


Fig. 2.14 Schematics of sensor and testing unit

2.2.5.4 Fuel cell testing unit

A typical fuel cell has anode, cathode and electrolyte. MEA preparation is shown in section 2.2.5.1. The humidified H_2 gas at anode and humidified O_2 at cathode were supplied using the in-built mass flow controller of fuel cell test station (FCTS) (M/s FCT-150S, France). The schematics of fuel cell testing unit are shown in Fig. 2.15. Cell temperature, humidification temperature and line temperature were controlled by in-built temperature controller. Current-voltage polarization and impedance studies of MEAs were studied using fuel cell test station. Electrochemical characterization (cyclic voltammetry) of diffusion electrodes in fuel cell set up were studied using multi-potentiostat (VMP-300 of M/s Biologic, France).

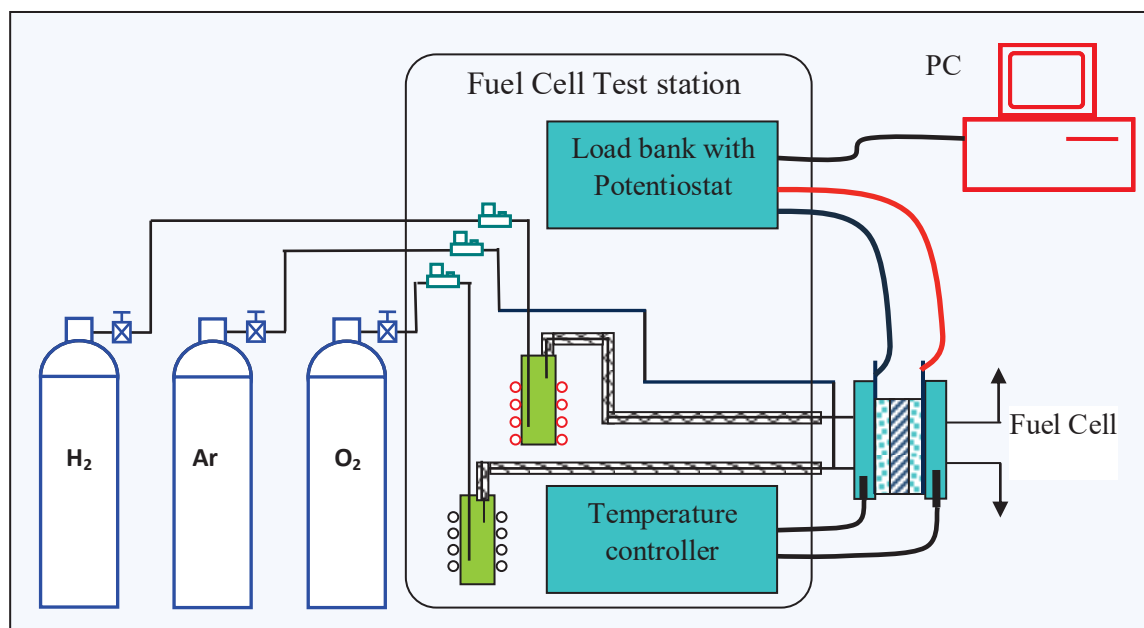


Fig. 2.15 Schematics of fuel cell test station

2.3 Conclusions

This chapter provided brief details of electrodeposition and characterization techniques used for carrying out research on the method of deposition of Pt, Pd and Pt_xPd_y alloy electrocatalysts on gas diffusion layer. The microstructure and electrochemical characterization tools utilized are described. The basic principles of experimental tools employed are discussed.

Chapter 3

Studies on deposition and characterization of electrocatalysts on carbon paper for application in PEM sensors

3.1 Introduction

Pt, Pd and Pt_xPd_y alloy are being investigated extensively as electrocatalysts in fuel cells and sensors^{20, 32, 122-124}. These noble metals and its alloys also find application in many other fields such as petroleum refineries, nitric acid production units, hydrogenation processes in chemical industries and as catalytic converters in automobiles. Particle size and microstructure of the electrocatalyst significantly influences the performance of fuel cells and sensors. Several techniques have been used for preparing the electrocatalyst in nano range. The methods of preparation of electrocatalyst include chemical reduction,¹²⁵ pulsed laser deposition,¹²⁶ sonochemical method,¹²⁷ chemical vapour deposition⁴¹, electrodeposition⁴⁷ (ED), and pulsed electrodeposition (PED) methods. Most commonly used method for electrocatalyst deposition are screen printing, spray coating and brush coating methods¹²⁸. These methods have limitation due to the possibility of non-utilization of significant extent of active sites⁴⁷. Chemical reduction methods for electro-catalyst deposition include impregnation-reduction⁴⁴ and Takenaka-Torikai method⁴⁵. These methods do not have control over the particle growth. Vapour deposition and pulsed laser deposition require high vacuum and expensive instrumental facility. To compensate for the effect of agglomeration or larger size particle, high loading of electrocatalyst is practised. Therefore, the present focus is to find an optimal method for deposition of electrocatalyst which is economically viable and has control over the particle size. ED methods are effective in tuning the particle size and also cost effective^{68, 129, 130}.

Preparation and deposition of Pt, Pd and Pt_xPd_y alloy electrocatalysts on GDL by brush coating (BC), ED and PED methods in the context of making gas diffusion electrodes are discussed in this chapter. ED and PED of Pt and Pd were carried out using both aqueous and ionic liquid electrolytes. Only aqueous electrolyte was used for pulsed electrodeposition of Pt_xPd_y alloy. The morphology and crystal structure of deposited electrocatalysts were characterized by field emission scanning electron microscope (FESEM) and grazing incidence X-ray diffraction (GIXRD). The prepared gas diffusion electrodes (GDE) find application in PEMHS.

3.2 Experimental

Diffusion electrode for application in PEM based sensors were made by deposition of electrocatalysts on to carbon paper based gas diffusion layer. Electrocatalysts attempted in the present study include Pt, Pd and Pt_xPd_y alloys. Deposition was carried out by brush coating, electrodeposition and pulsed electrodeposition. Both aqueous and ionic liquid electrolytes were used.

3.2.1 Preparation of gas diffusion electrodes for the application in PEMHS

3.2.1.1 Materials

1-methyl imidazole, chloro butane, acetonitrile, potassium tetrafluoroborate, ethyl acetate, and potassium hexachloroplatinate (K₂PtCl₆) were purchased from Sigma Aldrich. The ionic liquids 1-butyl-3-methylimidazolium tetrafluoroborate ([C4mim][BF₄]) and 1-butyl-3-methylimidazolium chloride ([C4mim][Cl]) electrolytes were synthesized as per the procedure given in literature ^{131, 132}. Palladium chloride (PdCl₂) used in the study was procured from M/s Ranbaxy, Chennai, India. GDL was bought from M/s Anabond Sainergy Fuel cell Pvt. Ltd, Chennai. GDL (3 cm²) used in the present study comprises of carbon paper (200 micron thickness) with a microporous layer of teflonised nanocarbon (25 micron

thickness) deposited on the surface. Pt supported on carbon (Pt/C-40%) was obtained from M/s Alfa Aesar, India.

Synthesis of [C4mim][Cl]: 1-methyl imidazole used in the study was purified by fractional distillation; 2:3 ratios of 1-methyl imidazole and chloro butane mixtures were taken in 1 L round bottom flask and refluxed for 48 h. The resulting mixture was washed thoroughly (4-5 times) with 1:1 ratios of acetonitrile and ethyl acetate. Finally, vacuum heating at 353 K was carried out to remove water completely. C4mimCl begins to crystallise and a white crystalline solid was obtained.

Preparation of [C4mim][BF4]: [C4mim][Cl] and potassium tetrafluoroborate were dissolved in water in 3:2 ratio and stirred for 12 h. Water was removed under vacuum by maintaining the temperature at 353 K. Further, dichloromethane and anhydrous magnesium sulphate were added to remove any residual moisture and kept aside for 1 h. The filterable residue of magnesium sulphate was removed. Volatile dichloromethane and the final trace of moisture in the above filtrate were removed under reduced pressure (0.2 bar) in a roto-evaporator. A light yellow [C4mim][BF4] viscous liquid was obtained.

The prepared ionic liquids were stored in vacuum desiccators to prevent absorbing moisture. The ionic liquids were purged with Ar to maintain the purity of the ionic liquid during the experiment.

3.2.1.2 Preparation/deposition of Pt electrocatalyst on gas diffusion layer

Pt electrocatalyst was deposited on GDL from both aqueous and ionic liquid electrolytes. From aqueous medium, deposition was attempted by BC, ED and PED methods. Catalyst for BC was prepared by taking Pt/C (50 %) catalyst (M/s Sigma Aldrich, India) along with 1:1 ratio of isopropanol and water. The mixture was ultrasonicated for 15 mins. 2.33 ml of 5% Nafion solution was added to the above mixture and again ultrasonicated for 15 mins.

Catalyst slurry thus prepared was brush coated on to the GDL and dried in an oven for 2 h at 333 K to remove volatile solvent.

Electrodeposition and pulsed electrodeposition of Pt were carried out in three electrode cell with constant stirring. Nafion impregnated GDL was used as the working electrode. Brush coated Pt/C catalyst based diffusion electrode and saturated calomel electrode (SCE) were used as the counter and reference electrodes respectively. Pt was electrodeposited on GDL at the optimum potential of -0.2 V from 3 mM of K_2PtCl_6 in 0.5 M H_2SO_4 for 10 mins^{39, 112-114}. PED of Pt on GDL was performed using the following electrochemical parameters: Lower potential (E_L) = 0 V, upper potential (E_U) = -0.2 V, on time (t_{on}) = 10 ms, off time (t_{off}) = 10 ms. After the deposition, the sample was washed with acetone and dried in oven at 333 K. The prepared samples were characterized.

Electrodeposition and pulsed electrodeposition of Pt on GDL in ionic liquid medium were also carried out in a three electrode cell. Nafion impregnated GDL, brush coated Pt/C catalyst on GDL and Pt wire were used as the working, counter and reference electrodes respectively. 70 mM of K_2PtCl_6 + [C4mim][BF₄] ionic liquid was used as the electrolyte and the temperature was maintained at 373 K. Before finding the characteristic potentials of Pt, the potential window of the electrolyte was determined by recording the cyclic voltammogram of [C4mim][BF₄] electrolyte. Prior to the electrodeposition, the deposition potential of Pt on GDL was determined by cyclic voltammetry (CV). Nucleation and growth kinetics of Pt on GDL was investigated by chronopotentiometry and chronoamperometry. The electrolyte solution was stirred during ED. The effect of deposition potential on the morphology was studied at various deposition potentials and optimum deposition potential was chosen ensuring surface coverage with minimum agglomeration. The diffusion electrode was washed, dried and characterized for surface morphology and microstructure.

3.2.1.3 Preparation/deposition of Pd electrocatalyst on gas diffusion layer

Palladium was electrodeposited and pulsed electrodeposited by using both aqueous and ionic liquid as electrolytes. Electrodeposition and pulsed electrodeposition were conducted in an electrolytic cell with Nafion impregnated GDL, brush coated Pt/C catalyst on GDL and SCE as working, counter and reference electrodes respectively. Both electrodeposition and pulsed electrodeposition were performed using PdCl_2 in 0.5 M HCl as electrolyte and the deposition potential reported in literature was adopted^{133, 134}. Electrodeposition was carried out at applied potential of -0.2 V for 10 mins^{47, 135-137}. Pulsed electrodeposition of Pd was carried using the following parameters $E_L = 0$ V, $E_U = -0.2$ V, $t_{\text{on}} = 10$ ms, $t_{\text{off}} = 10$ ms, and Nc (number of cycles) = 30,000. The electrodeposited and pulsed electrodeposited Pd on GDL was characterized after washing and drying.

Pd was also electrodeposited and pulsed electrodeposited on Nafion impregnated GDL using 12 mM of $\text{PdCl}_2 + [\text{C4mim}][\text{Cl}]$ as ionic liquid electrolyte. Electrodeposition and pulsed electrodeposition of Pd were carried using Nafion impregnated GDL, glassy carbon and Pt wire as working, counter and reference electrodes respectively. Before the deposition, the potential window of electrolyte and characteristics reduction potentials of Pd on GDL were determined by CV. Different potentials were applied for ED to study the microstructural change with applied potential. The optimum potential was selected to ensure uniform distribution of deposited catalyst with minimum particle size for both ED and PED. Both the samples were washed with acetone to remove the ionic liquid and dried in oven at 333 K. After that, the samples were dried at room temperature and characterized.

3.2.1.4 Preparation/deposition of Pt_xPd_y alloy electrocatalyst on gas diffusion layer

Pulsed electrodeposition of Pt_xPd_y alloy electrocatalyst was attempted from aqueous medium using Nafion impregnated GDL, brush coated Pt/C catalyst on GDL and SCE as the working,

counter and reference electrodes respectively. The electrolyte used for making Pt_xPd_y alloy electrodes was 1-3 mM PdCl₂ + 1-3 mM K₂PtCl₆ + 0.5 M H₂SO₄ and stirred continuously during deposition. In order to obtain Pt_xPd_y alloy electrodes of varying compositions of Pt and Pd, concentration of PdCl₂ was fixed at 3 mM and that of K₂PtCl₆ was varied in the range of 1 mM to 3 mM. High overpotential of -0.8 V was applied for electrodepositing Pt_xPd_y alloy to get the deposit in short duration compared to the potential used in the above studies for depositing Pt or Pd. PED of Pt_xPd_y alloy was carried out using the following parameters in three different electrolytes: E_L (lower potential) = 0 V, E_U (upper potential) = -0.8 V, t_{on} = 10 ms, t_{off} = 10 ms. After deposition, the samples were washed with acetone, dried in oven and characterized for morphology and crystal structure.

3.2.2 Characterization of Pt, Pd and Pt_xPd_y alloy based gas diffusion electrodes

The diffusion electrodes were characterized by FESEM, EDAX and GIXRD. Microstructure of the deposits was characterized by FESEM. The crystal structure of the deposits was studied by GIXRD at a grazing angle of 0.5 degrees. Elemental compositions of deposits were analyzed by inductively coupled plasma mass spectrometry (ICP-MS) and EDAX. Crystallite sizes of the deposits were calculated using Scherrer's formula. The lattice parameter was calculated by using the below mentioned equation (eq. 3.1)

$$a = \frac{n\lambda (\sqrt{h^2+k^2+l^2})}{2 \sin\theta} \quad (3.1)$$

The adhesion strength of electrodeposited Pd using ionic liquid and aqueous electrolytes over GDL was measured using linear scratch test equipment.

3.3 Results and discussions

3.3.1 Preparation of gas diffusion electrodes for the application in PEMHS

3.3.1.1 Preparation/deposition of Pt electrocatalyst on gas diffusion layer from aqueous electrolyte

Grazing incidence X-ray diffraction pattern of brush coated Pt/C catalyst on GDL (BC/Pt/C/GDL), electrodeposited Pt on GDL (ED/Pt/GDL/AQ), and pulsed electrodeposited Pt on GDL (PED/Pt/GDL/AQ) from aqueous electrolyte are shown in Fig. 3.1. The GIXRD pattern of all three GDE's shows a broad and low intense peak indicating that the deposited Pt particles are in nano range. Peaks at 39.8° , 46.2° , and 67.4° are attributed to fcc platinum (JCPDS No. 040802), and their corresponding planes are (111), (200) and (220) respectively. The calculated crystallite size for each lattice planes of Pt for brush coated, electrodeposited and pulsed electrodeposited samples are shown in Table 3.1. From the Table, it is evident that the crystallite size of Pt for BC/Pt/C/GDL is smaller than for PED/Pt/GDL/AQ and ED/Pt/GDL/AQ.

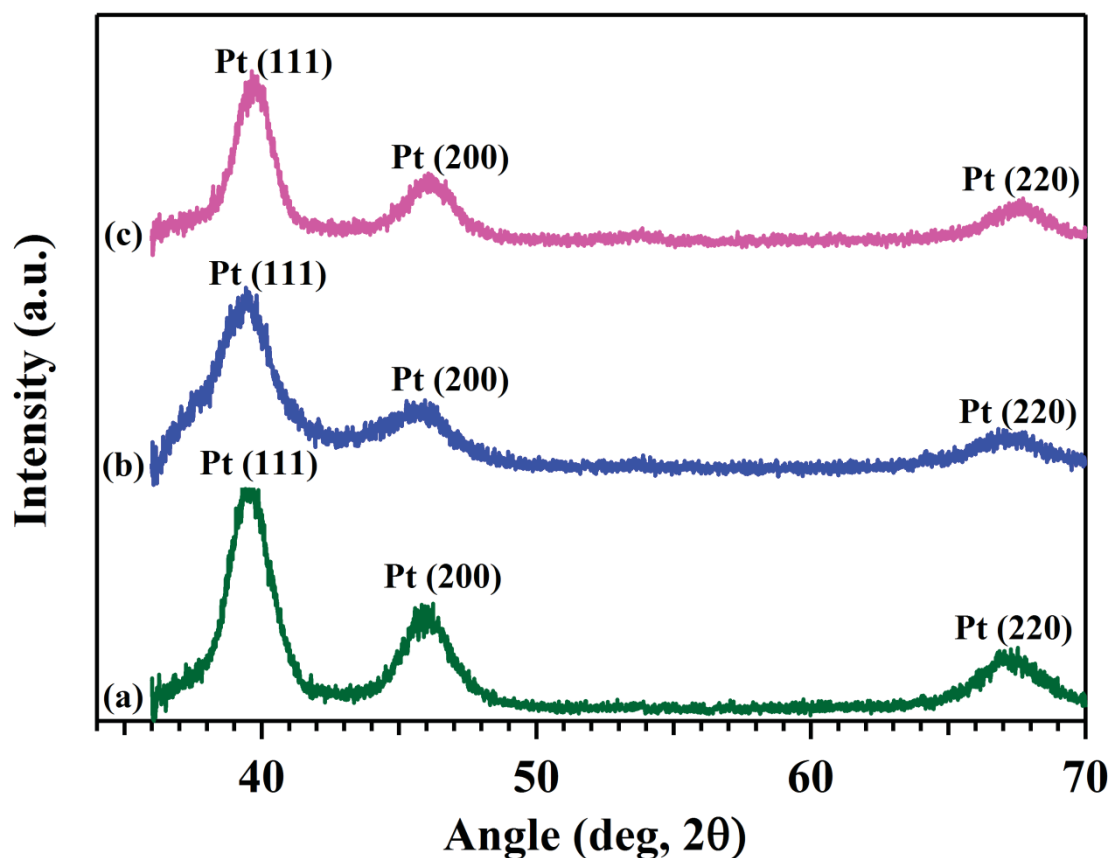


Fig. 3.1 Grazing incidence X-ray diffraction pattern of deposited Pt on gas diffusion layer (a) brush coated Pt/C commercial catalyst, (b) electrodeposited and (c) pulsed electrodeposited

Table 3.1 Crystallite sizes of Pt deposited on gas diffusion layer by brush coating, electrodeposition and pulsed electrodeposition methods

Angle (2θ)	BC/Pt/C/GDL d (nm)	ED/Pt/GDL/AQ d (nm)	PED/Pt/GDL/AQ d (nm)
39.8° (111)	4.71±0.29	8.96±1.53	5.38±1.32
46.2° (200)	4.41±0.54	9.34±1.15	4.70±1.21
67.4° (220)	3.99±0.34	11.44±1.46	8.93±1.12

Note: Brush coated Pt/C catalyst; electrodeposited Pt and pulsed electrodeposited Pt on gas diffusion layer are indicated as BC/Pt/C/GDL, ED/Pt/GDL/AQ and PED/Pt/GDL/AQ respectively.

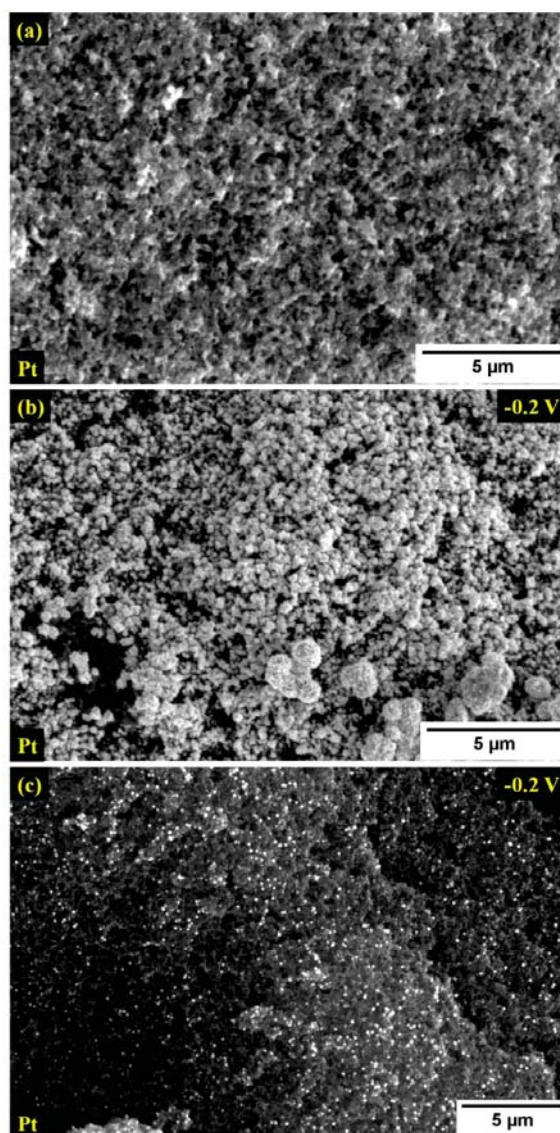


Fig. 3.2 Field emission scanning electron microscope images of electrocatalyst on gas diffusion layer (a) brush coated Pt/C (50 %), (b) electrodeposited Pt and (c) pulsed electrodeposited Pt

FESEM images of BC/Pt/C/GDL, ED/Pt/GDL/AQ and PED/Pt/GDL/AQ are shown in Fig. 3.2. Though the crystallite size is small for BC/Pt/C/GDL sample in comparison to ED/Pt/GDL/AQ and PED/Pt/GDL/AQ, the extent of agglomeration of crystallites is more as seen from the FESEM image of BC/Pt/C/GDL. FESEM image of PED/Pt/GDL/AQ shows a clear separation of particles when compared to ED/Pt/GDL/AQ and BC/Pt/C/GDL. Hence, PED/Pt/GDL/AQ contributes more to catalytic area than electrodeposited and brush coated samples. In brush coating method, active Pt catalytic sites are covered by Nafion preventing

the reactant gas from contacting Pt catalyst; whereas in ED method GDL is impregnated in 1 % Nafion prior to the deposition of Pt, avoids any coverage of Pt by Nafion. The 5% Nafion solution was diluted with the IPA to 1% and the electrodes were immersed in the Nafion IPA mixture for fixed time to achieve uniform loading of Nafion into carbon paper. This process was repeated until the required loading of Nafion is reached. The Nafion content was maintained at 30 % for the respective loading of catalyst. Prior to the deposition, the loading of catalyst is known and accordingly Nafion loading is made onto the carbon paper. The weight difference was measured before and after loading of Nafion. Pt ions diffused through the thin Nafion layer and were electrodeposited only at the regions with proper ionic and electronic conductivities^{138, 139}. Potentiostatic ED results in the continuous growth of the particle after initial nucleation process. The constant increase in diffusion layer thickness during ED decreases the current and thus reduces the deposition of catalyst at other sites leading to non-uniformity in deposition. Among all techniques, PED is a well known method for obtaining a uniform and nanocrystalline deposition of electrocatalyst. In PED, the potential is switched on (t_{on}) and off (t_{off}) between the applied reduction potential and zero potential at the electrode where electrodeposition occurs. PED reduces diffusion layer thickness by the reorganization of electroactive species at the interface during t_{off} . This offers deposition on various other sites which would bring about uniformity in PED^{68, 69}. PED gives high rate of nucleation compared to constant potential ED which enhances the electroactive area of catalyst with lower loading. This results in the formation of larger particles as seen from the FESEM image of ED/Pt/GDL/AQ. Thus, PED/Pt/GDL/AQ is expected to generate higher catalytic surface area because of formation of Pt particles of nano size with lesser agglomeration.

3.3.1.2 Preparation/deposition of Pt electrocatalyst on gas diffusion layer from

[C4mim][BF4] ionic liquid electrolyte

Electrochemical window for [C4mim][BF4] was determined by CV and is shown in Fig. 3.3 (a). The electrolyte was found to be stable in the potential range -2.8 to 1 V as reported in literature¹⁴⁰. Two small peaks were observed, one is at anodic (+0.4 V) and the other is at cathodic direction (-0.7 V). Most probably, the peak at -0.7 V is attributed to the reduction of water introduced, while transferring the ionic liquid to the electrolytic cell. Schroöder et al.¹⁴¹ and Brendan K Sweeny et al.¹⁴² reported that [C4mim][BF4] can quickly absorb moisture. They also studied the similar behaviour of [C4mim][BF4] ionic liquid in cyclic voltammetry as shown by Fig. 3.3 (a). Further, reported that the presence of water in [C4mim][BF4] ionic liquid electrolyte has a strong influence in the cyclic voltammetric experiments. The peak at + 0.4 V may be due to the oxidation of the reduced product of 1-butyl-3-methyl imidazolium cation, which is in accordance with the literature¹⁴³⁻¹⁴⁵. CV was carried out on gas diffusion electrode at the same scan rate of 10 mV/s for both [C4mim][BF4] and K₂PtCl₆ + [C4mim][BF4] electrolyte. In order to identify the characteristic reduction and oxidation potentials of Pt, CV was carried out in the potential range -2.6 to 0.6 V in K₂PtCl₆ + [C4mim][BF4] electrolyte and is shown in Fig. 3.3 (b). Cyclic voltammogram of Pt exhibits two peaks ($E_p^{C_1}$ and $E_p^{C_2}$) at cathodic side (at -0.53 V, -2.15 V) and one peak at anodic side at 0.66 V. The increased current was observed for K₂PtCl₆ + [C4mim][BF4] compared to pure [C4mim][BF4] electrolyte. Hence, the peaks $E_p^{C_1}$ and E_p^a are only due to the added K₂PtCl₆ and not from the electrolyte, since all other parameters are same except the addition of K₂PtCl₆ to [C4mim][BF4] electrolyte. Similar redox behaviour of Pt in [DEME][BF4] ionic liquid electrolyte was observed by Da Zhang et al.¹⁴⁰.

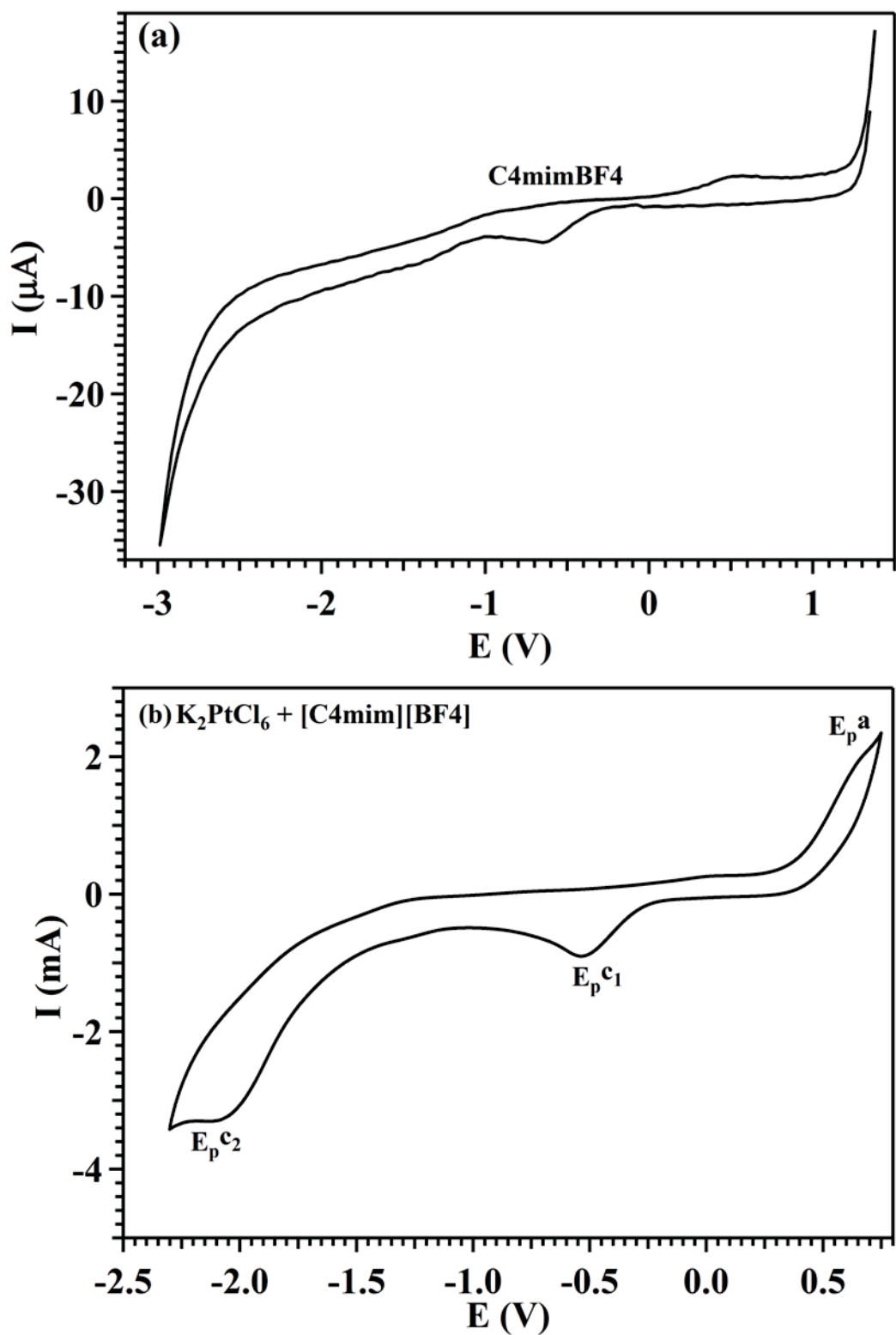


Fig. 3.3 Cyclic voltammogram of (a) 1-butyl-3-methylimidazolium tetrafluoroborate electrolyte (scan rate: 10 mV/s) and (b) $\text{K}_2\text{PtCl}_6 + [\text{C4mim}][\text{BF}_4]$ (scan rate: 10 mV/s) ; working electrode: GDL, counter electrode: glassy carbon, reference electrode: Pt wire

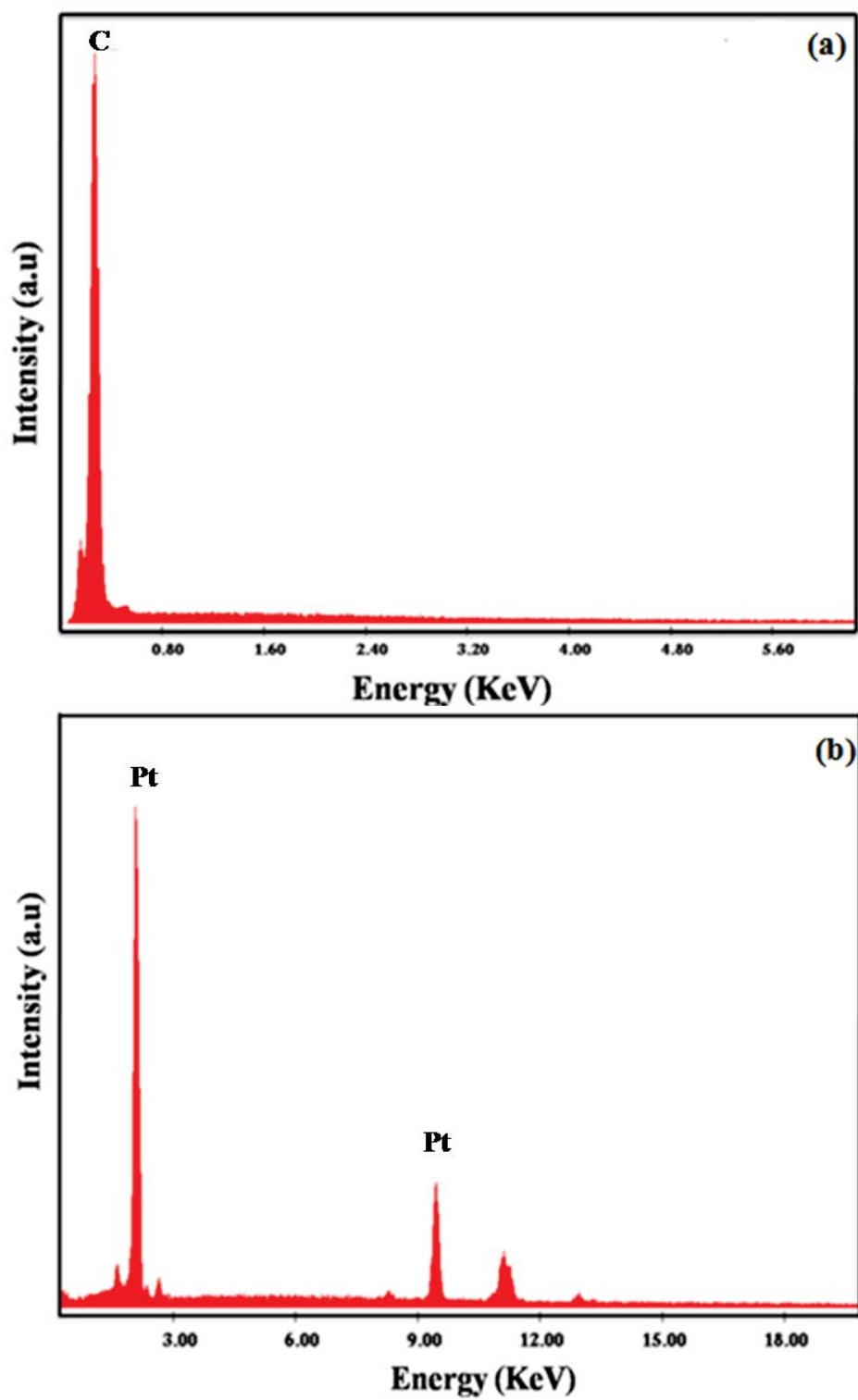


Fig. 3.4 (a) Pt electrodeposited on gas diffusion layer at -0.58 V and (b) Pt electrodeposited on gas diffusion layer at -2.17 V

The peak at -0.58 V may be due to the reduction of $[\text{PtCl}_6]^{2-}$ to $[\text{PtCl}_4]^{2-}$, the second peak at -2.17 V because of the reduction of $[\text{PtCl}_4]^{2-}$ to Pt (0) and the peak at 0.68 V corresponds to the oxidation of $[\text{PtCl}_4]^{2-}$ to $[\text{PtCl}_6]^{2-}$. Hence, the peak at -0.58 V is not expected to give the Pt electrodeposition whereas it occurs at -2.17 V. Therefore, in order to confirm the reduction of Pt (II) to Pt (0) at -2.17 V, the electrodeposition was carried out at -0.58 V and -2.17 V. After the deposition the samples were characterized by EDAX to identify the presence of Pt. EDAX spectrum of electrodeposited Pt on GDL using $[\text{C4mim}][\text{BF}_4]$ (ED/Pt/GDL/ $[\text{C4mim}][\text{BF}_4]$) at -2.17 V indicates a characteristic peak of Pt whereas no peak was observed for Pt deposition at -0.58 V as shown by Fig. 3.4 (a) and (b). This confirms that the peak at -0.58 V is due to the reduction of $[\text{PtCl}_6]^{2-}$ to $[\text{PtCl}_4]^{2-}$ and the latter peak at -2.17 V owing to the reduction of $[\text{PtCl}_4]^{2-}$ to Pt (0) ¹⁴⁰. Only limited studies have been reported for the growth of Pt on glassy carbon using $\text{K}_2\text{PtCl}_6 + [\text{C4mim}][\text{BF}_4]$ as electrolyte ^{140, 146}. Hence, the nucleation and growth kinetics of Pt were investigated prior to the deposition.

Chronopotentiometric studies on reduction of Pt on GDL using $\text{K}_2\text{PtCl}_6 + [\text{C4mim}][\text{BF}_4]$ as electrolyte were carried out at different current densities ranging from -2 mA to -6 mA and are shown in Fig. 3.5. The initial drop in potential is observed due to the formation of a double layer as well as due to the pseudocapacitor charging ¹⁴⁷. After the initial decrease in potential, there is a plateau formation. The potential remains stagnant for a few seconds, and this corresponds to the progress of a nucleation reaction. Afterwards, the overvoltage for reduction of Pt decreases owing to the formation of nuclei resulting in switching of the electrode potential to the next stable potential of the system. Chronopotentiogram shows two steps, first step is related to the reduction of Pt (IV) to Pt (II) and the second step is due to the reduction of Pt (II) to Pt (0). The reduction peak of Pt (IV) to Pt (0) observed in CV is in good agreement with chronopotentiogram.

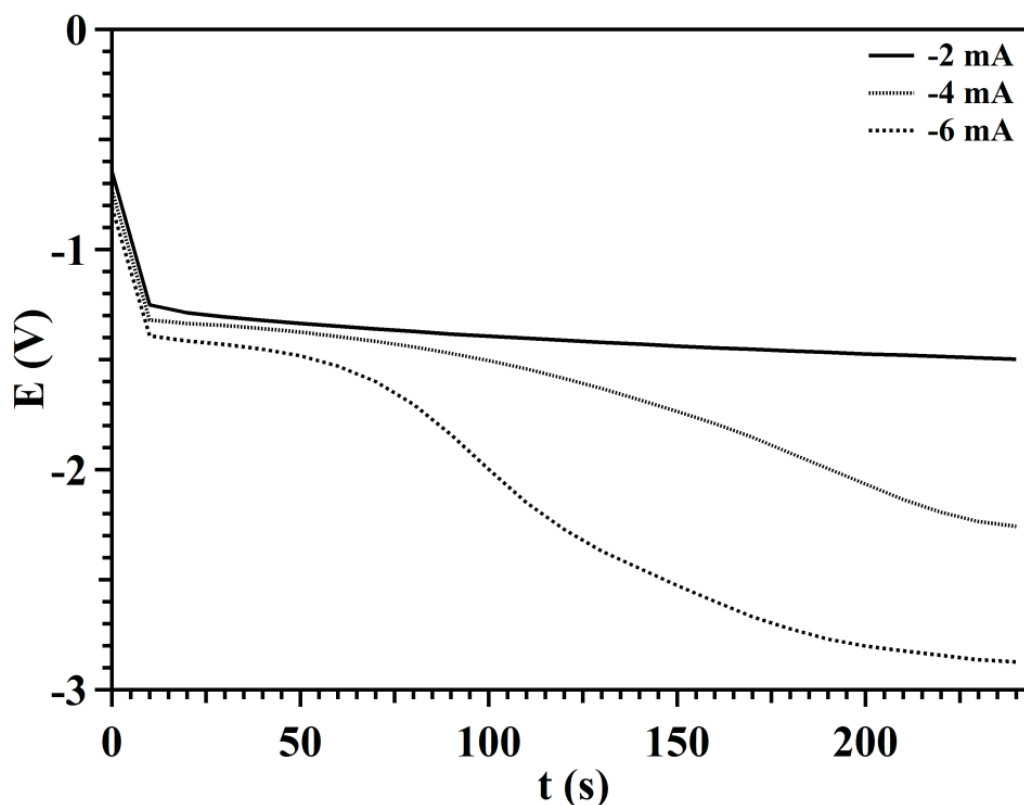


Fig. 3.5 Chronopotentiogram of 70 mM K_2PtCl_6 + [C4mim][BF₄] at 373 K

Chronoamperometry was performed to understand the nucleation and growth behaviour of Pt (IV) on GDL at 373 K in [C4mim][BF₄] ionic liquid medium. Typical chronoamperogram has the following behaviours: (1) initial increase in current due to the growth of individual nuclei and increase in the total number of nuclei in a short interval of time, (2) maximum current is reached once completion of the growth of independent nuclei is attained, and overlap occurs, and (3) decrease in current commences due to the overlap of hemispherical diffusion zones ¹⁴⁸. Chronoamperometry studies of Pt (IV) on GDL were carried out by varying the potential from -2.1 V to -2.6 V and the plot is shown in Fig. 3.6 (a). For over potential less than -2.2 V, steady state was reached immediately after the initial increase of current and this indicates the constant diffusion of Pt ion to the growing nuclei of Pt. In this case, the nuclei are far away from each other to undergo overlap, and hence the maximum current is not observed. Above -2.2 V, the high over potential leads to merging of individual nuclei formed initially in short span of time resulting in observation of the current transients

reaching maximum. Further decrease in current is due to the planar diffusion. The mechanism of nucleation and growth has been explained by Scharifker and Hills model.¹⁴⁹ This model explains whether a deposition follows instantaneous or progressive nucleation. Instantaneous growth happens slowly with small number of active sites, whereas progressive nucleation leads to fast growth of nuclei on many active sites during reduction. Theoretical plot of $(i/i_{\max})^2$ vs t/t_{\max} for instantaneous and progressive growth model are made by using equation (3.2) and (3.3).

For instantaneous nucleation

$$\left(\frac{i^2}{i_{\max}^2}\right) = \frac{1.952}{t/t_{\max}} \{1 - \exp[-1.2564 \left(\frac{t}{t_{\max}}\right)]\}^2 \quad (3.2)$$

And for progressive nucleation

$$\left(\frac{i^2}{i_{\max}^2}\right) = \frac{1.2254}{t/t_{\max}} \{1 - \exp[-2.3367 \left(\frac{t}{t_{\max}}\right)]\}^2 \quad (3.3)$$

I_{\max} and t_{\max} values were taken from chronoamperogram and the plot is made $(i/i_{\max})^2$ vs t/t_{\max} [Fig. 3.6 (b)]. Experimental and theoretical plots are compared to find the nucleation mechanism of platinum during electrodeposition in [C4mim][BF4] ionic liquid. Plot shows deviation from the theoretical line after t_{\max} and is likely due to the partial kinetic control of growth. Hence, Pt electrodeposition on GDL in [C4mim][BF4] ionic liquid follows 3D instantaneous nucleation growth.

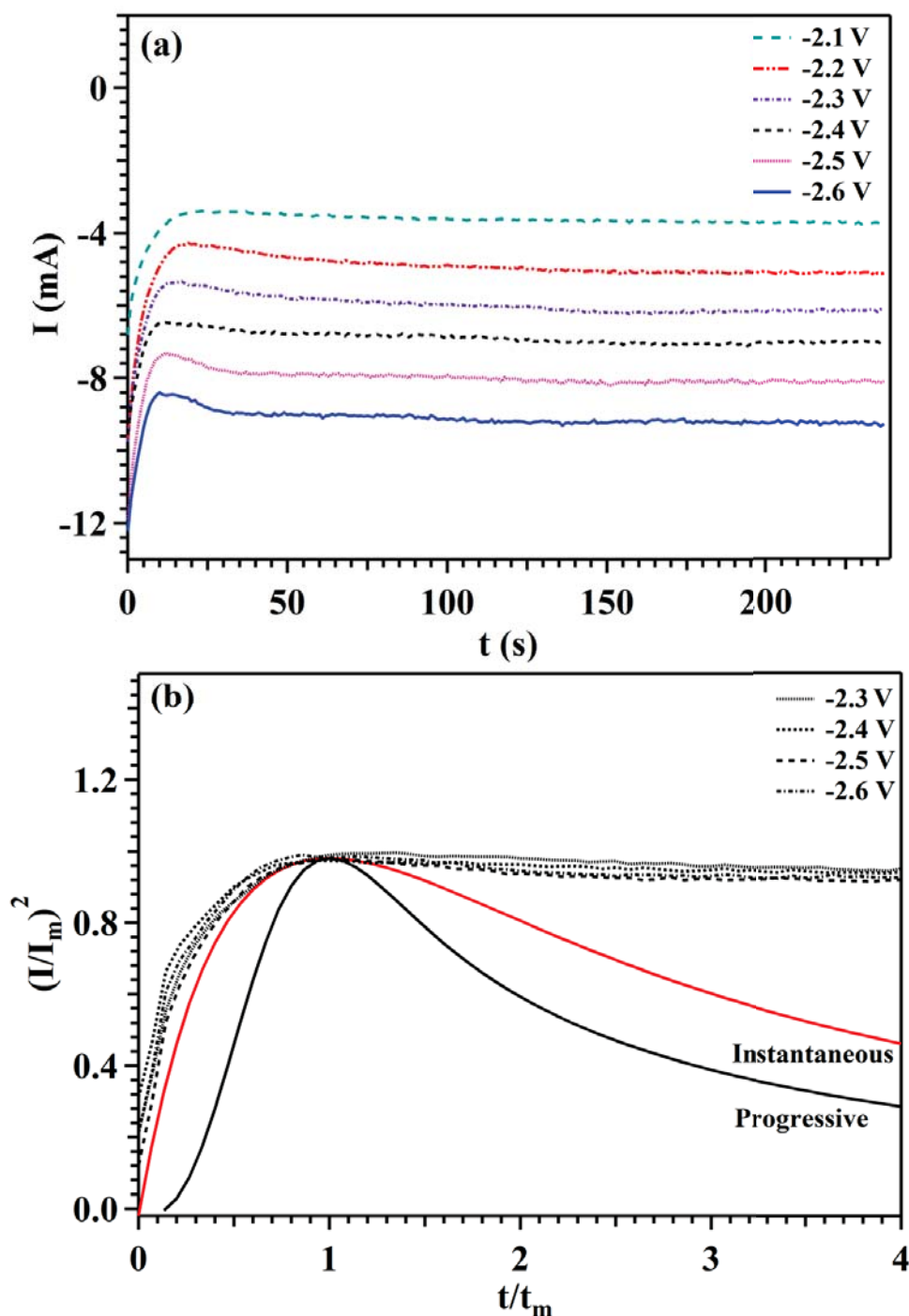


Fig. 3.6 (a) Chronoamperogram of Pt on gas diffusion layer in $[C4mim][BF4]$ ionic liquid electrolyte and (b) Fitting of chronoamperometric data with Scharifker Hills theoretical model of 3D progressive and instantaneous nucleation

Electrodeposition of Pt on GDL from $[C4mim][BF4]$ ionic liquid electrolyte was conducted by using the data obtained from cyclicvoltammetric, chronopotentiometric and chronoamperometric studies, which were carried out for 1 h at three different potentials of -

2.4, -2.5 and -2.6 V. These potentials are found to be high for Pt electrodeposition for commercial scale. It may be noted that this thesis presents a basic study of electrodeposition of Pt using [C4mim][BF4] electrolyte and further studies needs to be carried out by considering the economic point of view. So far, three different RTILs were reported for electrodepositing Pt such as 1-butyl-3-methylimidazolium tetrafluoroborate [C4mim][BF4], 1-butyl-3-methylimidazolium hexafluorophosphate [C4mim][PF6] and N,N-diethyl-N-methyl-N-(2-methoxyethyl)ammonium tetrafluoroborate [DEME][BF4]. The potential of deposition of Pt in both [C4mim][BF4] and [C4mim][PF6] electrolytes was found to be lower but, the Pt precursor used in this has some amount of water in it (Table 3.2). Hence, the present study was carried out using K₂PtCl₆ in [C4mim][BF4] ionic liquid electrolyte.

Table 3.2 Deposition potentials of Pt in [C4mim][BF4], [C4mim][PF6] and [DEME][BF4] ionic liquids

Pt precursor + IL	Deposition potential (V)
H ₂ PtCl ₆ .6H ₂ O + [C4mim][BF4]	-1.5
H ₂ PtCl ₆ .6H ₂ O + [C4mim][PF6]	-1.5
K ₂ PtCl ₆ + [DEME][BF4]	-2 and -3.5
H ₂ PtCl ₆ .6H ₂ O + [C4mim][BF4] (present work)	-2.4

Based on the surface coverage and particle size, the optimum potential was chosen for electrodeposition and pulsed electrodeposition of Pt on GDL for the application in sensors. Both potential and duration of deposition has an effect on the distribution of particle over the substrate. In this study, the effect of potential on Pt electrodeposition is studied and is possible to get well separated particles by reducing the loading of electrocatalyst. Field emission scanning electron microscope images of electrodeposited Pt on GDL using [C4mim][BF4] electrolyte (ED/Pt/GDL/[C4mim][BF4]) are shown in Fig. 3.7. Figures clearly show that an increase in the applied potential influences the morphology of Pt deposit

and change in potential from -2.4 V to -2.6 V significantly enhances the particle growth, leading to the formation of denser deposits. Denser deposits of Pt occurred at -2.5 V and -2.6 V compared to the deposit at -2.4 V, which eventually reduces the effective catalytic area. Optimum surface coverage and minimum agglomeration was observed for electrodeposited Pt at the potential of -2.4 V. Therefore, the optimum potential of -2.4 V was chosen for electro-deposition. Particle size was found to be less than 100 nm and similar observations were made by Ping et al.¹⁵ and Da Zhang et al.²⁶. Likewise, pulsed electrodeposition of Pt on GDL was carried out at the applied potential of -2.4 V. The FESEM image of pulsed electrodeposited Pt on GDL using [C4mim][BF4] ionic liquid (PED/Pt/GDL/[C4mim][BF4]) is also shown in Fig. 3.7 and this indicates a clear distinction between the particles.

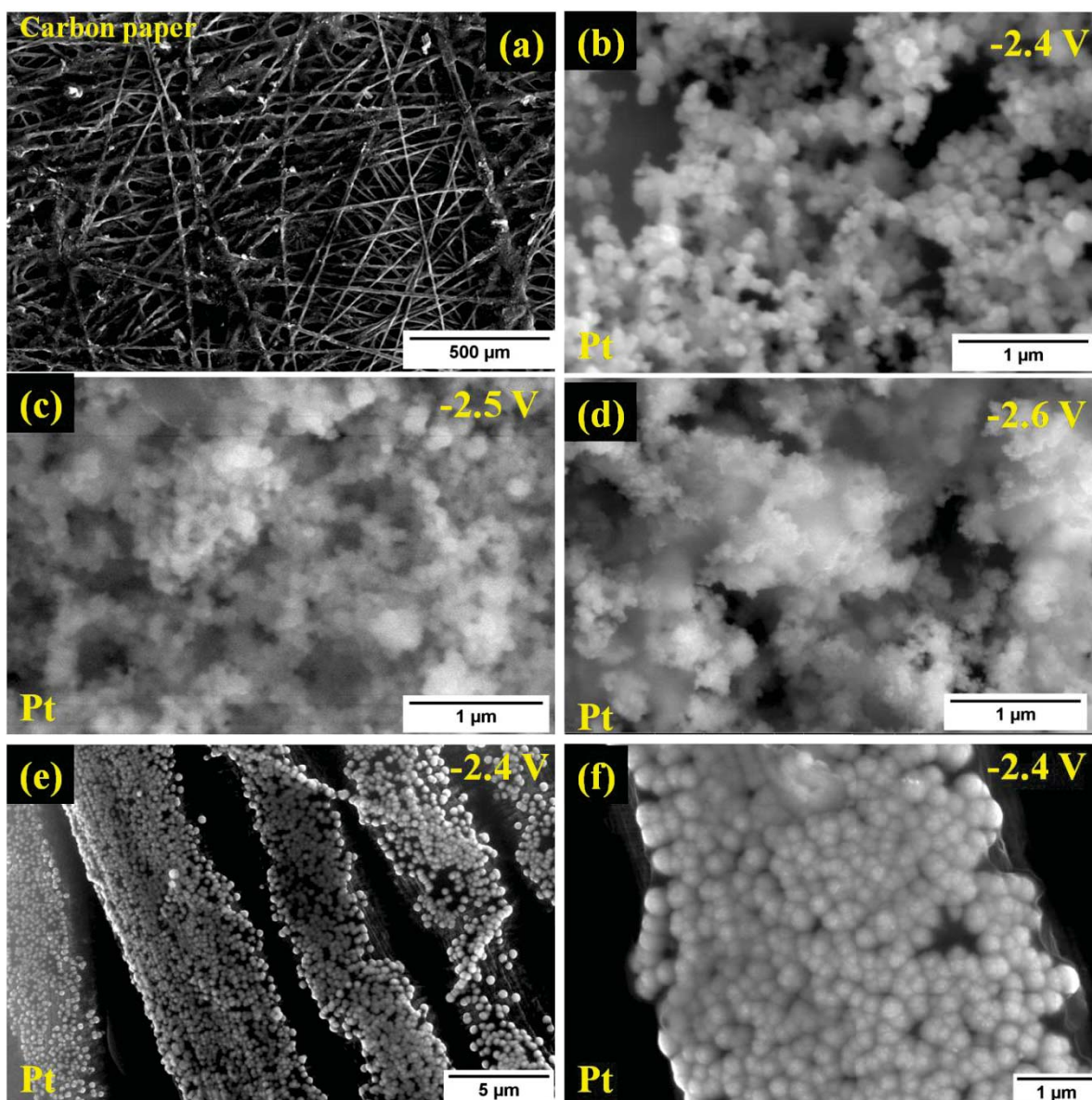


Fig. 3.7 Field emission scanning electron microscope images of (a) gas diffusion layer (GDL) electrodeposited Pt/GDL at the applied potential of (b) -2.4 V, (c) -2.5 V and (d) -2.6 V, and pulsed electrodeposited Pt/GDL at (e) -2.4 V (f) 1 μm resolution

Grazing incidence X-ray diffraction pattern of ED/Pt/GDL/[C4mim][BF₄] and PED/Pt/GDL/[C4mim][BF₄] are shown in Fig. 3.8. Peaks are of low intensity with broadening denoting the deposited particles are in nano range. Peaks at 39°, 46° and 67° are identified to be fcc structure of Pt (JCPDS No. 040802) with planes of (111), (200) and (220) respectively. Smaller crystallites of Pt were obtained for pulsed electrodeposited samples when compared to electrodeposited samples as seen from Table 3.3.

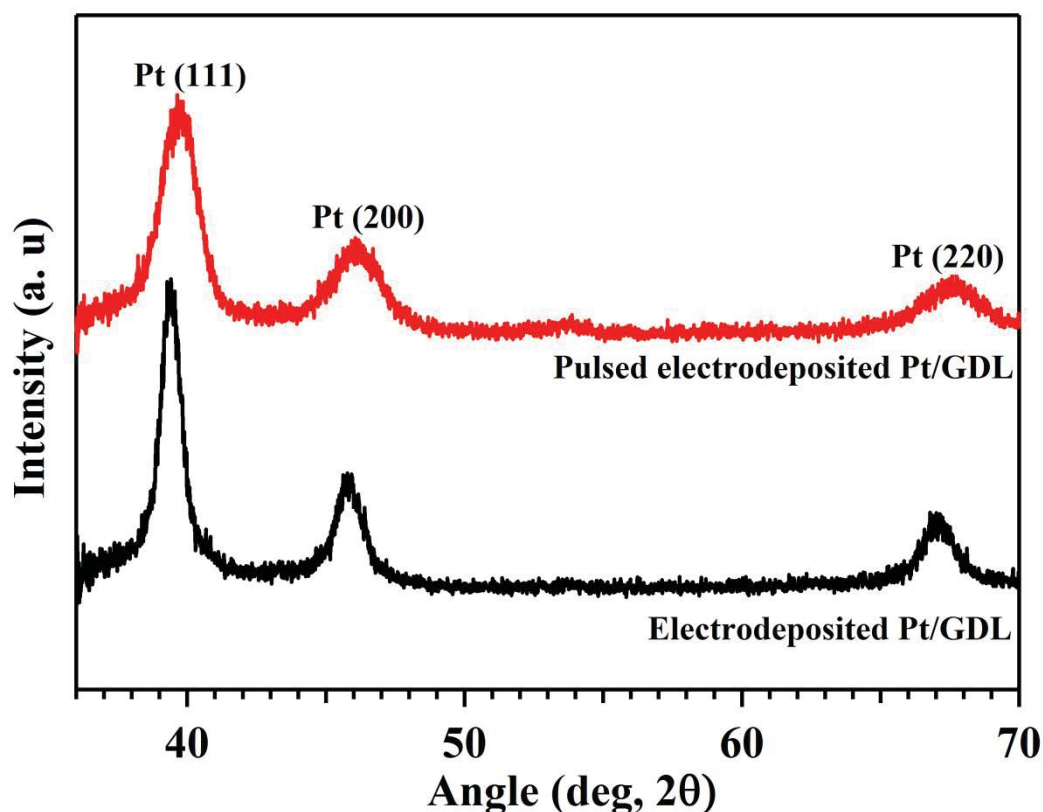


Fig. 3.8 Grazing incidence X-ray diffraction pattern of Pt on gas diffusion layer (a) electrodeposited and (b) pulsed electrodeposited

Table 3.3 Crystallite sizes of electrodeposited Pt on gas diffusion layer (Pt/GDL) and pulsed electrodeposited Pt/GDL from [C4mim][BF₄] ionic liquid electrolyte

Angle (2θ) (Pt)	ED/Pt/GDL/[C4mim][BF ₄] d (nm)	PED/Pt/GDL/[C4mim][BF ₄] d (nm)
39.4° (111)	8.0±1.0	5.0±0.32
46.0° (200)	7.3±1.21	4.6±0.5
67.5° (220)	7.0±1.03	4.1±0.31

Note: Electrodeposited and pulsed electrodeposited Pt on GDL using [C4mim][BF₄] ionic liquid electrolyte are indicated as ED/Pt/GDL/[C4mim][BF₄] and PED/Pt/GDL/[C4mim][BF₄] respectively

3.3.1.3 Preparation/deposition of Pd electrocatalyst on gas diffusion layer from aqueous electrolyte

Field emission scanning electron microscope images of electrodeposited (ED/Pd/GDL/AQ) and pulsed electrodeposited (PED/Pd/GDL/AQ) Pd on GDL using aqueous electrolyte are

given in Fig. 3.9. This figure indicates spherical particles with larger agglomerates of electrodeposited Pd whereas uniform distribution with spherical particles is observed for pulsed electrodeposited Pd.

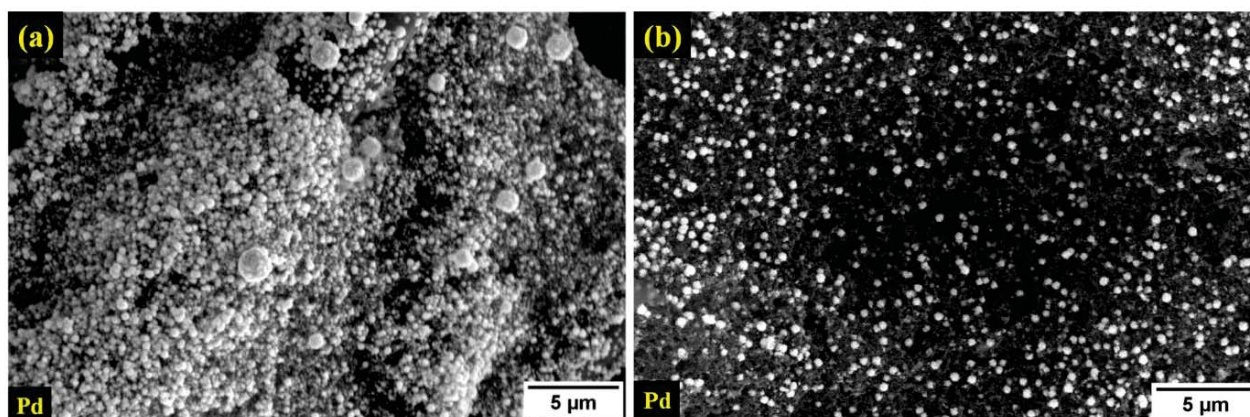


**Fig. 3.9 Field emission scanning electron microscope images of Pd on gas diffusion layer
(a) electrodeposited and (b) pulsed electrodeposited**

GIXRD pattern of ED/Pd/GDL/AQ and PED/Pd/GDL/AQ (Fig 3.10) shows peaks at 39.6° , 46.2° and 67.5° and are matching with palladium fcc structure (JCPDS Data No: 7440.06.4). Crystallite sizes of PED/Pd/GDL/AQ are found to be less than ED/Pd/GDL/AQ as shown by Table 3.4. Both FESEM and GIXRD pattern confirms the formation of nanoparticles of palladium.

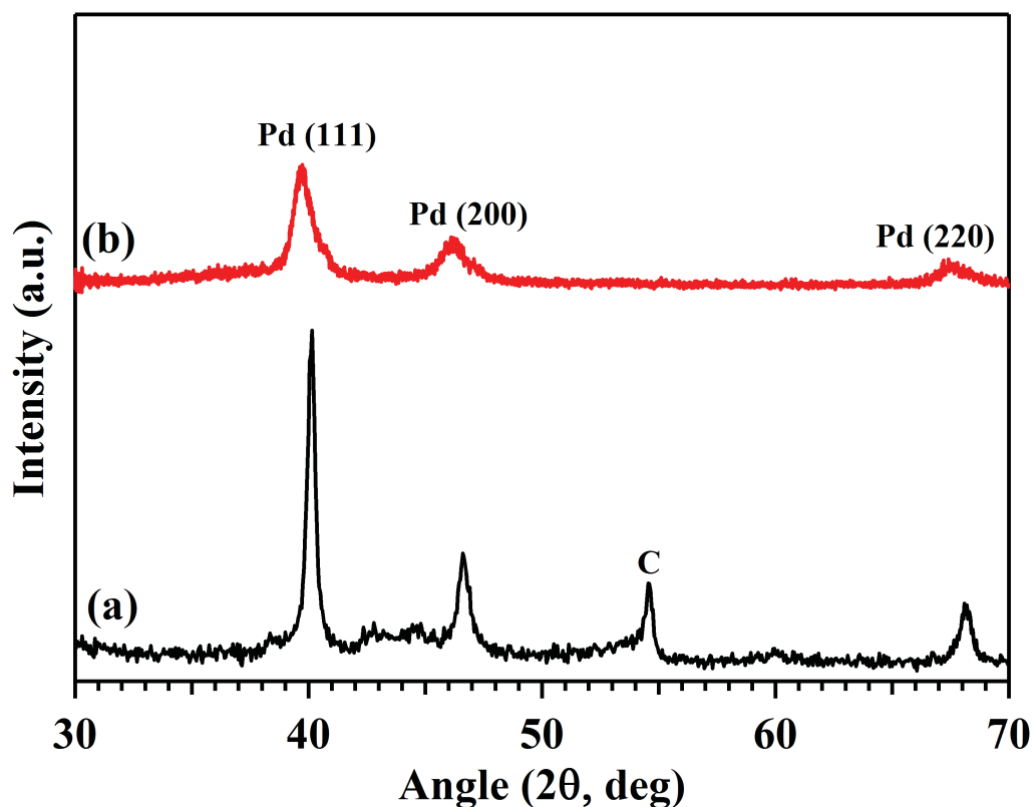


Fig. 3.10 Grazing incidence X-ray diffraction pattern of Pd on gas diffusion layer (a) electrodeposited and (b) pulsed electrodeposited

Table 3.4 Crystallite sizes of electrodeposited and pulsed electrodeposited Pd on gas diffusion layer using aqueous electrolyte

Angle (2θ)	Planes	ED/Pd/GDL/AQ d (nm)	PED/Pd/GDL/AQ d (nm)
39.6°	(111)	11.42±0.30	8.97±0.23
46.2°	(200)	14.94±0.12	9.37±0.10
67.5°	(220)	9.28±0.50	10.40±0.05

Note: electrodeposited and pulsed electrodeposited Pd on gas diffusion layer using aqueous electrolyte are indicated as ED/Pd/GDL/AQ and PED/Pd/GDL/AQ respectively

3.3.1.4 Preparation/deposition of Pd electrocatalyst on gas diffusion layer from

[C4mim][Cl] ionic liquid electrolyte

Electrochemical window of synthesized [C4mim][Cl] ionic liquid electrolyte is found to be 2.5 V i.e. from -1.7 to 0.8 V as shown in Fig. 3.11 (a). Jayakumar et al. also observed similar window for the [C4mim][Cl] ionic liquid electrolyte ¹⁵⁰⁻¹⁵³.

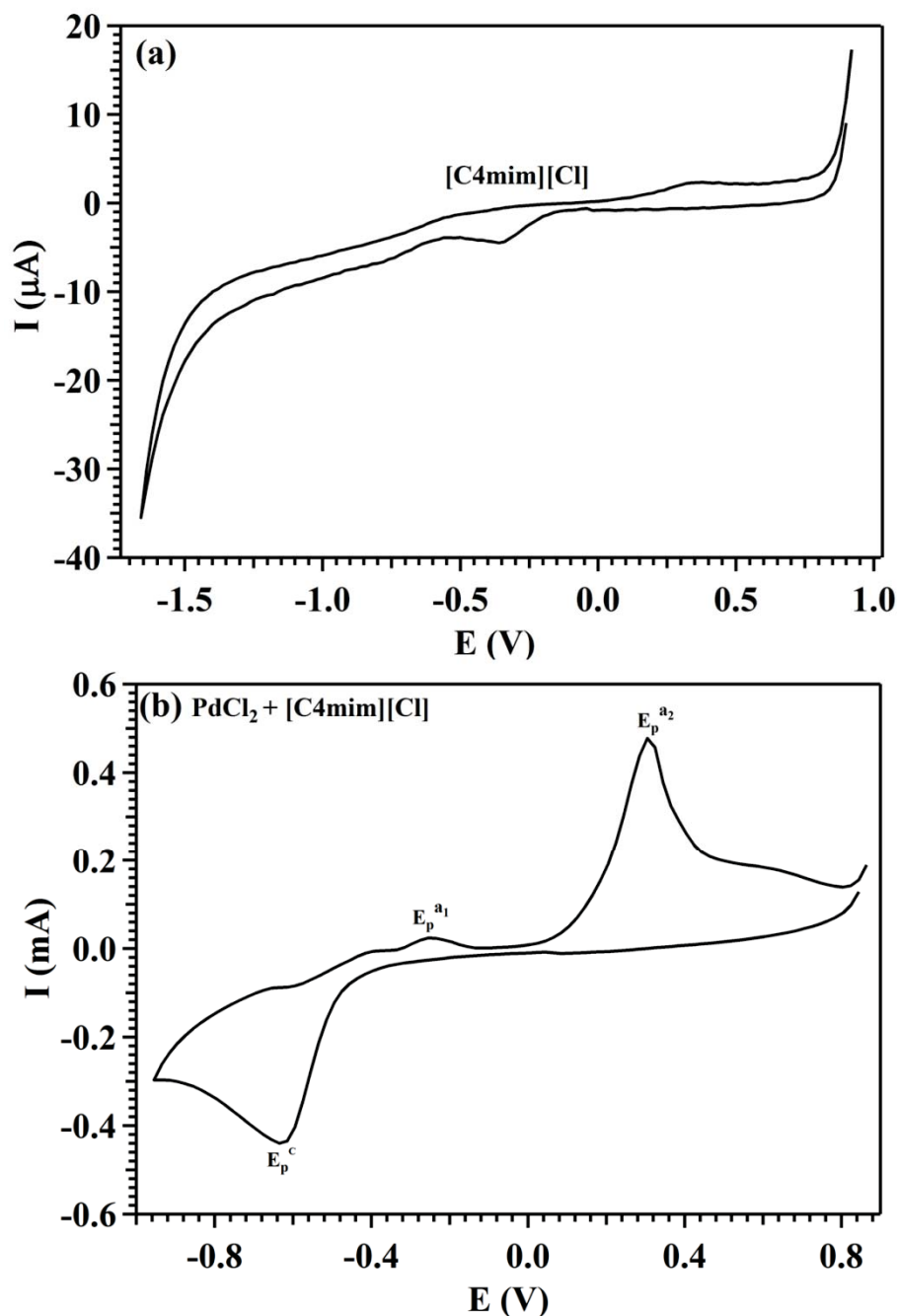


Fig. 3.11 Cyclic voltammogram of (a) 1-butyl-3-methylimidazolium chloride electrolyte (scan rate: 10 mV/s) and (b) $\text{PdCl}_2 + [\text{C4mim}][\text{Cl}]$ (scan rate: 10 mV/s); working electrode: GDL, counter electrode: glassy carbon, reference electrode: Pt wire

Thereafter, CV was conducted in $\text{PdCl}_2 + [\text{C4mim}][\text{Cl}]$ electrolyte to find the deposition potential of Pd on GDL. CV of Pd (Fig. 3.11 (b)) indicates a peak (E_p^c) at -0.63 V (Vs. Pt) and is due to the reduction of Pd (II) to Pd (0). The two oxidation peaks at -0.24 V ($E_p^{a_1}$) and 0.31 V ($E_p^{a_2}$) were observed when the scan was reversed from -0.95 V . Jayakumar et al.¹⁵⁰ studied the nucleation and growth behaviour of Pd on glassy carbon electrode using $\text{PdCl}_2 + [\text{C4mim}][\text{Cl}]$ as electrolyte. They reported that Pd on glassy carbon electrode followed the 3D instantaneous growth model. Electrodeposition of Pd on gas diffusion layer was carried out at four different deposition potentials close to the reduction peak potential (-0.79 V). The deposition potentials used were (-0.8 V , -0.9 V , -1.0 V & -1.1 V) and deposition were carried out for 2 h using $[\text{C4mim}][\text{Cl}]$ electrolyte.

Field emission scanning electron microscope images of ED/Pd/GDL/ $[\text{C4mim}][\text{Cl}]$ at various applied potentials are shown in Fig. 3.12. FESEM images of Pd show that increase in the applied potential influences morphology of the deposit¹⁵⁴. FESEM images indicate that the surface coverage is insufficient at -0.8 V and -0.9 V while at -1.1 V non uniform deposit with large lumps of Pd. At -1.0 V , uniform Pd deposits with good surface coverage was obtained, which is expected to give better catalytic activity compared to the deposits at higher or lower potentials. Hence the optimum potential of -1.0 V was selected for ED and PED of Pd on GDL. FESEM image of pulsed electrodeposited (Fig. 3.12 f) Pd shows separate particles with uniform distribution.

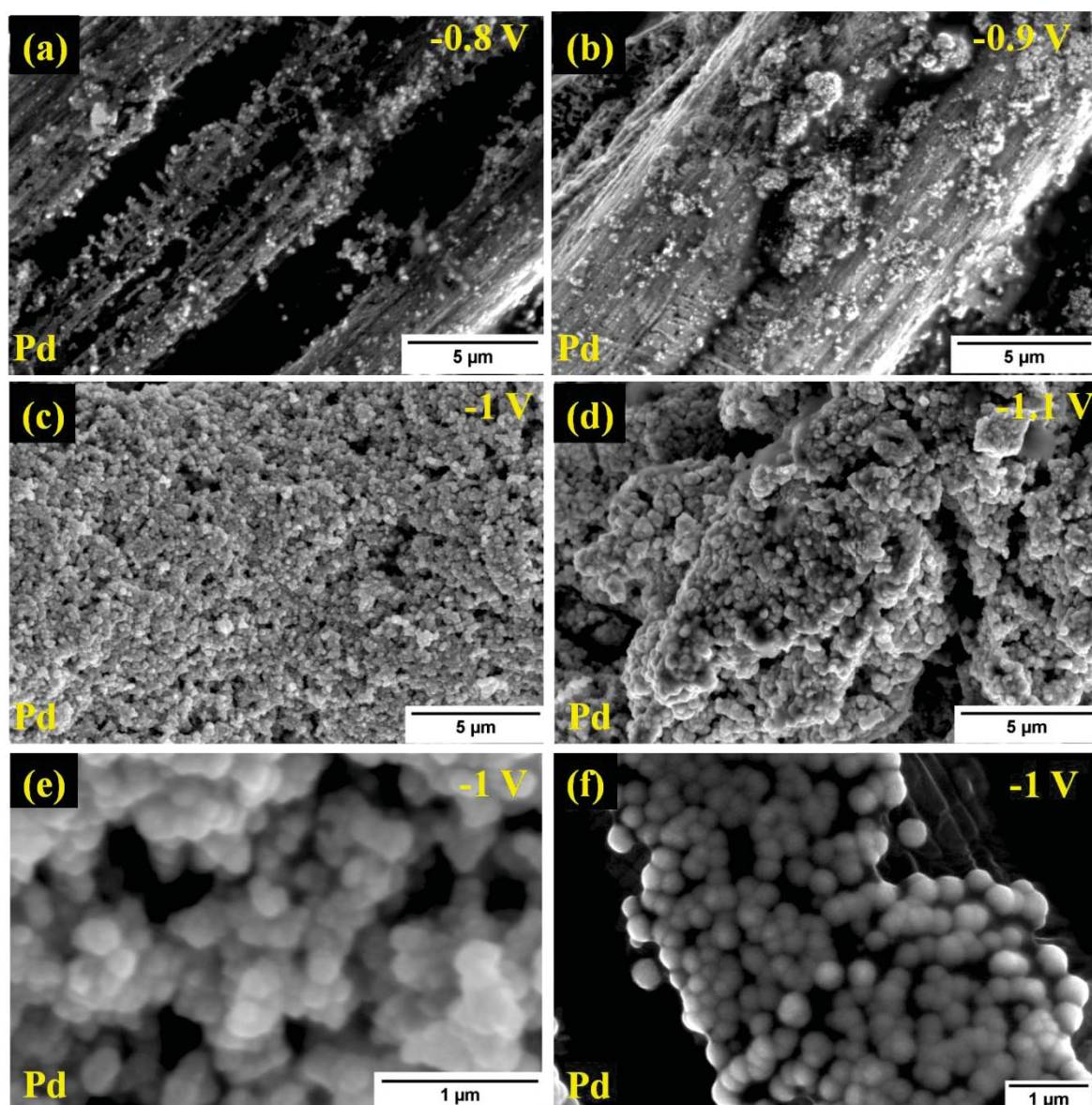


Fig. 3.12 Field emission scanning electron microscope images of electrodeposited Pd on gas diffusion layer using [C4mim][Cl] electrolytes at the applied potentials of (a) -0.8 V, (b) -0.9 V, (c) -1 V, (d) -1.1 V, (e) -1 V at 1 μm and (f) pulsed electrodeposited Pd at -1 V

FESEM images reveal that the Pd nanoparticles obtained are spherical in nature with an average size less than 100 nm. The reduction in size could also be due to the possible adsorption of RTIL onto the surface of the Pd due to its low interface tension. This reduces the tendency of the electrodeposited metal to undergo Ostwald Ripening¹⁵⁵. Moreover, the absence of oxygen functional groups on GDL due to the presence of supramolecular RTIL plays an important role in uniformly distributed nanoparticles across the GDL¹⁵⁶. The

particle sizes are uniform and the deposits are distributed over the entire surface of the GDL. Usage of IL for electrodeposition and pulsed electrodeposition has improved the adhesion of the deposit onto the substrate as compared to the aqueous electrolytes since it is devoid of H₂ evolution.

The energy dispersive X-ray spectrum of electrodeposited Pd on GDL using [C4mim][Cl] ionic liquid (ED/Pd/GDL/[C4mim][Cl]) illustrated in Fig. 3.13 shows the elemental signature of Pd. Hence, this confirms the presence of Pd nanoparticles.

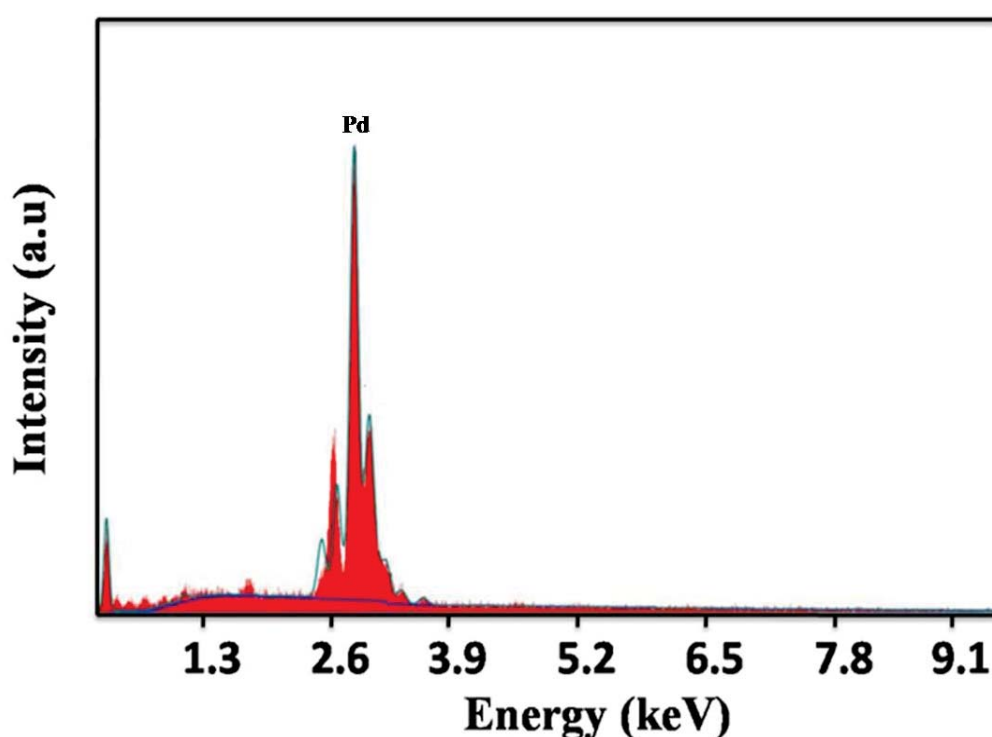


Fig. 3.13 Energy dispersive X-ray analysis of electrodeposited Pd on gas diffusion layer using [C4mim][Cl] electrolyte

Grazing incidence X-ray diffraction pattern of Pd shows peaks at 2θ values 40.2° , 46.6° , 68.1° as shown in Fig. 3.14, and corresponds to fcc with planes of (111) (200) and (220), respectively. The patterns match well with the JCPDS Data No: 7440.06.4. The other peak at 2θ value of 54° is from the GDL substrate and indexed to the JCPDS Data No: 89-8487¹⁵⁷. The crystallite sizes of ED/Pd/GDL/[C4mim][Cl] and pulsed electrodeposited Pd on GDL

using [C4mim][Cl] ionic liquid (PED/Pd/GDL/[C4mim][Cl]) are in the range of 10.7 to 17 nm and 4.25 to 7.11 nm as indicated in Table 3.5. Pulsed electrodeposited Pd on GDL has lesser crystallite size than that of electrodeposited.

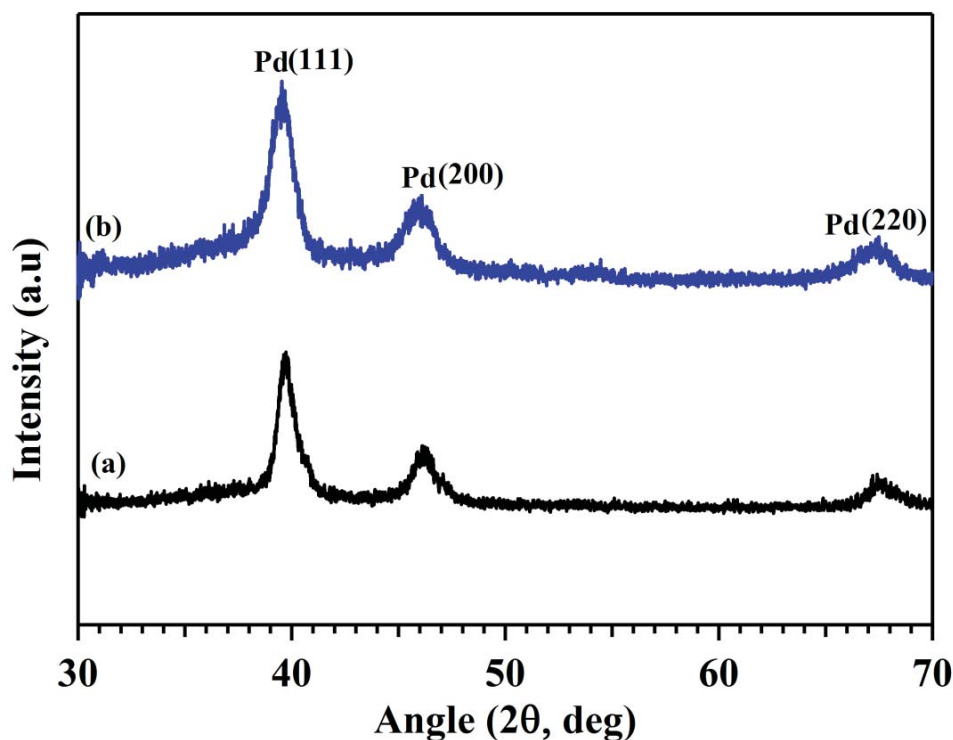


Fig. 3.14 Grazing incidence X-ray diffraction pattern of Pd on gas diffusion layer using [C4mim][Cl] electrolyte (a) electrodeposited and (b) pulsed electrodeposited

Table 3.5 Bragg angle and crystallite sizes of electrodeposited and pulsed electrodeposited Pd using [C4mim][Cl] electrolyte

Angle (2θ) (Pd)	ED/Pd/GDL/[C4mim][Cl] d (nm)	PED/Pd/GDL/[C4mim][Cl] d (nm)
40.11°(111)	12.12±0.66	5.03±0.20
46.64 (200)	10.60±0.32	4.25±0.33
68.15 (200)	16.80±0.34	7.11±0.45

Note: Electrodeposited and pulsed electrodeposited Pd on gas diffusion layer on GDL using [C4mim][Cl] ionic liquid electrolyte are represented as ED/Pd/GDL/[C4mim][Cl] and PED/Pd/GDL/[C4mim][Cl] respectively

Strong adhesion of electrocatalyst on GDL provides improved integrity and facilitates good electrochemical contact at electrode/electrolyte interface when it is used as electrocatalyst.

Scratch tests were carried out on the electrodeposited samples to see the adhesion of the electrocatalyst prepared using both aqueous and ionic liquid electrolytes. For instance, ED/Pd/GDL/[C4mim][Cl] and ED/Pd/GDL/AQ samples were taken for testing the adhesion. The scratch test of ED/GDL/Pd/AQ displayed a critical failure of the coating even at a minimal load of 1 N as shown in Fig. 3.15 (a). The scratch plot and SEM micrograph of Pd deposited GDL in RTIL medium is shown in Fig. 3.15 (b). The plot indicates absence of any such adhesive failure in the coating up to a test load of 2N. However, the load after 2 N produced only perforation in the coated layer, while other types of deformations such as buckling or spallation are not observed. Electrodeposited Pd via aqueous and RTIL electrolytes, using RTIL is observed to exhibit low defect density and superior coating morphology.

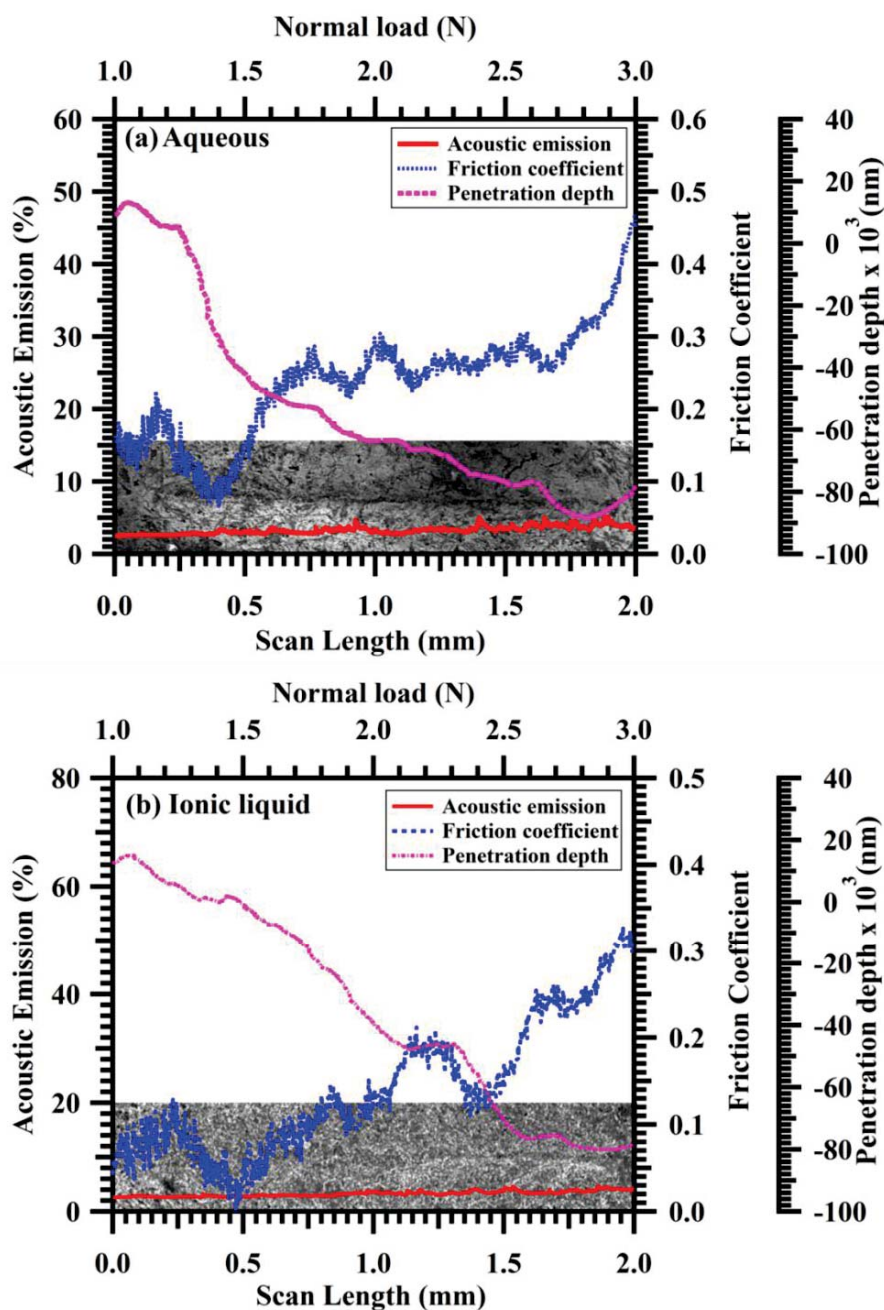


Fig. 3.15 Scratch plot and scanning electron micrograph of electrodeposited (a) Pd using PdCl_2/HCl electrolyte and (b) Pd from $\text{PdCl}_2/[\text{C4mim}][\text{Cl}]$ electrolyte

3.3.1.5 Preparation/deposition of Pt_xPd_y alloy electrocatalyst on gas diffusion layer from aqueous electrolyte

Alloying of Pt with Pd greatly improves the electrocatalytic activity due to the modification in the electronic structure of Pt. Electrodes with different compositions of Pt_xPd_y alloy were prepared by PED using different concentrations of electrolyte solution. ICP-MS analysis of

pulsed electrodeposited Pt_xPd_y indicated concentrations of Pt_1Pd_3 , Pt_1Pd_1 and Pt_4Pd_1 for the electrolyte concentrations of 3 mM PdCl_2 + 1 mM K_2PtCl_6 , 3 mM PdCl_2 + 3 mM K_2PtCl_6 and 1 mM PdCl_2 + 3 mM K_2PtCl_6 . The chemical compositions of the deposited Pt_xPd_y alloy were determined by ICP-MS analysis and EDAX spectroscopy are found to be $\text{Pt}_{28}\text{Pd}_{72}$, $\text{Pt}_{54}\text{Pd}_{46}$ and $\text{Pt}_{80}\text{Pd}_{20}$ for electrolyte concentrations of 3 mM PdCl_2 + 1 mM K_2PtCl_6 , 3 mM PdCl_2 + 3 mM K_2PtCl_6 and 1 mM PdCl_2 + 3 mM K_2PtCl_6 respectively. The EDAX spectrum of Pt_xPd_y alloys are shown in Fig. 3.16.

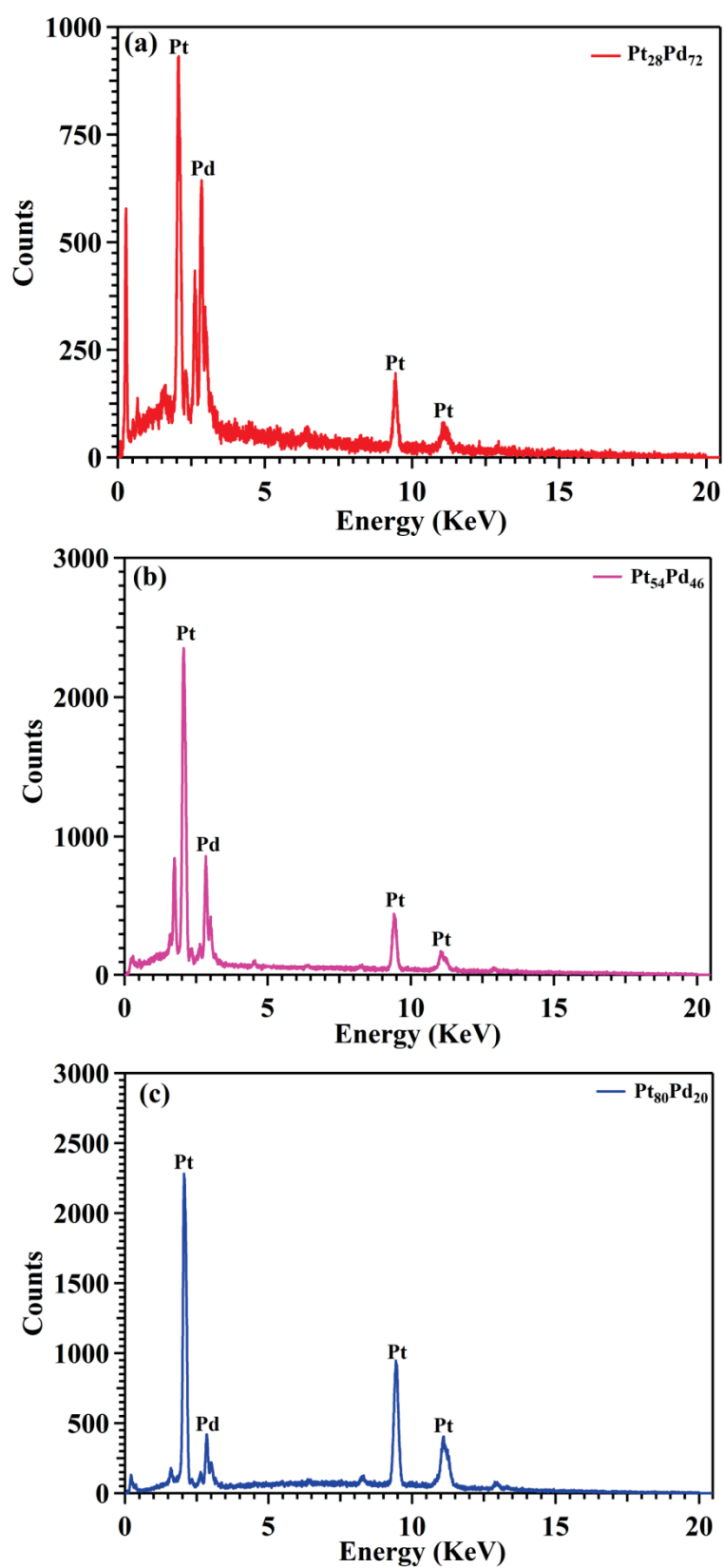


Fig. 3.16 Energy dispersive X-ray analysis of pulsed electrodeposited catalyst on gas diffusion layer using aqueous electrolyte (a) $\text{Pt}_{80}\text{Pd}_{20}$, (b) $\text{Pt}_{54}\text{Pd}_{46}$ and (c) $\text{Pt}_{28}\text{Pd}_{72}$

Field emission scanning electron microscope images of pulsed electrodeposited Pt_xPd_y alloy on GDL using aqueous electrolyte at a pulse width of 10 ms and at 0.2 ms (PED/ Pt_xPd_y /GDL/AQ) with various compositions of Pt_xPd_y alloys (PED/ $Pt_{28}Pd_{72}$ /GDL/AQ, PED/ $Pt_{54}Pd_{46}$ /GDL/AQ PED/ $Pt_{80}Pd_{20}$ /GDL/AQ) are shown in Fig. 3.17. It is evident from the figure that particles deposited are spherical in shape. In order to ascertain the distribution of Pt and Pd in Pt_xPd_y alloy on GDL, EDAX mapping was carried out. The profile indicates that Pt and Pd (Fig. 3.17 d and e) are well covered over the surface of GDL. The alloy formation of Pt_xPd_y is evident from the merged mapping of Pt and Pd (Fig. 3.17 f).

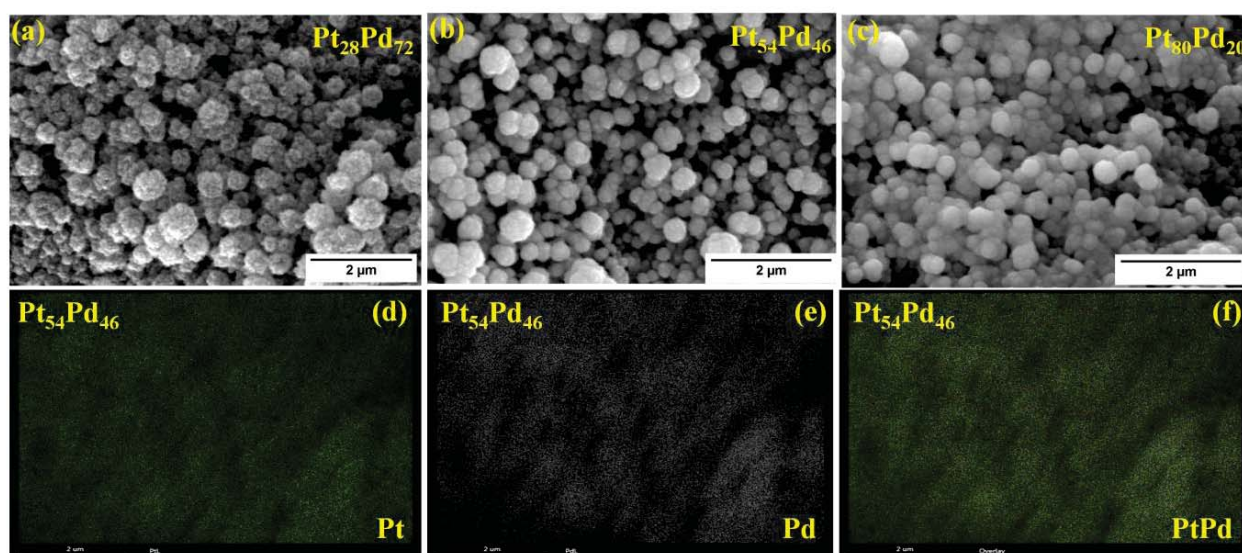


Fig. 3.17 Field emission scanning electron microscope images of pulsed electrodeposited of catalyst on gas diffusion layer using aqueous electrolyte (a) $Pt_{28}Pd_{72}$, (b) $Pt_{54}Pd_{46}$ and (c) $Pt_{80}Pd_{20}$. Energy dispersive X-ray mapping of $Pt_{54}Pd_{46}$ alloy (d) Pt, (e) Pd and (f) merging of Pt and Pd

Grazing incidence X-ray diffraction pattern of Pt, $Pt_{28}Pd_{72}$, $Pt_{54}Pd_{46}$ and $Pt_{80}Pd_{20}$ are shown in Fig. 3.18. Pt peaks are interpreted with JCPDS data card no. 7440.05.3 which are characteristics of fcc. The peaks correspond to the planes of (111), (200) and (220). The (111) plane was used to calculate the lattice parameter and crystallite size. GIXRD of $Pt_{28}Pd_{72}$, $Pt_{54}Pd_{46}$ and $Pt_{80}Pd_{20}$ show peaks with a shift in 2θ value to that of Pt as well as Pd. The

atomic radii of Pt (0.139 nm) and Pd (0.137 nm) ¹⁵⁸ are very close. Bragg angle and lattice parameter are indicated in Table 3.6. The 2θ value of Pt rich $\text{Pt}_{80}\text{Pd}_{20}$ is shifted to higher value compared to that of Pt. The inclusion of Pd to the larger size Pt has lead to the increased lattice parameter of $\text{Pt}_{80}\text{Pd}_{20}$, whereas ¹⁵⁹ addition of Pt to smaller size Pd does not alter the lattice parameter in $\text{Pt}_{28}\text{Pd}_{72}$ as seen from Table 3.6. Intermediate lattice parameter and 2θ are observed for the similar ratios of Pt and Pd ($\text{Pt}_{54}\text{Pd}_{46}$). Peak shift and change in lattice parameter indicate the formation of Pt_xPd_y alloy ¹⁶⁰⁻¹⁶². EDAX mapping also confirms alloy formation. Crystallite sizes of the present electrodes are given in Table 3.6, and the sizes are observed in the range between 8 and 11 nm.

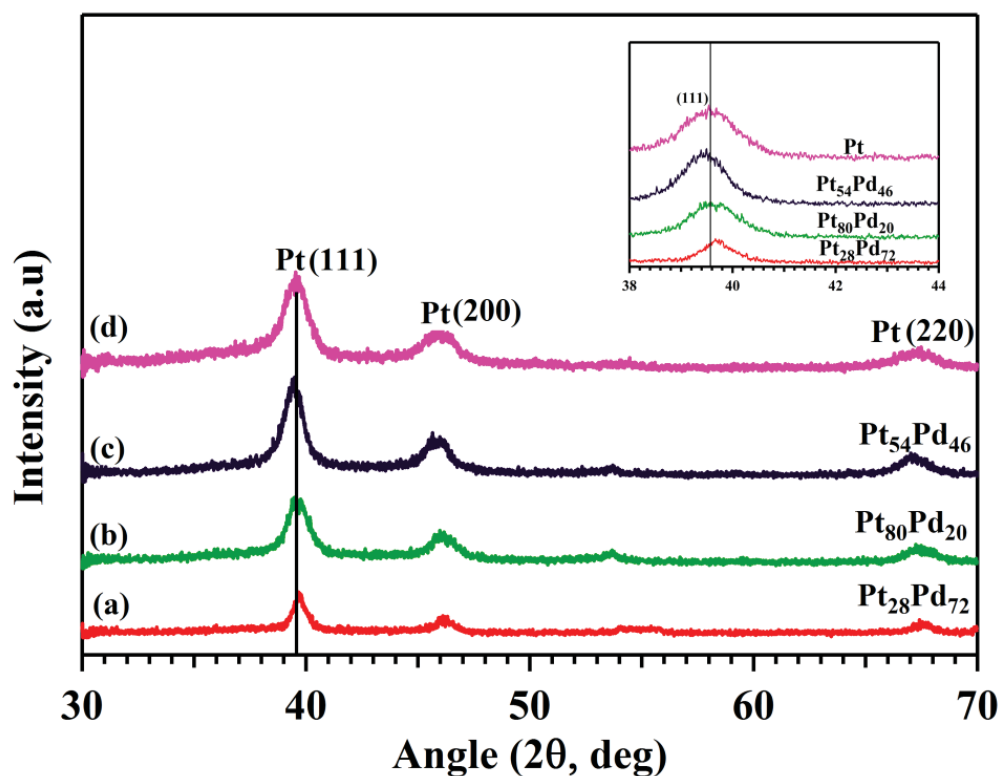


Fig. 3.18 Grazing incidence X-ray diffraction pattern of pulsed electrodeposited of catalyst on gas diffusion layer using aqueous electrolyte (a) $\text{Pt}_{28}\text{Pd}_{72}$, (b) $\text{Pt}_{80}\text{Pd}_{20}$, (c) $\text{Pt}_{54}\text{Pd}_{46}$ and (d) Pt

Inset: Expanded image of Pt_xPd_y electrodes of (111) plane

Table 3.6 Bragg angle, lattice parameter and crystallite sizes of pulsed electrodeposited Pt₂₈Pd₇₂, Pt₅₄Pd₄₆ and Pt₈₀Pd₂₀ on gas diffusion layer

Pt _x Pd _y alloy	Angle (2θ) (111)	Lattice parameter (nm)	Crystallite size d (nm)
Pt ₂₈ Pd ₇₂	39.63° ± 0.09	0.392	7.54±0.23
Pt ₅₄ Pd ₄₆	39.43° ± 0.14	0.393	7.74±0.15
Pt ₈₀ Pd ₂₀	39.51° ± 0.21	0.396	8.25±0.11

3.4 Conclusions

Pt, Pd and Pt_xPd_y alloy electrocatalysts were deposited on GDL for application in PEMHS. Pt electrocatalysts on GDL were prepared by brush coating, electrodeposition and pulsed electrodeposition methods. The characterization of brush coated, electrodeposited and pulsed electrodeposited Pt on GDL was carried out by FESEM, EDAX and GIXRD. FESEM images indicate larger agglomerates of Pt for brush coated samples compared to electrodeposited ones. Hence, further studies were carried out only on electrodeposited and pulsed electrodeposited electrodes. Electrodeposition and pulsed electrodeposition of Pt and Pd were carried out by using both aqueous and ionic liquid electrolytes. On comparing the morphology and microstructure of electrodeposited and pulsed electrodeposited Pt and Pd electrocatalyst, pulsed electrodeposition method is found to be highly suitable for getting good catalytic area for application in PEMHS. Pt_xPd_y alloys of three different compositions were electrodeposited by PED on GDL using aqueous electrolyte and characterized. GIXRD of the samples confirmed the formation of Pt_xPd_y alloy. The GIXRD pattern also showed the change in lattice parameter of Pt_xPd_y alloy compared to Pt because of alloying. Compositional analyses of three alloys were carried out by EDAX spectroscopy. EDAX analysis indicated the alloy composition to be Pt₂₈Pd₇₂, Pt₅₄Pd₄₆ and Pt₈₀Pd₂₀.

Chapter 4

Development of PEM fuel cell based amperometric H₂ sensor with catalyst deposited gas diffusion electrode

4.1 Introduction

Hydrogen measurement is a technical challenge and extensive R&D is carried out to develop sensors for the purpose. Sensors based on catalytic oxidation of hydrogen¹⁶³, thermal conductivity¹⁶⁴, resistance change³, and electrochemical devices¹⁶⁵ have been reported. Pellistor and thermoelectric catalytic sensors^{14, 166} operate by change-in-resistance as a result of an exothermic reaction between H₂ and oxygen (O₂). Catalytic sensors work at high temperatures, and need the presence of O₂^{163, 164}. Thermal conductivity sensors are very sensitive to the flow rate change of the gas. Metal oxide sensors¹⁶⁵ function as chemoresistors where surface gets altered because of reduction of chemisorbed O₂ by H₂ resulting in change of surface conductivity. Electrochemical sensors^{20, 22, 23} are well established commercially due to miniaturization, low power consumption and operation at ambient temperature. Electrochemical sensors comprise of conductometric, potentiometric and amperometric devices^{20, 22, 23, 165}. Potentiometric sensors¹⁶⁷ give non-linear response, where it relates electromotive force with concentration logarithmically. Hence, potentiometric sensors are suitable to be used in an environment with low concentration of hydrogen. Whereas, an amperometric hydrogen sensor²⁵ responds linearly with the concentration of analyte. Therefore, amperometric sensors can be used for detecting analyte concentrations in a wide range.

Solid electrolyte based sensors are deemed to be superior to those with that of liquid electrolyte since it avoids the leakage of electrolyte, corrosion and impurities associated with liquid electrolyte thereby increasing the lifetime of the sensor¹⁶⁸. Among the solid electrolytes, polymer electrolyte based sensors are found to be efficient due to its ease of

operation and compactness. Nafion¹⁶⁸⁻¹⁷⁰ is a commonly used solid proton conducting polymer electrolyte in amperometric sensors.

Polymer electrolyte based H₂ sensor (PEMHS) is a fuel cell device operating in galvanic mode. The response behaviour of electrochemical sensors is significantly influenced by the three phase boundary (analyte-electrolyte-electrode) at the electrochemical interface at anode hence care has to be taken during the design of a sensor. The following aspects need to be considered before configuring PEMHS: (1) optimum porosity of the electrode to allow the diffusion of analyte to the interface and (2) suitable electrocatalyst with high surface area to increase the rate of redox process. This charge transfer reaction at the interface influences the sensor signal. Various types of diffusion electrodes were developed for the above purpose. In commercially available amperometric hydrogen sensors,²⁵ Pt catalyst slurry was prepared with Teflon solution and was coated on a porous Teflon film and used as sensing electrodes. The porous structure of Teflon allows the electrolyte solutions to flow through and also the hydrophobic nature of Teflon on Pt surface prevents it from being unduly wetted by the electrolyte. Liquid electrolytes impose problems such as leakage of electrolyte, corrosion and impurities, thereby decreasing the lifetime of the sensor¹⁶⁸. Hence, solid polymer membranes are being attempted as electrolyte, typically Nafion (sulphonated tetrafluoroethylene) is used as proton conducting electrolyte due to good conductivity, chemical stability and non permeability to hydrogen. Electrocatalyst film can also be transferred directly onto Nafion membrane via screen printing and decal methods. Coating of catalyst by these methods suffers by agglomeration and this aspect is already discussed in detail in the previous chapter. Present sensor design uses electrodeposited Pt catalyst on gas diffusion layer (carbon paper) as diffusion electrodes and these electrodes are hot pressed on both sides of the Nafion membrane to get better three phase contact, stability and less dependence of response on flow rate. The electrodeposition of catalyst was carried out on Nafion impregnated GDL so that Pt

deposited on the surface which will have both ionic and electronic conductivity. Hence, the present design is aimed to achieve large number of three phase boundaries to have high active area at the electrochemical interface. Thus the present study is an attempt to develop sensor with improved sensitivity, short response time, less flow rate dependence and minimum catalyst loading by employing GDL and ED methods for preparing sensing electrodes of sensor. PED gives high rate of nucleation compared to constant potential ED which enhances the active area of catalyst requiring lower catalyst loading. In this study, development of amperometric H₂ sensor with electrodeposited Pt and Pd on GDL using aqueous and ionic liquid electrolytes are reported. Pulsed electrodeposited Pt_xPd_y alloy on GDL was also attempted to be used as sensing electrodes in PEMHS.

4.2 Experimental

4.2.1 Preparation of membrane electrode assembly

Nafion 117 membrane was pre-treated prior to the preparation of membrane electrode assembly (MEA) by boiling with 3% H₂O₂ solution for 1 h for removing the oxidizable impurities. After that, the membrane was boiled in 0.5 M H₂SO₄ for 2 h to protonate the membrane and then cleaned with boiling de-ionized water for 2 h. Finally, the cleaned membrane was used as the electrolyte. Membrane electrode assemblies were made using the above cleaned membrane.

MEA was prepared by hot-pressing sensing (3 cm²) and counter (3 cm²) electrodes on either side of Nafion membrane at 393 K, 50 bar for 120 s. Sensing and counter electrodes of MEA used in making Pt, Pd and Pt_xPd_y alloy sensors are indicated in Table 4.1. Loading of electrocatalyst was maintained with 0.5 mg/cm².

Table 4.1 Sensing and counter electrodes used for membrane electrode assembly for the application in proton exchange membrane based H₂ sensor

Sensing electrode	Counter electrode
BC/Pt/C/GDL	BC/Pt/C/GDL
ED/Pt/GDL/AQ	ED/Pt/GDL/AQ
PED/Pt/GDL/AQ	PED/Pt/GDL/AQ
ED/Pt/GDL/[C4mim][BF ₄]	ED/Pt/GDL/[C4mim][BF ₄]
PED/Pt/GDL/[C4mim][BF ₄]	ED/Pt/GDL/[C4mim][BF ₄]
PED/Pd/GDL/ AQ	PED/Pt/GDL/ AQ
ED/Pd/GDL/[C4mim][Cl]	BC/Pt/C/GDL
PED/Pt _x Pd _y /GDL/AQ	PED/Pt/GDL/AQ

Note: BC/Pt/C/GDL- Brush coated Pt/C electrocatalysts on gas diffusion layer, electrodeposited and pulsed electrodeposited Pt and Pd on gas diffusion layer using aqueous electrolyte are indicated as ED/Pt/GDL/AQ PED/Pt/GDL/AQ, PED/Pd/GDL/ AQ. Electrodeposited and pulsed electrodeposited Pt and Pd on GDL using [C4mim][BF₄] and [C4mim][Cl] ionic liquid electrolytes are represented as ED/Pt/GDL/[C4mim][BF₄], PED/Pt/GDL/[C4mim][BF₄], ED/Pd/GDL/[C4mim][Cl]. Pulsed electrodeposited Pt_xPd_y alloy on gas diffusion layer using aqueous electrolyte is indicated as PED/Pt_xPd_y/GDL/AQ.

4.2.2 Sensor assembly

Membrane electrode assembly of sensors with different sensing electrodes and counter electrodes indicated in Table 4.1 were assembled in a separate polycarbonate sensor housing discs and tested for H₂ sensing. A pin-hole barrier was positioned at the sensing side to limit the flow of H₂/Ar. In addition to the pin-hole barrier, GDL also acts as the diffusion barrier at the sensing side.

4.2.3 Testing of sensor performance

The assembly of sensor was discussed in chapter 2 (section 2.2.5.2). Sensors were tested for sensing H₂ in the concentration ranges 1 to 5% of H₂/Ar. The current generated during the oxidation of H₂ was acquired using Agilent data acquisition system and data was recorded with respect to time. Different concentrations of H₂ and argon mixtures were prepared by using mass flow controller and it is passed to the sensing side of the sensor and counter

electrode was exposed to atmosphere. The mechanical barrier with pin-hole (0.1 mm) at the sensing side limits the supply for the oxidation of H₂. The response behaviour of the sensors with all the sensing electrodes mentioned in Table 4.1 was recorded towards H₂ in argon atmosphere. Based on the sensor performance, sensors were extensively investigated for repeatability, long-term stability, detection limit etc. of sensors. Sensor response of pulsed electrodeposited Pd based diffusion electrodes prepared using aqueous electrolyte operated in two electrode mode was not satisfactory since it takes much longer response time. Hence, the response behaviour of electrodeposited Pd using [C4mim][Cl] ionic liquid electrolyte based diffusion electrodes were studied in three electrode mode. The potential to be applied for sensing H₂ in three electrode mode was determined by recording cyclic voltammogram separately in argon and H₂ at the sensing side. Cyclic voltammetry was carried out in three electrode mode using Pd diffusion electrode, brush coated Pt/C and Pt wire as working, counter and reference electrodes respectively. The optimum potential was chosen by comparing the CV recorded in argon and H₂, where H₂ signal to baseline (argon) ratio is high. H₂ sensing characteristics were tested by applying of 0.8 V vs Pt wire at the working electrode.

To calculate the detection limit, standard deviation (σ) of baseline value with argon was calculated. The minimum detection limit of the sensor was calculated using the following equation:

$$\text{Detection limit} = \frac{3 \sigma (\mu\text{A})}{\text{Sensitivity } (\mu\text{A/ppm})} \quad (4.1)$$

Influence of temperature, flow-rate and relative humidity were studied for the sensors whose long-term stability was satisfactory. The temperature of the sensor was regulated using mini cooling system for studying the effect of temperature on the sensor signal.

4.2.4 Electrochemical characterization

Electrochemical surface area of BC/Pt/C/GDL, ED/Pt/GDL/AQ and PED/Pt/GDL/AQ were determined by in-situ cyclic voltammetry measurement (hydrogen pump mode)¹⁷¹⁻¹⁷³. In order to measure the ECSA of the sensing electrode, barrier was not incorporated in the assembled sensor at the sensing side. Argon was flown at the sensing side and H₂ was passed at the counter electrode side. Cyclic voltammetry (CV) was performed using multi-potentiostat and the potential was applied in the range 0 to +1 V at the scan rate of 10 mV/s and the stability of the catalyst was studied by recording the CV for 48 h. The obtained current vs voltage plot could be converted in terms of current vs time to calculate the electrochemical surface area. The charge associated with hydrogen desorption region was obtained by integrating the area under the potential range 0 and +0.4 V. ECSA of ED/Pt/GDL/[C4mim][BF₄], PED/Pt/GDL/[C4mim][BF₄], PED/Pd/GDL/AQ, ED/Pd/GDL/[C4mim][Cl] and PED/Pt_xPd_y/GDL/AQ were measured using ex-situ cyclic voltammetry. The evolution of molecular hydrogen could not be controlled in electrochemical surface area measurement using hydrogen pump mode as there was two or three orders of difference was observed between the anodic and cathodic peak. Hence, adopted the procedure reported by Stefan Rudi et al.¹⁷⁴ Cyclic voltammetry was carried out using Pt or Pt_xPd_y alloy on gas diffusion layer as working electrodes in 0.5 M H₂SO₄ electrolyte at the scan rate of 200 mV/s. Pt sheet and Ag/AgCl were used as counter and reference electrodes respectively. The solution was purged with argon continuously. CV scan was optimized in the potential range of -0.2 to 1.2 V vs Ag/AgCl. Cyclic voltammogram of Pt/GDL and Pt_xPd_y/GDL showed a slightly different potential limits for desorption of hydrogen that are mentioned in the respective sub-section. Adsorption region was not taken for ECSA since there was no clear distinction of double layer capacitance. Third cycle of CV was taken for ECSA calculation and the same is shown in the figures. ECSA measured using this method showed

a considerable difference as that of hydrogen pump mode. The charge associated with hydrogen desorption region was obtained by integrating the area and the equation for calculation of electrochemical surface area (ECSA) is given below

$$\text{Electrochemical active area} = \frac{\text{Charge } (\mu\text{C}/\text{cm}^2)}{210 (\mu\text{C}/\text{cm}^2) \times \text{Pt loading } (\text{mg}/\text{cm}^2)} \quad (4.2)$$

210 ($\mu\text{C}/\text{cm}^2$) is the charge correspond to the oxidation of monolayer adsorption/desorption of H_2 on smooth Pt surface.

Impedance spectra were recorded while sensing 4 % H_2/Ar (in-situ) in the frequency range of 100 kHz to 10 mHz at the applied potential of 10 mV for all the sensors. Charge transfer resistance values were estimated by fitting the curve using a simple equivalent circuit for studying the variation in charge transfer resistance at the electrode–electrolyte interface.

4.3 Results and discussions

4.3.1 Sensing mechanism

Amperometric H_2 sensor is a galvanic device in which chemical energy is converted to electrical energy. Sensor signal leads were connected in series with the current measuring device (Agilent 34972 A data acquisition system/switch unit). When the data acquisition system operated in current mode, the system offers minimum input impedance and hence there is no load imposed on the sensor cell. Therefore the sensor was operated in short circuited mode. The cell is represented as $\text{H}_2, \text{M}_a/\text{Nafion}/\text{M}_c, \text{O}_2$ where M_a and M_c represents anode and cathode electrocatalyst respectively. H_2 at the sensing side gets oxidized and oxidized protons are conducted through the proton conducting electrolyte to cathode. The electron produced in the oxidation flows through the external circuit and reaches the cathode.

Oxygen reduction reaction takes place by the reaction of O₂ with proton and electron at the cathode. The overall cell reaction is given below



The flux of H₂/Ar reaching sensing electrode is limited by pin hole diffusion barrier such that HOR becomes the rate-determining step of the electrochemical reaction. The oxidation of H₂ at sensing electrode is diffusion controlled process because of limiting H₂ supply at the anode. The flux is correlated to the concentration of H₂ by Fick's first law of diffusion¹⁷⁵. Faraday's law relates the number of moles of H₂ being pumped per unit time (J) to the current and is given by²⁰

$$J = \frac{I}{2F} \quad (4.4)$$

Fick's first law relates J and concentration gradient by

$$J = AD \frac{\partial C}{\partial x} \quad (4.5)$$

where A - area of electrode (m²), D - diffusion coefficient of H₂ (m²/s), $\frac{\partial C}{\partial x}$ - concentration gradient. By relating equation (4.4) and (4.5) get

$$I = 2FAD \frac{\partial C}{\partial x} \quad (4.6)$$

where I-current (coulombs/s) and F- Faraday's constant (C/mol).

4.3.2 Hydrogen sensing behaviour of PEMHS with Pt/GDL diffusion electrodes

4.3.2.1 Response behaviour of PEMHS with brush coated Pt/GDL, electrodeposited Pt/GDL, pulsed electrodeposited Pt/GDL as sensing electrodes prepared using aqueous electrolyte

Sensor response of PEMHS with brush coated Pt/C catalyst on gas diffusion layer (BC/Pt/C/GDL) and electrodeposited Pt on gas diffusion layer using aqueous electrolyte (ED/Pt/GDL/AQ) for 0.5 % - 4 % H₂/Ar are shown in Fig. 4.1 and Fig. 4.2 respectively. Response of sensor with pulsed electrodeposited Pt on gas diffusion layer using aqueous electrolyte (PED/Pt/GDL/AQ) for 0.5 % - 4 % H₂/Ar is given in Fig. 4.3. Sharp and stable response was observed for PED/Pt/GDL/AQ sensor than ED/Pt/GDL/AQ and BC/Pt/C/GDL sensors. Although the response time of BC/Pt/C/GDL sensor is lesser, noise increases with the rise in the concentration of H₂.

FESEM (Fig. 3.2) image of BC/Pt/C/GDL showed predominant agglomeration of particles, which ultimately reduces three-phase contacts in sensing H₂. Whereas FESEM (Fig. 3.2) images of ED/Pt/GDL/AQ and PED/Pt/GDL/AQ showed a finer distribution of particles, which lead to the enhanced three-phase contacts in the sensors. Further, the adhesion of catalyst onto the support is crucial in sensing application, otherwise during sensor testing the particles have higher tendencies to coalesce to form larger particles. This ultimately affects the sensor performance¹⁷⁶. Pulsed electrodeposition method provides better adhesion compared to the brush coating and electrodeposition methods. The particles are distributed uniformly over the surface in pulsed electrodeposited samples as proven by the FESEM images (Fig. 3.2).

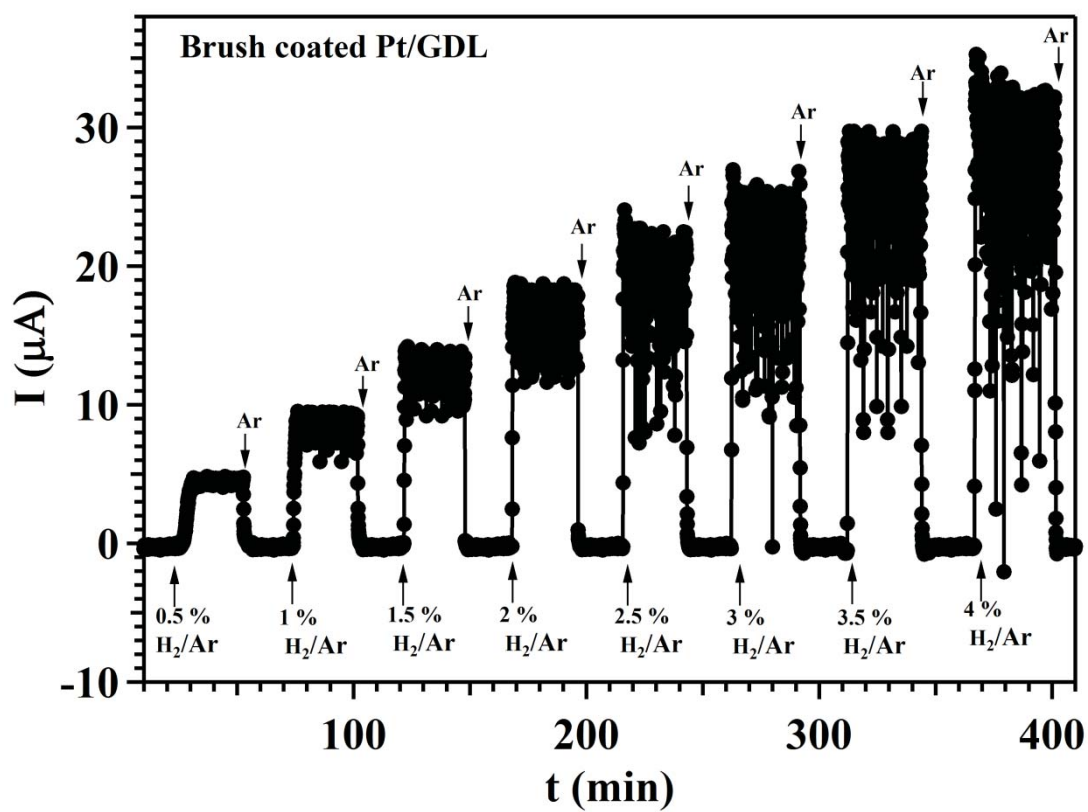


Fig. 4.1 Hydrogen response behaviour of sensor with brush coated Pt on gas diffusion layer

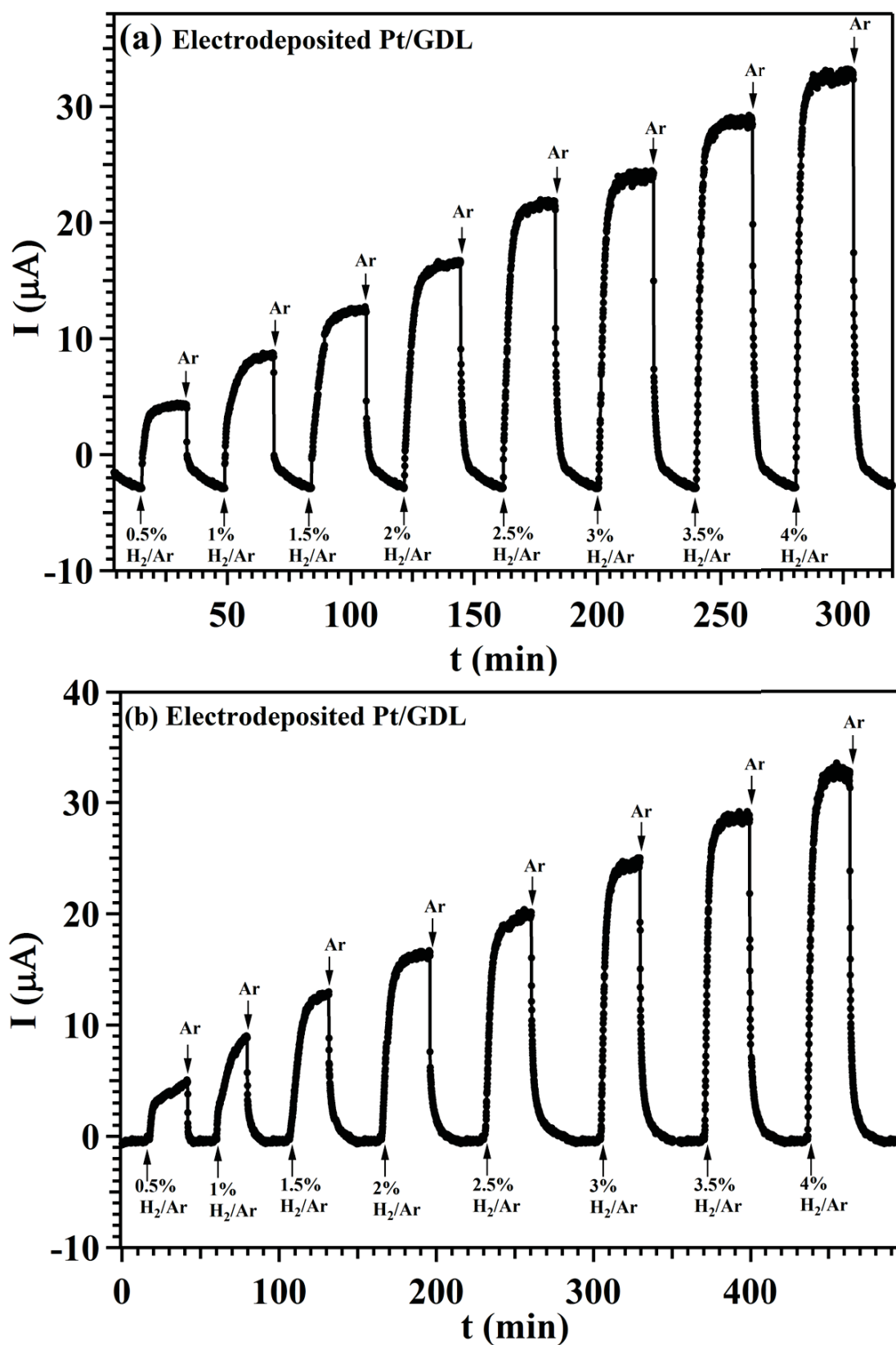


Fig. 4.2 Hydrogen response behaviour of sensor with electrodeposited Pt on gas diffusion layer using aqueous electrolyte (a) initial (b) after 48 h

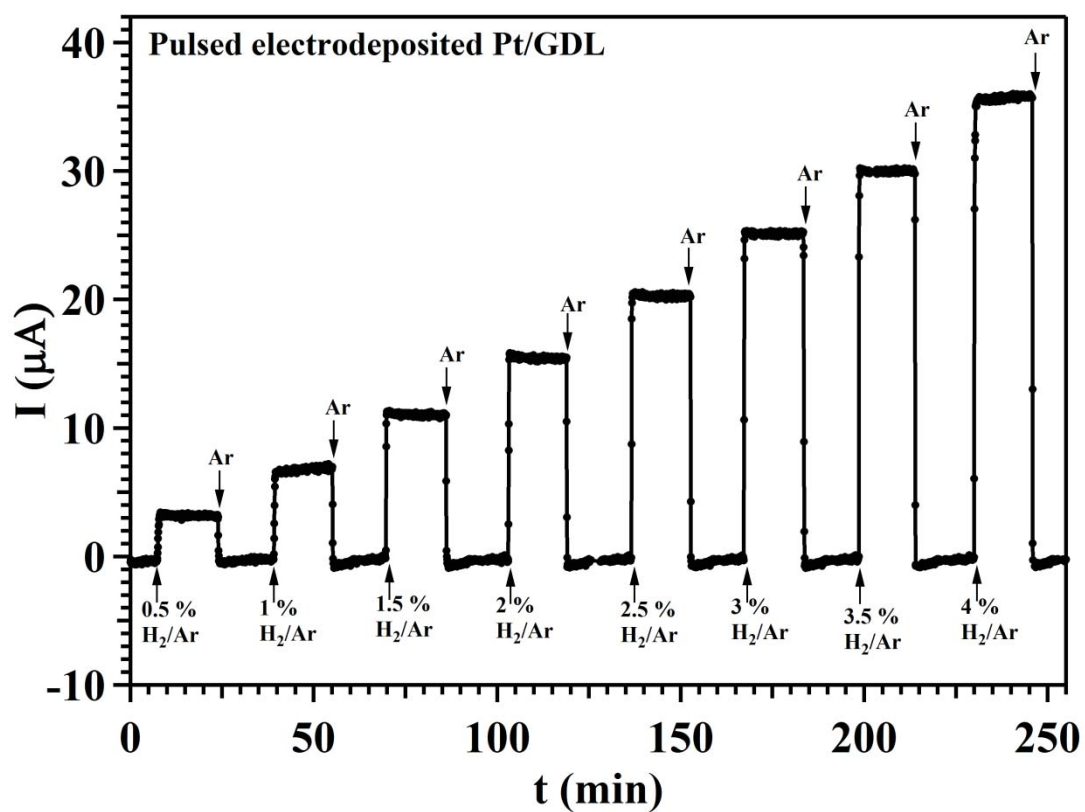


Fig. 4.3 Hydrogen response behaviour of sensor with pulsed electrodeposited Pt on gas diffusion layer using aqueous electrolyte

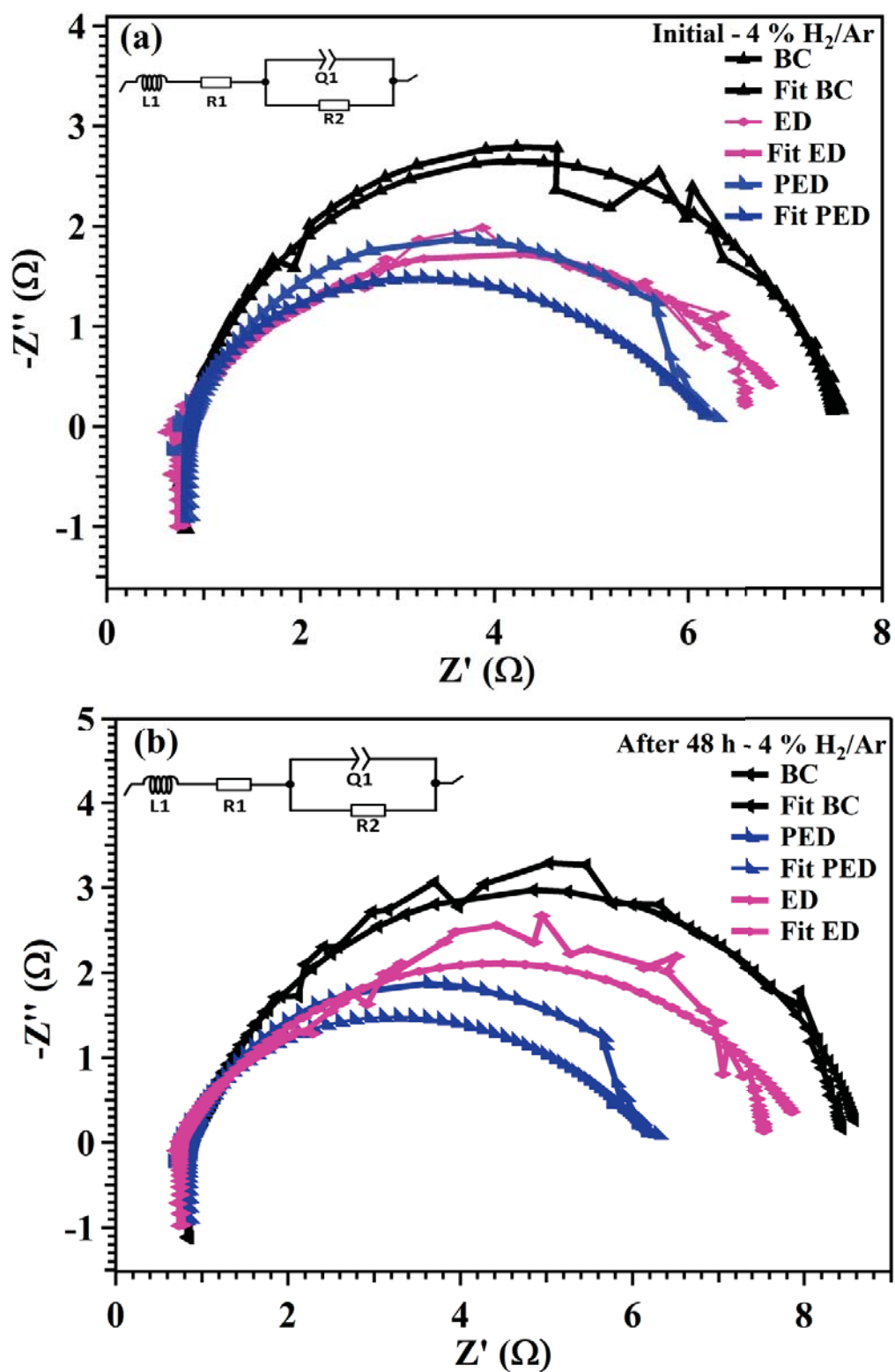


Fig. 4.4 Impedance spectrum of sensors with brush coated (BC), electrodeposited (ED) and pulsed electrodeposited (PED) Pt electrocatalyst on gas diffusion layer (a) initial and (b) after 48 h

In-situ electrochemical impedance spectra of sensors with BC/Pt/C/GDL, ED/Pt/GDL/AQ, and PED/Pt/GDL/AQ were taken initially and after 48 h while passing 4 % H₂/Ar and are shown in Fig. 4.4 (a) and Fig. 4.4 (b). Impedance spectra were recorded from high frequency to low frequency. Impedance spectra illustrate a semicircle which indicates that there is a charge transfer resistance and non-ideal capacitance elements are in parallel combination as shown by the equivalent circuit (Fig. 4.4., inset). The negative value of the impedance at high frequency range observed in Fig. 4.4 corresponds to the inductance offered by the current connecting leads. At extremely high frequency the non-ideal capacitor part acts as short circuit and that of at low frequency non-ideal capacitor behaves as open circuit. Hence, at high frequency the current is completely shunted through the non-ideal capacitor and therefore, the effective impedance is zero. The intercept at high frequency on the real axis corresponds to the ohmic resistance of the electrolyte. In contrast, at low frequency all the current is forced through the resistor and the effective impedance of the model is given by the impedance of the resistor. At intermediate frequency the impedance model will have both non-ideal capacitor and resistor elements. Table 4.2 signifies that PED/Pt/GDL/AQ has much lesser charge transfer resistance and lesser interfacial capacitance leading to the reduced noise and better stability. The higher capacitance, higher charge transfer resistance, less electrochemical active area (Table 4.2) and substantial agglomeration as shown by FESEM image (Fig. 3.2) of BC/Pt/C/GDL sensor elucidate the apparent current fluctuations detected in BC/Pt/C/GDL sensor response¹⁷⁷⁻¹⁷⁹. The response of BC/Pt/C/GDL sensor testing after 48 h denotes only noise and it is ascribed to the fact that the electrode/electrolyte interface has deteriorated. This is explained by the increased capacitance, decreased ECSA and decreased charge transfer resistance values obtained after 48 h of sensor testing. Fig. 4.5 shows the cyclic voltammogram of BC/Pt/C/GDL, ED/Pt/GDL/AQ and PED/Pt/GDL/AQ sensing electrodes taken initially and after 48 h of sensor testing for electrochemical active

area measurement. All the catalysts showed a peak in the hydrogen adsorption-desorption region i.e. from 0 to 0.37 V. ECSA values of the electrodes were calculated by integrating the peak obtained in the hydrogen desorption region. Comparing the voltammogram at initial and after 48 h of BC/Pt/C/GDL and ED/Pt/GDL/AQ electrodes, it is evident that current density has decreased which reflects that the ECSA of the catalyst has changed due to the agglomeration caused during the sensor testing, PED/Pt/GDL/AQ electrode showed only a slight change in ECSA when compared to electrodeposited and brush coated samples.

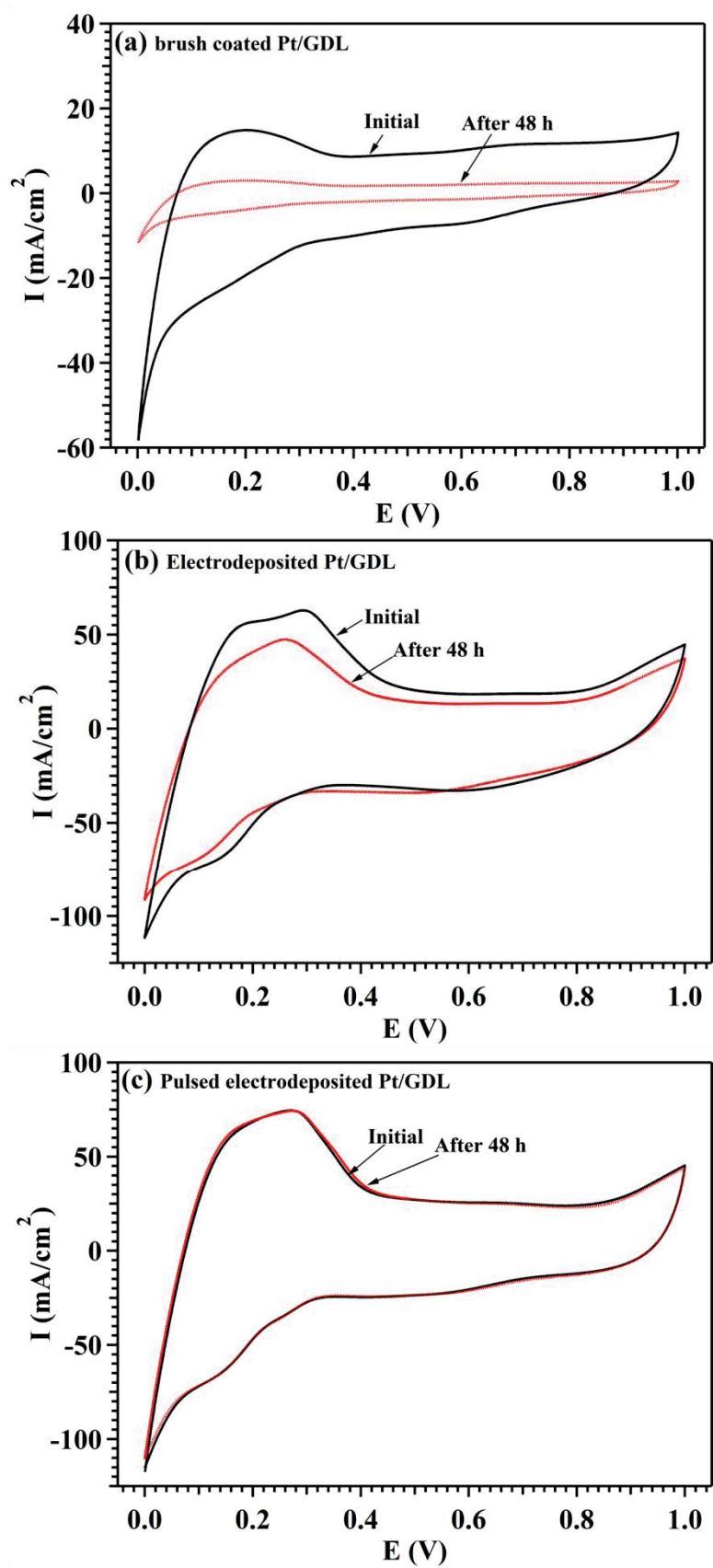


Fig. 4.5 Cyclic voltammogram of sensor with Pt electrocatalyst on gas diffusion layer (a) brush coated, (b) electrodeposited and (c) pulsed electrodeposited

Though noise was lesser in ED/Pt/GDL/AQ sensor, response ($t_{90\%}$) and recovery time (Fig. 4.6 (a)) are observed to be longer compared to PED/Pt/GDL/AQ sensor and further the response and recovery time get enhanced after 48 h of testing (Fig. 4.6 (a)). The potential cycling of electrocatalyst leads to the increased particle size in brush coated and electrodeposited Pt samples which eventually leads to the loss of electrochemical active area.

¹⁷⁷ The loss of ECSA of brush coated, electrodeposited and pulsed electrodeposited samples follows in the order BC/Pt/C/GDL > ED/Pt/GDL/AQ > PED/Pt/GDL/AQ. Sensitivity, response time, electrochemical active area and charge transfer resistance of BC/Pt/C/GDL, ED/Pt/GDL/AQ and PED/Pt/GDL/AQ sensors are displayed in Table 4.2.

Table 4.2 Response behaviours of sensors with brush coated, electrodeposited and pulsed electrodeposited Pt on gas diffusion layer using aqueous electrolyte

Characteristics of sensor	BC/Pt/C/GDL	ED/Pt/GDL/AQ	PED/Pt/GDL/AQ
Response time	1-5 s	360 –1254 s	115 -30 s
Electrochemical active area (m^2/g)	2	15	26
Sensitivity ($\mu\text{A}/\%$)	-	-	9.7
Stability	Signal degraded after 48 h	Increased response time after 48 h	Signal was found to be stable with stable response time
Capacitance (F) (initial and after 48 h)	0.042 & 0.082	0.012 & 0.023	0.0058 & 0.0057
Charge transfer resistance (Ω) (initial and after 48 h)	7.87 & 8.39	6.39 & 7.39	5.35 & 5.12

Note: Brush coated Pt/C electrocatalysts, electrodeposited and pulsed electrodeposited Pt and Pd on gas diffusion layer using aqueous electrolyte are indicated as BC/Pt/C/GDL, ED/Pt/GDL/AQ and PED/Pt/GDL/AQ respectively.

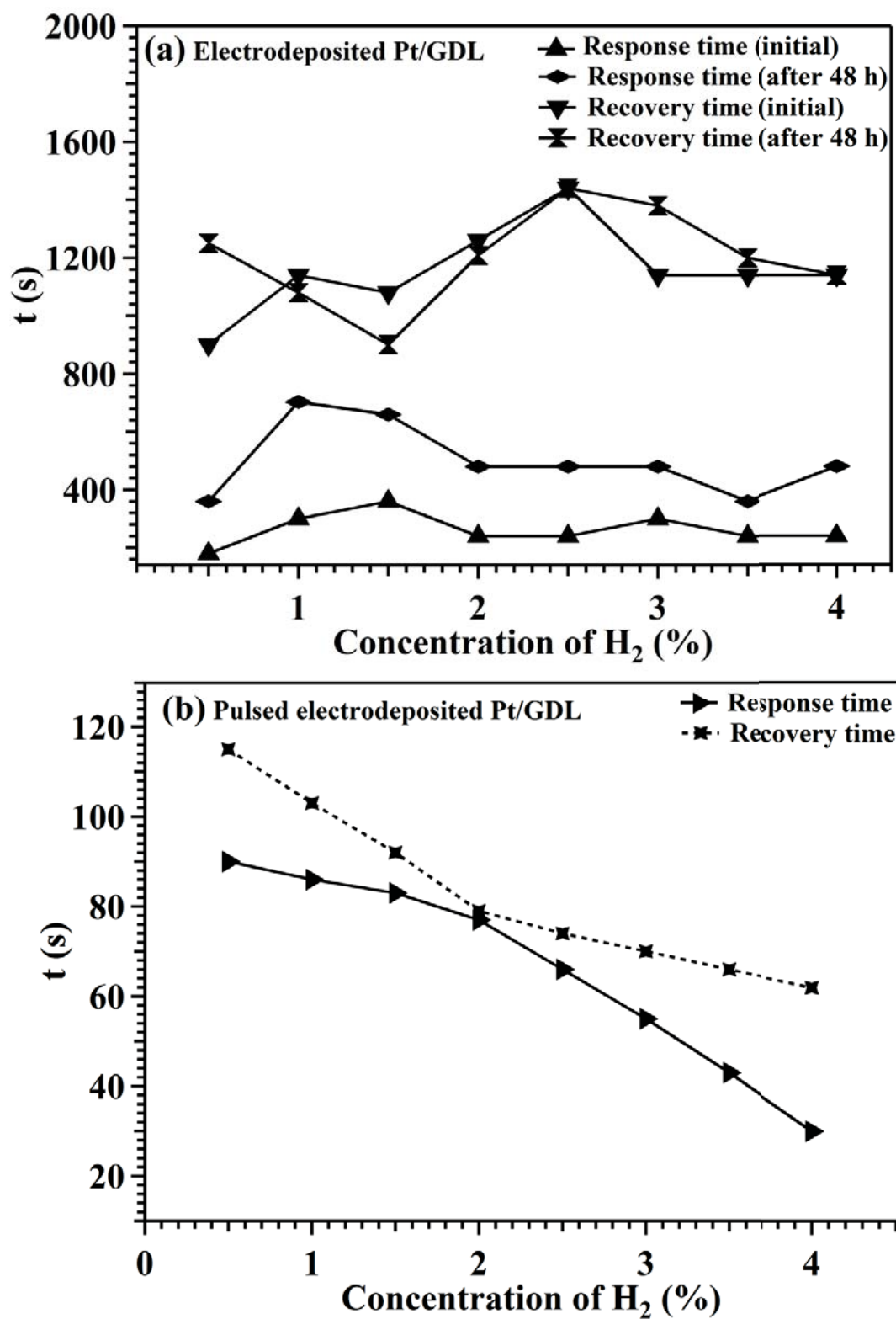


Fig. 4.6 Response and recovery times of sensor with Pt deposited on gas diffusion layer using aqueous electrolyte (a) electrodeposited Pt/GDL and (b) pulsed electrodeposited Pt/GDL

Response and recovery times of the sensors vary with respect to the pore volume and electrochemical active surface area of the diffusion electrode. If the pore volume is fixed for all three sensors, the response time directly depends on the electrochemical active area ⁴². Electrochemical active area of BC/Pt/C/GDL, ED/Pt/GDL/AQ, and PED/Pt/GDL/AQ sensors are shown in Table 4.2. The stable electrochemical active area and low charge transfer resistance of PED/Pt/GDL/AQ sensor contributes to the improved sensor performance than ED/Pt/GDL/AQ and BC/Pt/C/GDL sensor. The response and recovery time of PED/Pt/GDL/AQ is shown in Fig. 4.6 (b) and is found to decrease with increase in concentration (0.5 – 4 %) which implies that the more number of H₂ can diffuse deeper into the electrode, which leads to the activation of more catalytic sites of Pt than at low concentration resulting in shorter response time of 115-30 s for 1% - 5 % concentration of H₂/Ar.

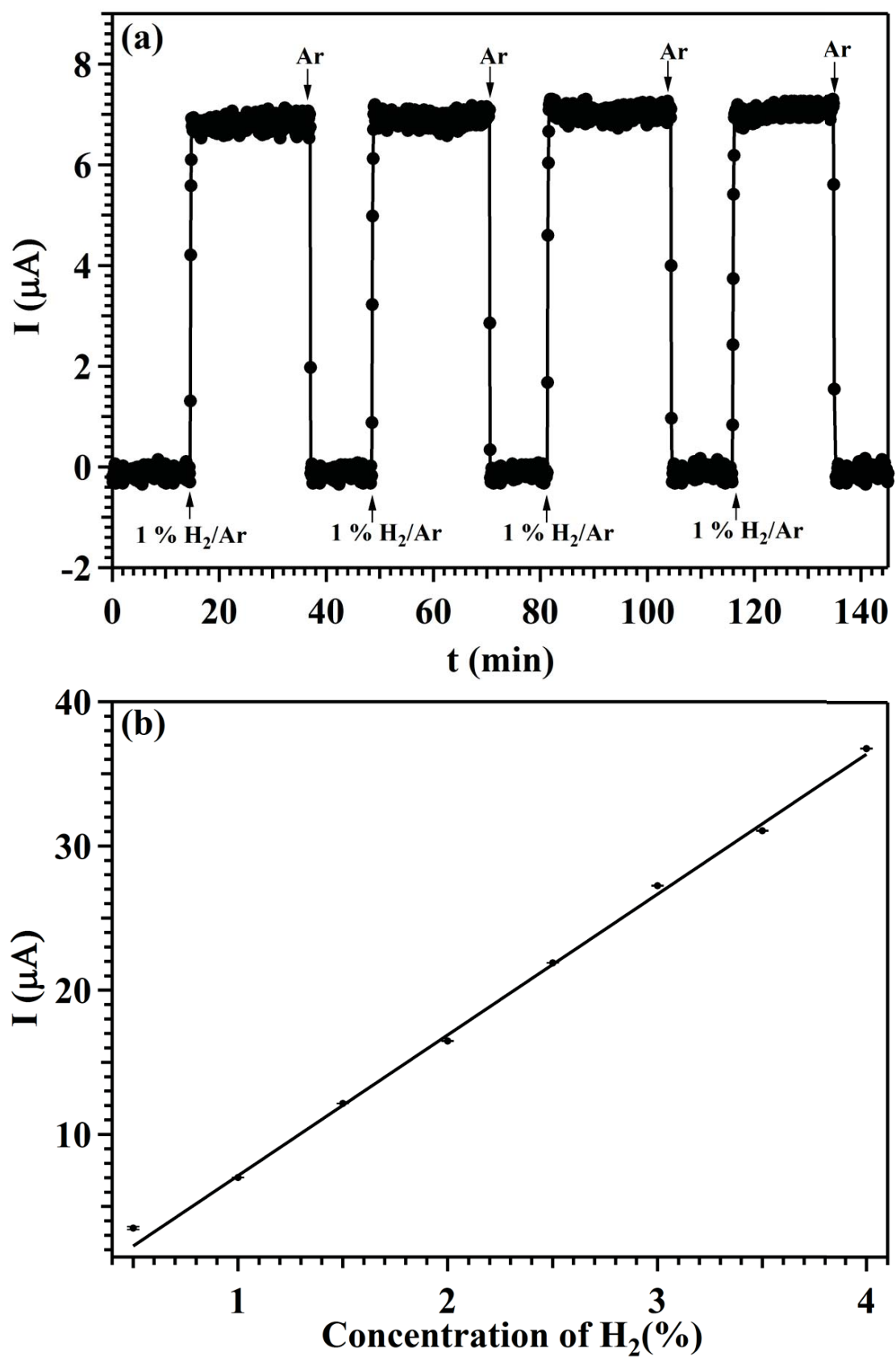


Fig. 4.7 Pulsed electrodeposited Pt on gas diffusion layer using aqueous electrolyte based sensor (a) Repeatability of 1% H_2/Ar and (b) Calibration plot

Repeatability of sensor response to 1 % H₂/Ar of PED/Pt/GDL/AQ is shown in Fig. 4.7 (a). The sensor response is found to be repeatable. PED/Pt/GDL/AQ sensor has better stability; short response time and minimum detection limit (Table 4.3). Hence, PED/Pt/GDL/AQ sensing electrode is the best suited for use in amperometric H₂ sensing application.

Table 4.3 Response behaviour of sensor with pulsed electrodeposited Pt on gas diffusion layer using aqueous electrolyte to H₂/Ar

H₂ sensor characteristics	PED/Pt/GDL/AQ
Sensitivity (μA/%)	9.75
Response time (s)	115-30
Recovery time (s)	90-62
Detection limit (%)	0.0275

Note: pulsed electrodeposited Pt on gas diffusion layer using aqueous electrolyte are indicated as PED/Pt/GDL/AQ

Calibration plot of PED/Pt/GDL/AQ based sensor is indicated in Fig. 4.7 (b). Sensor signal value for each concentration with their standard deviations of PED/Pt/GDL/AQ sensor is indicated in Table 4.4 and the standard deviation of the sensor signal is found to be minimal and hence the spread in values is not visible in the calibration plot.

Table 4.4 Sensor signal with their standard deviations for pulsed electrodeposited Pt on gas diffusion layer

Concentration of H₂ (%)	I (μA)
0.50	3.2 ± 0.30
1.00	6.9 ± 0.02
1.50	11.0 ± 0.10
2.00	15.4 ± 0.03
2.50	20.3 ± 0.03
3.00	25.3 ± 0.07
3.50	30.0 ± 0.04
4.00	35.7 ± 0.07

The sensitivity of PED/Pt/GDL/AQ sensor is adequate for sensing H₂ concentration in percentage level. Hydrogen sensors with electrocatalyst coated on either side of the Nafion membrane showed significant variation in the sensor performance with change in flow rate. Amperometric H₂ sensors with Pt catalyst prepared by chemical reduction method and decal method were reported by Sakthivel et al.¹⁸⁰, Murugesan et al.¹⁸¹ and Lu et al.⁴⁴ Sakthivel et al.¹⁸⁰ tested the sensor performance at a fixed flow rate of 80 sccm and they also studied the effect of flow rate on the sensor signal. Thus, a change of flow rate of ± 20 sccm showed a variation in the sensor signal from 425 μ A to 325 μ A (23 % error) whereas Murugesan et al.¹⁸¹ performed at a fixed flow rate of 300 sccm and there was no significant change when the flow rate was changed by 300 ± 75 sccm. The large deviation in the sensor signal was observed when the change was more than 25 % of the fixed flow rate. Lu et al.⁴⁴ reported a variation of sensor signal from 123 μ A to 115 μ A for a change of flow rate from 60 sccm to 40 sccm. Response behaviour of PED/Pt/GDL/AQ for 1 % H₂/Ar with varying the flow rates from 50 sccm to 400 sccm is given in Fig. 4.8.

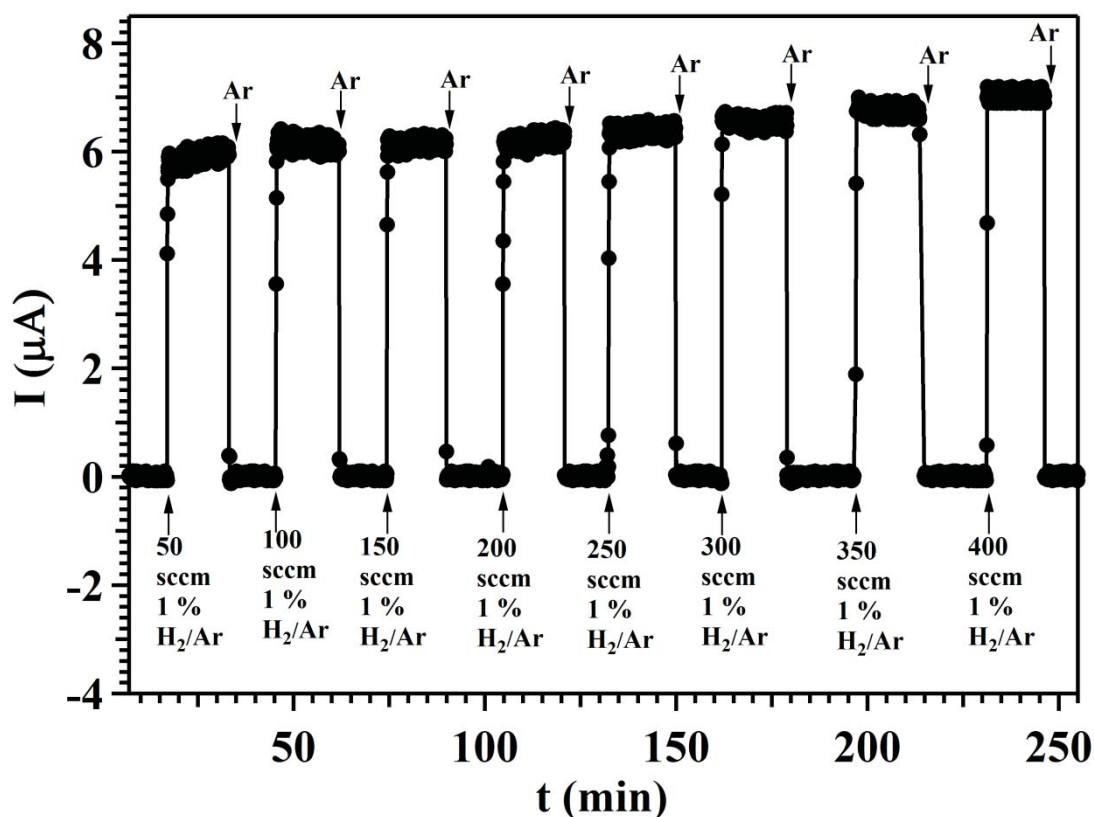


Fig. 4.8 response behaviour of sensor with pulsed electrodeposited Pt on gas diffusion layer using aqueous electrolyte for 1% H₂/Ar with various flow rates (50 sccm to 400 sccm)

Increasing the flow rate from 50-400 sccm varied the signal from 6.0 μA to 6.7 μA the error is found to be less than 10 %. Moreover, doubling the flow rate from 200 sccm to 400 sccm leads to 12 % (6.9 μA) error. Hence, the flow rate variation on sensor performance is much less in the present sensor. Other two important factors that affect the sensor performances are relative humidity (RH) and temperature. The ionic conductivity of Nafion membrane depends on water content and it varies with a change in RH and temperature. Fig. 4.9 exhibits a linear variation of current with concentration of H₂/Ar at different RH, i.e. at 60-80 %. From the figure, it is clear that RH has an impact on the sensor response for concentrations greater than 2 % H₂/Ar.

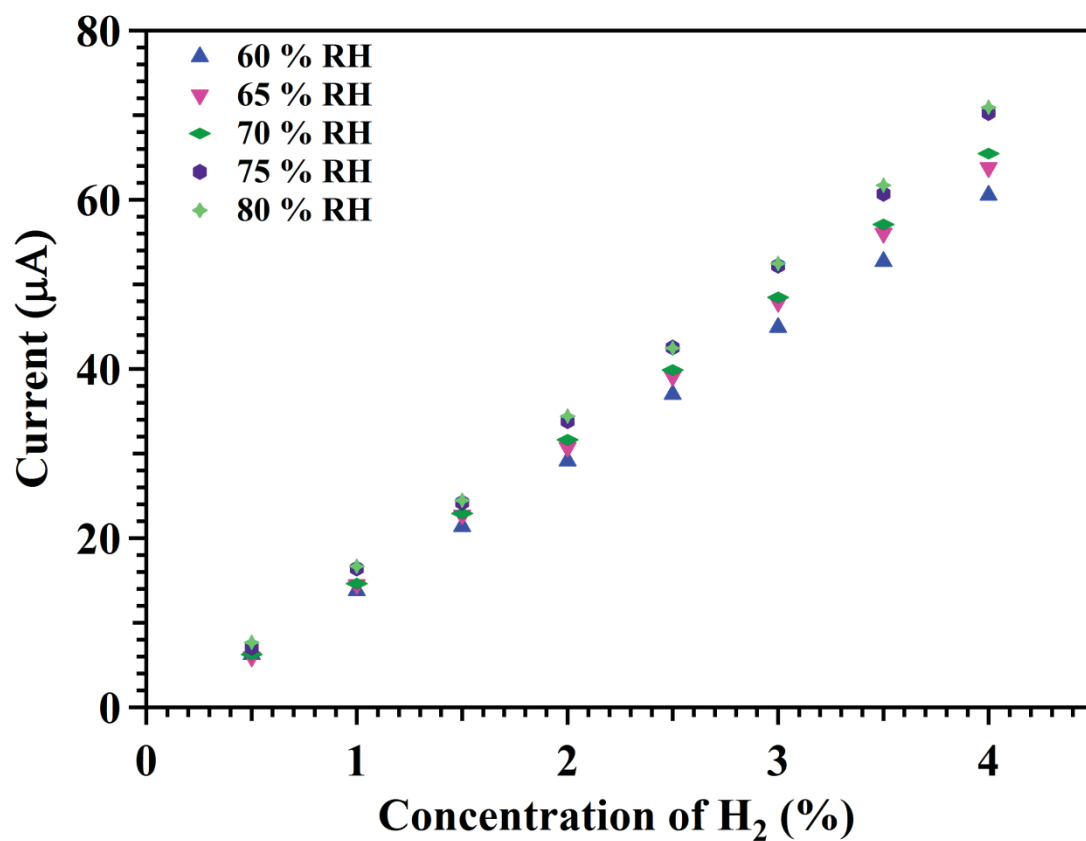


Fig. 4.9 Calibration plot of sensor with pulsed electrodeposited Pt on gas diffusion layer using aqueous electrolyte at different RH 60-80 %

The effect of temperature on the sensor performance is illustrated in Fig. 4.10. The plot reveals that the variation of temperature from 293-313 K does not affect the sensor signal significantly and the error is less than 7 %.

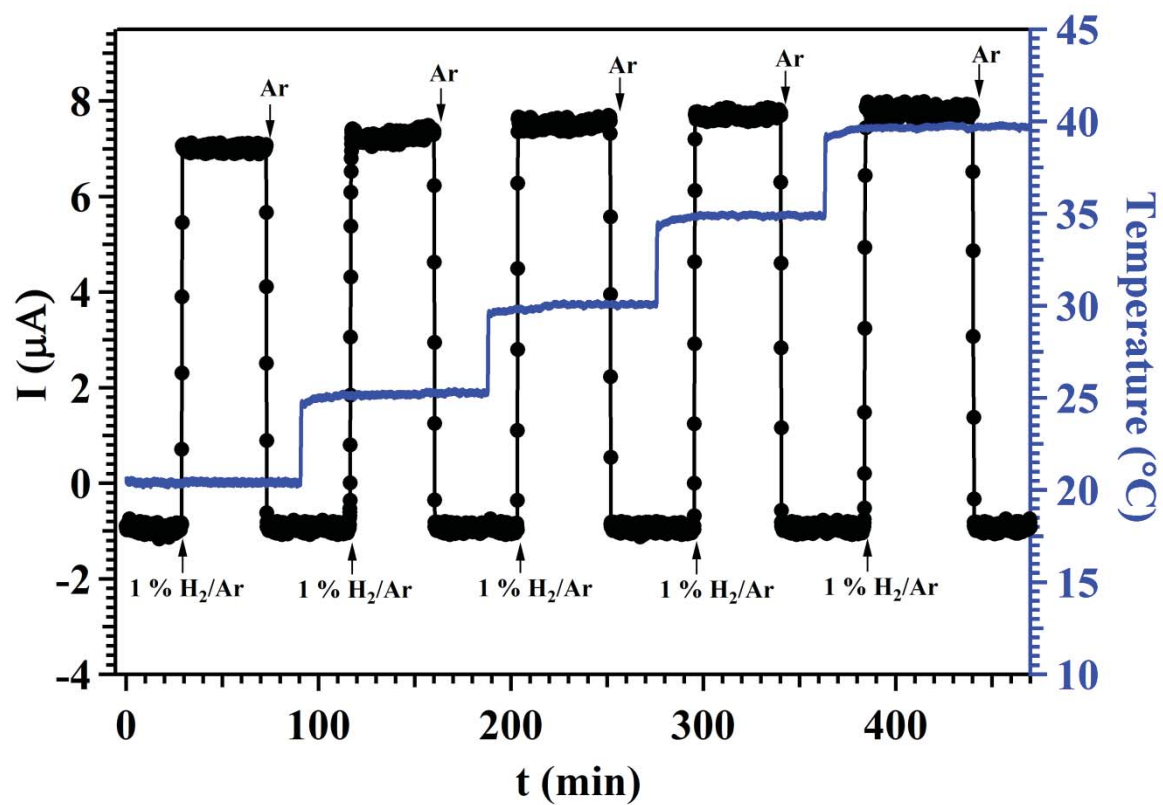


Fig. 4.10 Sensor with pulsed electrodeposited Pt on gas diffusion layer using aqueous electrolyte response behaviour of 1% H_2/Ar at five different temperatures (293-313 K)

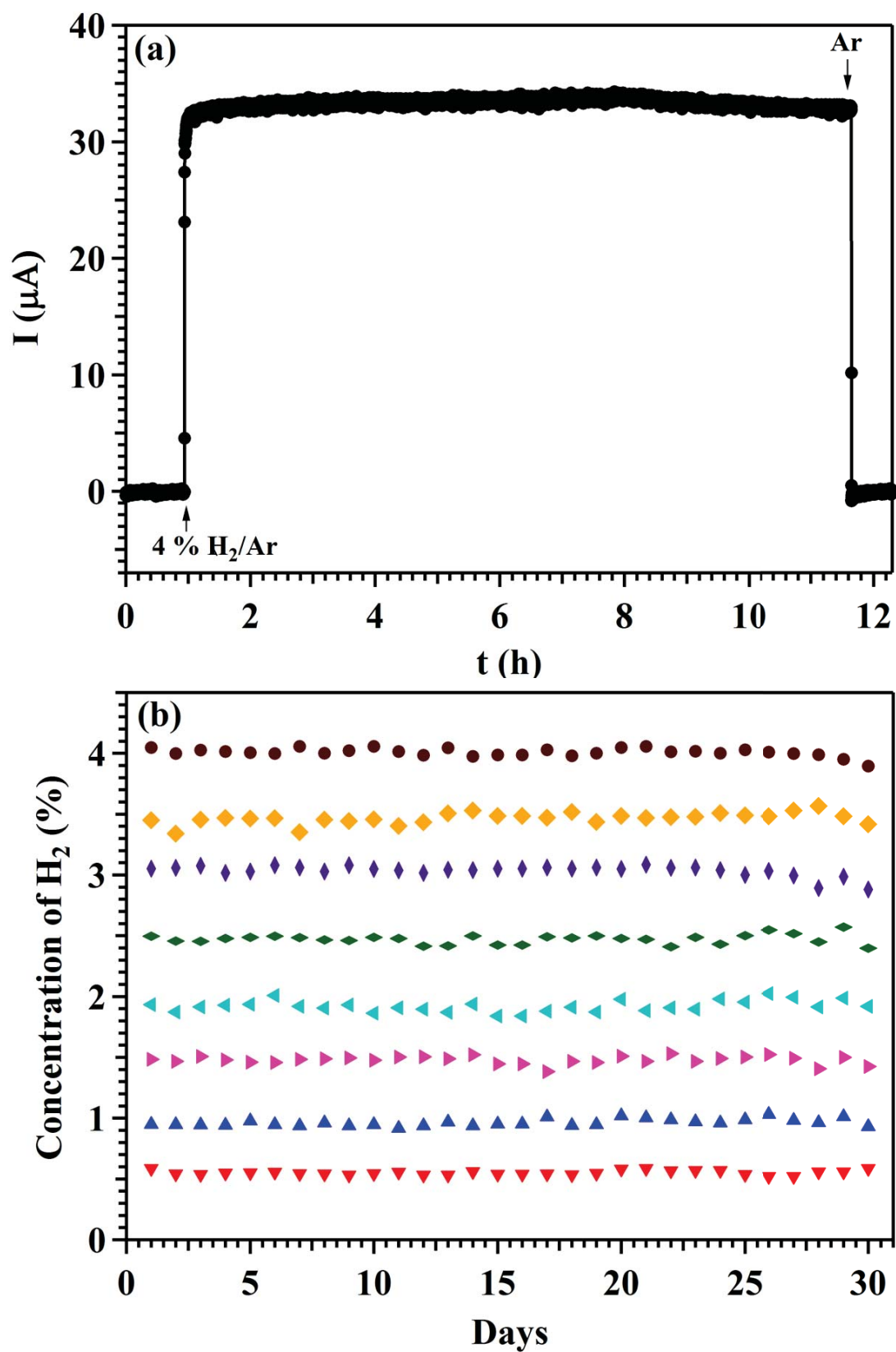


Fig. 4.11 Sensor with pulsed electrodeposited Pt on gas diffusion layer using aqueous electrolyte (a) Signal stability of 4% H_2/Ar and (b) Long-term stability

Stability of sensor with PED/Pt/GDL/AQ signal for 4 % H₂/Ar is shown in Fig. 4.11 (a). The sensor signal is found to be stable over a significant period (12 h). Fig. 4.11 (b) shows the long-term stability of the sensor for a period of four weeks. Generally, the catalyst agglomeration and less adhesion on the substrate are the main cause for catalyst degradation. Pt particles deposited are well separated from each other in PED when compared to the constant potential deposition and hence the probability of getting agglomerated is less in the case of PED. Pulse electrodeposition can produce finer particles with homogenous distribution over the substrate with better adhesion than the constant potential deposition. The good adhesion of pulsed electrodeposited sample contributes to the high stability/durability of the deposit. One can obtain improved adhesion using pulsed electrodeposition (PED) method compared to the constant potential deposition due to higher instantaneous current density achieved during PED. In PED, the potential is turned off (t_{off}) periodically so that the ions near the interface will be discharged to an extent and this allows the easier passage of ions during the time of deposition (t_{on}) which, gives higher current efficiency whereas constant potential deposition leads to the growth of charged layer till the duration of deposition eventually decreases the current efficiency of deposition.

Extensive investigations on hydrogen sensors with brush coated Pt, electrodeposited Pt and pulsed electrodeposited Pt on GDL revealed that sensor with pulsed electrodeposited electrodes exhibited better sensitivity and stability. The sensor also displayed less flow rate dependency compared to the previously reported sensors ^{44, 88, 181}. Improved response behaviour of hydrogen sensor with pulsed electrodeposited electrodes is attributed to the higher electrochemical active area and lower charge transfer resistance.

4.3.2.2 Hydrogen sensing behaviour of sensors with electrodeposited Pt/GDL and pulsed electrodeposited Pt/GDL using [C4mim][BF4] as electrolyte

Response behaviour and repeatability of 4 % H₂/Ar sensor with ED/Pt/GDL/[C4mim][BF4] sensor are shown in Fig. 4.12 (a) and Fig. 4.12 (b), respectively. The sensor responds to each concentrations of H₂/Ar and attains the steady state. The sensor retraces to the baseline immediately when the flow was cut off. Thus, it indicates that the sensor senses H₂/Ar with stable response and recovery of the signal. Response and repeatability of 4 % H₂/Ar sensor with PED/Pt/GDL/[C4mim][BF4] are shown in Fig. 4.13 (a) and Fig. 4.13 (b), respectively.

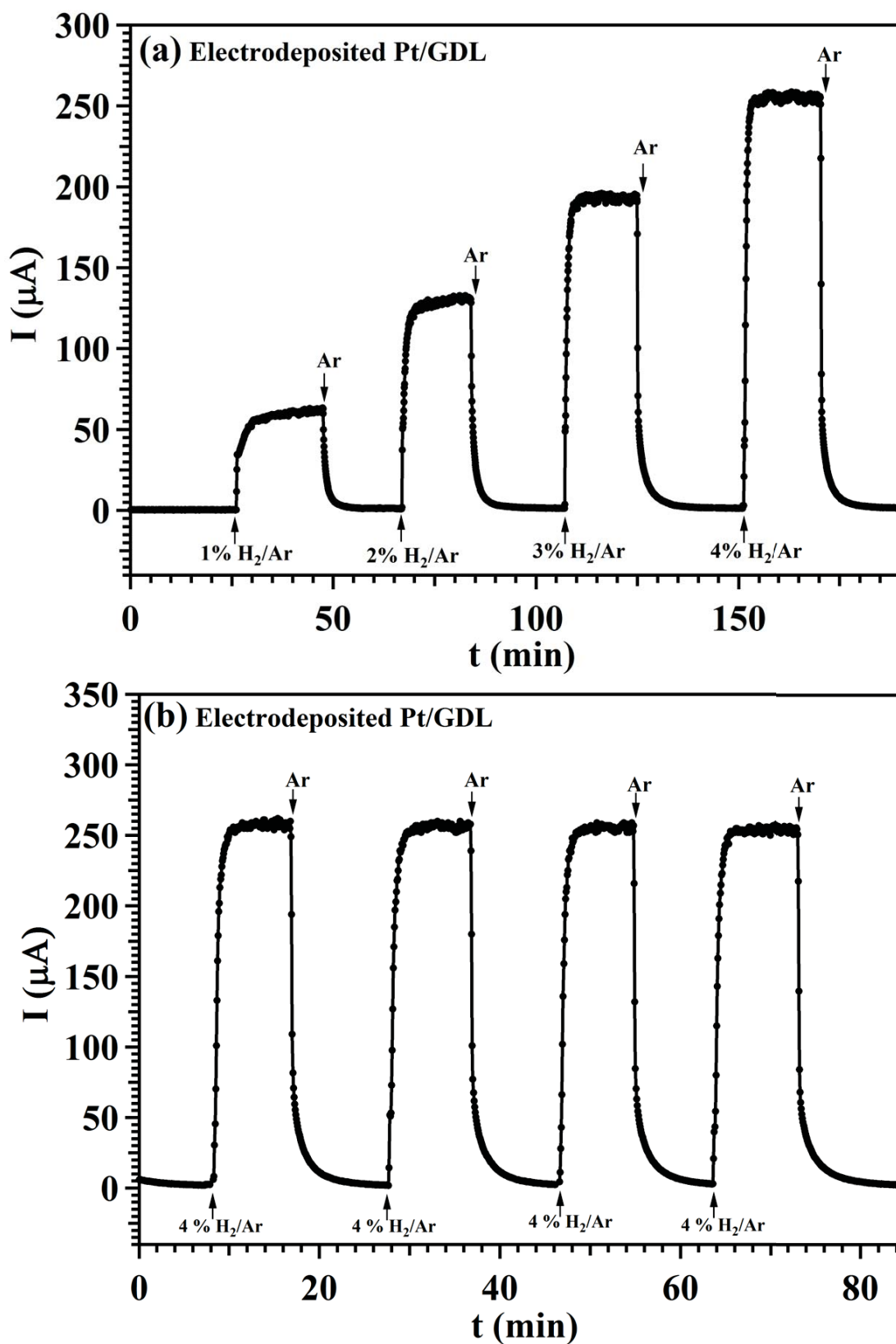


Fig. 4.12 Sensor with electrodeposited Pt on gas diffusion layer using $[C4mim][BF_4]$ ionic liquid electrolyte (a) response behaviour and (b) repeatability for response of 4 % H_2/Ar

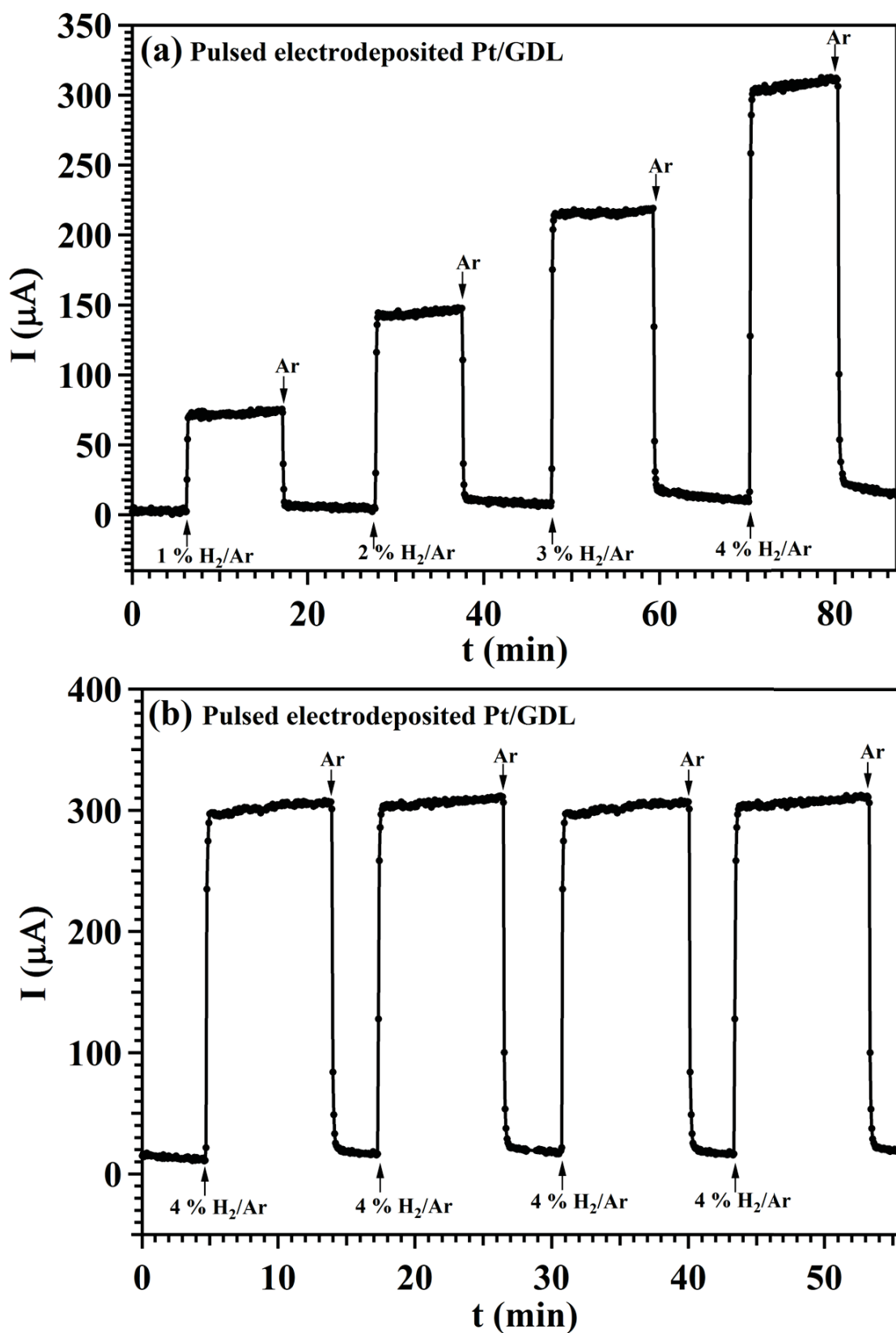


Fig. 4.13 Sensor with pulsed electrodeposited Pt on gas diffusion layer using $[\text{C4mim}][\text{BF}_4]$ ionic liquid electrolyte (a) response behaviour and (b) repeatability for response of 4 % H_2/Ar

The average value was taken for each concentration from the response curve of the sensors. The resulting current is plotted against the concentration of hydrogen. The calibration plot of sensors shows that the current signal varies linearly with concentration. The sensitivity of the sensors is obtained from the slope of the plot. Sensitivities of ED/Pt/GDL/[C4mim][BF4] and PED/Pt/GDL/[C4mim][BF4] sensors are found to be 65.6 $\mu\text{A}/\%$ and 77.7 $\mu\text{A}/\%$. PED/Pt/GDL/[C4mim][BF4] sensor exhibited higher sensitivity than ED/Pt/GDL/[C4mim][BF4] due to larger ECSA. Fig. 4.14 shows that both electrodeposited and pulsed electrodeposited samples exhibited a peak in the hydrogen desorption region. ECSA of ED/Pt/GDL/[C4mim][BF4] and PED/Pt/GDL/[C4mim][BF4] was calculated in hydrogen desorption region (Table 4.5). Pulsed electrodeposited Pt has high ECSA compared to electrodeposited one and is due to the uniform distribution of particles on GDL in pulsed electrodeposited samples.

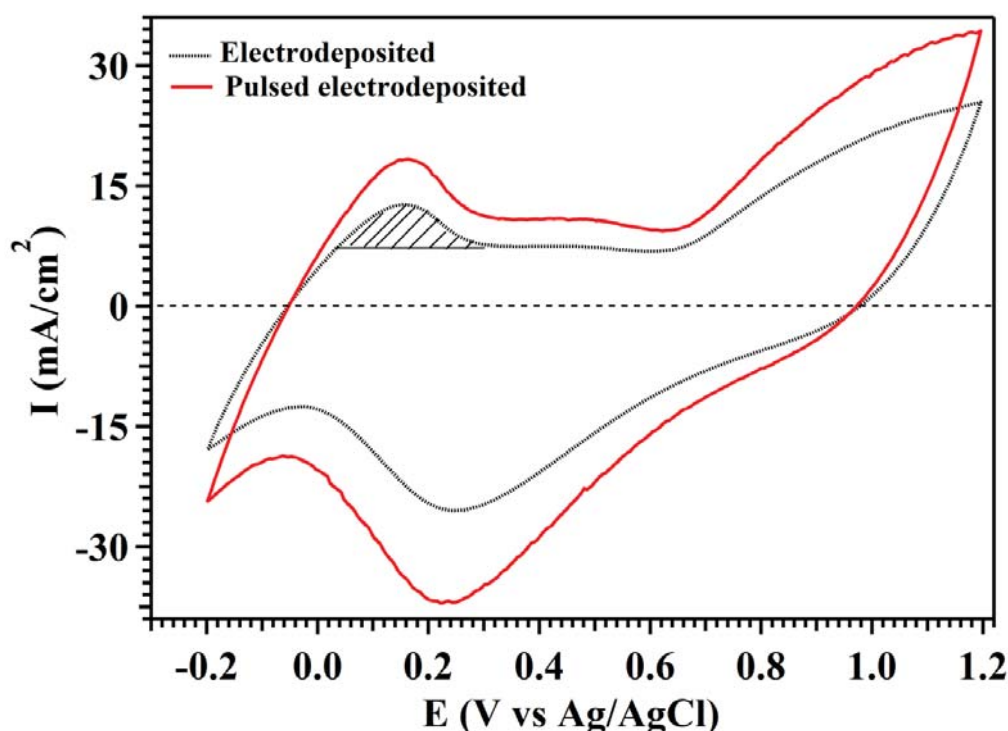


Fig. 4.14 Cyclic voltammogram of sensors with electrodeposited and pulsed electrodeposited Pt on gas diffusion layer using [C4mim][BF4] ionic liquid electrolyte (Loading: 0.5 mg/cm², scan rate: 200 mV/s)

The plot of response and recovery time of sensors with ED/Pt/GDL/[C4mim][BF₄] and PED/Pt/GDL/[C4mim][BF₄] vs. concentration of H₂/Ar is shown in Fig. 4.15. From Table 4.5, the response time (t_{90}) of PED/Pt/GDL/IL sensor is observed to be much less than that of the ED/Pt/GDL/[C4mim][BF₄] sensor. This is because of high electrochemical active area of PED/Pt/GDL/[C4mim][BF₄] electrode as is evident from the FESEM image (Fig. 3.7).

Table 4.5 Comparison of amperometric H₂ sensing behaviour of electrodeposited and pulsed electrodeposited Pt on gas diffusion layer using [C4mim][BF₄] ionic liquid electrolyte

Sensor	Potential limit used for integration of charge for ECSA (V)	ECSA (m ² /g)	Response time (s)	Sensitivity (μA/%)	Detection limit (%)
Electrodeposited Pt	0.04 – 0.29	16	60-176	65.6	0.1593
Pulsed electrodeposited Pt	0.039 – 0.35	27	12-16	77.7	0.0381

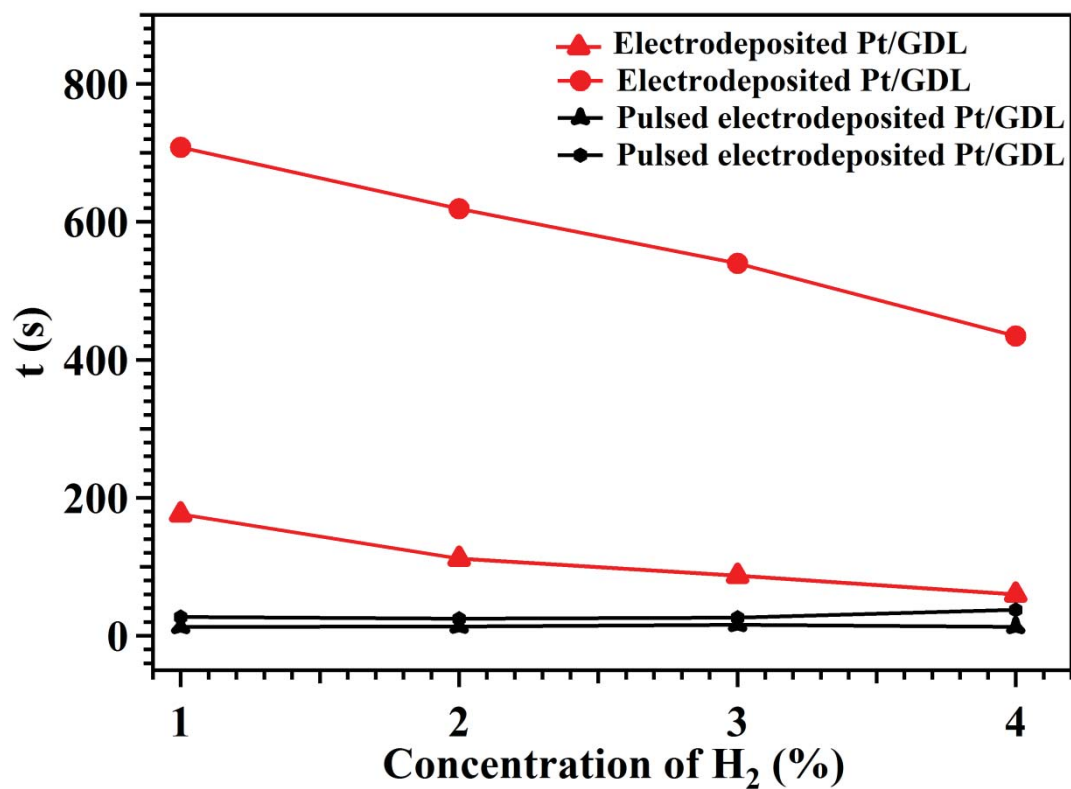


Fig. 4.15 Response and recovery times of sensor with Pt deposited on gas diffusion layer using [C4mim][BF₄] ionic liquid electrolyte

Response and recovery times of the sensor directly depend on the catalytic surface area of the sensing electrode. Response and recovery times decrease with increase in concentration of H₂/Ar¹⁸².

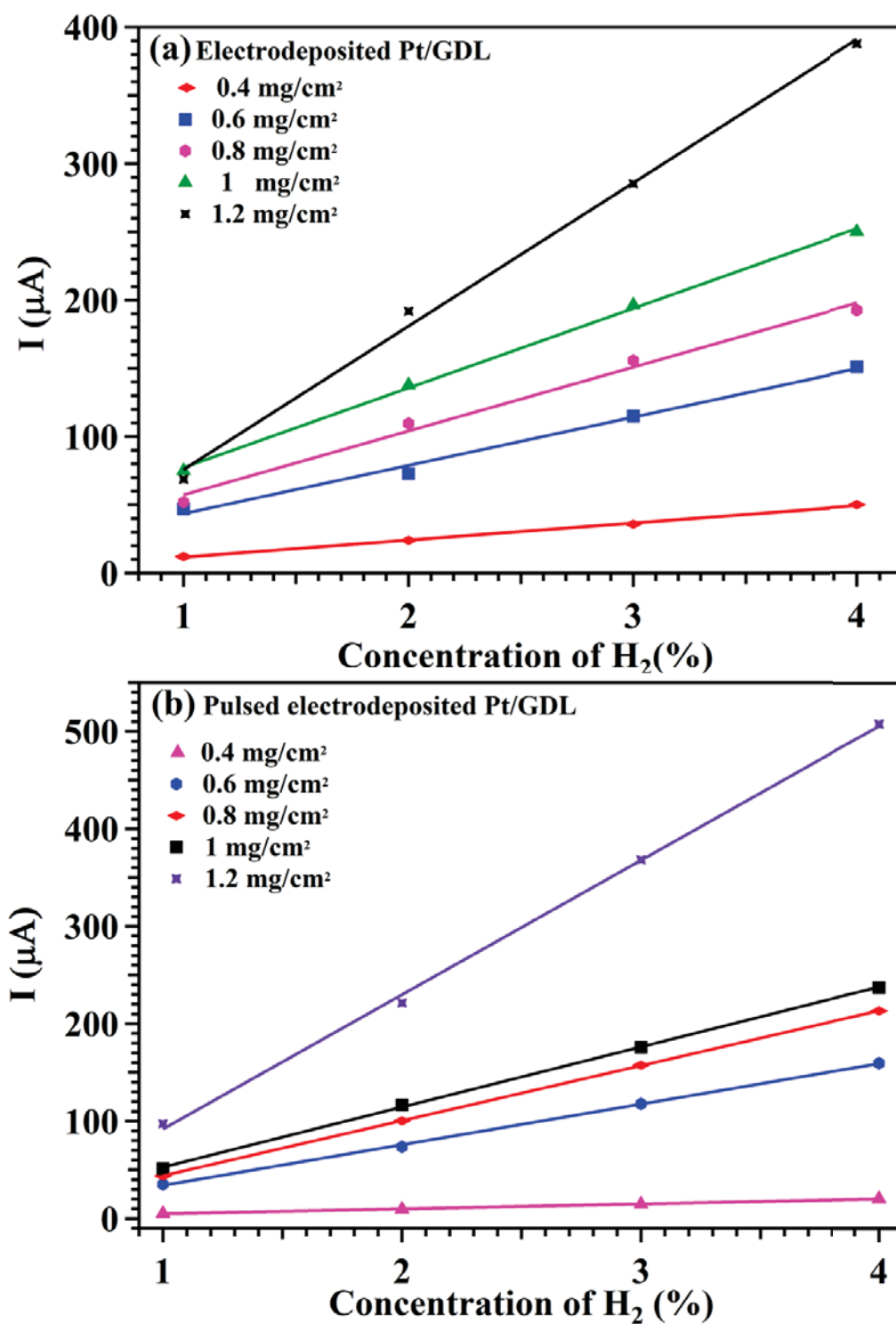


Fig. 4.16 Calibration plot of H₂ sensors with five different loadings of Pt deposited on gas diffusion layer using [C4mim][BF₄] ionic liquid electrolyte (a) electrodeposited and (b) pulsed electrodeposited

Fig. 4.16 (a) and Fig. 4.16 (b) indicate the calibration plot of sensors with different loadings of Pt on GDL of ED/Pt/GDL/[C4mim][BF₄] and PED/Pt/GDL/[C4mim][BF₄]. Sensitivity

of sensor increases with Pt loading in both ED/Pt/GDL/[C4mim][BF4] and PED/Pt/GDL/[C4mim][BF4] sensors owing to the enhancement of active area when the loading increases. The improvement in sensitivity with loading of Pt is attributed to the particles are being distributed without any agglomeration even at the higher loading of Pt.

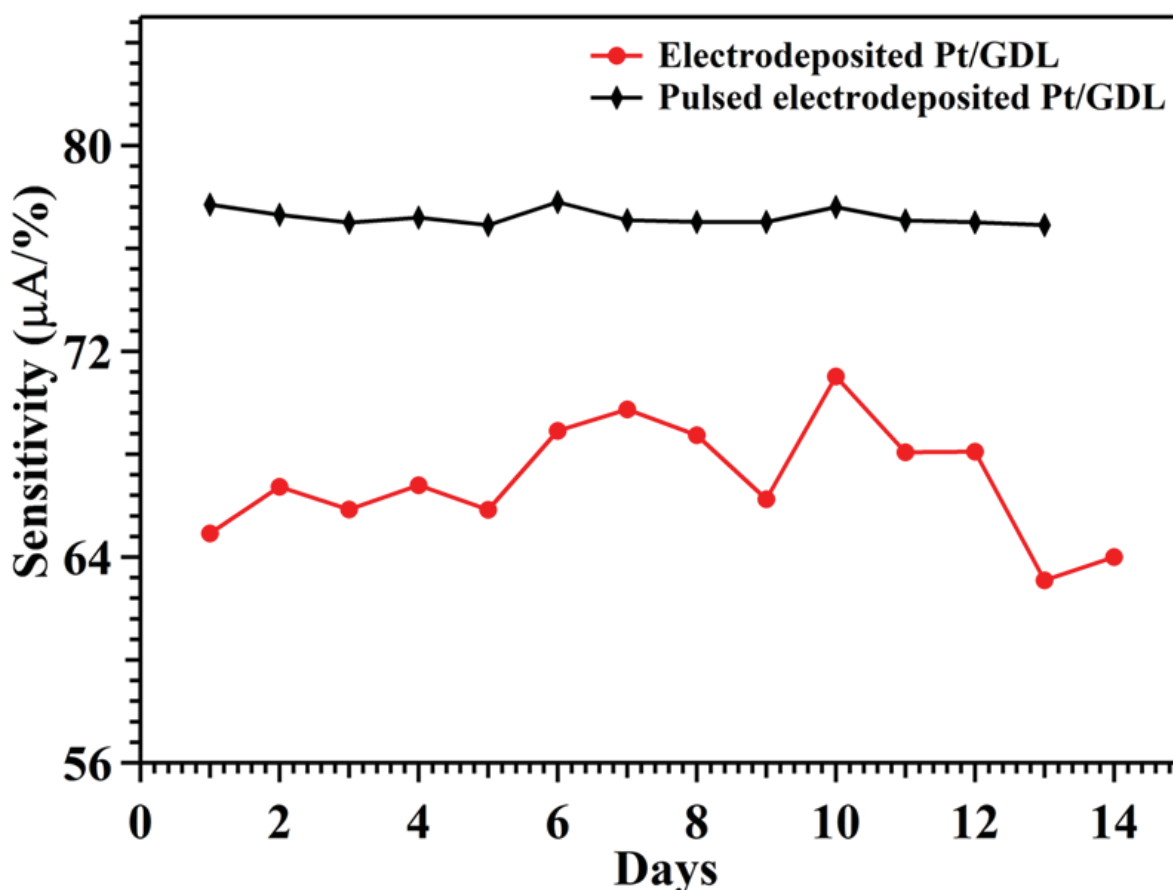


Fig. 4.17 Long-term Stability sensors with electrodeposited and pulsed electrodeposited Pt at different loadings on gas diffusion layer using [C4mim][BF4] of ionic liquid electrolyte

The long-term stability of the sensors was studied by recording the sensor signal for two weeks, and the plot is shown in Fig. 4.17. Improved sensor performance owing to the use of RTILs has been observed and reported in the literature^{28, 74}.

Electrodeposition and pulsed electrodeposition of Pt from ionic liquid electrolyte furnishes higher electrochemical active area compared to that of Pt electrodeposited from aqueous

electrolyte. The use of RTIL in electrodeposition methods controls the morphology. Electrodeposition and pulsed electrodeposition via ionic liquid electrolytes give better adhesion of the catalyst onto the support. Thus, improves the three phase contacts between the reactant, electrode and electrolyte which ultimately influence the integrity of the catalyst on the support compared to aqueous electrolyte ²⁸.

4.3.3 Hydrogen sensing behaviour of sensors with pulsed electrodeposited Pd/GDL as sensing electrode

Pd exhibits high sticking coefficient for H₂ and is a promising catalyst for dissociation of H₂. Hence, Pd was also attempted as electrocatalyst for H₂ sensing. It is clear from our studies that response to hydrogen decreased significantly in the case of sensors with brush coated Pt and Pt electrodeposited using aqueous electrolyte. Similar behaviour was expected in the case of Pd and hence H₂ sensors with electrodes having brush coated Pd and Pd electrodeposited using aqueous electrolyte were not investigated. Studies were carried out with pulsed electrodeposited Pd/GDL in aqueous electrolyte and electrodeposited Pd/GDL using ionic liquid electrolyte.

4.3.3.1 Response behaviour of sensor with pulsed electrodeposited Pd/GDL using aqueous electrolyte

Response behaviour of sensor with PED/Pd/GDL/AQ for H₂/Ar in the concentration range 1-5 % is shown in Fig. 4.18 (a). Fig. 4.18 (b) presents the repeatability of the sensor for 4 % H₂/Ar. Fig. 4.18 (a) clearly indicates that response takes much longer time to reach the steady state. Similar behaviour is also seen from the repeatability plot (Fig. 4.18 (b)).

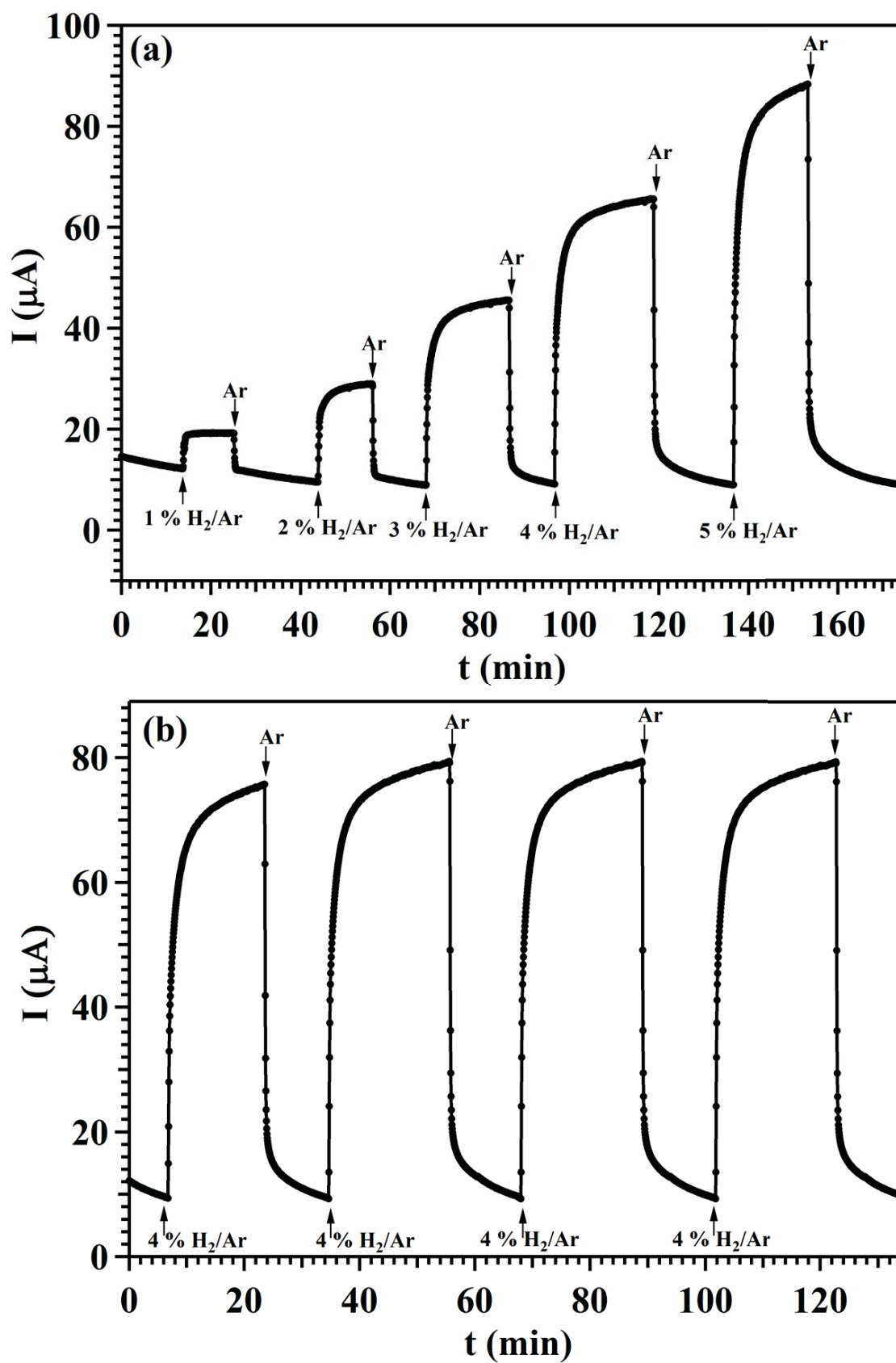


Fig. 4.18 Sensor with pulsed electrodeposited Pd on gas diffusion layer (a) response behaviour and (b) repeatability of 4 % H_2/Ar

Response time for PED/Pd/GDL/AQ sensor is found to be very much higher than for PED/Pt/GDL/AQ and PED/Pt/GDL/[C4mim][BF₄] sensors. Hence, irrespective of the method used for preparation of Pd electrocatalyst on GDL, the sensor in two electrode configuration takes much longer response time to achieve steady state. This is because of O₂ adsorbed on the surface of Pd. Hence, pristine Pd is not a recommended electrocatalyst for H₂ sensing in two electrode mode.

4.3.3.2 Response behaviour of sensor with electrodeposited Pd/GDL using [C4mim][Cl] ionic liquid electrolyte as sensing electrode

Cyclic voltammetry (CV) was carried out to find the optimum potential for sensing H₂. CV was recorded from 0 to +1 V at the scan rate of 50 mV/s with Ar gas, as well as H₂/Ar mixture at sensing electrode side (anode side) and the cathode side was exposed to air. The optimum potential for sensing H₂ was determined from the voltammogram such that signal to baseline ratio is high. H₂ sensing characteristics were tested in three electrode mode by applying the experimentally determined optimum potential of 0.8 V vs Pt wire at the working electrode.

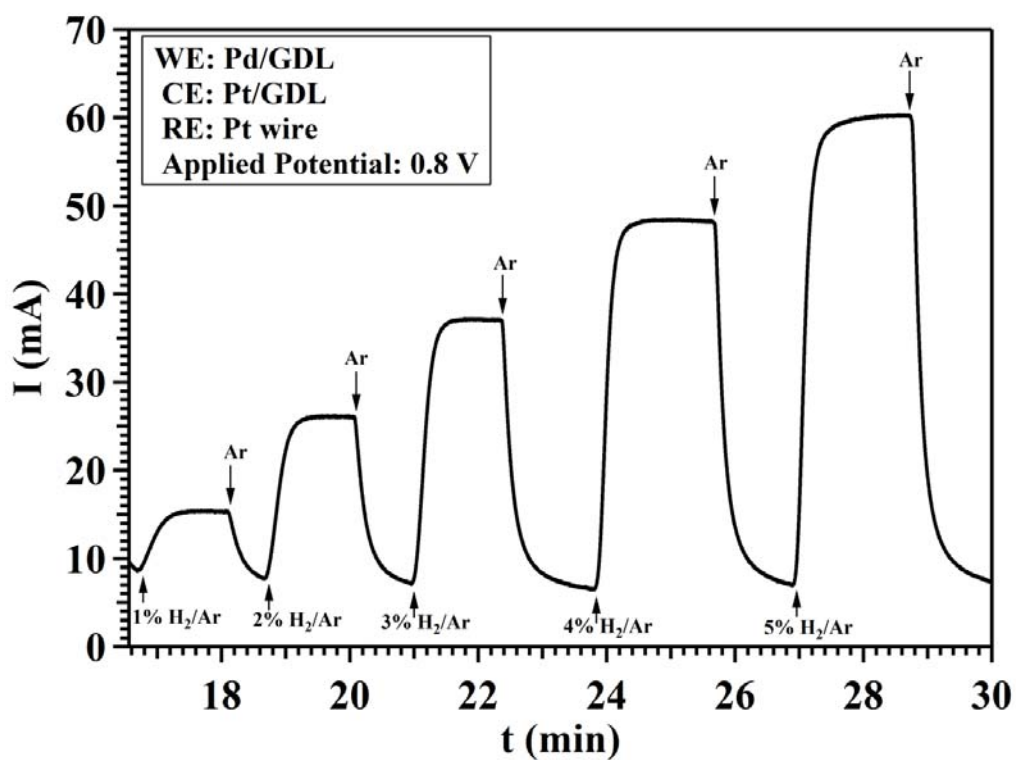


Fig. 4.19 Response behaviour sensor with electrodeposited Pd on GDL using [C4mim][Cl] electrolyte

Response behaviour of the sensor for various concentrations of H₂/Ar was recorded in three electrode mode and is shown in Fig. 4.19.

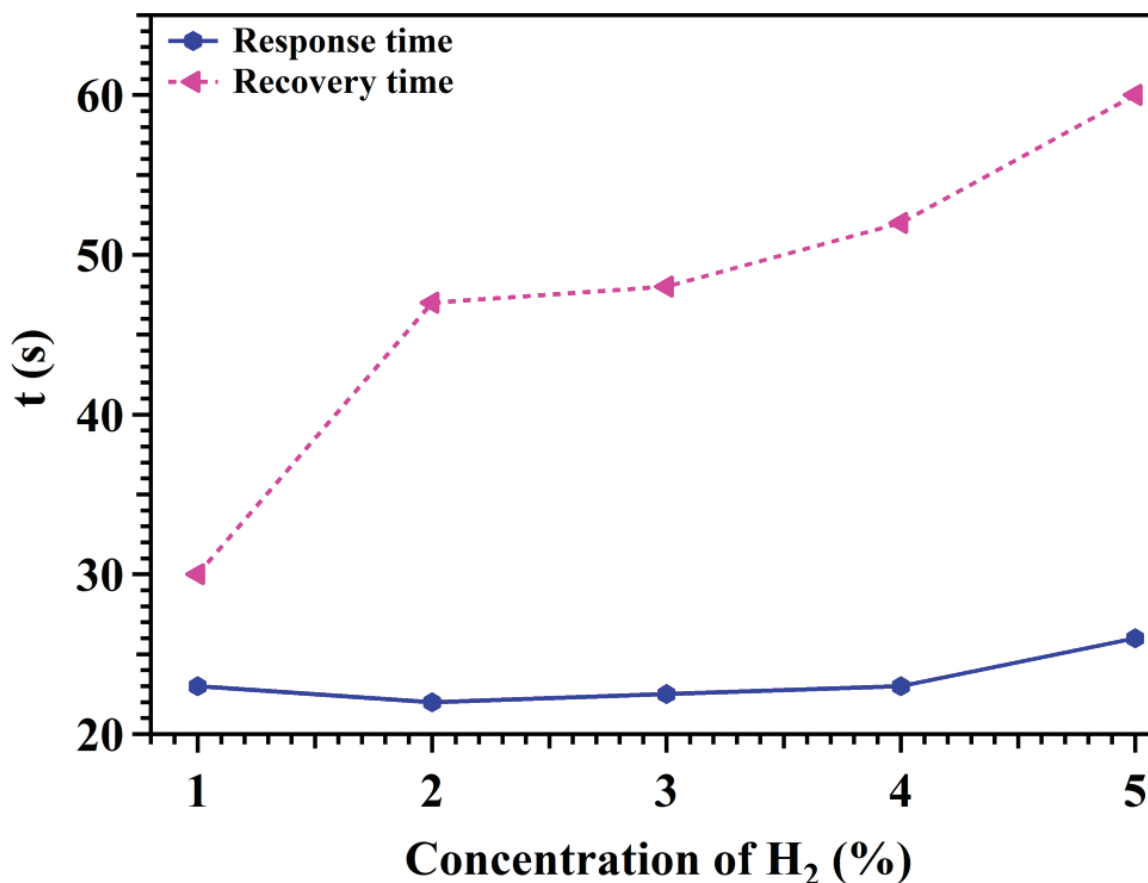


Fig. 4.20 Response and recovery times of electrodeposited Pd on GDL using [C4mim][Cl] electrolyte based sensor

Response (t_{90}) and recovery time of the sensor for 1-5 % concentration of H₂ is shown in Fig. 4.20. From the plot, it is evident that response time of the sensor is in the range 22-26 s. Repeatability for 5% H₂/Ar and the calibration plot of the sensor in the concentration range 1-5% are shown in Fig. 4.21 (a) and Fig. 4.21 (b) respectively. The sensitivity of the sensor is 0.011 A/%. The sensor shows linear response behaviour since the supply of H₂ to the sensing electrode is a diffusion-limited process¹⁷⁵. The flow of H₂ is diffusion limited because of the pin-hole barrier at the anode and it is the rate determining step for the reaction of H₂ and O₂. If the rate of oxidation of H₂ is limited, then the change in current is directly proportional to concentration of H₂.

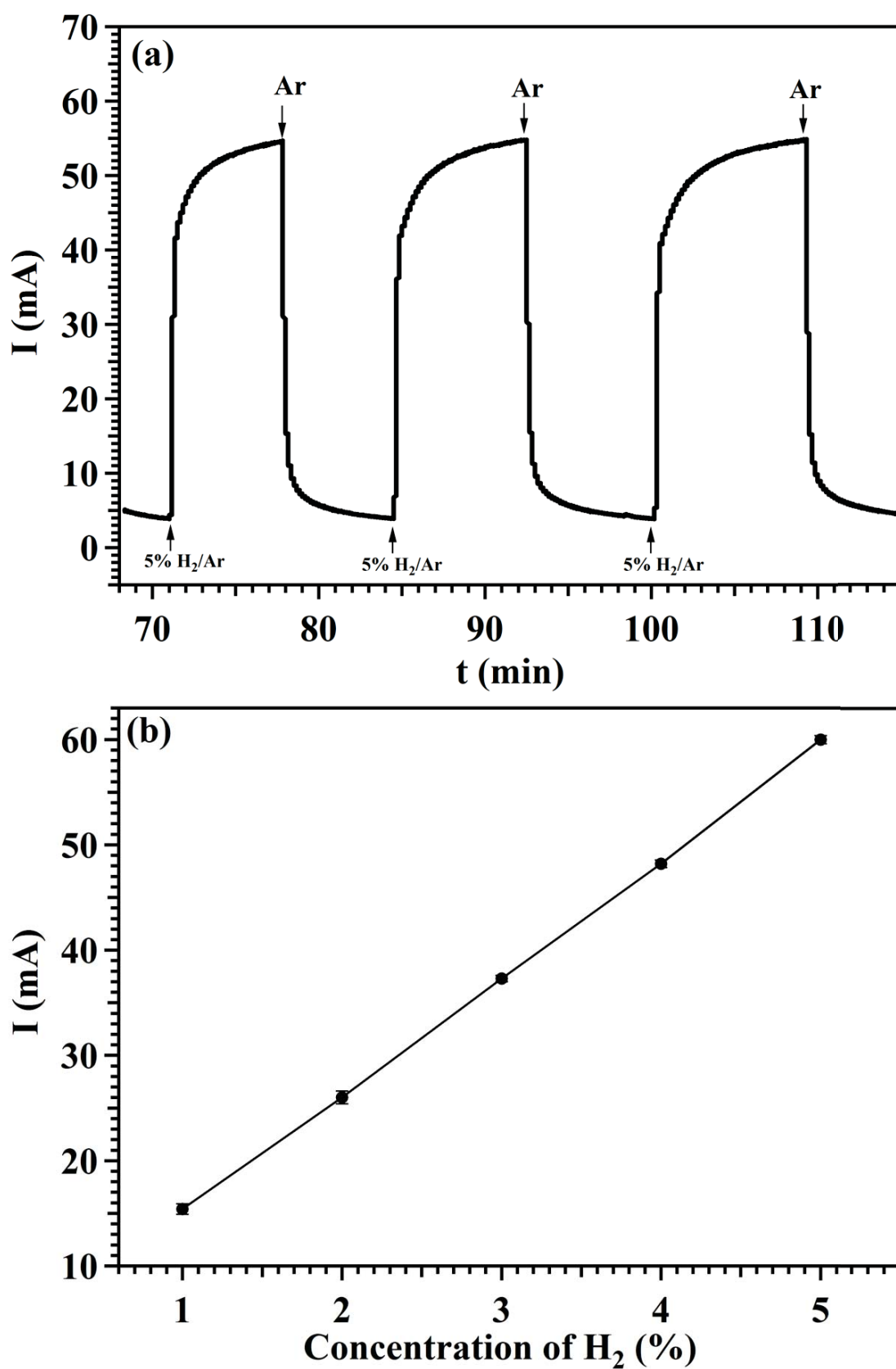


Fig. 4.21 Sensor with electrodeposited Pd on gas diffusion layer using [C4mim][Cl] ionic liquid electrolyte (a) Repeatability for 5% H₂/Ar and (b) Calibration plot

The sensitivity and response time of electrodeposited Pd on GDL is enhanced in three electrode mode operation owing to the application of potential which facilitates the faster rate of electrochemical reaction. Hence, Pd based amperometric H₂ sensor could be very well operated in three electrode mode to get shorter response time and higher sensitivity.

4.3.4 Hydrogen sensing behaviour of sensor with Pt_xPd_y /GDL diffusion electrodes as sensing electrode

It is clear from the studies carried out on H₂ sensors in two electrode mode with diffusion electrodes having Pt and Pd as electrocatalyst that both Pt and Pd can serve as electrocatalyst but, have deficiencies with respect to sensitivity and response time. Hence, an attempt was made to develop H₂ sensors with Pt_xPd_y alloy as electrocatalyst.

Cyclic voltammogram of sensors with Pt_xPd_y alloy as electrocatalyst is shown in Fig. 4.22. Pt_xPd_y alloys showed a peak in the hydrogen desorption region hence the ECSA was calculated in different potential limits and are indicated in Table 4.6. ECSA estimated for various alloy compositions (Pt₅₄Pd₄₆, Pt₂₈Pd₇₂ and Pt₈₀Pd₂₀) are shown in Table 4.6.

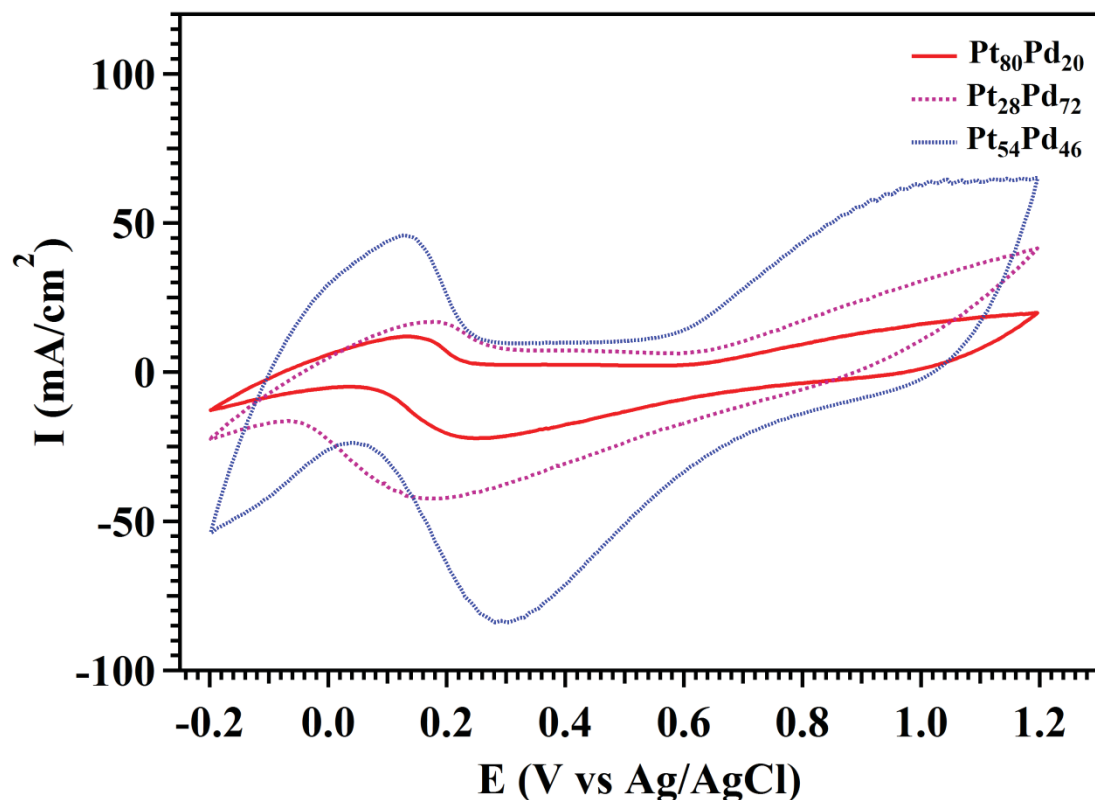


Fig. 4.22 Cyclic voltammogram of sensors with pulsed electrodeposited Pt_xPd_y alloy electrocatalyst

(Loading: 0.5 mg/cm^2 , scan rate: 200 mV/s)

ECSA follows in the order $\text{Pt}_{54}\text{Pd}_{46} > \text{Pt}_{28}\text{Pd}_{72} > \text{Pt}_{80}\text{Pd}_{20}$. Hoa van Hien et al.¹⁸³ also reported higher ECSA for $\text{Pt}_{51}\text{Pd}_{49}$ deposited by chemical vapour deposition method in comparison to other combinations of alloys. It is observed highest ECSA for alloy composition of $\text{Pt}_{54}\text{Pd}_{46}$ ($33 \text{ m}^2/\text{g}$).

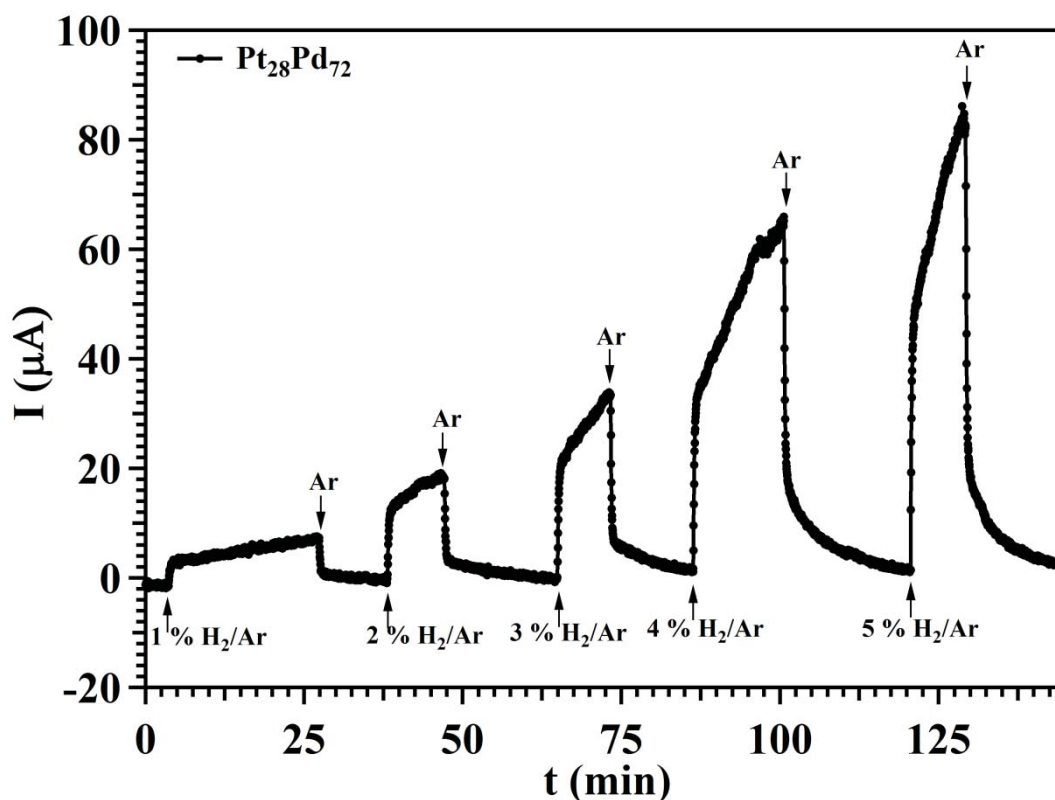


Fig. 4.23 Hydrogen response behaviour of sensor with pulsed electrodeposited Pt₂₈Pd₇₂ alloy electrodes

The H₂/Ar response behaviour of sensor with Pt₂₈Pd₇₂/GDL electrode is shown in Fig. 4.23. It is evident from the figure that limiting current is not attained for all the concentrations of H₂/Ar. In Pd rich alloy, Pd forms oxide film on the surface which inhibits the chemisorptions of H₂¹⁸⁴. Hence Pd rich Pt_xPd_y alloy does not attain steady state unless the oxide is removed and hence the sensor takes much longer time to establish the steady state. Even though the ECSA is higher for Pt₂₈Pd₇₂ sensor as indicated in Table 4.6, the oxide present at the surface limits the response time to an unacceptable level. Hence, the response behaviour of sensor with Pt₂₈Pd₇₂ was not investigated further. Fig. 4.24 indicates the response behaviour of H₂/Ar in the case of sensors with diffusion electrodes having alloy electrocatalyst of composition Pt₅₄Pd₄₆, and Pt₈₀Pd₂₀.

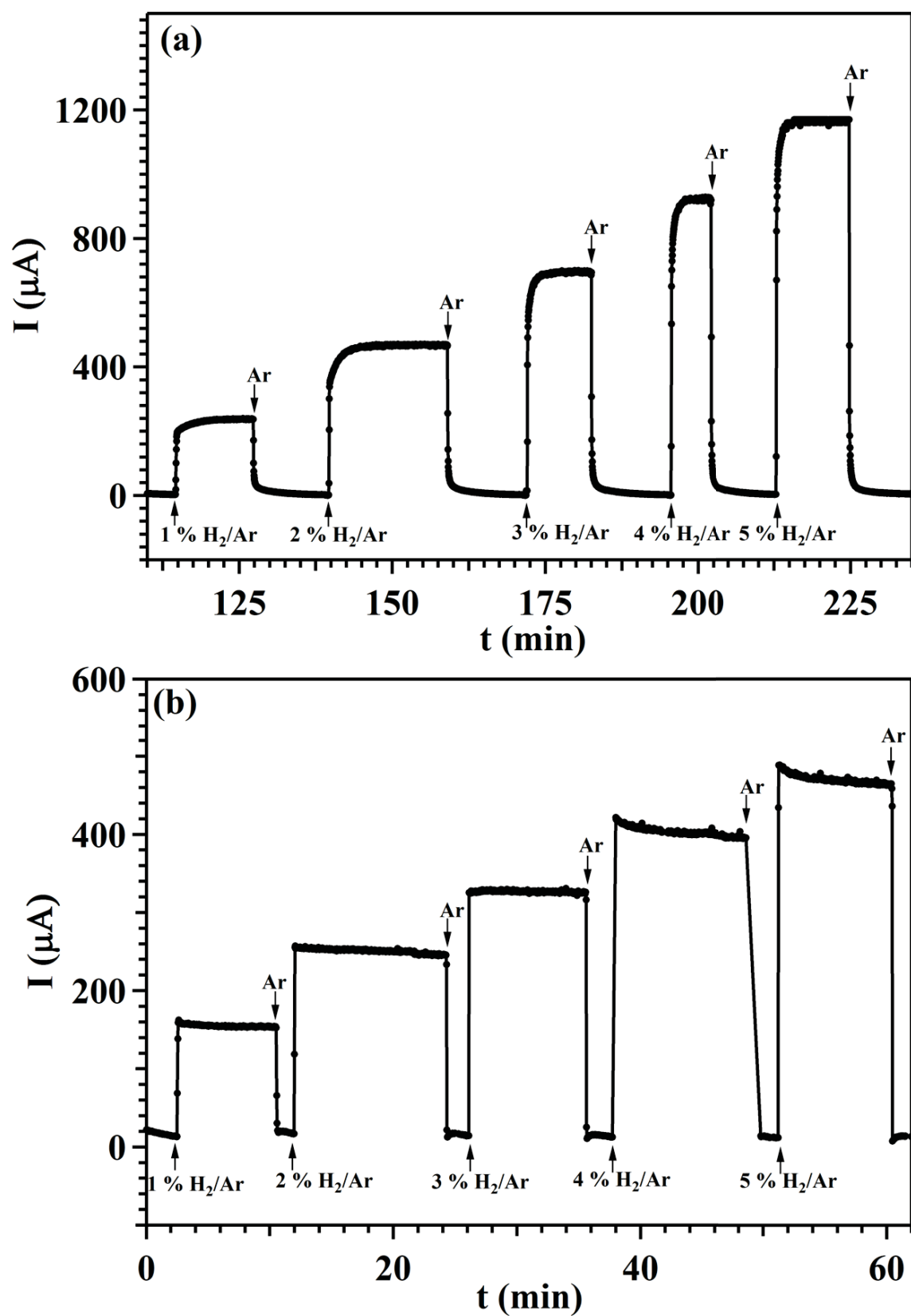


Fig. 4.24 Response behaviour of sensors with pulsed electrodeposited Pt_xPd_y alloy electrodes (a) $Pt_{54}Pd_{46}$ and (b) $Pt_{80}Pd_{20}$

Fig. 4.25 shows the calibration plot of sensors with pulsed electrodeposited $\text{Pt}_{54}\text{Pd}_{46}$, and $\text{Pt}_{80}\text{Pd}_{20}$ sensors. It can be inferred from the figure that sensor with $\text{Pt}_{54}\text{Pd}_{46}$ alloy has the highest sensitivity compared to pristine Pt and $\text{Pt}_{80}\text{Pd}_{20}$ electrode based sensors. The sensitivity gets enhanced with increase in Pd content in Pt_xPd_y alloy but deteriorates when Pd content increases very significantly. Our experimental observations indicate that at 46 % of Pd in Pt_xPd_y alloy improved the sensitivity and response time compared to pristine Pt. The higher sensitivity of $\text{Pt}_{54}\text{Pd}_{46}$ corresponds to higher ECSA value compared to the other alloy compositions as seen from Table 4.6.

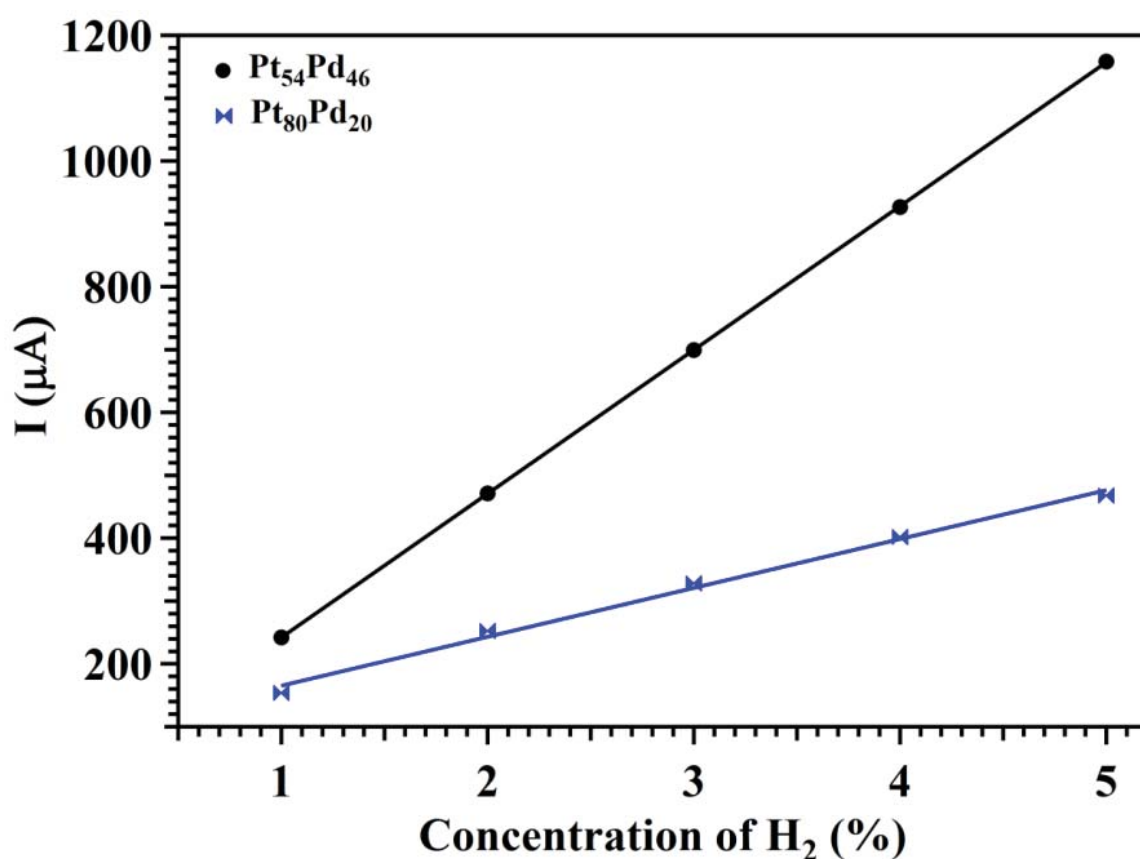


Fig. 4.25 Calibration plot of sensor with pulsed electrodeposited $\text{Pt}_{54}\text{Pd}_{46}$ and $\text{Pt}_{80}\text{Pd}_{20}$ alloy electrodes

Plot bearing the response and recovery time of Pt, $\text{Pt}_{54}\text{Pd}_{46}$, and $\text{Pt}_{80}\text{Pd}_{20}$ alloy sensors are shown in Fig. 4.26.

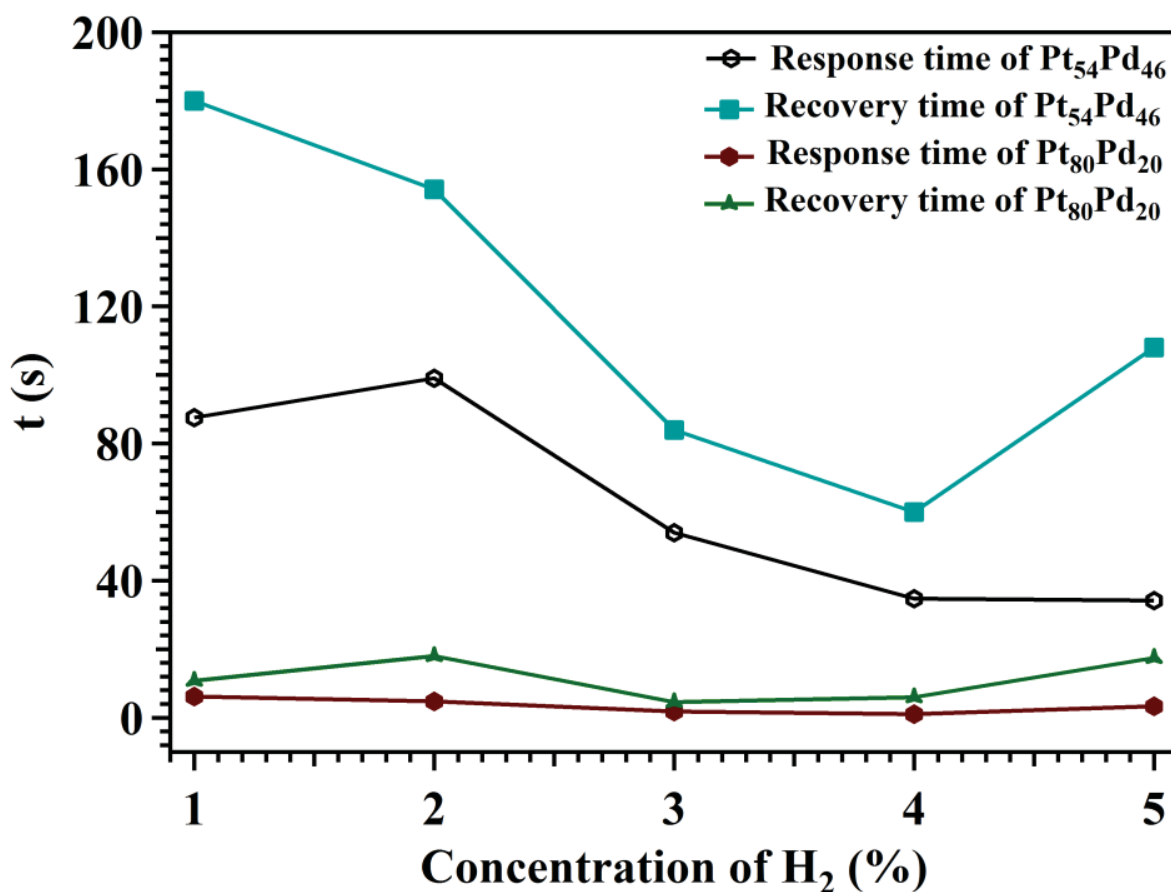


Fig. 4.26 Response and recovery times of sensors with pulsed electrodeposited Pt_xPd_y alloy on gas diffusion layer

Notably, the decrease in response and recovery time with respect to increasing concentration of H₂ is due to the activation of more catalytic sites. The response time of the sensor is improved when the Pt content increases in Pt_xPd_y alloy as observed from Table 4.6. Response and recovery time of Pt₈₀Pd₂₀ sensor achieves steady state faster than that of Pt₅₄Pd₄₆ sensor. Sensitivity and response time are dependent on the ECSA and the ratios of Pt and Pd respectively as indicated in Table 4.6.

Table 4.6 Hydrogen sensing characteristics of sensor with pulsed electrodeposited Pt_xPd_y alloy diffusion electrodes

sensor	Potential limit used for integration of charge for ECSA (V)	ECSA (m^2/g)	Sensitivity ($\mu A/\%$)	Response Time (s)	Detection limit (%)
$Pt_{28}Pd_{72}$	-0.072 – 0.27	17	-	-	-
$Pt_{54}Pd_{46}$	0.019 – 0.33	51	228	34-99	0.0305
$Pt_{80}Pd_{20}$	-0.075 – 0.31	12	78	1.5-6.24	0.0258

Sensitivity and response time are found to be better for Pt_xPd_y alloy compared to the pristine Pt and Pd. Pd has a high sticking coefficient towards H_2 which leads to spontaneous adsorption of H_2 and PdH_x alters the electronic structure of Pt in alloy to favour the hydrogen oxidation reaction¹⁵⁸. Minimum detection limit of $Pt_{54}Pd_{46}$ and $Pt_{80}Pd_{20}$ alloys are shown in Table 4.6. $Pt_{54}Pd_{46}$ alloy sensor shows a detection limit of 0.0305 % H_2/Ar and is found to be the minimum value compared to the other sensors.

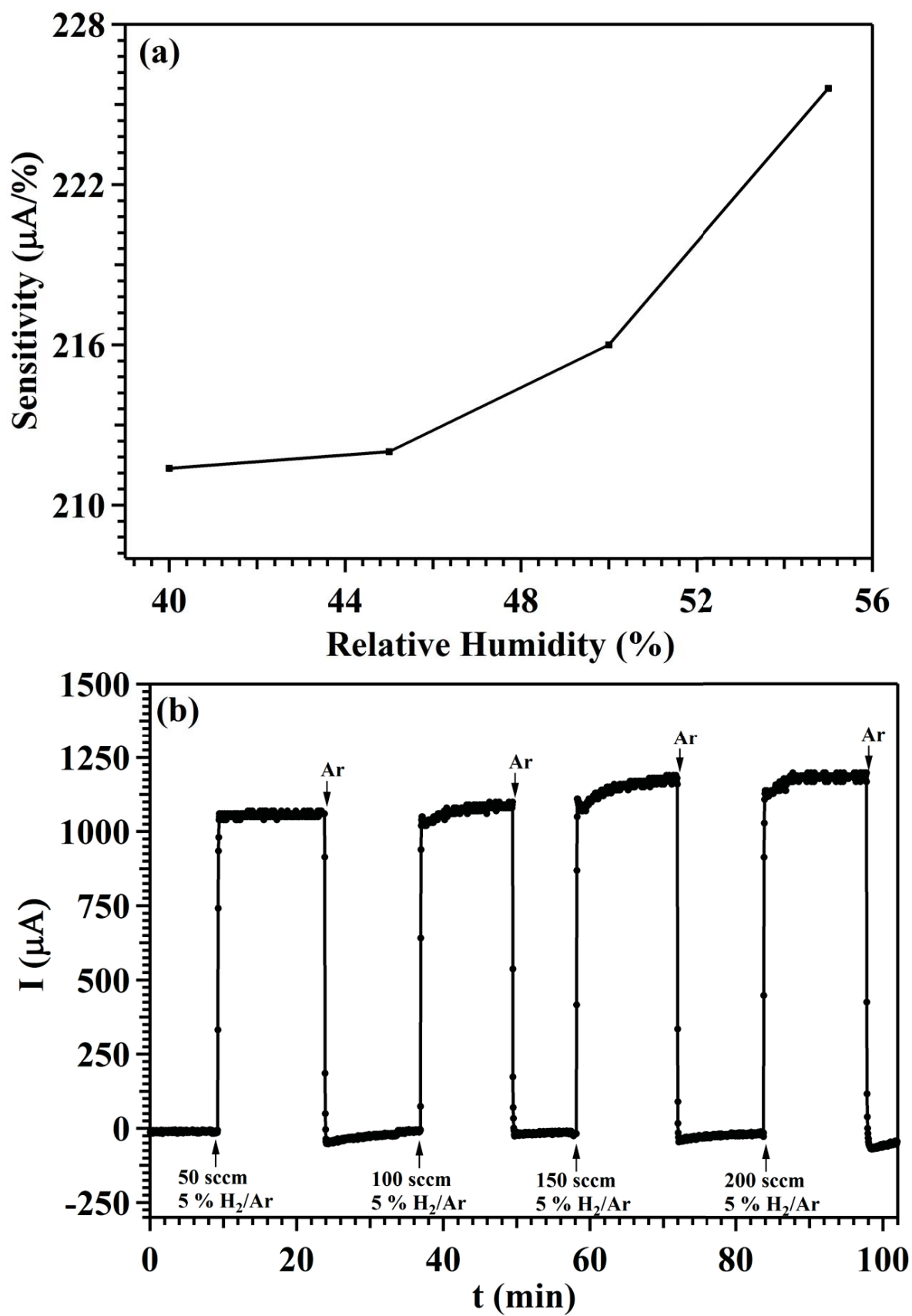


Fig. 4.27 (a) Effect of RH and (b) flow rate on the sensor response for $\text{Pt}_{54}\text{Pd}_{46}$ alloy on gas diffusion layer based sensors

The repeatability, long-term stability, influence of relative humidity (RH) and flow rate effect on the sensor response was studied for Pt₅₄Pd₄₆ sensor since it has optimal response behaviour in comparison to other sensors. The sensor response of Pt₅₄Pd₄₆ sensor was studied at different RH to see the effect of RH on the sensor signal. Fig. 4.27 (a) indicates that a change of RH from 40 to 50 % has an impact on sensitivity which gets altered from 75 $\mu\text{A}/\%$ to 70 $\mu\text{A}/\%$. Electrodeposition of electrocatalyst on GDL for the application in amperometric H₂ sensor has an advantage with respect to flow rate dependence on sensor response. The effect of flow rate on the sensor response of Pt₅₄Pd₄₆ was studied and is shown in Fig. 4.27 (b).

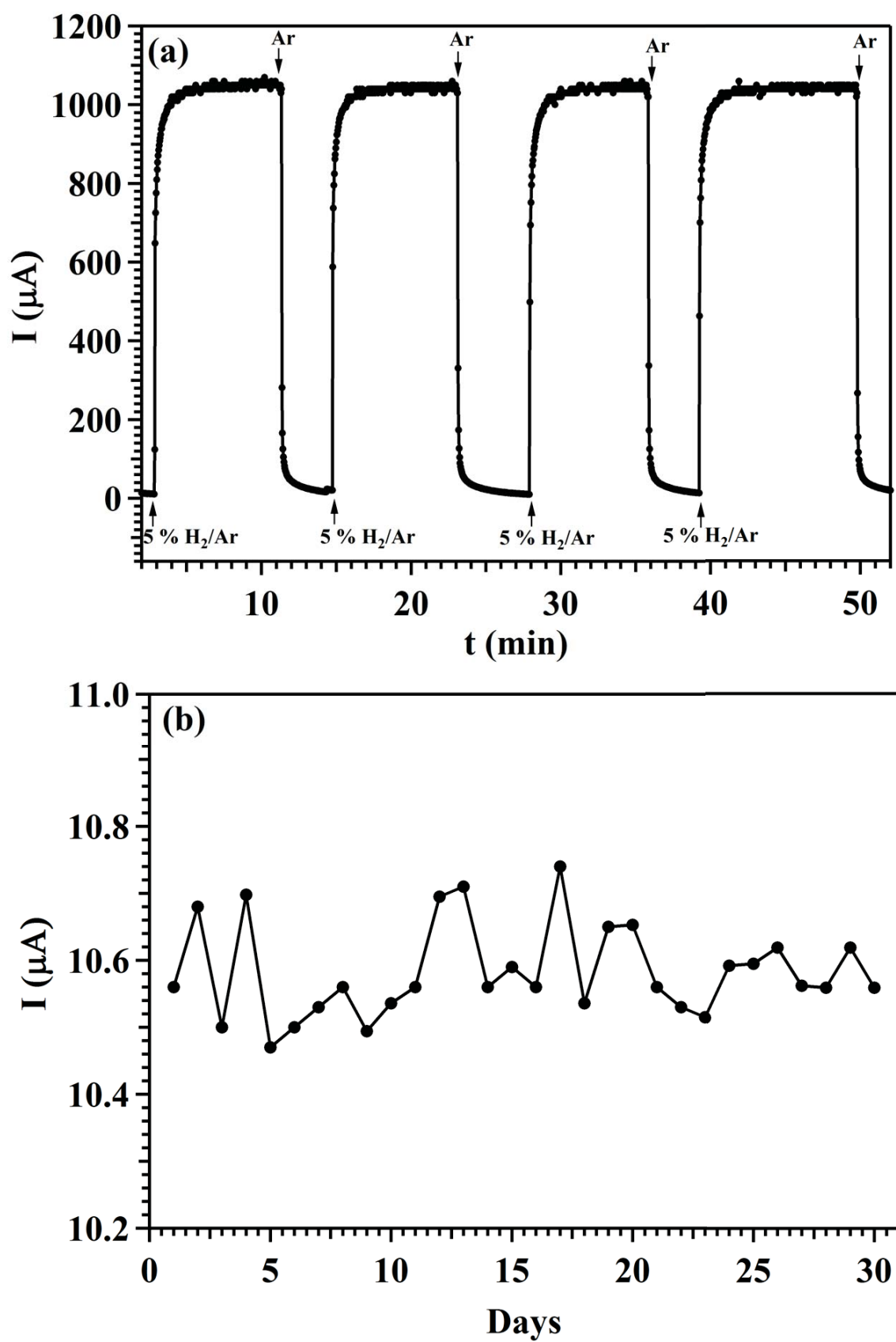


Fig. 4.28 Sensor with pulsed electrodeposited $\text{Pt}_{54}\text{Pd}_{46}$ alloy on gas diffusion layer (a) repeatability of 5 % H_2/Ar of $\text{Pt}_{54}\text{Pd}_{46}$ and (b) long-term stability for 5 % H_2/Ar

Flow rate variation from 100 sccm to 200 sccm has altered the sensor signal from 1085 $\mu\text{A}/\%$ to 1183 $\mu\text{A}/\%$ and the value is found to be well within the acceptable range. Repeatability and long-term stability of $\text{Pt}_{54}\text{Pd}_{46}$ sensor for 5 % H_2/Ar are shown in Fig. 4.28 (a) and (b). Standard deviation of sensor signal was calculated from the repeatability of sensor response for each concentration four times and the values are indicated in Table 4.7.

Table 4.7 Response current with standard deviation of sensor with $\text{Pt}_{54}\text{Pd}_{46}$ alloy diffusion electrode

Concentration of H_2 (%)	Current (μA)	Standard deviation	Response time (s)
1	155.4	± 3.3	11
2	333	± 2.4	18
3	558	± 4.2	60
4	789	± 9.6	66
5	1056	± 3.6	49

Table 4.8 Sensor characteristics of Pt and Pt_xPd_y alloy electrocatalysts on gas diffusion layer based electrodes with sensors reported in literature

Sensing electrode	Sensitivity ($\mu\text{A}/\%$)	Response time (s)	ECSA (m^2/g)
PED/Pt/GDL/AQ	9.75	115-30	26
PED/Pt/GDL/[C4mim][BF ₄]	77.7	12-16	29
PED/ $\text{Pt}_{54}\text{Pd}_{46}$ /GDL/AQ	228	34-99	33
PED/ $\text{Pt}_{80}\text{Pd}_{20}$ /GDL/AQ	78	1.5-6.24	16

Table 4.8 compares the sensitivity and response time of Pt and $\text{Pt}_{54}\text{Pd}_{46}$ sensors. The diffusion electrodes for PEMHS prepared by PED method is found to give better sensitivity and response time than by electrodeposition and brush coating methods. PED method has better control over the particle size than the other deposition methods. On comparing the sensitivity

and response time of Pt and Pt₅₄Pd₄₆ alloy, Pt₅₄Pd₄₆ alloy showed improved response time and higher sensitivity which is attributed to the high ECSA. The alloying of Pt with Pd reduces the expensive Pt and improves the sensitivity and response time. Alloying of Pt with Pd modifies the electronic structure of Pt that contributes to the better catalytic area in Pt_xPd_y alloy. The d-band centre of metal becomes low when it is alloyed with other metals and thus attribute to the optimum adsorption of hydrogen neither strong nor too weak. This may be the reason for the enhanced activity of Pt_xPd_y over pristine Pt or Pd¹⁸⁵.

The sensitivity and response time of the Pt_xPd_y was found to be better compared to the pristine Pt and Pd sensing electrodes. The equal proportions of Pt and Pd in Pt_xPd_y alloy gives higher sensitivity owing to the higher ECSA value over the other compositions of Pt and Pd. Alloying of Pt with 20 % Pd gives short response time compared to the Pt₅₄Pd₄₆ and pristine Pt and Pd electrodes. Higher or equal ratios of Pt in Pt_xPd_y alloy are able to facilitate reaching the steady state in lesser time than the other ratios with lower concentration of Pt. In terms of optimal sensitivity and response time of pulsed electrodeposited Pt_xPd_y alloy electrocatalyst, the order is Pt₅₄Pd₄₆ > Pt IL ≈ Pt₈₀Pd₂₀ > Pt and Pt₈₀Pd₂₀ < Pt IL < Pt < Pt₅₄Pd₄₆ respectively.

Table 4.9 compares the present amperometric H₂ sensors with the sensors reported in literature. The sensitivity of the pulsed electrodeposited electrocatalyst based sensors is comparable with reported sensors. Pulsed electrodeposition or electrodeposition of electrocatalyst on GDL substrate reduces the effect of flow rate of H₂ on the sensor response. GDL also facilitates better dispersion of catalyst enhancing electrocatalytic area. The effect of flow rate on the sensor response is not advisable in the field application. Lu et al. ^[38] and Sakthivel et al. ^[39] observed non-linearity in sensor response with increasing concentration of H₂/Ar. Lu et al. reported that the sensor lose its linearity above 1.15 % due to excess water and heat generated by the reaction with increasing concentration of H₂. In the present sensor

this is prevented because of hydrophobicity incorporated into GDL by Teflonization. The sensitivity of these amperometric H_2 sensors directly depends on the H_2 flux at the sensing electrode which in turn depends on the pore size in the Teflon mechanical barrier. The flux of gas reaching the sensing electrode is minimized using small pore sized mechanical barrier such that the flux of H_2 is reduced. The use of mechanical barrier with pin-hole is advantageous in sodium cleaning or cold trap regeneration since any sodium aerosol produced does not reach the sensing electrode. Due to smaller pore size, the sensitivity of the sensor is lesser in the present sensor in comparison to similar sensors reported in the literature. The dynamic range of the present sensor is from ppm to percentage level with a minimum detection limit of ~ 300 ppm of $Pt_{54}Pd_{46}$ /GDL based sensor.

Table 4.9 Comparison of present amperometric H₂ sensor performances with sensors reported in literature

Electrocatalyst	loading (mg/cm ²)	Preparation method	Concentration range (ppm)	Response time (s)	Sensitivity (μA/ppm)	Ref.
Pt/Nafion	4.99	IR method by NaBH ₄	0-4508	120-180	0.0744	⁹⁰
Pt/C/Nafion	3	HP-Method	1260-5250	100-500	0.716	⁴²
Pt/Nafion	3	IR method by HCOOH	560-11,500	20-50	0.017	⁴⁴
Pt/Nafion	3.05	IR method by NaBH ₄	1-100000	10-50	0.01	⁸⁸
Pt/Nafion	N.A.	Screen printing	50-20000	35-60	0.0022	⁴³
Pt _x Pd _y /Nafion	N.A.	TT-method	100-1000	24 to 37	1.62	⁴⁵
Pt-MWNT/Nafion	1	Decal Transfer	100-1000	33	3.60	⁹²
Ag/Pt-MWNT	1.1	CR by NaBH ₄	5-1000	180	1.1	⁹³
Pt ₅₄ Pd ₄₆ /GDL	0.5	PED	0-50000	34-99	0.022	Present sensor
Pt ₈₀ Pd ₂₀ /GDL	0.5	PED	0-50000	1.5-6.24	0.005	Present sensor

Note: Electrodeposition-ED, pulsed electrodeposition-PED, IR- Impregnation-Reduction, TT- Takenata-Torikai, CR- Chemical reduction, HP- Hot pressed

Huber et al.¹² report on "Response time measurement of hydrogen sensors" showed a maximum response time (t_{90}) of 57 ± 8 s for CAT sensor and a minimum response time of 2.8 ± 0.2 s (Table 4.10).

Table 4.10: Response time reported in Huber et al.¹² document

Sensor Type	Response time
TC	2.8±0.2
MIS-FET	3.4±0.3
MOS I	4.8±0.3
MOS II	23.1±0.2
CAT	57±8

Table 4.11: Response time reported in the present thesis

Sensing electrode	mode of operation two/three electrode mode	Response time (s)
PED/Pt/GDL/AQ	Two	115-30
PED/Pt/GDL/[C4mim][BF4]	Two	12-16
PED/Pt ₅₄ Pd ₄₆ /GDL/AQ	Two	34-99
PED/Pt ₈₀ Pd ₂₀ /GDL/AQ	Two	1.5-6.24
ED/Pd/GDL/[C4mim][Cl]	Three	22-26

The response time of sensors with PED/Pt/GDL/[C4mim][BF4], PED/Pt₈₀Pd₂₀/GDL/AQ and ED/Pd/GDL/[C4mim][Cl] reported in the present study is comparable with Hubert et al.¹² except the sensors with PED/Pt/GDL/AQ and PED/Pt₅₄Pd₄₆/GDL/AQ. Three electrode mode of operation (Table 4.11) was found to give shorter response time and hence future studies of sensor with PED/Pt/GDL/AQ and PED/Pt₅₄Pd₄₆/GDL/AQ in three electrode mode has to be carried out for improving the response time of sensors.

4.4 Conclusions

Pt, Pd and Pt_xPd_y alloy diffusion electrodes were prepared by electrodeposition methods and used for development of PEM fuel cell based amperometric H₂ sensor. The amperometric H₂ sensor performance of pulsed electrodeposited Pt using ionic liquid electrolyte showed a better sensitivity than aqueous electrolyte due to the better control of particle size and also

owing to the improved adhesion of the electrocatalysts since H_2 evolution was avoided during electrodeposition. Sensor with Pd diffusion electrode in two electrode mode exhibited higher response time to reach the steady state but, in three electrode mode operation of sensor gave much higher sensitivity and short response time over two electrode mode. Hence, sensor with Pd diffusion electrode needs to be operated in three electrode mode for achieving the steady state with short response time. Sensor having diffusion electrode with Pt_xPd_y alloy of composition $Pt_{54}Pd_{46}$ in two electrode mode gave better response behaviour for H_2 in Ar compared to pristine Pt in two electrode mode. The alloy also reduced the expensive Pt content in electrode by nearly 50 %. The sensing behaviour also showed that the flow rate dependency gets greatly reduced due to the use of diffusion electrodes for electrocatalyst deposition for sensor application. By adopting electrodeposition method for sensor application was greatly reduced the catalyst loading to 0.5 mg/cm^2 and also avoided the catalyst wastage in the present study compared to the conventional method used for depositing the electrocatalysts. The developed PEMHS is intended to be used in monitoring hydrogen concentrations during sodium cleaning and cold trap regeneration applications in fast reactor technology. For these applications, the response time of 60 seconds is sufficient since the hydrogen concentration is measured in an inert ambient. For these applications, the sensor is used along with the commercial sensor for redundancy. The commercial sensor (NUCON H_2 sensor using Citi-Tech (UK) sensor transducer) used for these applications has a response time of about 90 seconds. The sensor presently developed is having shorter response time than the mentioned commercial sensor.

Chapter 5

Deposition, characterization and application of pulsed electrodeposited Pt_xPd_y alloy based gas diffusion electrodes in PEMFC

5.1 Introduction

Proton exchange membrane fuel cell (PEMFC) is an emerging energy convertor for sustainable development¹⁸⁶⁻¹⁸⁹. Commercial application of PEMFC is challenging due to the high cost of electrocatalyst used. Platinum is the commonly used electrocatalyst for hydrogen oxidation (HOR) and oxygen reduction reactions (ORR). The rate of ORR is six times slower compared to HOR^{190, 191}. Hence, the loading of Pt required is higher at cathode than at anode. Though Pt is the outperforming catalyst for ORR in PEMFC, cost and stability of the catalyst are the major limitations for commercialization in a large-scale. The adsorption of hydrogen and oxygen on metal surface is mainly depending on its electronic structure. The interaction of metal d-band with H_2 , hybridizes to form bonding ($d-\sigma$) and anti-bonding ($d-\sigma$)* orbitals. This model seems to be reasonable for ORR also with reference to Stamenkovic et al.¹⁹². The metals used in HOR and ORR has filled ($d-\sigma$) orbital and the extent of filling ($d-\sigma$)* decides the catalytic activity of the electrocatalyst. An increased filling of anti-bonding orbital leads to weaker binding of metal with adsorbate and this filling is determined by the location of d-band centre. Higher the d-band centre stronger is the binding between metal and adsorbate if the d-band centre is low weaker is the binding (vice-versa). Platinum binds too strongly with oxygen due to high d-band centre. Alloying Pt introduces an irregularity in the Pt lattice eventually leads to the neither too weak nor too strong binding with oxygen. Thus, facilitates better adsorption kinetics for ORR¹⁹³. Hence, to improve the stability of the catalyst without compromising the catalytic activity for ORR, Pt has been alloyed with other metals. Alloying of Pt is commonly accepted owing to the desired change of electronic structure and surface effects^{158, 194}. Pd is the next active metal to Pt for ORR since it has similar lattice structure as

Pt and also economical. Guo et al.¹⁹⁵ observed that alloying of Pt with Pd significantly enhanced the morphology of Pt-Pd alloy.

Many methods have been adopted for the deposition of Pt_xPd_y alloy for the application in PEMFC. They include chemical reduction of electrocatalyst precursors using ethylene glycol, formic acid¹⁹⁶, $NaBH_4$ as reducing agents¹⁹⁷, surfactant assisted synthesis¹⁹⁸, electrodeposition¹⁹⁹, one-step dealloying²⁰⁰ and pulsed electrodeposition (PED)^{49, 201, 202}. PED method has advantages like easy fabrication, low cost, high purity and better control of microstructure when compared to other conventional methods²⁰¹.

Herein, studies were carried out on pulse electrodeposition of Pt_xPd_y alloy on gas diffusion layer (GDL) in three different ratios of Pt and Pd for the first time for fuel cell application. PED method plays an important role for controlling the particle size of the deposit. This method makes the electrode fabrication easier and allows us to achieve high surface area for the electrochemical reactions with minimum loading of the catalyst.

5.2 Experimental

Gas diffusion electrodes were made by pulsed electrodeposition of electrocatalysts on GDL for application in PEM fuel cell. Electrocatalysts used in the present investigation comprises of Pt and Pt_xPd_y alloy and deposition was also carried out by brush coating of Pt/C commercial electrocatalyst on GDL for purpose of comparison.

5.2.1 Pulsed electrodeposition of Pt_xPd_y alloy electrocatalysts on gas diffusion layer

Pulsed electrodeposition of Pt and Pt_xPd_y alloy electrocatalyst was conducted on Nafion impregnated GDL in three electrode configuration with constant stirring. GDL on which electrocatalyst is to be deposited was made as working electrode and brush coated Pt/C catalyst on GDL was used as counter electrode. Saturated calomel electrode was chosen as reference electrode for the electrodeposition. Electrodeposition of pristine Pt on GDL was

carried out using 3 mM of K_2PtCl_6 in 0.5 M H_2SO_4 . Three different compositions of PdCl_2 and K_2PtCl_6 in 0.5 M H_2SO_4 was taken to deposit Pt_xPd_y alloys of three different compositions. The concentrations of electrolytes used for deposition are given in Table 5.1.

Table 5.1 Electrolyte concentrations used for pulsed electrodeposition of Pt_xPd_y alloy on gas diffusion layer

Concentration of K_2PtCl_6 (mM)	Concentration of PdCl_2 (mM)
3 mM PdCl_2	1 mM K_2PtCl_6
3 mM PdCl_2	3 mM K_2PtCl_6
1 mM PdCl_2	3 mM K_2PtCl_6

Pulsed electrodeposition of Pt and Pt_xPd_y alloy on GDL was carried out at pulse potentials of E_L (lower potential) = 0 V, E_U (upper potential) = -0.8 V. In order to choose the optimum pulse width for deposition, pulsed electrodeposition of Pt was studied by carrying out deposition at four different pulse widths such as t_{on} = 0.2 ms, 2 ms, 20 ms and 200 ms. The t_{off} was kept at 20 ms in all the cases. Pulsed electrodeposition of Pt_xPd_y alloy on GDL was carried out at a pulse width of t_{on} = 0.2 ms, t_{off} = 20 ms. Duration of deposition was maintained until similar loadings (0.05 mg/cm^2) of Pt were obtained for the electrodes to be used as anode. Duration of deposition for preparing Pt and Pt_xPd_y alloy for cathode diffusion electrodes were maintained until the loading was found to be at 0.1 mg/cm^2 . Thereafter, the prepared samples were washed with acetone and dried.

5.2.2 Characterization of Pt and Pt_xPd_y alloy based gas diffusion electrodes

Pulsed electrodeposited Pt, and Pt_xPd_y alloy based diffusion electrodes were characterized for their morphology, elemental compositions, crystal structure and particle size by FESEM, EDAX, GIXRD and HRTEM. Chemical compositions of Pt_xPd_y alloy was analysed by ICP-MS. Samples for ICP-MS analysis were prepared by dissolving the pulsed electrodeposited

Pt_xPd_y alloy in aqua regia. Scherrer's formula was employed to calculate the crystallite size of the deposits. Alloy formation of Pt_xPd_y was confirmed by HRTEM analysis and sample for analysis was prepared by sonicating Pt_xPd_y/GDL in methanol and drop casted the solution on copper grid. Details of the instruments used are provided in chapter 2.

5.2.3 Preparation of membrane electrode assembly

Membrane electrode assemblies (MEAs) for use in fuel cells were prepared by hot-pressing the anode and cathode diffusion electrodes onto the Nafion membrane (212 R) at 393 K, 50 bar pressure for 120 s. Fig. 5.1 indicates MEA with an electrode areas of 5 cm² and 25 cm².

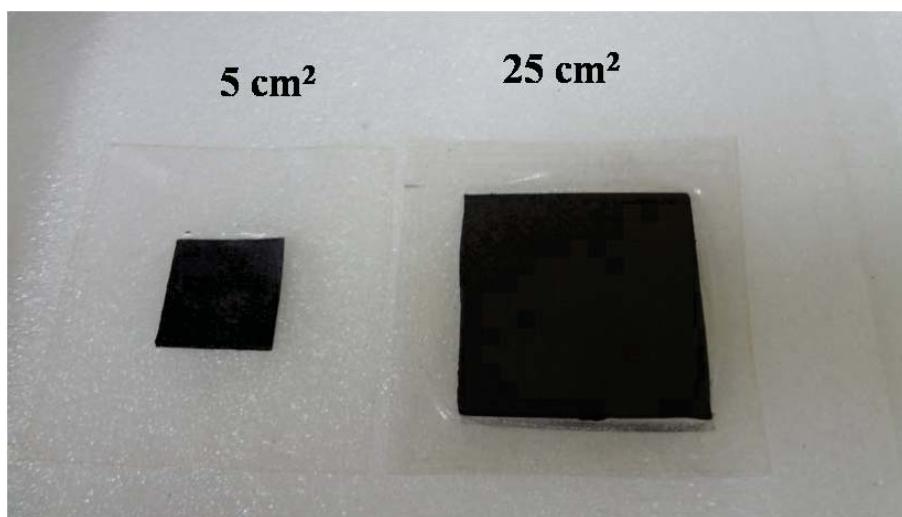


Fig. 5.1 Membrane electrode assemblies of PEM fuel cell with 5 cm² and 25 cm² electrode area

MEAs were made using diffusion electrodes with pulsed electrodeposited Pt on GDL at four different pulse widths as cathode with a loading of 0.1 mg/cm². Diffusion electrodes with pulsed electrodeposited Pt on GDL at a fixed pulse width of 0.2 ms with a loading of 0.05 mg/cm² were used as anode. These MEAs were assembled in fuel cell set-up to study the effect of pulse widths of Pt deposition on the electrochemical active area and charge transfer resistance of the cell. Details of the sub assemblies are presented in Table 5.2.

The fuel cell performance of Pt and Pt_xPd_y alloy electrodes were studied by making MEA with pulsed electrodeposited Pt_xPd_y alloys and pristine Pt at 0.2 ms pulse width on GDL as cathodes and pulsed electrodeposited Pt diffusion electrodes as anode. The loading of Pt and Pt_xPd_y alloy on GDL at cathode side was maintained at 0.1 mg/cm² and that of anode at 0.05 mg/cm² as indicated in Table 5.3. For comparison purposes MEA was also made with commercial Pt/C electrocatalyst with a loading of 0.1 mg/cm² at cathode and 0.05 mg/cm² at anode.

Table 5.2 Loading of electrocatalyst and pulse width used for pulsed electrodeposition of Pt on gas diffusion layer as anode and cathode

Cathode electrocatalyst			Anode electrocatalyst		
Catalyst	Loading (mg/cm ²)	Pulse width (ms)	Catalyst	loading (mg/cm ²)	Pulse width (ms)
Pt	0.1	0.2	Pt	0.05	0.2
Pt	0.1	2	Pt	0.05	0.2
Pt	0.1	20	Pt	0.05	0.2
Pt	0.1	200	Pt	0.05	0.2

Table 5.3 Loading of electrocatalyst and pulse width used for pulsed electrodeposition of Pt_xPd_y alloy on gas diffusion layer as cathode and for pulsed electrodeposition of Pt on gas diffusion layer as anode

Cathode electrocatalyst			Anode electrocatalyst		
Catalyst	Loading (mg/cm ²)	Pulse width (ms)	Catalyst	Loading (mg/cm ²)	Pulse width (ms)
Pt ₂₈ Pd ₇₂	0.1	0.2	Pt	0.05	0.2
Pt ₅₁ Pd ₄₉	0.1	0.2	Pt	0.05	0.2
Pt ₈₁ Pd ₁₉	0.1	0.2	Pt	0.05	0.2

5.2.4 Assembly of proton exchange membrane fuel cell

The PEM fuel cell consists of components like end plates, mono-polar plates (graphite), current collectors, gas diffusion electrodes (GDEs), etc. are shown in Fig. 5.2 (a). MEA is formed by sandwiching the Nafion memberane (Nafion 212R) between anode and cathode gas diffusion electrodes at 393 K, 50 bar pressure for 120 s. The assembly of PEM fuel cell (Fig. 5.2 (b)) is made by placing the MEA between two monopolar plates for the supply of gas followed by gold coated (5 μm) copper plate used as current collectors on both sides. The assembly is finally enclosed by two stainless steel end plates with provision for gas inlet and outlet. After assembling the cell, uniform torque of 5 Nm was applied for tightening the cell. Across leak was tested by passing argon at anode and checking the leak at cathode. Gas leak tightness of fuel cells was ensured prior to the testing. Totally six cells were made, five cells with an area of 5 cm^2 and one with 25 cm^2 electrode area. Further details of diffusion electrodes are shown in Table 5.4.

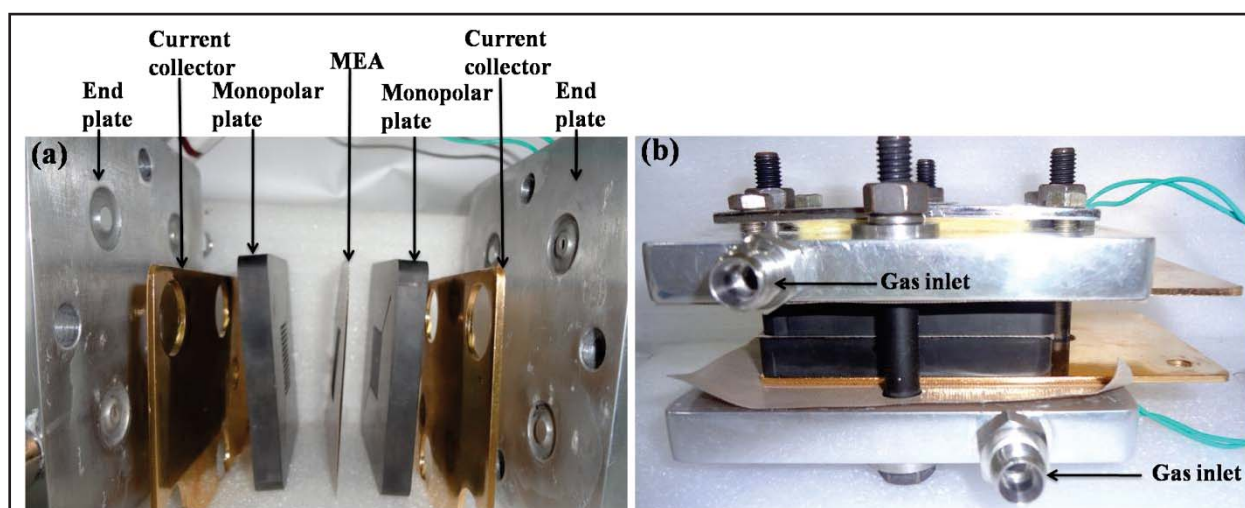


Fig. 5.2 (a) Components of proton exchange membrane fuel cell and (b) Assembly of proton exchange membrane fuel cell

Table 5.4 PEM fuel cells assembled and tested

Cathode electrocatalyst			Anode electrocatalyst			Area
Catalyst	Loading (mg/cm ²)	Pulse width (ms)	Catalyst	Pulse width (ms)	loading (mg/cm ²)	(cm ²)
Pt	0.1	0.2	Pt	0.2	0.05	5
Pt ₂₈ Pd ₇₂	0.1	0.2	Pt	0.2	0.05	5
Pt ₅₁ Pd ₄₉	0.1	0.2	Pt	0.2	0.05	5
Pt ₈₁ Pd ₁₉	0.1	0.2	Pt	0.2	0.05	5
Pt/C commercial	0.1	-	Pt/C commercial	-	0.05	5
Pt ₅₁ Pd ₄₉	0.1	0.2	Pt	0.2	0.05	25

5.2.5 Electrochemical characterizations of membrane electrode assembly

MEAs (5 cm²) assembled in standard fuel cell configuration were characterized for electrochemical active surface area by cyclic voltammetry. Hydrogen adsorption - desorption voltammetric studies were carried out in-situ using the fuel cell set up at scan rate of 50 mV/s in the potential range 0 to 1 V. Impedance spectra were recorded for all the cells under operating condition with H₂ at anode side and O₂ at the cathode side using the real time impedance measurement option available in fuel cell test station. Measurements were carried out in the frequency range of 1 kHz to 10 mHz under an applied potential of 10 mV. Polarizing potential of 0.5 V was applied and the discharge current of 1 A/cm² was observed.

5.2.6 Performance evaluation of fuel cell

Fuel cell performance was ascertained for six MEAs shown in Table 5.4 under the following conditions: cell temperature; 323 K, humidification temperature; 313 K and line temperature; 323 K. The flow rates of H₂ at anode and O₂ at cathode were maintained at 100 sccm and 200 sccm respectively. The fuel cell test station with assembled fuel cell is shown in Fig. 5.3. The

fuel cell catalysts were activated by keeping the discharge potential of fuel cell at 0.5 V for 4 h with H_2 flow maintained at anode side and O_2 at cathode side. Thereafter, the current-voltage polarization curve was recorded in the potential range from open circuit potential to 0.3 V at the scan rate of 50 mV/s. Fuel cell discharge at constant potential (0.5V) was also studied to ascertain the stability of the cells.

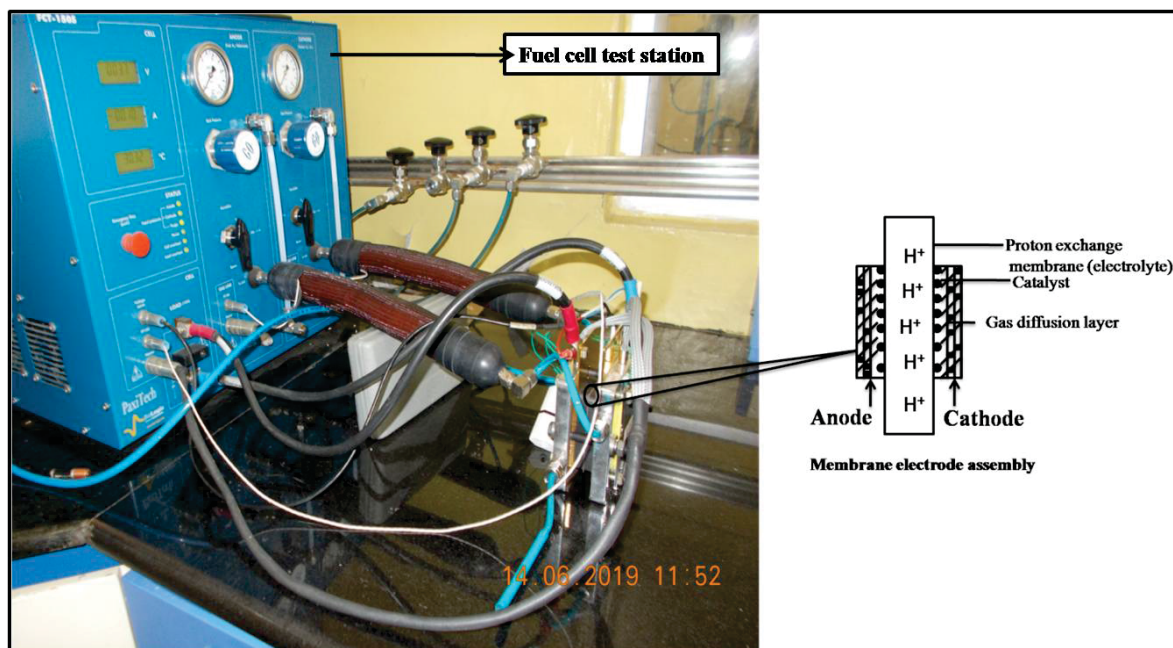


Fig. 5.3 Fuel cell set up with test station

5.3 Results and discussions

5.3.1 Physicochemical characterizations of Pt and Pt_xPd_y alloy on gas diffusion layer

The chemical composition of deposited Pt_xPd_y alloy in gas diffusion electrodes was dependent on the concentrations of Pt and Pd in electrolyte solutions used for pulsed electrodeposition. ICP-MS analysis of stripped out Pt_xPd_y on diffusion electrodes indicated Pt/ Pd ratios as Pt_1Pd_3 , Pt_1Pd_1 and Pt_4Pd_1 for the electrolyte concentrations of 3 mM $PdCl_2$ + 1 mM K_2PtCl_6 , 3 mM $PdCl_2$ + 3 mM K_2PtCl_6 and 1 mM $PdCl_2$ + 3 mM K_2PtCl_6 respectively. The ratios of Pt and Pd in Pt_xPd_y alloys were also confirmed by EDAX and are found to be similar to that obtained by ICP-MS analysis. EDAX analysis of Pt_xPd_y showed

compositions of Pt₂₈Pd₇₂, Pt₅₁Pd₄₉ and Pt₈₁Pd₁₉ (Fig 5.4). EDAX analysis indicated 0.8 % of chloride in Pt₈₁Pd₁₉ sample and was removed by washing thoroughly with acetone prior to other characterizations.

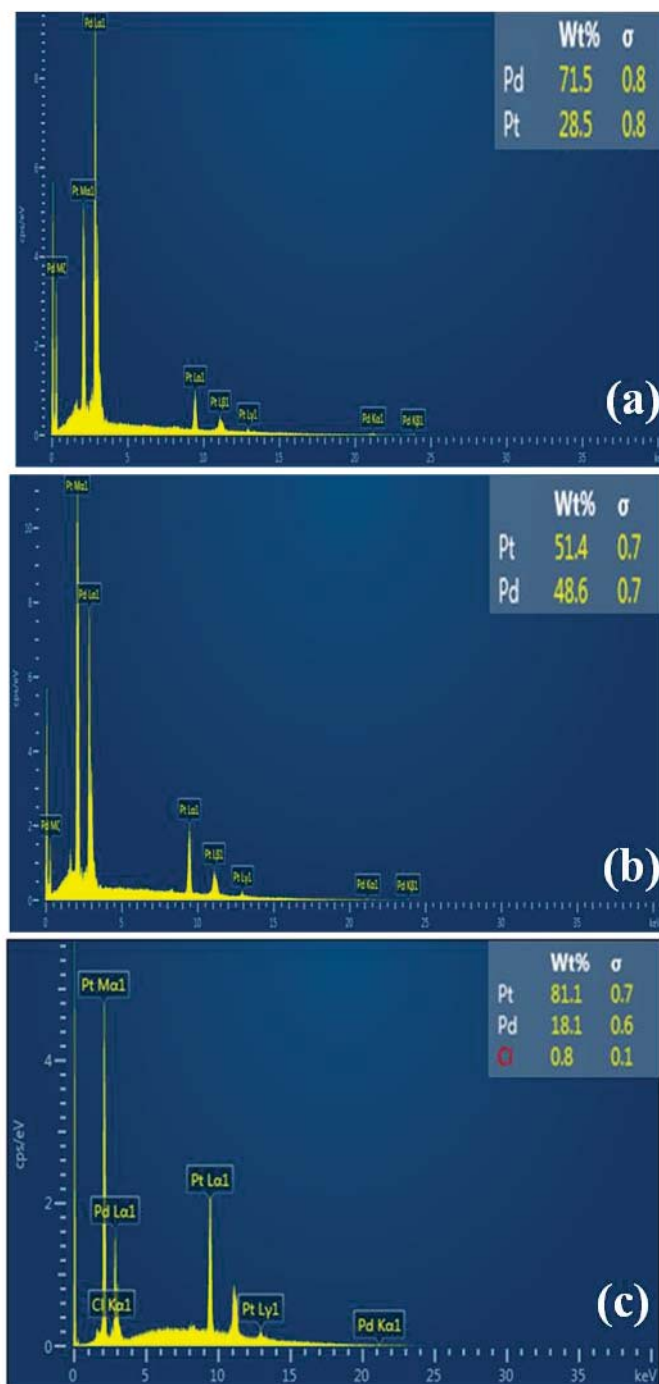


Fig. 5.4 Energy dispersive X-ray analysis of pulsed electrodeposited Pt_xPd_y alloy on gas diffusion layer (a) Pt₂₈Pd₇₂, (b) Pt₅₁Pd₄₉ and (c) Pt₈₁Pd₁₉

Field emission scanning electron microscope images of pulsed electrodeposited Pt on GDL at various pulse widths are shown in Fig. 5.5. Spherical particles and particle size is getting reduced with decreasing pulse width. Hence, Pt, Pd and Pt_xPd_y alloy based diffusion electrodes were prepared at a pulse width of 0.2 ms to obtain higher electrocatalytic area for fuel cell application.

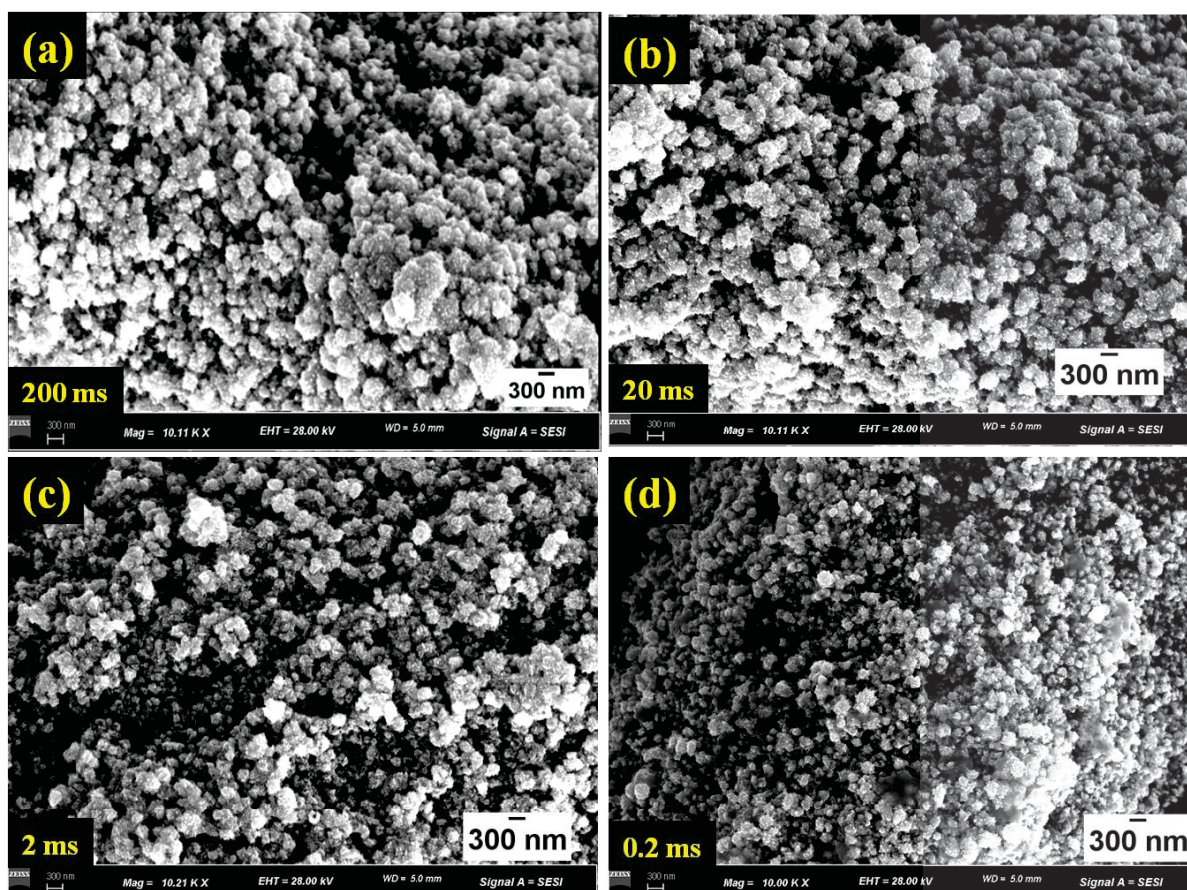


Fig. 5.5 Field emission scanning electron microscope images of pulsed electrodeposited Pt on gas diffusion layer at different pulse widths of (a) 200 ms, (b) 20 ms, (c) 2 ms and (d) 0.2 ms

FESEM images of pulsed electrodeposited Pt_xPd_y alloys exhibited spherical particles with uniform coverage over GDL (Fig. 5.6). Chapter 3 (Fig. 3.17) indicated that EDAX mapping of $Pt_{54}Pd_{46}$ alloy showed uniform distribution of Pt and Pd over the surface of GDL prepared by pulsed electrodeposition method.

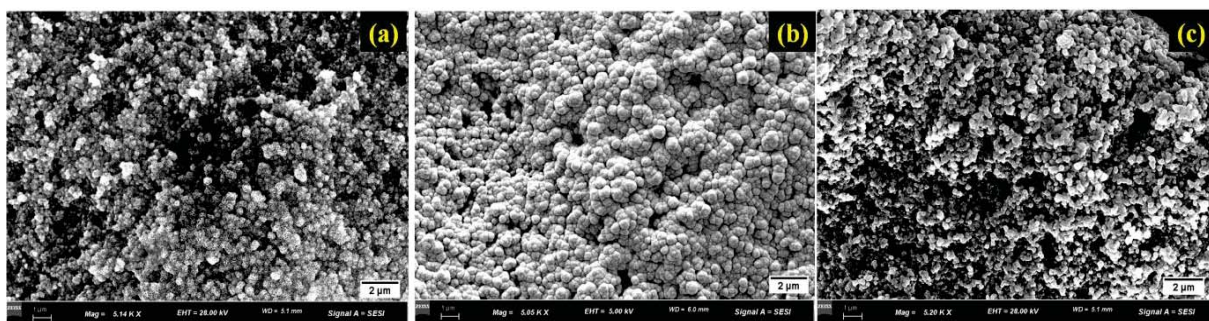


Fig. 5.6 FESEM images of pulsed electrodeposited Pt_xPd_y alloys on gas diffusion layer at 0.2 ms pulse width (a) $Pt_{28}Pd_{72}$, (b) $Pt_{51}Pd_{49}$ and (c) $Pt_{81}Pd_{19}$

Grazing incidence X-ray diffraction pattern of Pt, $Pt_{81}Pd_{19}$, $Pt_{51}Pd_{49}$ and $Pt_{28}Pd_{72}$ are shown in Fig. 5.7. GIXRD patterns of all the deposited electrocatalysts exhibit peaks at 39.32° , 45.71° , 66.9° and their corresponding planes are (111), (200) and (220) (JCPDS card no. 7440.05.3). This confirms that Pt_xPd_y has fcc crystal structure.

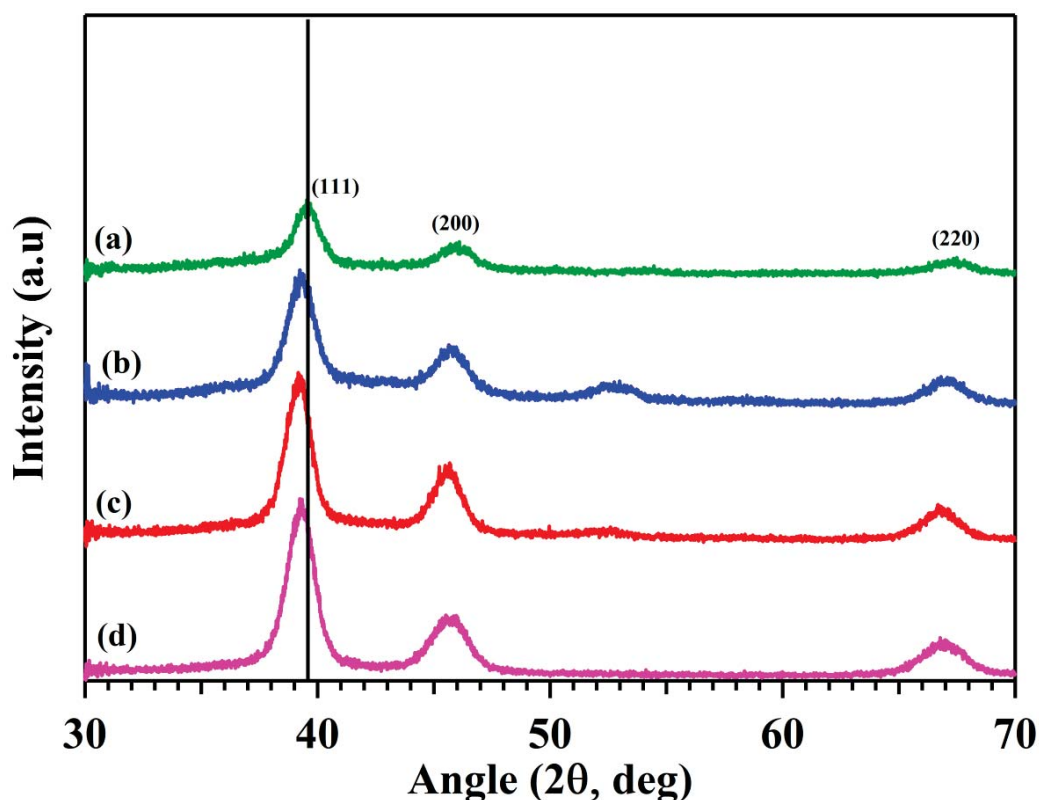


Fig. 5.7 Grazing incidence X-ray diffraction pattern of Pt, Pd and Pt_xPd_y alloy: (a) Pt (b) $Pt_{81}Pd_{19}$ (c) $Pt_{51}Pd_{49}$ (d) $Pt_{28}Pd_{72}$

The slight shift in 2θ value and also change in lattice parameter is observed for Pt_xPd_y alloy compared to pure Pt which is an indication of the presence of alloy. 2θ value corresponding to (111) plane and lattice parameters of Pt and Pt_xPd_y alloy are shown in Table 5.5. Crystallite sizes of pulsed electrodeposited Pt and Pt_xPd_y alloy on GDL for (111) are shown in Table 5.5 and the sizes are found to be between 2.55 and 3.64 nm.

Table 5.5 Bragg angle, lattice parameter and crystallite sizes of pulsed electrodeposited $Pt_{28}Pd_{72}$, $Pt_{51}Pd_{49}$ and $Pt_{81}Pd_{19}$ on gas diffusion layer

Pt_xPd_y alloy	Angle (2θ) (111)	Lattice parameter (nm) (111)	Lattice parameter (nm) (200)	Lattice parameter (nm) (220)	Crystallite size (d) (nm)
Pt	39.32 ± 0.004	0.393	0.393	0.392	3.64 ± 0.12
$Pt_{28}Pd_{72}$	39.27 ± 0.002	0.396	0.393	0.392	3.00 ± 0.21
$Pt_{51}Pd_{49}$	39.17 ± 0.005	0.393	0.396	0.394	2.96 ± 0.19
$Pt_{81}Pd_{19}$	39.31 ± 0.008	0.394	0.395	0.393	2.55 ± 0.12

TEM images of representative $Pt_{51}Pd_{49}$ alloy were recorded. Fig. 5.8 (a, and b) shows the TEM images with an average particle size of 4.6 nm as revealed from histogram (Fig 5.8 (f)). The high magnification HRTEM images indicate that the particles are spherical and well distributed (Fig. 5.8 (c)). Fig. 5.8 (d) shows lattice spacing of 0.229 nm in between the lattice spacing of pure Pt (0.23 nm with (111) lattice plane)²⁰³ and Pd (0.224 nm with (111) lattice plane)²⁰⁴. The ring pattern shown (Fig.5.8 (e)) by selected area electron diffraction (SAED) indicating that pulsed electrodeposited $Pt_{51}Pd_{49}$ alloy on GDL is polycrystalline in nature (JCPDS No. 04-001-0001).

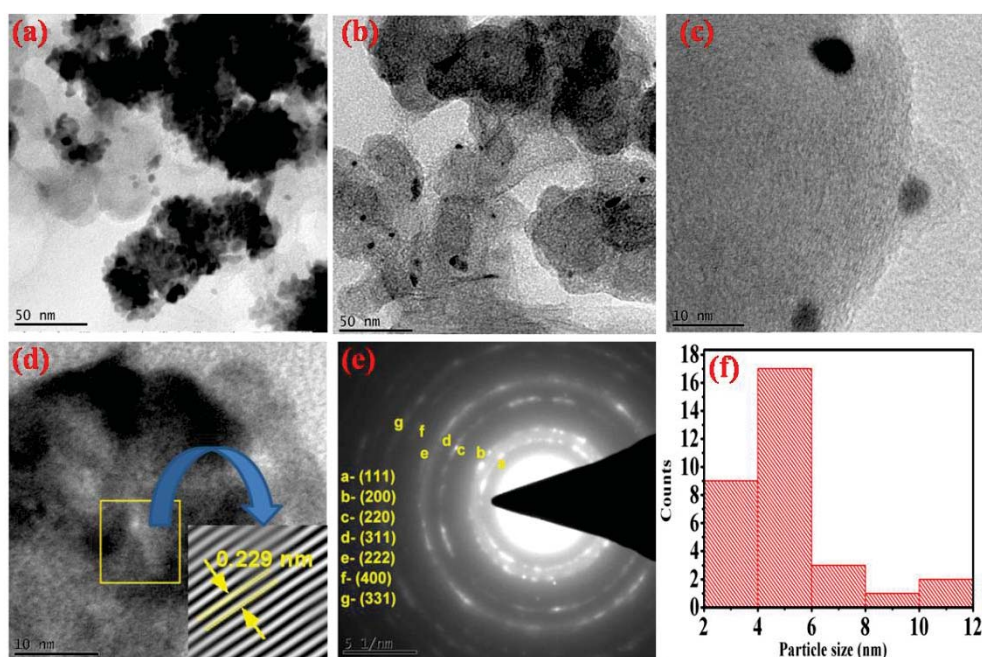


Fig. 5.8 (a) TEM image, (b) to (d) HRTEM images, (e) SAED pattern and (f) particle size distribution

5.3.2 Electrochemical characterizations of membrane electrode assemblies

In order to understand the effect of pulse width on the catalytic area of Pt deposited on GDL, deposition was carried out at different pulse widths. Cyclic voltammogram of pulsed electrodeposited Pt at different pulse width is shown in Fig. 5.9 (a). ECSA was calculated using eq. (4.2) (section 4.2.4) by substituting the integrated charge. ECSA increases with decreasing pulse width (Fig. 5.9 (b)) due to lesser agglomeration and reduced particle size at lower pulse width. This aspect is further confirmed by FESEM images (Fig. 5.5). ECSA increases in the order 200 ms < 20 ms < 2 ms < 0.2 ms (Table 5.6). Electrochemical impedance studies of pulsed electrodeposited Pt based gas diffusion electrodes at different pulse widths further substantiates the enhanced electrochemical activity with decreasing pulse width.

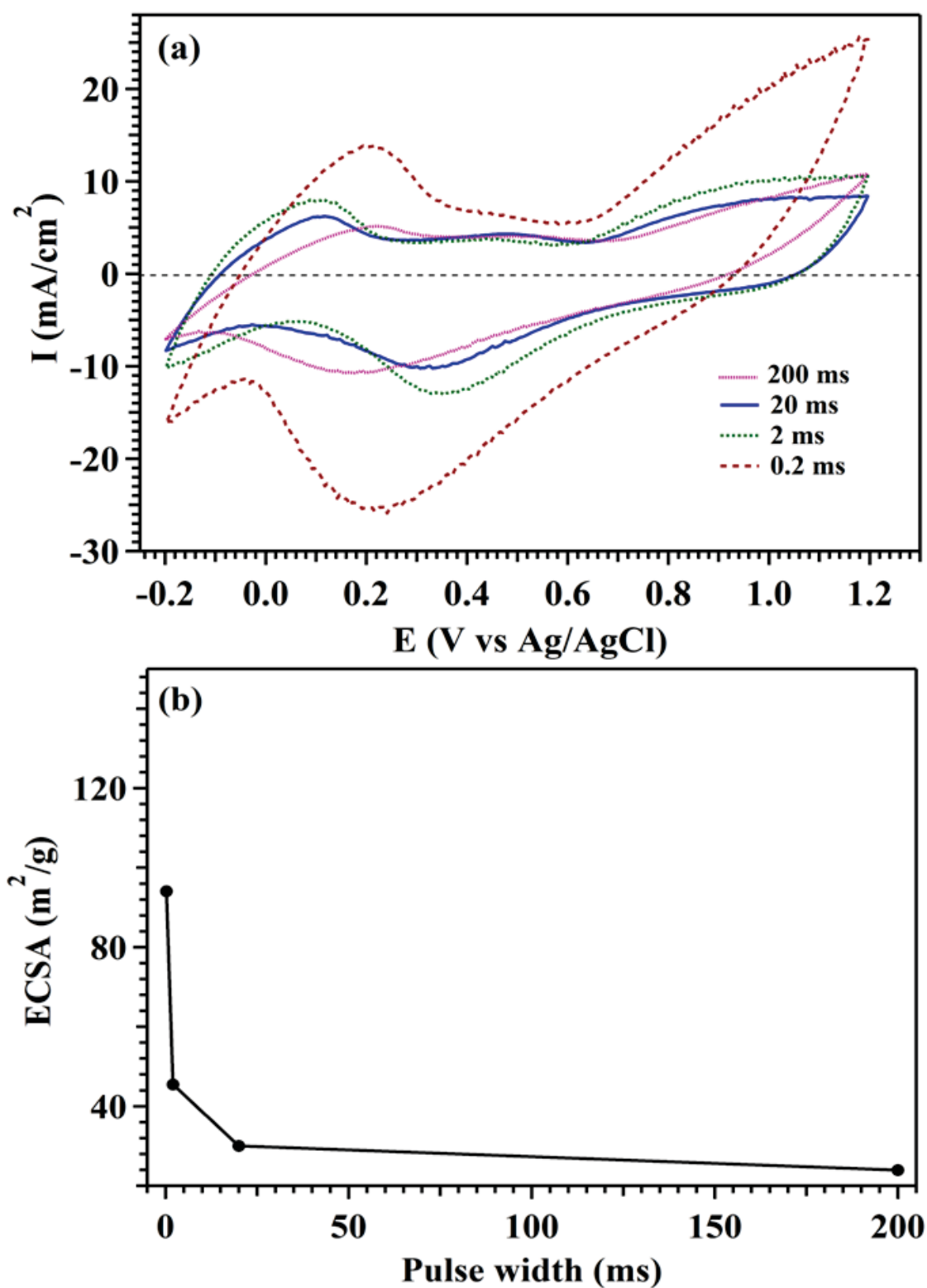


Fig. 5.9 (a) Cyclic voltammogram of pulsed electrodeposited Pt on gas diffusion layer at various pulse widths (Loading: 0.1 mg/cm², scan rate: 200 mV/s) and (b) Plot of ECSA vs pulse width

Table 5.6 Electrochemical surface area of pulsed electrodeposited Pt on GDL at various pulse widths

Pulsed electrodeposited Pt on GDL at various pulse widths	Potential limit used for integration of charge for ECSA (V)	ECSA (m²/g)
200 ms	0.119 - 0.34	24
20 ms	0.001 - 0.25	30
2 ms	-0.052 - 0.27	45
0.2 ms	0.040 – 0.39	98

The impedance spectra shown in Fig. 5.10 and Fig. 5.11 indicated a semicircle with two characteristic features: (i) a high frequency intercept on the real axis corresponding to total ohmic resistance, electrolyte resistance of single cell and (ii) a single elongated semicircle, the diameter of which is ascribed to the charge transfer resistance, pulsed electrodeposited cathode electrocatalysts. The impedance spectra are fitted with resistor and non-ideal capacitor in parallel combination and their equivalent circuits are displayed in Fig. 5.10 and Fig. 5.11 as insets. It can be seen from both Fig. 5.10 and Fig. 5.11 that, electrolyte resistance of the cells are not varying much with the electrocatalysts representing minimal effect of electrocatalysts on the electrolyte resistance of the fuel cell. On the other hand, charge transfer resistance changes significantly for different pulsed electrodeposited Pt and Pt_xPd_y alloy electrocatalysts. It is an important parameter, since it can give a direct correlation with the ORR kinetics; a low value indicates a high catalytic activity. The estimated charge transfer resistance of pulsed electrodeposited Pt at various pulse widths and Pt_xPd_y alloy electrocatalysts on GDL follows the decreasing order: 200 ms > 20 ms > 2 ms > 0.2 ms and Pt₂₈Pd₇₂ > Pt/C > Pt₈₁Pd₁₉ > Pt₅₁Pd₄₉ respectively (Table 5.7 and Table 5.8). Low charge transfer resistance of pulsed electrodeposited Pt at a pulse width of 0.2 ms and pulsed electrodeposited Pt₅₁Pd₄₉ are expected to give higher electrocatalytic activity for ORR.

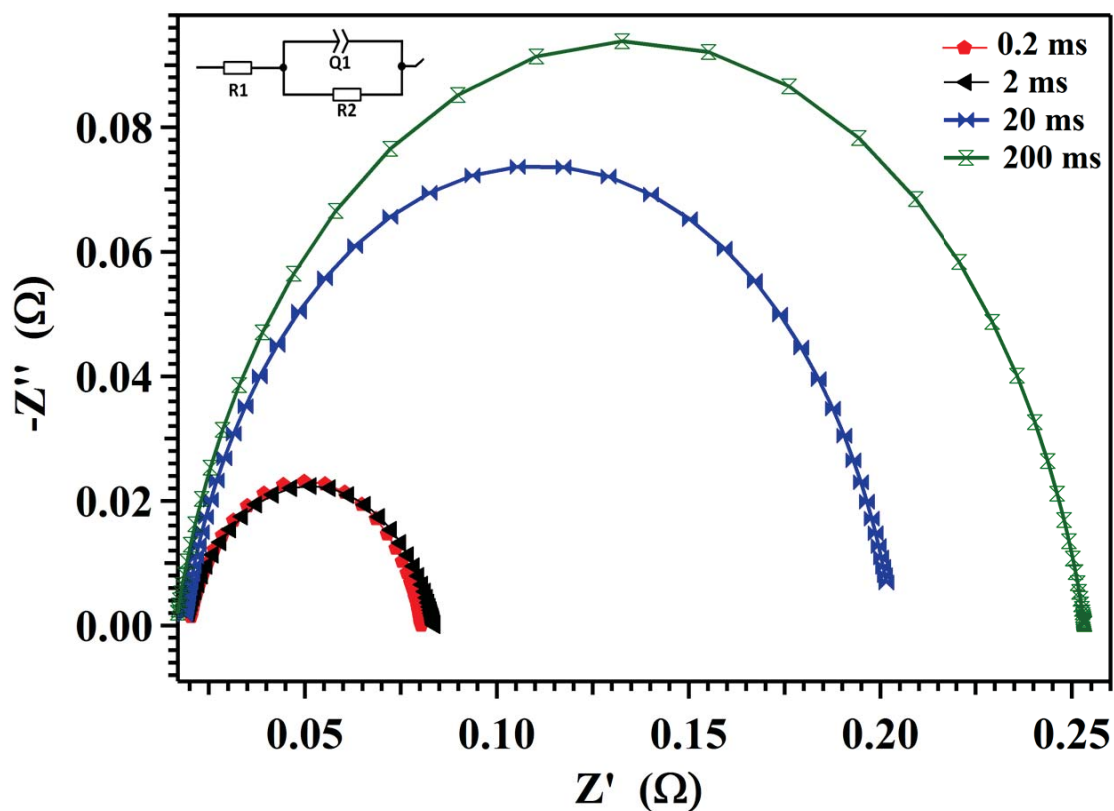


Fig. 5.10 Impedance spectrum of fuel cell with pulsed electrodeposited Pt diffusion electrode at different pulse widths as cathode and pulsed electrodeposited Pt at 0.2 ms as anode (R_1 - Ohmic resistance, R_2 - Charge transfer resistance and Q_1 - Non-ideal capacitance)

Table 5.7 Electrochemical impedance of pulsed electrodeposited Pt diffusion electrode at different pulse widths

Pulsed electrodeposited Pt at a pulse width (ms)	Ohmic resistance (R_1) (Ω)	Charge transfer resistance (R_2) (Ω)	Non-ideal capacitance (Q_1) (F)
0.2	0.019	0.060	0.067
2	0.019	0.064	0.093
20	0.019	0.190	0.095
200	0.019	0.237	0.100

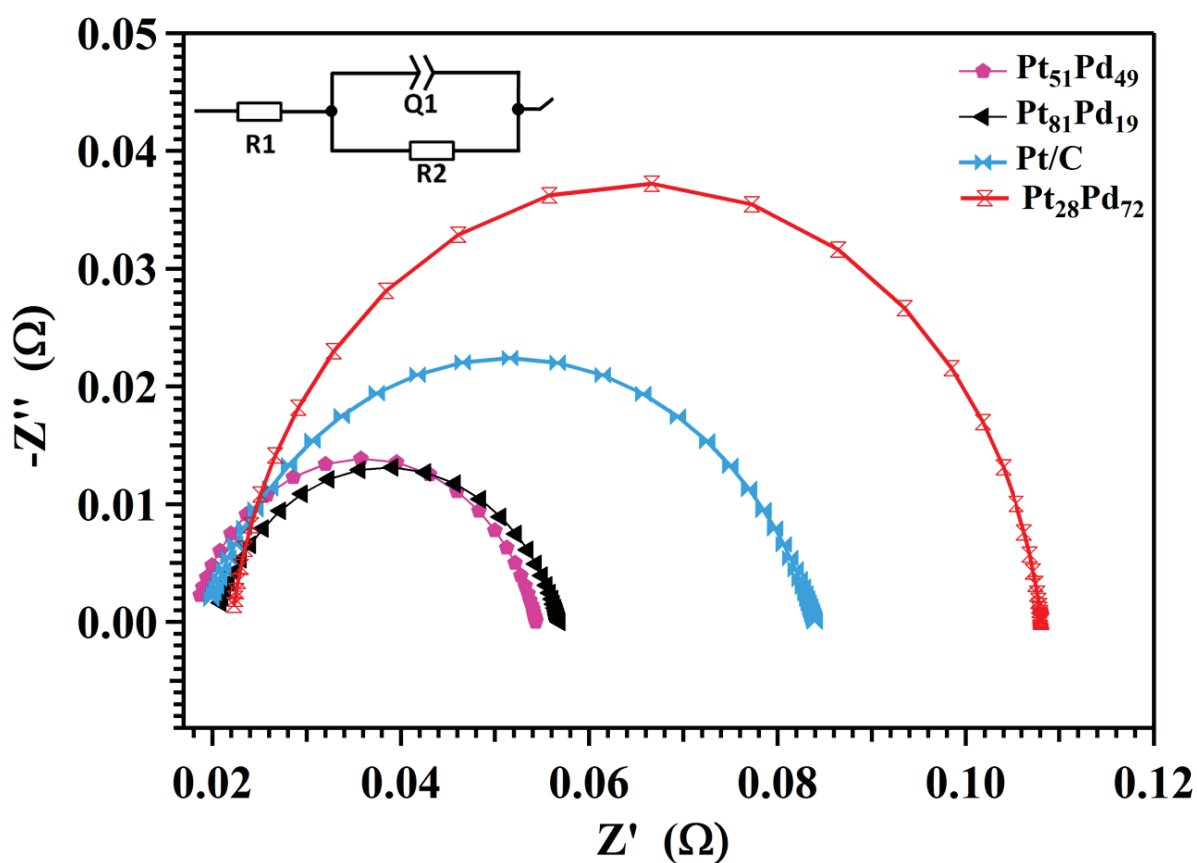


Fig. 5.11 Electrochemical impedance spectrum of Pt/C commercial catalyst and pulsed electrodeposited Pt_xPd_y alloy electrocatalysts on gas diffusion layer (R_1 - Ohmic resistance, R_2 - Charge transfer resistance and Q_1 - Non-ideal capacitance)

Table 5.8 Electrochemical impedance of Pt/C commercial catalyst and pulsed electrodeposited Pt_xPd_y alloy electrocatalysts on gas diffusion layer

Electrocatalysts	Ohmic resistance (R_1) (Ω)	Charge transfer resistance (R_2) (Ω)	Non-ideal capacitance (Q_1) (F)
Pt/C	0.018	0.086	0.029
$\text{Pt}_{51}\text{Pd}_{49}$	0.018	0.046	0.057
$\text{Pt}_{81}\text{Pd}_{19}$	0.018	0.050	0.062
$\text{Pt}_{28}\text{Pd}_{72}$	0.018	0.1063	0.180

Cyclic voltammogram of brush coated and pulsed electrodeposited Pt_xPd_y alloy electrodes are shown in Fig. 5.12. ECSA values were calculated from the integrated charge in different potential limits as indicated by Table 5.9. ECSA values of electrocatalysts are shown in Table 5.9 and is in the order $Pt_{51}Pd_{49} > Pt_{81}Pd_{19} > Pt/C > Pt_{28}Pd_{72}$.

Table 5.9 Electrochemical surface area of brush coated Pt/C/GDL and pulsed electrodeposited Pt_xPd_y on GDL

Pulsed electrodeposited Pt/C and Pt_xPd_y alloy on GDL	Potential limit used for integration of charge for ECSA (V)	ECSA (m^2/g)
$Pt_{28}Pd_{72}$	-0.05 – 0.30	38
$Pt_{51}Pd_{49}$	-0.068 – 0.30	101
Pt/C	-0.075 – 0.226	62
$Pt_{81}Pd_{19}$	0.031 – 0.32	55

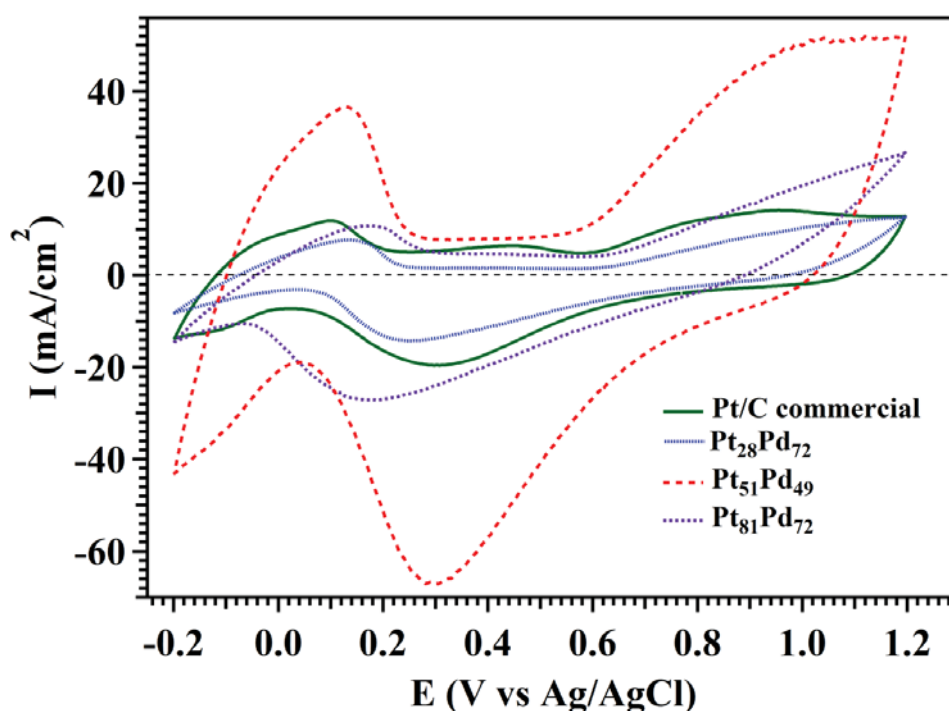


Fig. 5.12 Cyclic voltammogram of Pt/C commercial catalyst and pulsed electrodeposited Pt_xPd_y alloy electrocatalysts on gas diffusion layer (Loading: 0.1 mg/cm^2 scan rate: 200 mV/s)

5.3.3 Performance evaluation of fuel cells assembled with catalyst deposited diffusion electrodes

Electrochemical active area and charge transfer resistance of diffusion electrodes indicated that pulsed electrodeposited Pt and Pt_xPd_y alloys on GDL at 0.2 ms exhibited maximum electrochemical active area and minimum R_{ct} . Hence, fuel cell performance was evaluated for diffusion electrodes with pulsed electrodeposited Pt and Pt_xPd_y alloys deposited at 0.2 ms pulse width (used as cathode electrocatalysts). Pulsed electrodeposited Pt on GDL at 0.2 ms pulse width was used as anode for all the cells used in the study.

Proton exchange membrane fuel cell performance for diffusion electrode with brush coated Pt/C on GDL and pulsed electrodeposited Pt_xPd_y alloy electrocatalysts on GDL are shown in Fig. 5.13. Pulsed electrodeposited $Pt_{51}Pd_{49}$ alloy on GDL is found to have higher power density over other compositions of Pt_xPd_y alloy catalyst and Pt/C commercial catalyst. The fuel cell performance of pulsed electrodeposited $Pt_{51}Pd_{49}$ alloy (loading of Pt – 0.05 mg/cm²) electrocatalyst is comparable with that of pulsed electrodeposited Pt (Fig. 5.13) (0.1 mg/cm²). This is attributed to high ECSA (Table 5.9) and low R_{ct} values (Table 5.8) of $Pt_{51}Pd_{49}$ alloy. Current density vs time plot at 0.5 V is shown in Fig. 5.14.

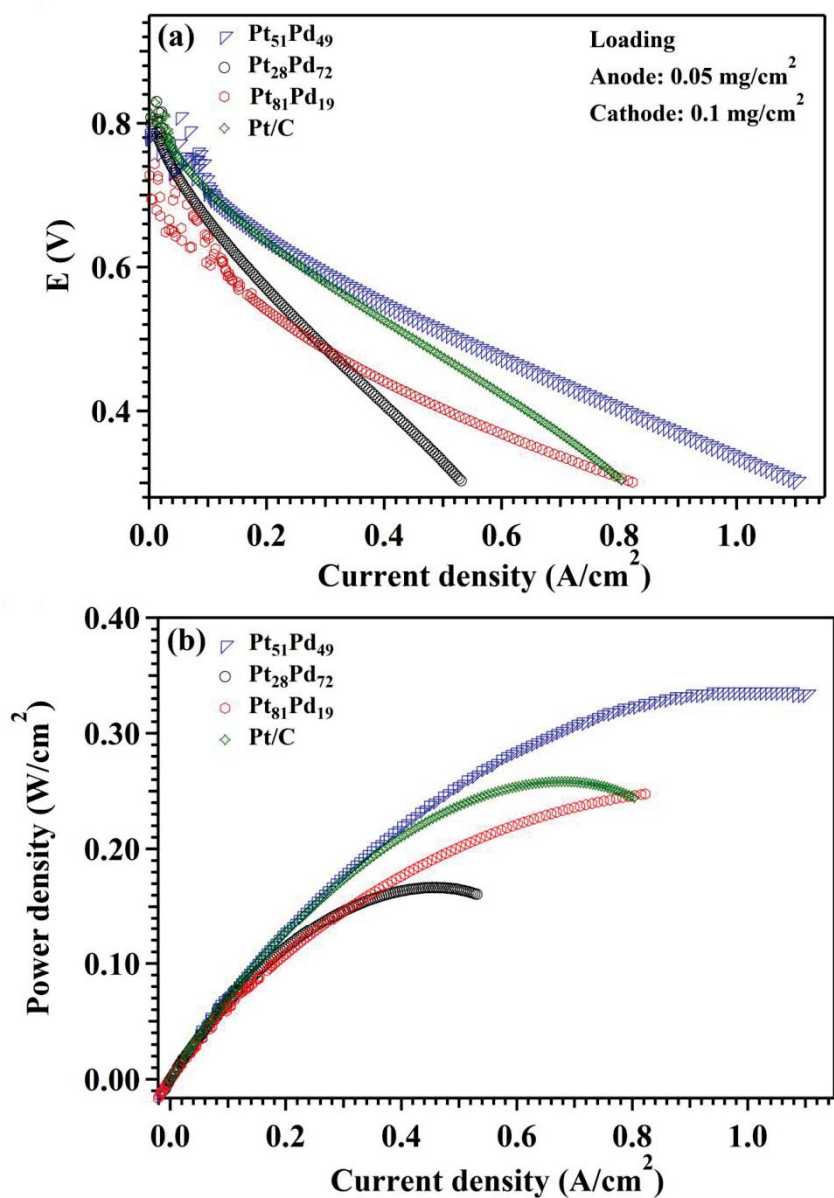


Fig. 5.13 Proton exchange membrane fuel cell performance of pulsed electrodeposited Pt_xPd_y alloy electrocatalysts on gas diffusion layer (5 cm²) (a) current density vs E and (b) current density vs power density

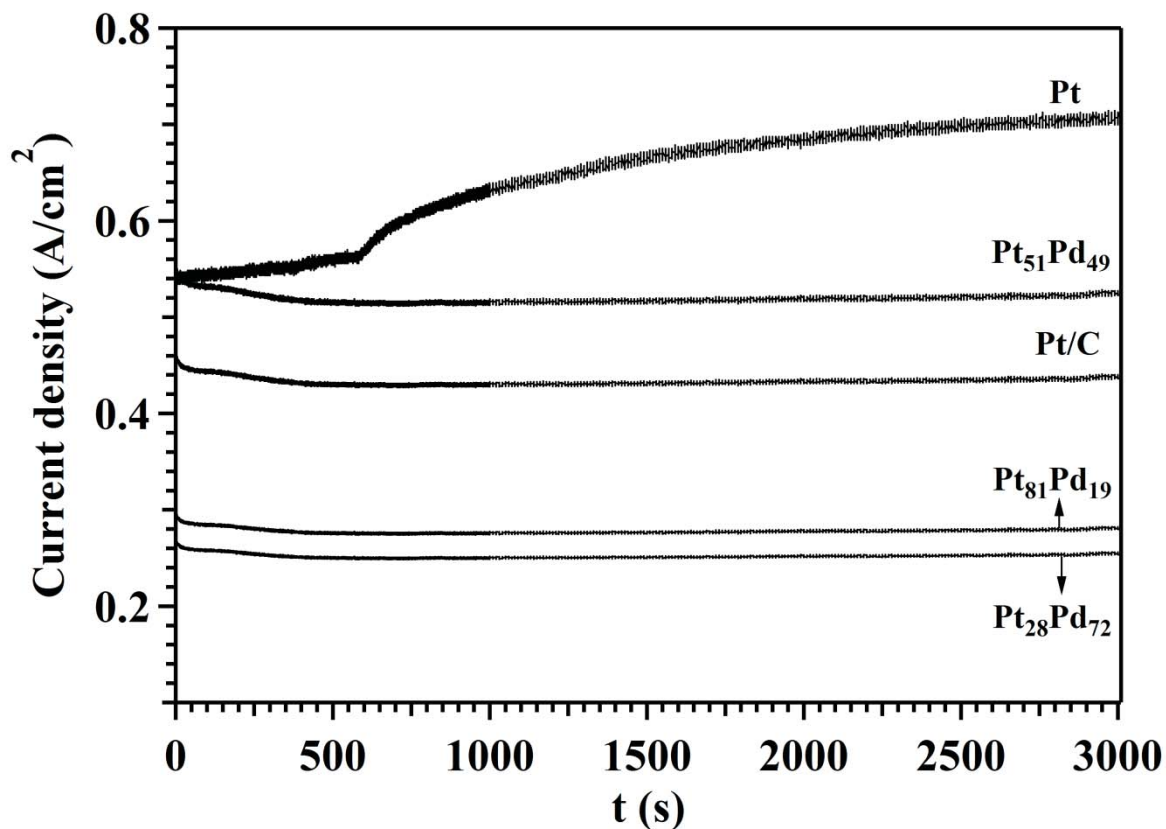


Fig. 5.14 Plot of current density vs time at 0.5 V

Table 5.10 and Fig. 5.14 shows that current density for fuel cell performance of Pt_xPd_y as ORR catalyst at 0.5 V is in the order $Pt > Pt_{51}Pd_{49} > Pt/C \text{ commercial} > Pt_{81}Pd_{19} > Pt_{28}Pd_{72}$. $Pt_{51}Pd_{49}$ alloy catalyst exhibits higher performance in fuel cell over other ratios of Pt/Pd in Pt_xPd_y alloy. Upon comparing the fuel cell performance of $Pt_{51}Pd_{49}$ alloy with literature, using pulsed electrodeposition for deposition of electrocatalyst reduced the loading of electrocatalyst for the same current density reported in literature (Table 5.11).

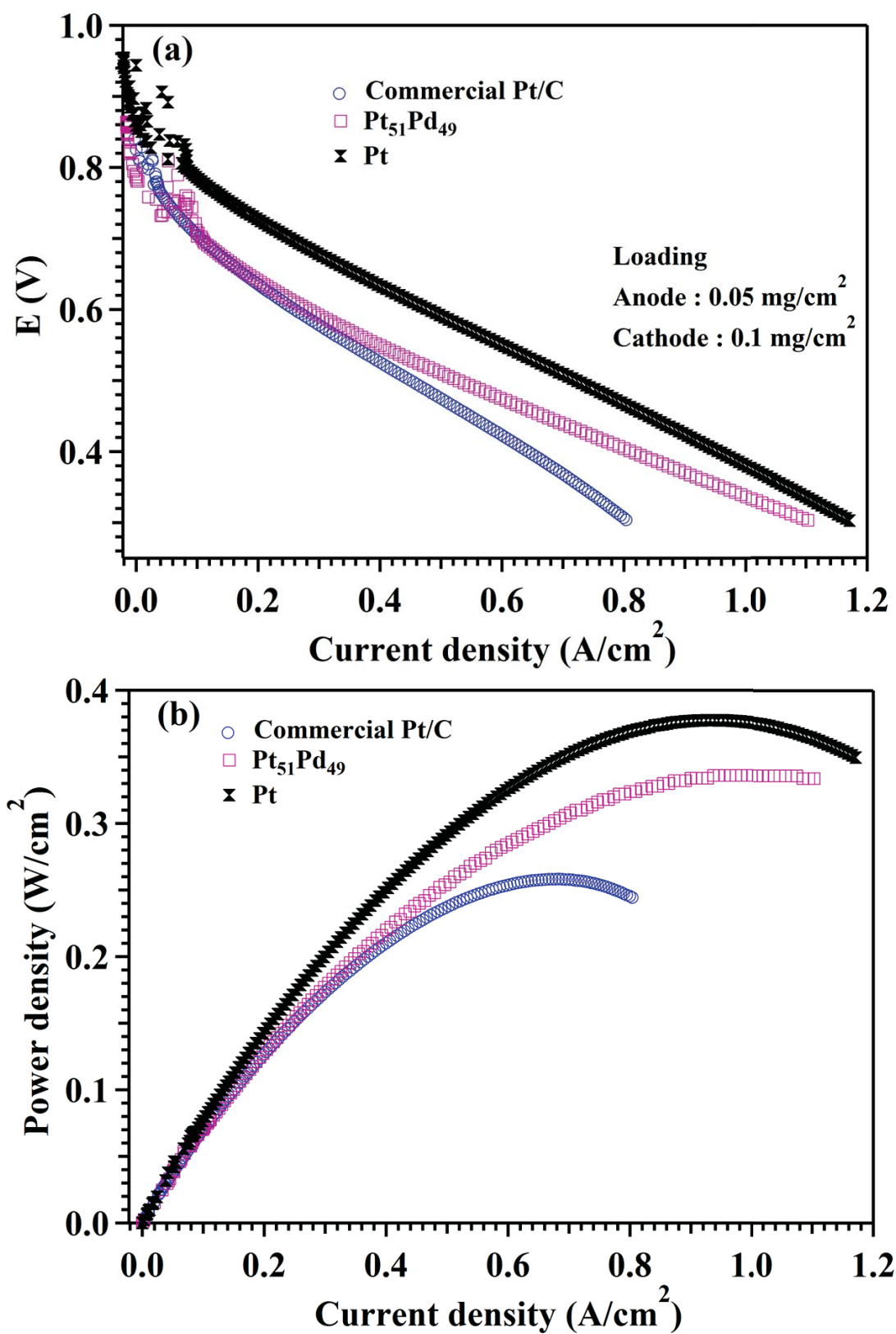


Fig. 5.15 Proton exchange membrane fuel cell performance for pulsed electrodeposited Pt, $\text{Pt}_{54}\text{Pd}_{49}$ alloy and brush coated commercial Pt/C catalyst (5 cm^2) (a) current density vs E and (b) current density vs power density

Table 5.10 Proton exchange membrane fuel cell performance of pulsed electrodeposited Pt_xPd_y on gas diffusion layer at a loading of 0.1 mg/cm^2

Electrocatalysts	Maximum power density (W/g_{Pt})	Current density (A/cm^2) @ 0.5 V
Pt/C commercial	2580	0.435
$\text{Pt}_{51}\text{Pd}_{49}$	6588	0.520
$\text{Pt}_{81}\text{Pd}_{19}$	3049	0.256
$\text{Pt}_{28}\text{Pd}_{72}$	5928	0.278
Pt	3760	0.714

The electrode area of pulsed electrodeposited $\text{Pt}_{51}\text{Pd}_{49}$ alloy on GDL was extended to 25 cm^2 and it gave similar performance as that of 5 cm^2 electrode area with a slight change in maximum power density of 0.314 W/cm^2 and its I-V curve is indicated in Fig. 5.16.

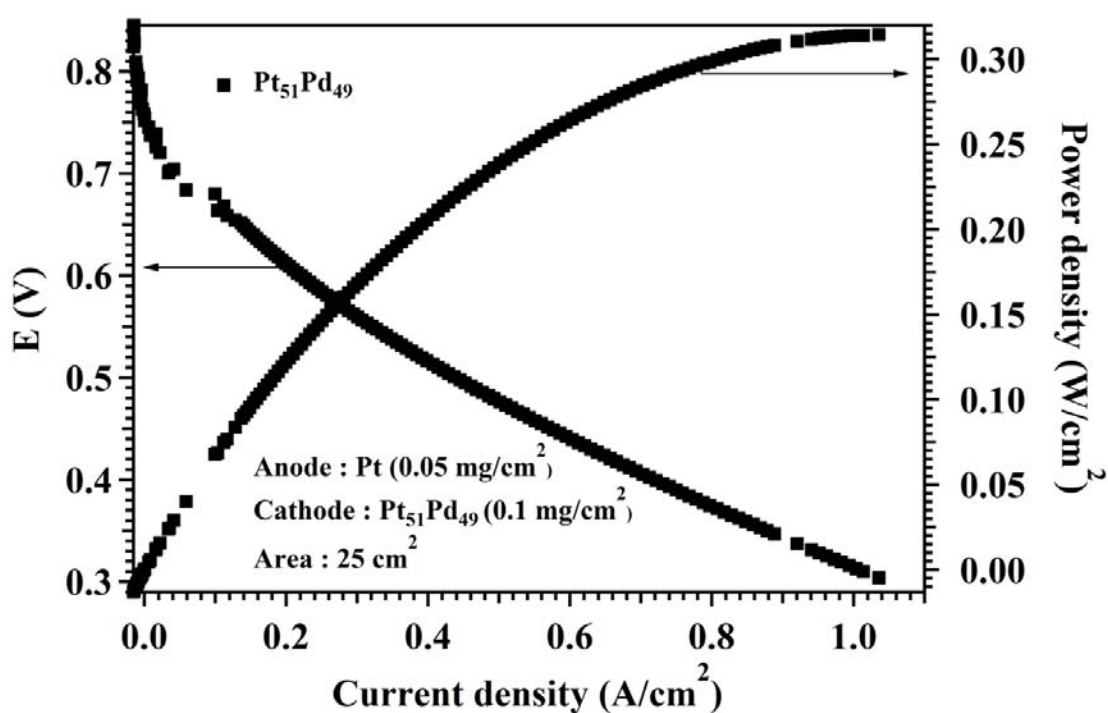


Fig. 5.16 Proton exchange membrane fuel cell performance of pulsed electrodeposited $\text{Pt}_{51}\text{Pd}_{49}$ alloy electrocatalysts on gas diffusion layer (25 cm^2)

Table 5.11 Comparison of single fuel cell performance of present pulsed electrodeposited Pt_xPd_y alloy electrocatalysts on GDL with reported Pt_xPd_y alloy electrocatalysts in literature

Electrocatalysts	Method adopted for preparation	Loading of catalyst (mg/cm^2)	Current density (mA/cm^2)
Pt on Pd/C ⁹⁷	NaBH ₄ -reduction	0.30	424 (@0.6 V)
Pt/C catalyst coated membrane ²⁰⁵	Spray coating	0.029	3000 (0.4 V) at 3 bar
Pt/C catalyst coated membrane ²⁰⁶	Spray coating	0.1	3250 (0.2 V) at cell temp. 313 K
Pt/C ⁹⁹	Pulsed electrodeposition	0.68	380 (@ 0.8 V)
Pt/C ¹⁰⁰	Pulsed potential deposition	0.22	324 (@ 0.5 V)
TiO ₂ /Pt ₇₀ Pd ₃₀ ¹⁰¹	Chemical reduction	0.40	820 (@ 0.6 V)
TiO ₂ /Pt ₅₀ Pd ₅₀ ¹⁰¹	Chemical reduction	0.40	716 (@ 0.6 V)
Pt ₁ Pd ₁ /CNT ²⁰⁷	microwave (MW) assisted, polyol reduction route	0.5	600 (@ 0.52 V)
Pt (present studies)	Pulsed electrodeposition	0.10	714 (@ 0.5 V)
Pt ₅₁ Pd ₄₉ /GDL (present studies)	Pulsed electrodeposition	0.10	520 (@ 0.5 V)

Comparison of PEM fuel cell performance of pulsed electrodeposited Pt and Pt₅₁Pd₄₉ on GDL with reported single cell performance of Pt_xPd_y alloys are shown in Table 5.11. Fuel cell performance of Pt and Pt₅₁Pd₄₉/GDL alloy with low loading of 0.1 and 0.05 mg/cm^2 gives considerable output current density at 0.5 V and is achieved due to the use of pulsed electrodeposition method for deposition of catalyst. Pulsed electrodeposition method has better control over the microstructure and better dispersion of electrocatalyst over other chemical reduction methods. The improved dispersion of catalyst results in increased activity

^{208, 209}. Effective utilization of Pt₅₁Pd₄₉/GDL catalysts was achieved by depositing the catalysts on Nafion impregnated GDL. Alloying of Pt with Pd causes a lattice strain to the Pt lattice and this might contribute to better performance for ORR. Use of Pt_xPd_y alloy for ORR result in enhanced performance with 50 % loading of Pt compared to pure Pt due to the change in d-band center of Pt in Pt_xPd_y alloy favouring ORR activity ²¹⁰⁻²¹². Membrane coated catalyst is found to give better performance as reported by M. Breiwieser et al.²⁰⁵ (3 A/cm²) and Klinglee et al.²⁰⁶ (3.25 A/cm²) but they have used Nafion 211 (25 micron) thickness and performed fuel cell operation at 353 K. Also, M. Breiwieser et al. observed 3 A/cm² under the pressurised condition of 3 bar for both H₂ and O₂. Hence, pressure, temperature of operation as well as the membrane thickness decides the current density of PEM fuel cell. Future studies will be carried out on the effect of different thickness Nafion membrane, back pressure and also different cell temperature on the fuel cell performances.

5.4 Conclusions

Facile fabrication of Pt_xPd_y alloy electrocatalysts on GDL was carried out by pulsed electrodeposition method. Pulsed electrodeposition of Pt at 0.2 ms pulse width gave better catalytic area compared to other pulse widths. The deposited Pt_xPd_y electrocatalysts at an optimum pulse width of 0.2 ms by pulsed electrodeposition method indicated a spherical morphology in FESEM images with an average particle size of 4-6 nm confirmed by HRTEM studies. The Pt/Pd ratio of Pt_xPd_y alloys prepared using three different electrolytes having varying ratios of Pt and Pd was found to be Pt₈₁Pd₁₉, Pt₅₁Pd₄₉ and Pt₂₈Pd₇₂ and were indexed to fcc crystal structure by GIXRD and SAED. The electrocatalytic activity of the deposited diffusion electrodes was investigated by ECSA measurements and impedance studies. The alloy with composition, Pt₅₁Pd₄₉ showed minimal charge transfer resistance and maximum ECSA. The fuel cell performance of diffusion electrodes with Pt_xPd_y alloys follows in the order Pt₅₁Pd₄₉ > Pt₈₁Pd₁₉ > Pt/C commercial > Pt₂₈Pd₇₂. MEA with Pt₅₁Pd₄₉ alloy

electrocatalyst used lower loading of Pt (0.05 mg/cm^2) at cathode and Pt (0.05 mg/cm^2) at anode compared to pulsed electrodeposited Pt at cathode with a loading of 0.1 mg/cm^2 and Pt at anode (0.05 mg/cm^2). The use of pulsed electrodeposition method for electrocatalyst reduced Pt loading considerably. Improved fuel cell performance was observed for $\text{Pt}_{51}\text{Pd}_{49}$ alloy compared to the conventional method of coating the Pt/C commercial catalyst. Single cell performance of $\text{Pt}_{51}\text{Pd}_{49}$ (Pt loading: 0.05 mg/cm^2) alloy is comparable with that of pulsed electrodeposited Pt (0.1 mg/cm^2). Enhanced fuel cell performance of $\text{Pt}_{51}\text{Pd}_{49}$ alloy is due to higher dispersion, electronic structure and improved interaction of Pt and Pd in alloy.

Chapter 6

Summary and Scope for Future Research

The thesis covers investigations carried out towards development of diffusion electrodes by electro deposition of Pt, Pd and Pt_xPd_y alloy electrocatalysts. The diffusion electrodes found application in amperometric H_2 sensors and fuel cells. Pulsed electrodeposition method was chosen and conditions for deposition optimised for depositing the electrocatalysts on gas diffusion layer (GDL). Facile fabrication of diffusion electrodes with better control of particle size and reduced loading of expensive electrocatalysts was realised. Electrodeposition was carried out using both aqueous and ionic liquid electrolytes. The use of ionic liquid electrolyte in electrodeposition avoids H_2 evolution and also acts like surfactants to control the particle growth during electrodeposition. Amperometric hydrogen sensor operating in fuel cell mode was developed and performance evaluation carried out. PEM fuel cells with pulsed electrodeposited alloy electrocatalyst was assembled and tested.

6.1 Summary

6.1.1 Studies on deposition and characterization of electrocatalysts on carbon paper for application in PEM sensors

The Pt, Pd and Pt_xPd_y alloy electrocatalysts were deposited on GDL by electrodeposition and pulsed electrodeposition methods for the application in proton exchange membrane based hydrogen sensors (PEMHS). Pt/C commercial catalysts were also coated on GDL by brush coating method for comparison. FESEM studies of brush coated Pt, electrodeposited Pt and pulsed electrodeposited Pt on GDL indicated more uniform distribution of spherical particles in pulsed electrodeposited samples in comparison to the other two methods. Pt was electrodeposited using $[C4mim][BF_4]$ ionic liquid electrolyte for sensor application. Prior to the electrodeposition, deposition behaviour was studied by carrying out cyclic voltammetry,

chronopotentiometry and chronoamperometry. Cyclic voltammetric studies of $\text{K}_2\text{PtCl}_6 + [\text{C4mim}][\text{BF}_4]$ showed the peak potential for Pt reduction at -2.17 V and this was also confirmed by EDAX analysis by electrodeposited Pt at -2.17 V. Chronopotentiometric and chronoamperometric studies of Pt confirmed the formation of nuclei at peak potential. By matching chronoamperometric data with Scharifker and Hills theoretical model, it was found that the nucleation of Pt on GDL surface follows instantaneous growth model. Based on the results of the above studies, electrodeposition of Pt in $\text{K}_2\text{PtCl}_6 + [\text{C4mim}][\text{BF}_4]$ electrolyte was carried out at three different applied potentials such as -2.4 V, -2.5 V and -2.6 V. The optimum surface coverage was observed at the potential of -2.4 V. This potential was used for electrodeposition and pulsed electrodeposition of Pt on GDL for sensor application. Pd was electrodeposited on GDL using $\text{PdCl}_2 + [\text{C4mim}][\text{Cl}^-]$ ionic liquid electrolyte. Peak deposition potential of Pd on GDL was observed at -0.79 V from the cyclic voltammogram of the above electrolyte. Electrodeposition of Pd on GDL was performed at four different applied potentials such as -0.8 V, -0.9 V, -1 V and -1.1 V and the optimum surface coverage was exhibited at -1 V. This potential was used for electrodeposition and pulsed electrodeposition of Pd on GDL for sensor application. Pt and Pd were also electrodeposited on GDL from aqueous medium at the applied potential of -0.2 V using 3 mM $\text{K}_2\text{PtCl}_6 + 0.5$ M H_2SO_4 and $\text{PdCl}_2 + 0.5$ M HCl respectively for comparison. Deposition from ionic liquid electrolytes showed well adhered and spherical morphology of electrodeposited Pt and Pd as illustrated by the FESEM images. GIXRD analysis confirmed Pt and Pd have fcc crystal structure without any other impurities. Energy dispersive X-ray analysis indicated the presence of Pt and Pd on GDL for electrodeposited samples. Pt_xPd_y alloy electrocatalysts was pulsed electrodeposited on GDL using $\text{K}_2\text{PtCl}_6 + \text{PdCl}_2 + 0.5$ M H_2SO_4 electrolyte. Three different ratios of Pt and Pd in Pt_xPd_y alloys were prepared using three different concentrations of Pt and Pd in the electrolyte solutions used for deposition. Compositions of

Pt_xPd_y alloy were found to be Pt₂₈Pd₇₂, Pt₅₄Pd₄₆ and Pt₈₀Pd₂₀ on analysis by ICP-MS and EDAX analysis. FESEM images of pulsed electrodeposited Pt_xPd_y alloy on GDL denote spherical particles and EDAX mapping showed uniform distribution of Pt and Pd. Shift in 2θ values in GIXRD pattern and change in lattice parameter confirmed the alloy formation.

6.1.2 Development of PEM fuel cell based amperometric H₂ sensor with catalyst deposited diffusion electrode

Pulsed electrodeposition of Pt, Pd and Pt_xPd_y alloys were carried on GDL for preparation of diffusion electrodes to be used as sensing and counter electrodes in PEMHS. Pt and Pd electrocatalysts on GDL were also electrodeposited using ionic liquid electrolytes and sensor performance compared with that prepared using aqueous electrolytes. Hydrogen sensing behaviour of sensor in two electrode mode with pulsed electrodeposited electrocatalysts on GDL showed better sensitivity and short response time compared to sensors made with brush coated and electrodeposited electrodes. By adopting gas diffusion electrode for sensor application, reduced flow rate dependence of sensor signal was achieved. Sensor with Pt based diffusion electrode prepared from ionic liquid electrolyte gave better sensitivity and response time in comparison to aqueous electrolyte owing to the improved adhesion and better morphology. Pd diffusion electrode based sensor takes much longer time to reach steady and hence it can only be operated in three electrode mode. Three electrode mode of operation of Pd diffusion electrode based sensor gave much faster response and sensitivity compared to two electrode mode. The use of ionic liquid avoids H₂ evolution during electrodeposition. The use of alloy in sensor application enhanced the catalytic activity due to the change in d-band center, which was favourable for fast kinetics of hydrogen oxidation reaction on alloy surface. Amperometric H₂ sensor with Pt₅₄Pd₄₆ alloy diffusion electrode as anode exhibited higher sensitivity compared to pristine Pt and other Pt_xPd_y alloys. Sensor with pulsed electrodeposited Pt₈₀Pd₂₀ alloy diffusion electrode gave much shorter response

time. The alloy based diffusion electrode sensor also requires lesser quantity of expensive Pt. The loading of Pt was reduced to 0.5 mg/cm^2 by utilizing electrodeposition method for sensor application. Sensitivity of the present sensor is comparable with H_2 sensors reported in literature.

6.1.3 Deposition, characterization and application of pulsed electrodeposited Pt_xPd_y alloy based gas diffusion electrodes in PEMFC

Diffusion electrode with pulsed electrodeposited Pt_xPd_y alloy on GDL was developed for application in proton exchange membrane fuel cell. In order to optimise the pulse width for deposition, pulsed electrodeposition of Pt on GDL was carried at four different on time pulse widths (0.2, 2, 20 and 200 ms) and off time pulse width was fixed at 20 ms. FESEM image of Pt at a pulse width of 0.2 ms indicated a reduced particle in comparison to depositions carried out at other pulse widths. The pulse width for deposition of Pt_xPd_y alloy was optimised at 0.2 ms on time pulse width and off time pulse width was fixed at 20 ms. FESEM and HRTEM studies proved that the Pt_xPd_y alloy has spherical morphology. GIXRD and SAED pattern confirms Pt_xPd_y alloy has fcc crystal structure. EDAX and ICP-MS analysis showed Pt_xPd_y with compositions of $\text{Pt}_{81}\text{Pd}_{19}$, $\text{Pt}_{51}\text{Pd}_{49}$ and $\text{Pt}_{28}\text{Pd}_{72}$. Fuel cell polarization studies of diffusion electrodes with pulsed electrodeposited electrocatalysts indicated that the performance are in the order of $\text{Pt} \approx \text{Pt}_{51}\text{Pd}_{49} > \text{Pt}_{81}\text{Pd}_{19} > \text{Pt/C commercial} > \text{Pt}_{28}\text{Pd}_{72}$. This in turn was supported by the ECSA and charge transfer values of the above electrocatalysts. The loading of $\text{Pt}_{51}\text{Pd}_{49}$ alloy used was 0.1 mg/cm^2 and in that Pt loading was only 0.05 mg/cm^2 . The power density of $\text{Pt}_{51}\text{Pd}_{49}$ alloy diffusion electrode is comparable with that of pristine Pt. Alloying of Pt with other metals alter the electronic structure of Pt by inducing an irregularity in the Pt lattice. This result in the lowering of d-band center in alloys for oxygen reduction reaction compared to pristine Pt.

6.2 Conclusions

- Pulsed electrodeposition method for the preparation of Pt and Pt_xPd_y alloy electrocatalysts was found to be superior in comparison to constant potential deposition and by brush coating method.
- The H_2 sensing behaviour of $\text{Pt}_{54}\text{Pd}_{46}$ alloy showed better sensitivity and response time in comparison to pristine Pt and Pd electrocatalyst. This is because of higher ECSA, lesser charge transfer resistance, change in the electronic structure and synergistic effect of alloy.
- The ionic liquid electrolyte assisted electrodeposition gave well adhered Pt and Pd particles compared to aqueous electrolyte assisted electrodeposition eventually leading to improved sensitivity and response time. Hence, future study will be undertaken for depositing Pt_xPd_y alloy using ionic liquid electrolyte and studying the H_2 sensing behaviour.
- Higher power density and current density for PEM fuel cell was achieved in the case of pulsed electrodeposited $\text{Pt}_{51}\text{Pd}_{49}$ alloy in comparison to pulsed electrodeposited pristine Pt, $\text{Pt}_{28}\text{Pd}_{72}$, and $\text{Pt}_{81}\text{Pd}_{19}$ alloy due to higher ECSA, lesser charge transfer resistance, change in the electronic structure and synergistic effect of alloy.

6.3 Scope for future studies

Three electrode mode operation of amperometric H_2 sensors are expected to give better selectivity, shorter response time and higher sensitivity than two electrode mode due to application of external voltage as a driving force for the reaction. Further, the function of Nafion proton conducting electrolyte depends on water content and sensor signal varies with respect to the relative humidity. To eliminate the humidity effect on the sensor, composite membranes are required to be developed. Also, alloy electrocatalysts are playing crucial role

in improving the performance as well as stability of fuel cell and sensor. Hence, it has lot of scope in future. Prevention of corrosion and poisoning of electrocatalysts is challenging. Therefore, the following works can be carried out in the future.

- 1) Sensors with Pt and Pt_xPd_y alloy electrocatalysts based diffusion electrodes needs to be operated in three electrode mode to get improved sensitivity, selectivity and response time.
- 2) In this thesis, single-cell performance with small electrode area (5 cm^2 and 25 cm^2) is reported. This can also be carried out at large electrode area and also for fuel cell stacks in order to extend for large-scale operation.
- 3) Corrosion and poisoning of electrocatalysts are major issues due to the continuous potential cycling of fuel cells and sensors. Alloys of Pt with Pd, Ru, Cr electrocatalyst are found to improve the stability and the kinetics of HOR and ORR. Hence, pulsed electrodeposition of the above electrocatalysts on gas diffusion layer needs to be carried out.

References

1. L. Boon-Brett, J. Bousek, G. Black, P. Moretto, P. Castello, T. Hübert and U. Banach, *Int. J. Hydrogen Energy*, 2010, 35, 373-384.
2. T. Hübert, L. Boon-Brett, G. Black and U. Banach, *Sens. Actuators B: Chem.*, 2011, 157, 329-352.
3. T. M. David, P. Sagayaraj, P. Wilson, C. Ramesh, N. Murugesan, E. Prabhu, A. S. R. Murthy and S. Annapoorani, *J. Electrochem. Soc.*, 2016, 163, B15-B18.
4. M. A. Butler, *Appl. Phys. Lett.*, 1984, 45, 1007-1009.
5. J. Zosel, G. Schiffel, F. Gerlach, K. Ahlborn, U. Sasum, V. Vashook and U. Guth, *Solid State Ionics*, 2006, 177, 2301-2304.
6. G. Velayutham, C. Ramesh, N. Murugesan, V. Manivannan, K. Dhathathreyan and G. Periaswami, *Ionics*, 2004, 10, 63-67.
7. P. Shaver, *Rev. Sci. Instrum.*, 1969, 40, 901-905.
8. D. Dwivedi, R. Dwivedi and S. Srivastava, *Sens. Actuators B: Chem.*, 2000, 71, 161-168.
9. K. Potje-Kamloth, *Chem. Rev.*, 2008, 108, 367-399.
10. M. Shivaraman, I. Lundström, C. Svensson and H. Hammarsten, *Electron. Lett.*, 1976, 12, 483-484.
11. M. T. Soo, K. Y. Cheong and A. F. M. Noor, *Sens. Actuators B Chem.*, 2010, 151, 39-55.
12. T. Hübert, L. Boon-Brett, G. Black and U. Banach, *Sens. Actuators B Chem.*, 2011, 157, 329-352.
13. M. V. K. Azhagan, M. V. Vaishampayan and M. V. Shelke, *J. Mater. Chem. A*, 2014, 2, 2152-2159.
14. J. Firth, A. Jones and T. Jones, *Combust. Flame*, 1973, 20, 303-311.
15. H. A. Daynes, 1933.
16. G. Jessop, *J. Sci. Instrum.*, 1966, 43, 777.
17. G. Pollak-Diener and E. Obermeier, *Sens. Actuators B: Chem.*, 1993, 13, 345-347.
18. I. Simon and M. Arndt, *Sens. Actuators B: phys.*, 2002, 97, 104-108.
19. M. Ando, *Trends Anal. Chem.*, 2006, 25, 937-948.
20. G. Korotcenkov, S. D. Han and J. R. Stetter, *Chem. Rev.*, 2009, 109, 1402-1433.
21. L. P. Martin, A.-Q. Pham and R. S. Glass, *Solid State Ionics*, 2004, 175, 527-530.
22. C. Park, S. Akbar and W. Weppner, *J Mater. Sci.*, 2003, 38, 4639-4660.
23. Z. Samec, F. Opekar and G. J. Crijns, *Electroanal.*, 1995, 7, 1054-1058.
24. N. Miura, T. Harada, Y. Shimizu and N. Yamazoe, *Sens. Actuators B: Chem.*, 1990, 1, 125-129.
25. J. R. Stetter and J. Li, *Chem. Rev.*, 2008, 108, 352-366.
26. C. Ramesh, G. Velayutham, N. Murugesan, V. Ganesan, K. Dhathathreyan and G. Periaswami, *J. solid state electrochem.*, 2003, 7, 511-516.
27. R. P. O'Hayre, *Fuel cell fundamentals*, John Wiley & Sons, 2006.
28. E. Jayanthi, N. Murugesan, A. Suneesh, C. Ramesh and S. Anthonysamy, *J. Electrochem. Soc.*, 2017, 164, H5210-H5217.
29. B. Sørensen and G. Spazzafumo, *Hydrogen and fuel cells: emerging technologies and applications*, Academic Press, 2018.
30. B. D. Adams and A. Chen, *Mater. Today*, 2011, 14, 282-289.
31. X. Zhong, Y. Qin, X. Chen, W. Xu, G. Zhuang, X. Li and J. Wang, *Carbon*, 2017, 114, 740-748.
32. H. Duan and C. Xu, *Electrochim. Acta*, 2015, 152, 417-424.
33. Y. Jiao, Y. Zheng, M. Jaroniec and S. Z. Qiao, *Chem. Soc. Rev.*, 2015, 44, 2060-2086.
34. N. Sammes, *Fuel cell technology: reaching towards commercialization*, Springer Science & Business Media, 2006.
35. L. Blomen and M. N. Mugerwa, *Plenum Press, Berlin* 1993.
36. M. M. Mench, *Fuel cell engines*, John Wiley & Sons, 2008.
37. G. D. Harper, *New York: McGraw-Hil*, 2008.

38. S. Srinivasan, *Fuel cells: from fundamentals to applications*, Springer Science & Business media, 2006.
39. A. Hermann, T. Chaudhuri and P. Spagnol, *Int. J. Hydrog. Energy*, 2005, 30, 1297-1302.
40. G.-Q. Lu and A. Wieckowski, *Curr. Opin. Colloid Interface Sci.*, 2000, 5, 95-100.
41. C. Ramesh, G. Velayutham, N. Murugesan, V. Ganesan, K. Dhathathreyan and G. Periaswami, *J solid state electrochem.*, 2003, 7, 511-516.
42. Y.-C. Liu, B.-J. Hwang and I.-J. Tzeng, *J Electrochem. Soc.*, 2002, 149, H173-H178.
43. C. Ramesh, N. Murugesan, M. Krishnaiah, V. Ganesan and G. Periaswami, *J Solid State Electrochem.*, 2008, 12, 1109-1116.
44. X. Lu, S. Wu, L. Wang and Z. Su, *Sens. Actuators B: Chem.*, 2005, 107, 812-817.
45. Y.-C. Weng and K.-C. Hung, *Sens. Actuators B: Chem.*, 2009, 141, 161-167.
46. A. C.-C. Chang, R. Louh, D. Wong, J. Tseng and Y. Lee, *Int. J. Hydrog. Energy*, 2011, 36, 8794-8799.
47. S. D. Thompson, L. R. Jordan and M. Forsyth, *Electrochim. Acta*, 2001, 46, 1657-1663.
48. S. Woo, I. Kim, J. K. Lee, S. Bong, J. Lee and H. Kim, *Electrochim. Acta*, 2011, 56, 3036-3041.
49. F. Fouda-Onana, N. Guillet and A. AlMayouf, *J. Power Sources*, 2014, 271, 401-405.
50. S. Ghashghaie, S. S. Ahmadi, B. Raissi, R. Riahifar, M. S. Yaghmaee and M. Javaheri, *Mater. Lett.*, 2015, 141, 23-26.
51. K.-T. Jeng, W.-M. Huang and N.-Y. Hsu, *Mater. Chem. Phys.*, 2009, 113, 574-578.
52. R.-F. Louh, A. C. Chang, V. Chen and D. Wong, *Int. J. Hydrog. Energy*, 2008, 33, 5199-5204.
53. C. Felix, T.-C. Jao, S. Pasupathi and B. G. Pollet, *J. Power Sources*, 2013, 243, 40-47.
54. H. Morikawa, N. Tsuihiji, T. Mitsui and K. Kanamura, *J. Electrochem. Soc.*, 2004, 151, A1733-A1737.
55. Z. Jabbari, B. Nassernejad, N. Fallah, M. Javanbakht and N. Afsham, *Surf. Eng.*, 2019, 1-8.
56. J.-S. Do, Y.-Y. Chen and M.-L. Tsai, *Int. J. Hydrog. Energy*, 2018, 43, 14848-14858.
57. X. Yang, Y. Zhang, X. Hao, Y. Song, X. Liang, F. Liu, F. Liu, P. Sun, Y. Gao and X. Yan, *Sens. Actuators B: Chem.*, 2018, 273, 635-641.
58. P. Frontera, A. Malara, S. Stelitano, S. G. Leonardi, A. Bonavita, E. Fazio, P. Antonucci, G. Neri, F. Neri and S. Santangelo, *Mater. Chem. Phys.*, 2016, 170, 129-137.
59. Y. Guan, F. Liu, B. Wang, X. Yang, X. Liang, H. Suo, P. Sun, Y. Sun, J. Ma and J. Zheng, *Sens. Actuators B: Chem.*, 2017, 239, 696-703.
60. B. M. Koraishy, J. P. Meyers and K. L. Wood, *J. Electrochem. Soc.*, 2011, 158, B1459-B1471.
61. A. Wolz, S. Zils, M. Michel and C. Roth, *J. power sources*, 2010, 195, 8162-8167.
62. N. Afsham, N. Fallah, B. Nassernejad, M. Javanbakht and Z. Jabbari, *Ionics*, 2019, 1-12.
63. C. Guzman, Y. Verde, E. Bustos, F. Manriquez, I. Terol, L. G. Arriaga and G. Orozco, *ECS Transactions*, 2009, 20, 413-423.
64. C.-T. Hsieh, Y.-Y. Liu and A. K. Roy, *Electrochim. Acta*, 2012, 64, 205-210.
65. J. Liu, L. Cao, W. Huang and Z. Li, *J. electroanal. chem.*, 2012, 686, 38-45.
66. I. Gurrappa and L. Binder, *Sci. Tech. Adv. Mater.*, 2008, 9, 043001.
67. E. Alfonso, J. Olaya and G. Cubillos, in *Crystallization-Science and Technology*, IntechOpen, 2012.
68. K. H. Choi, H. S. Kim and T. H. Lee, *J. Power Sources*, 1998, 75, 230-235.
69. J. Tang and K. Azumi, *Electrochim. Acta*, 2011, 56, 1130-1137.
70. J. J. Whalen, J. D. Weiland and P. C. Searson, *J. Electrochem. Soc.*, 2005, 152, C738-C743.
71. Z. He, J. Chen, D. Liu, H. Tang, W. Deng and Y. Kuang, *Mater. Chem. Phys.*, 2004, 85, 396-401.
72. S. Guerin and G. S. Attard, *Electrochem. Commun.*, 2001, 3, 544-548.
73. S. Guerin and G. S. Attard, *Electrochem. Commun.*, 2001, 3, 544-548.
74. P. He, H. Liu, Z. Li and J. Li, *J. Electrochem. Soc.*, 2005, 152, E146-E153.
75. F. Endres, A. Abbott and D. R. MacFarlane, *Electrodeposition from Ionic Liquids*, Wiley, 2017.
76. A. P. Abbott and K. J. McKenzie, *Phys. Chem. Chem. Phys.*, 2006, 8, 4265-4279.
77. T. Welton, *Chem. rev.*, 1999, 99, 2071-2084.

78. D. Wei and A. Ivaska, *Anal. Chim. Acta*, 2008, 607, 126-135.
79. M. Armand, F. Endres, D. R. MacFarlane, H. Ohno and B. Scrosati, *Nat. mater.*, 2009, 8, 621-629.
80. G. G. Eshetu, M. Armand, H. Ohno, B. Scrosati and S. Passerini, *Energy Environ. Sci.*, 2016, 9, 49-61.
81. S. Z. El Abedin, M. Pölleth, S. Meiss, J. Janek and F. Endres, *Green Chem.*, 2007, 9, 549-553.
82. P. Migowski, D. Zanchet, G. Machado, M. A. Gelesky, S. R. Teixeira and J. Dupont, *Phys. Chem. Chem. Phys.*, 2010, 12, 6826-6833.
83. K. Iwata, H. Okajima, S. Saha and H.-o. Hamaguchi, *Acc. Chem. Res.*, 2007, 40, 1174-1181.
84. F. Alcaide, G. Álvarez, J. A. Blázquez, P. L. Cabot and O. Miguel, *Int. J. Hydrogen Energy*, 2010, 35, 5521-5527.
85. X.-m. Chen, Z.-x. Cai, Z.-y. Huang, M. Oyama, Y.-q. Jiang and X. Chen, *Electrochim. Acta*, 2013, 97, 398-403.
86. N. Doan, T. Sundqvist, P. Hiekkataipale, J. Korhonen, T. Kallio, J. Ruokolainen, K. Kontturi and C. Johans, *Int. J. Electrochem. Sci*, 2015, 10, 2535-2553.
87. S. D. Thompson, L. R. Jordan and M. Forsyth, *Electrochim. Acta*, 2001, 46, 1657-1663.
88. M. Sakthivel and W. Weppner, *Sens. Actuators B: Chem.*, 2006, 113, 998-1004.
89. H. Cheh, *J. Electrochem. Soc.*, 1971, 118, 551-557.
90. B. Hwang, Y. Liu and W. Hsu, *J. New Mater. Electrochem. Syst.*, 2001, 4, 69-76.
91. Y.-C. Weng, K.-C. Hung, J.-C. Wang, Y.-G. Lee, Y.-F. Su and C.-Y. Lin, *Sens. Actuators B: Chem.*, 2010, 150, 264-270.
92. M. Rashid, T.-S. Jun and Y. S. Kim, *J Korean Electrochem. Soc.*, 2014, 17, 18-25.
93. M. Rashid, T.-S. Jun, Y. Jung and Y. S. Kim, *Sens. Actuators B: Chem.*, 2015, 208, 7-13.
94. S. Xie, S.-I. Choi, N. Lu, L. T. Roling, J. A. Herron, L. Zhang, J. Park, J. Wang, M. J. Kim and Z. Xie, *Nano lett.*, 2014, 14, 3570-3576.
95. E. Antolini, S. C. Zignani, S. F. Santos and E. R. Gonzalez, *Electrochim. Acta*, 2011, 56, 2299-2305.
96. M. F. Hossain and J. Y. Park, *Int. J. Electrochem. Sci.*, 2015, 10, 6213-6226.
97. S. J. Bae, S. J. Kim, K. S. Nahm and P. Kim, *Int. J. Hydrogen Energy*, 2011, 36, 9115-9122.
98. Y.-H. Cho, B. Choi, Y.-H. Cho, H.-S. Park and Y.-E. Sung, *Electrochem. Commun.*, 2007, 9, 378-381.
99. H. Kim, N. P. Subramanian and B. N. Popov, *J. Power Sources*, 2004, 138, 14-24.
100. J. J. Burk and S. K. Buratto, *J. Phys. Chem. C*, 2013, 117, 18957-18966.
101. S.-Y. Huang, P. Ganesan and B. N. Popov, *ACS Catal.*, 2012, 2, 825-831.
102. F. Alcaide, G. Álvarez, P. L. Cabot, O. Miguel and A. Querejeta, *Int. J. Hydrogen Energy*, 2010, 35, 11634-11641.
103. J.-J. Lv, J.-N. Zheng, H.-B. Zhang, M. Lin, A.-J. Wang, J.-R. Chen and J.-J. Feng, *J. Power Sources*, 2014, 269, 136-143.
104. F. Scholz, *Electroanalytical methods*, Springer, 2010.
105. P. T. Kissinger and W. R. Heineman, *J. Chem. Ed.*, 1983, 60, 702.
106. A. J. Bard, L. R. Faulkner, J. Leddy and C. G. Zoski, *Electrochemical methods: fundamentals and applications*, Wiley New York, 1980.
107. E. R. Brown and J. R. Sandifer, *Physical methods of chemistry*, 1986, 2, 273.
108. H. Gerischer, *Interscience Publishers Inc., New York 1954.*, 1956, 60, 521-522.
109. M. Paunovic, *J. electroanal. chem. interfacial electrochem.*, 1967, 14 447-447.
110. M. E. Orazem and B. Tribollet, *Electrochemical impedance spectroscopy*, John Wiley & Sons, 2017.
111. J. I. Goldstein, D. E. Newbury, J. R. Michael, N. W. Ritchie, J. H. J. Scott and D. C. Joy, *Scanning electron microscopy and X-ray microanalysis*, Springer, 2017.

112. A. Khursheed, *Scanning electron microscope optics and spectrometers*, World scientific, 2011.
113. T. Pradeep, *Nano: the essentials*, Tata McGraw-Hill Education, 2007.
114. D. B. Williams and C. B. Carter, in *Transmission electron microscopy*, Springer, 1996, pp. 3-17.
115. B. D. Cullity and S. R. Stock, *Elements of x-ray diffraction*, Prentice Hall, Upper Saddle River, NJ, 2001.
116. P. Scherrer, *Phys*, 1918, 2, 98-100.
117. B. Ben-Nissan, A. Choi, R. Roest, B. Latella and A. Bendavid, in *Hydroxyapatite (Hap) for Biomedical Applications*, Elsevier, 2015, pp. 21-51.
118. A. Choi, B. Ben-Nissan, A. Bendavid and B. Latella, in *Thin Film Coatings for Biomaterials and Biomedical Applications*, Elsevier, 2016, pp. 117-141.
119. S. T. Gonczy and N. Randall, *Int. J. Appl. Ceram. Technol.*, 2005, 2, 422-428.
120. H. E. Taylor and H. M. TAYLOR, *Inductively coupled plasma-mass spectrometry: practices and techniques*, Academic press, 2001.
121. S. H. Nam, W. R. Masamba and A. Montaser, *Anal. Chem.*, 1993, 65, 2784-2790.
122. A. Brouzgou, S. Song and P. Tsiakaras, *Appl. catal. b environ*, 2012, 127, 371-388.
123. M. K. Debe, *Nature*, 2012, 486, 43-51.
124. E. Antolini, *Energy Environ. Sci.*, 2009, 2, 915-931.
125. J. Zhang, X. Wang, C. Wu, H. Wang, B. Yi and H. Zhang, *React. Kinet. Catal. Lett.*, 2004, 83, 229-236.
126. N. Cunningham, E. Irissou, M. Lefevre, M.-C. Denis, D. Guay and J.-P. Dodelet, *Electrochem. Solid State Lett.*, 2003, 6, A125-A128.
127. Y. Xing, *J. Phys. Chem. B*, 2004, 108, 19255-19259.
128. M. Uchida, Y. Aoyama, N. Eda and A. Ohta, *J. Electrochem. Soc.*, 1995, 142, 4143-4149.
129. J. Tang and K. Azumi, *Electrochimica Acta*, 2011, 56, 1130-1137.
130. I. Gurrappa and L. Binder, *Sci. Technol. Adv. Mater.*, 2008, 9, 043001.
131. P. Giridhar, K. Venkatesan, T. Srinivasan and P. Vasudeva Rao, *J. Radioanal. Nucl. Chem.*, 2005, 265, 31-38.
132. S. A. Dharaskar, K. L. Wasewar, M. N. Varma, D. Z. Shende and C. Yoo, *Arab. J. Chem.*, 2016, 9, 578-587.
133. S. Salomé, R. Rego, A. Querejeta, F. Alcaide and M. C. Oliveira, *Electrochim. Acta*, 2013, 106, 516-524.
134. F. Sarto, E. Castagna, M. De Francesco, T. Dikonimos, L. Giorgi, S. Lecci, M. Sansovini and V. Violante, *Int. J. Hydrogen Energy* 2014, 39, 14701-14711.
135. K. Itaya, H. Takahashi and I. Uchida, *J electroanal. chem. interfacial electrochem.*, 1986, 208, 373-382.
136. C. Paoletti, A. Cemmi, L. Giorgi, R. Giorgi, L. Pilloni, E. Serra and M. Pasquali, *J. Power Sources*, 2008, 183, 84-91.
137. N. Georgolios, D. Jannakoudakis and P. Karabinas, *J. electroanal. chem. interfacial electrochem.*, 1989, 264, 235-245.
138. J. Lee, J. Seo, K. Han and H. Kim, *J. power sources*, 2006, 163, 349-356.
139. O. Antoine and R. Durand, *Electrochem. Solid-State Lett.*, 2001, 4, A55-A58.
140. D. Zhang, W. C. Chang, T. Okajima and T. Ohsaka, *Langmuir*, 2011, 27, 14662-14668.
141. U. Schröder, J. D. Wadhawan, R. G. Compton, F. Marken, P. A. Suarez, C. S. Consorti, R. F. de Souza and J. Dupont, *New J Chem.*, 2000, 24, 1009-1015.
142. B. K. Sweeny and D. G. Peters, *Electrochem. commun.*, 2001, 3, 712-715.
143. Y. Katayama, S. Dan, T. Miura and T. Kishi, *J. Electrochem. Soc.*, 2001, 148, C102-C105.
144. J. Fuller and R. T. Carlin, *J. Chem. Crystallogr.*, 1994, 24, 489-493.
145. L. Xiao and K. E. Johnson, *J. Electrochem. Soc.*, 2003, 150, E307-E311.
146. P. He, H. Liu, Z. Li and J. Li, *J Electrochem. Soc.*, 2005, 152, E146-E153.

147. F. Lantelme and J. Chevalet, *J. electroanal. chem. interfacial electrochem.*, 1981, 121, 311-327.
148. P. Lai and M. Skylas-Kazacos, *J. electroanal. chem. interfacial electrochem.*, 1988, 248, 431-440.
149. B. Scharifker and G. Hills, *Electrochim. Acta*, 1983, 28, 879-889.
150. M. Jayakumar, K. Venkatesan and T. Srinivasan, *Electrochim. Acta*, 2007, 52, 7121-7127.
151. P. Giridhar, K. Venkatesan, B. P. Reddy, T. Srinivasan and P. V. Rao, *Radiochim. Acta*, 2006, 94, 131-136.
152. S. Shrestha, M. Nagib and E. J. Biddinger, *J Electrochem. Soc.*, 2016, 163, D74-D82.
153. S. Shrestha, E. Gjoka and E. J. Biddinger, *ECS Transact.*, 2014, 64, 267-274.
154. J.-K. Chang, C.-H. Huang, W.-T. Tsai, M.-J. Deng, I.-W. Sun and P.-Y. Chen, *Electrochim. Acta*, 2008, 53, 4447-4453.
155. M. Antonietti, D. Kuang, B. Smarsly and Y. Zhou, *Angew. Chem. Int. Ed.*, 2004, 43, 4988-4992.
156. Z. Wang, Q. Zhang, D. Kuehner, X. Xu, A. Ivaska and L. Niu, *Carbon*, 2008, 46, 1687-1692.
157. A. Kaniyoor and S. Ramaprabhu, *Electrochim. Acta*, 2012, 72, 199-206.
158. Y. Lu, Y. Jiang and W. Chen, *Nano Energy*, 2013, 2, 836-844.
159. H. Li, Q. Xin, W. Li, Z. Zhou, L. Jiang, S. Yang and G. Sun, *Chem. Comm.*, 2004, 2776-2777.
160. A. Arico, P. Antonucci, E. Modica, V. Baglio, H. Kim and V. Antonucci, *Electrochim. Acta*, 2002, 47, 3723-3732.
161. Z. Ma, P. Cheng and T. Zhao, *J. Membr. Sci.*, 2003, 215, 327-336.
162. W. Wang, Q. Huang, J. Liu, Z. Zou, Z. Li and H. Yang, *Electrochem. Commun.*, 2008, 10, 1396-1399.
163. C.-H. Han, D.-W. Hong, I.-J. Kim, J. Gwak, S.-D. Han and K. C. Singh, *Sens. Actuators B: Chem.*, 2007, 128, 320-325.
164. E.-B. Lee, I.-S. Hwang, J.-H. Cha, H.-J. Lee, W.-B. Lee, J. J. Pak, J.-H. Lee and B.-K. Ju, *Sens. Actuators B: Chem.*, 2011, 153, 392-397.
165. E. Bakker and M. Telting-Diaz, *Anal. Chem.*, 2002, 74, 2781-2800.
166. J. F. McAleer, P. t. Moseley, P. Bourke, J. O. W. Norris and R. Stephan, *Sens. Actuators*, 1985, 8, 251-257.
167. N. Maffei and A. K. Kuriakose, *Sensors and Actuators B: Chemical*, 2004, 98, 73-76.
168. F. Opekar and K. Štulík, *Anal. Chim. Acta*, 1999, 385, 151-162.
169. F. Opekar, *Electroanal.*, 1992, 4, 133-138.
170. B. Adhikari and S. Majumdar, *Prog. Polym. Sci.*, 2004, 29, 699-766.
171. J. Lobato, M. Rodrigo, J. Linares and K. Scott, *J. Power Sources*, 2006, 157, 284-292.
172. Y. Verde, G. Alonso-Nuñez, M. Miki-Yoshida, M. Jose-Yacamán, V. H. Ramos and A. Keer, *Catal. today*, 2005, 107, 826-830.
173. X. Wang, I.-M. Hsing and P. L. Yue, *J. Power Sources*, 2001, 96, 282-287.
174. S. Rudi, C. Cui, L. Gan and P. Strasser, *Electrocatalysis*, 2014, 5, 408-418.
175. N. Miura, H. Kato, Y. Ozawa, N. Yamazoe and T. Seiyama, *Chem. Lett.*, 1984, 13, 1905-1908.
176. R. L. Borup, J. R. Davey, F. H. Garzon, D. L. Wood and M. A. Inbody, *J. Power Sources*, 2006, 163, 76-81.
177. R. L. Borup, J. R. Davey, F. H. Garzon, D. L. Wood and M. A. Inbody, *J. Power Sources*, 2006, 163, 76-81.
178. A. Hassibi, R. Navid, R. W. Dutton and T. H. Lee, *J. Appl. Phys.*, 2004, 96, 1074-1082.
179. P. Sedlak, J. Sikula, V. Sedlakova, M. Chvatal, J. Majzner, M. Vondra, P. Kubersky, S. Nespurek and A. Hamacek, 2013.
180. M. Sakthivel and W. Weppner, *Sensors*, 2006, 6, 284-297.
181. N. Murugesan, C. Ramesh, N. Sanil, M. Krishnaiah, S. S. Raj and V. Ganesan, *Sens. Actuators B: Chem.*, 2013, 182, 598-604.
182. Y.-C. Liu, B.-J. Hwang and I.-J. Tzeng, *J. Electrochem. Soc.*, 2002, 149, H173-H178.

183. H. Van Hien, T. D. Thanh, N. D. Chuong, D. Hui, N. H. Kim and J. H. Lee, *Compos. Part B Eng.*, 2018, 143, 96-104.
184. E. Voogt, A. Mens, O. Gijzeman and J. Geus, *Surf. Sci.*, 1997, 373, 210-220.
185. K. Jiang, S. Back, A. J. Akey, C. Xia, Y. Hu, W. Liang, D. Schaak, E. Stavitski, J. K. Nørskov and S. Siahrostami, *Nat. commun.*, 2019, 10, 1-11.
186. M. Miller and A. Bazylak, *J. Power Sources*, 2011, 196, 601-613.
187. Y. Wang, K. S. Chen, J. Mishler, S. C. Cho and X. C. Adroher, *Appl. energy*, 2011, 88, 981-1007.
188. W. R. W. Daud, R. Rosli, E. Majlan, S. Hamid, R. Mohamed and T. Husaini, *Renew. Energy*, 2017, 113, 620-638.
189. C.-Y. Liu and C.-C. Sung, *J. Power Sources*, 2012, 220, 348-353.
190. M. K. Debe, *Nature*, 2012, 486, 43.
191. F. Jaouen, E. Proietti, M. Lefèvre, R. Chenitz, J.-P. Dodelet, G. Wu, H. T. Chung, C. M. Johnston and P. Zelenay, *Energy Environ. Sci.*, 2011, 4, 114-130.
192. V. Stamenkovic, B. S. Mun, K. J. Mayrhofer, P. N. Ross, N. M. Markovic, J. Rossmeisl, J. Greeley and J. K. Nørskov, *Angew. Chem. Int. Ed.*, 2006, 45, 2897-2901.
193. J. Rossmeisl, G. S. Karlberg, T. Jaramillo and J. K. Nørskov, *Faraday discuss.*, 2009, 140, 337-346.
194. S. J. Yoo, H. Y. Park, T. Y. Jeon, I. S. Park, Y. H. Cho and Y. E. Sung, *Angew. Chem. Int. Ed.*, 2008, 47, 9307-9310.
195. S. Guo, S. Dong and E. Wang, *Chem. Commun.*, 2010, 46, 1869-1871.
196. Y. Lu, S. Du and R. Steinberger-Wilckens, *Appl. Catal. B*, 2016, 187, 108-114.
197. J. B. Joo, P. Kim, W. Kim, Y. Kim and J. Yi, *J. Appl. Electrochem.*, 2009, 39, 135-140.
198. Z. Liu, C. Yu, I. A. Rusakova, D. Huang and P. Strasser, *Top. Catal.*, 2008, 49, 241-250.
199. S. Lertviriyapaisan and N. Tantavichet, *Int. J. Hydrogen Energy* 2010, 35, 10464-10471.
200. J. Erlebacher and J. Snyder, *ECS Transactions*, 2009, 25, 603-612.
201. D. Dang, H. Zou, Z. a. Xiong, S. Hou, T. Shu, H. Nan, X. Zeng, J. Zeng and S. Liao, *ACS Catal.*, 2015, 5, 4318-4324.
202. H. Kim and B. N. Popov, *Electrochem. Solid-State Lett.*, 2004, 7, A71-A74.
203. Y. Lu, Y. Jiang, H. Wu and W. Chen, *J. Phys. Chem. C*, 2013, 117, 2926-2938.
204. M. Khan, A. B. Yousaf, M. Chen, C. Wei, X. Wu, N. Huang, Z. Qi and L. Li, *J. Power Sources*, 2015, 282, 520-528.
205. M. Breitwieser, M. Klingele, B. Britton, S. Holdcroft, R. Zengerle and S. Thiele, *Electrochem. Commun.*, 2015, 60, 168-171.
206. M. Klingele, B. Britton, M. Breitwieser, S. Vierrath, R. Zengerle, S. Holdcroft and S. Thiele, *Electrochem. Commun.*, 2016, 70, 65-68.
207. A. Bharti and G. Cheruvally, *Int. J. Hydrog. Energy*, 2018, 43, 14729-14741.
208. H. A. Gasteiger, S. S. Kocha, B. Sompalli and F. T. Wagner, *Appl. Catal., B*, 2005, 56, 9-35.
209. D. Dang, S. Liao, F. Luo, S. Hou, H. Song and P. Huang, *J. Power Sources*, 2014, 260, 27-33.
210. J. Kitchin, J. K. Nørskov, M. Barteau and J. Chen, *J. chem. phys.*, 2004, 120, 10240-10246.
211. J. Greeley, J. K. Nørskov and M. Mavrikakis, *Annu. rev. phys. chem.*, 2002, 53, 319-348.
212. L. A. Kibler, A. M. El-Aziz, R. Hoyer and D. M. Kolb, *Angew. Chem. Int. Ed.*, 2005, 44, 2080-2084.